PROCESS PHYSICS:
From Information Theory to Quantum Space and Matter

By

Reginald T. Cahill

.

This book is dedicated to the memory of Dayton C. Miller of the Case School of Applied Science, Cleveland, Ohio. His extensive and high quality detection of absolute motion was one of the great experiments of the last century. He was ignored by the physics community simply because in his era it was believed, as it is now, that absolute motion was incompatible with special relativistic effects, and so it was accepted, without any evidence, that his experiments were wrong. His experiences showed yet again that few in physics actually accept that it is an evidence based science, as Galileo long ago discovered also to his great cost.

Contents

Chapter 1

Introduction

This book is about a new and very radical information-theoretic approach to comprehending and modelling reality. It is called *Process Physics* because it uses a process model of time rather than, as in current physics, a non-process geometrical model of time, a model so successfully developed and used by Galileo, Newton, Einstein and others that for many physicists the phenomenon of time is actually identified with this geometrical model. Now, for the first time in the history of physics, we have a model of time that includes the distinctions between past, present and future. These distinctions cannot be made in the geometrical model of time. For this reason we can call the current prevailing physics *Non-Process Physics*. In *Process Physics* we turn to a fundamental reformulation of the key concepts in physics. This entails that we must identify both the successes and failures of the *Non-Process Physics*, for it almost succeeded.

The radical starting point is to model reality as a self-organising semantic information system. This is 'information' that is accessible and meaningful to reality itself, but not, in the main, accessible by us, even including the experimental scientists. This means in part that we reject that notion that matter and space are 'substances' or 'things' obeying 'laws'. That kind of phenomenological modelling of reality has reached its limits. Indeed right through the last century, after the discovery of the intriguing quantum phenomena, the idea had begun to emerge that reality had some 'informational' aspects to it, though this notion never successfully matured into a new modelling. First it is necessary to analyse how the older physics modelled reality, and it did so using only a syntactical information system. Essentially that means that it used a symbol based system, with symbols assigned to stand for various given entities, such as electrons, electric fields and the like. As well rules or laws were proposed to determine how the symbols were to be manipulated and used for computations. This approach gave us the famous equations of physics. Such a system is all syntax. It's like a game of chess - the pieces are rearranged according to prescribed rules. Of course that a science such as physics could successfully exploit a syntactical system was a major development - it was

the hallmark of the last 400 years. In such a system the only sense of meaning is that the symbol manipulators, us, may attach meanings to the symbols. While such meaning might inspire and guide us, it certainly has no significance for the symbols themselves. In *Process Physics* the daunting problem of how reality itself may be ascribed as having internal meaning has been tackled and developed to such a level that this book is now warranted, although clearly much remains to be done - this book is about the early stages of this new approach.

So the new concept of a semantic information system is developed here. This is very subtle as we must deal with such a system, somewhat paradoxically, by using syntax, that is by using mathematical symbols. As explained in Part I the symbols are essentially a way of bootstrapping the semantic system. Being a semantic information system with meaning determined by the system self-organising, there is a sense in which reality is being modelled as a self-referencing system. Of course as Gödel showed in the 1930's there is a sense in which even certain syntactical systems can be made self-referencing. But this was only used to show how limited such systems are; if they are self-consistent then they are incomplete. This means that there are statements that one can construct within the syntax but for which one cannot determine whether or not they followed from the axioms for that syntax. This meant that syntactical systems had, in the end, serious limitations. In the semantic information system we avoid a strict axiomatised syntax by introducing the notion of self-referential noise. This is a way of modelling the limitations on self-referencing - basically reality cannot be all-knowing about itself, if you like. This is implemented by using stochastic or random processes injected at each stage of the processing time, actually an iterative modelling of time with a stochastic disordering process competing against an ordering process. So we have an order/disorder system at the 'start-up' of the modelling, but most significantly one which has no notion of space, matter or any of the other well known phenomena of physics. Curiously the mathematics of the bootstrapping system is that of a stochastic neural network, a system originally inspired by the apparent operation of biological brains. Here, however, the stochastic neural network mathematics was inspired by the discovery that conventional quantum field theories could almost be reformulated in the mathematical language of stochastic neural networks. In such systems the information is represented by connection patterns, and not by symbols. Information is then processed by interactions between the patterns, and because of the randomness, such systems can actually generate new 'information' patterns. Amazingly, as shown in detail herein, there is good evidence that the system self-organises patterns that show all the characteristics of a quantum space and quantum matter, and the idea is that these patterns of relationships are self-recognising. That means that the behaviour of the informational patterns is determined internally, they are not prescribed. To the extent so far reached by this approach we see emergent phenomena of a quantum field theory with many of the attributes of the current standard model of 'particle physics'. That is, we see, for the first time, the emergence of quantum phenomena,

where no assumptions about such phenomena were placed into the system at the start-up. So we see the logical necessity for quantum phenomena. Such phenomena seems to be necessary once we use the notion of semantic as distinct from syntactical information. So quantum phenomena are an attribute of semantic information systems. This convergence of the form of a deep theory of reality with the operation of biological brains is not at all strange. Both systems are dealing with internally meaningful information. Manipulating symbols is of very limited value.

The emergent quantum phenomena are embedded in an emerging space, a quantum foam system itself; so space is also a consequences of implementing a semantic information system approach. This quantum space, like quantum matter, is essentially nothing but internal information, and it is fractal; relationships within relationships and so on. Because the space is self-organising it actually 'grows' in size over time, and so naturally exhibits the key feature of an expanding universe. The distinction between space and matter is only about how the information is encoded. For matter the information is topologically encoded, and so is preserved, except when space and matter are together dissipated at a quantum-foam in-flow singularity, a new form of black hole.

General considerations, which require a great deal of further work, suggested that the inertia of matter may be a consequence of how the information patterns that are quantum matter are processed, that once in motion that motion is preserved by the very nature of the information processing. This represents a very novel explanation for inertia - the property of systems to stay in uniform motion unless acted upon by some externally imposed influence, that is by a 'force'. But this explanation also suggested that such motion was 'absolute motion', meaning that motion relative to space itself should be meaningful and measurable. As well arguments were constructed that suggested that the phenomenon of gravity was caused by the differential processing of the information subsystems that constitute quantum space and quantum matter. The net result of that difference being manifested as a relaxation of space towards matter. Matter was essentially destroying the spatial system, and it in turn essentially 'flowed' towards matter. Of course this is not a flow of something through space, but rather a restructuring of the spatial patterns. These two insights led to two major predictions: first that absolute motion should be observable, and second that the absolute motion data should reveal a component of the motion amounting to a flow towards matter. In this case we would expect to see, for example, a flow past the earth towards the sun, and such a flow is now apparent in data from the experiment by Miller in the 1920's. This flow should not be confused with the older aether concept. That concept had a particulate system, the aether, flowing through a smooth geometrical space. That was a dualistic system. At this stage we come to the end of the information-theoretic Part I of this book. Before this is further developed we should test against observation and experiment some of the key predictions that have emerged so far: space having quantum structure, absolute motion being meaningful and observable, and

that gravity was a relaxation of the quantum structure of space towards matter. Of course these last two predictions are in total disagreement with Einstein's theories. For that reason such notions are totally banned in physics.

In Part II and III of the book we report on what can only be described as an amazing sequence of developments that emerged from looking for observational and experimental tests of these predictions of the information-theoretic Process Physics. Part II deals with the new theory of gravity and its elegant dynamical explanation of the so-called 'dark matter' effect, while Part III deals with the extensive range of experiments that have detected absolute motion. First, it turns out that both the Newtonian and Hilbert-Einstein theories of gravity may be reformulated in the language of a 'fluid-flow' system, in the latter case for a certain class of metrics. This class includes the external Schwarzschild metric, which is the metric in which all but one of the so-called tests of that theory were done. Hence the many successes of these theories are not inconsistent with a flow interpretation of gravity. Of course Newton's theory of gravity has always been cast in a force law formalism, giving the famous inverse square law, namely that the gravitational force exerted by a lump of matter should decrease with the inverse of the square of the distance. This law was based on the analysis by Kepler of the motion of the planets about the sun. It seemed to work just fine. The Hilbert-Einstein theory of gravity, on the other hand, was supposed to have explained gravity as a distortion, caused by matter, of the geometry of the four dimensional spacetime construct. However in all but one of the tests the gravity part of this spacetime mathematical formalism is nothing more than Newton's inverse square law in heavy mathematical disguise. The obtuse mathematics of General Relativity, as this theory is called, had resulted in nothing less than total confusion. By introducing an exact but much more explicit choice of mathematical variables, it turns out that General Relativity, in the case of the Schwarzschild metric, reduces exactly to Newton's theory of gravity, written as an in-flow, with only a minor difference associated with how matter, say a planet, responds to the in-flow, as specified by the so-called geodesic equation. The difference is related to special relativity effects that are important only if the planet has a high enough speed. So the celebrated tests of General Relativity actually had very little to do with gravity.

What is not well known amongst gravity experts is that there are many so-called 'gravitational anomalies'. These include the borehole anomaly discovered by geophysicists, the strange behaviour of pendula, especially during solar eclipses, and various effects associated with atomic clocks also during such eclipses, and other effects. These are gravitational phenomena that are inexplicable within either of the two prevailing theories. Another anomaly is in fact well known as the issue of the so-called 'dark matter'. The stars in spiral galaxies rotate, essentially, about the centre of the galaxy, but the speeds of rotation of the stars, particularly towards the outer limits, are much larger than can be explained by either of the two prevailing theories. The popular 'explanation' for this is that such galaxies are filled with enormous

quantities of unseen and undetected matter, called 'dark matter'. This 'dark matter' is intended to provide the extra gravitational force required to maintain these high orbital rotational speeds. However when the in-flow formalism was being studied it was discovered that a simple modification of that formalism appeared to offer a dynamical explanation for this 'dark matter' effect. This implied that there was no such stuff as 'dark matter', but only a new manifestation of the gravitational in-flow effect. So Newton's inverse square law was too special, and gravity simply had much richer modes of behaviour. This extra in-flow dynamics was such that it produced no observable effects for the planets in orbit about the sun. But it does manifest itself in subtle ways, such as in the borehole anomaly.

This extra dynamics meant that gravity now involved two fundamental constants, the famous Newtonian gravitational constant G, and a new constant which determines the strength of the new dynamical effect. But what was the value of the new constant? In late 2003 the in-flow dynamics became sufficiently well understood that the borehole anomaly data from the 1980's could be analysed. Amazingly the new gravitational constant turned out to have the same value, within experimental errors, as another long known constant called the fine structure constant, $\alpha \approx 1/137$. In atomic physics this constant determines the quantum properties of atoms and molecules. It essentially sets the probability for a charged particle to emit or absorb a photon. So it is a measure of randomness within known quantum systems. That the same probability measure was now turning up in gravity effects immediately suggested that the quantum structure of space had been discovered. That space was indeed a quantum foam system, and that the randomness was presumably some residual manifestation of the self-referential noise within the information-theoretic process physics. Space was being revealed as a quantum process. It was not some smooth featureless geometry, as had been supposed by physicists for hundreds of years. But a more startling development rapidly followed. With this new 'quantum foam' dynamics manifesting in gravitational in-flows, even though the flow equation are themselves classical-type equations, it was found that these equations possessed solutions corresponding to gravitational in-flows towards a point in space, an in-flow that did not require the presence of matter to initiate or sustain the in-flow. This amounted to the discovery of a fundamentally new phenomenon - the gravitational attractor - a new form of black hole. Here the quantum foam maintained its own relaxational in-flow. The most amazing property of these attractors is that their gravitational force decreases almost like the inverse of the distance, rather than as the inverse of the square of the distance. But that is precisely the force law that explains the strange rotational behaviour of spiral galaxies. So it turns out that spiral galaxies had been formed by the existence of a gravitational attractor, such an attractor pre-existing the galaxy itself, and being responsible for the formation of the galaxy. These in-flows result in a region where the in-flow speed exceeds the speed of light, resulting in the formation of a black hole event horizon. But of course these black holes are very different to those of General Relativity, for they

produce an inverse square law behaviour. These in-flow quantum-foam black hole singularities have an effective mass determined by the nature of the attractor, and which is directly related to the in-flow effect throughout the galaxy. That is, unlike in General Relativity, the effective mass of the black hole at the centre of galaxies is determined by in-flow dynamics. In contrast, according to General Relativity such galactic black holes are formed by the collapse of enormous numbers of stars into the black hole, and the resulting total mass of the black hole would depend contingently on the history of each particular galaxy. Astronomers and astrophysicists had found a different effect, namely that the effective mass of the supermassive black hole was related to the size of the so-called 'dark matter' effect, just as the new theory of gravity is now predicting. Basically the 'dark matter' effect is a quantum foam in-flow effect - it is a macroscopic quantum gravity effect.

Contrary to long held beliefs in physics, the magnitude of quantum gravity effects are determined by the fine structure constant, and not by the Planck scales which are determined by G, $\hbar$ and c. So quantum gravity effects are present at the 1/137 relative level, i.e. resulting in 0.2% effects in measurements of G. Basically these experiments were being contaminated by quantum gravity effects. But now we can easily turn this around to our advantage; Cavendish-type laboratory experiments can now be used to study quantum gravity effects.

A dramatic consequence of these developments is that Newton's Universal Law of Gravitation is quite restricted in its region of validity - it is not universal at all. It only applies to the case of small test particles external to a large matter system, so long as that system did not form by matter being drawn in by a pre-existing attractor. This is the situation for the solar system. Of course General Relativity was constructed to agree with this Newtonian theory of gravity in the non-relativistic limit. So General Relativity is flawed, not by its special relativity underpinnings, which remain valid in Process Physics, but by its inheritance of a flawed account of gravitational phenomena.

The other fundamental prediction of the *Process Physics* was that absolute motion should be observable. Ever since the famous Michelson-Morley experiment of 1887 physicists, particularly at the urging of Einstein, have believed that no such experiments had or ever could detect absolute motion. However this turns out to be one of the greatest blunders of physics. The Michelson and Morley experiment actually detected a speed of some 8 km/s, which was based on their analysis of their observed and published fringe shifts. So why is it believed in physics that the result had been "null"? Well they used Newtonian physics in the analysis of the data, and this gave a speed of 8km/s, which is significantly smaller than the expected speed of 30km/s which should have been seen due to the orbital motion of the earth about the sun. So Michelson and Morley dismissed their own discovery of absolute motion. It was only in 2002 that the fringe shifts observed by Michelson and Morley were finally understood. There are three key physical aspects to this interferometer apparatus: (i) there is a difference in propagation times between the

two arms caused by absolute motion, with this difference resulting in fringes shifting as the apparatus is rotated, (ii) that time difference is affected by a differential Fitzgerald-Lorentz contraction of the two arms of the interferometer, and effects (i) and (ii) result in a null effect, i.e. no fringe shifts on rotation of the device, unless (iii) it operates within a gas, for then the cancellation between effects (i) and (ii) is incomplete. Operating in a vacuum Michelson type interferometers do give a null effect, they simply then fail as absolute motion 'speedometers'. But in the presence of a gas they do operate as speedometers. Analysing the Michelson-Morley fringe shift data then gives a speed of some 360km/s. Not only is absolute motion of the solar system observable, it has a very large speed. There are at least seven experiments that have detected absolute motion. Some were Michelson interferometer devices using different gases, which allowed the gas effect in (iii) to be confirmed, but two of the experiments were done using travel times of radio frequency (RF) signals along coaxial cables. The results are all consistent with what is now a known speed and direction of absolute motion of the solar system. The most extensive of the interferometer experiments was carried out by Dayton Miller during 1925/26 at Mt. Wilson. In 2002 the data from that experiment was found, and subjected to analysis, as shown here. Not only did this data confirm the observations of the other absolute motion experiments, but it also revealed evidence of the flow of space past the earth towards the sun, as is now required of the new theory of gravity. Even more amazing is that this data, together with data from other experiments, has now revealed the presence of flow turbulence. So gravitational waves have been detected. It is even possible that the Michelson-Morley experiment of 1887 also detected these gravitational waves. These gravitational waves are very different to those predicted by the general theory of relativity, and which are being sought using the long baseline static vacuum Michelson interferometers. Considering that the general theory of relativity had totally failed to explain the rotational properties of spiral galaxies, and the various other gravitational anomalies, it should really be regarded as a discredited and failed theory of gravity.

It needs to be emphasised that the observation of absolute motion is completely consistent with the special relativistic effects, such as time dilation and length contraction. Indeed the length contraction effect is a critical aspect in understanding the operation of the interferometers as absolute motion detectors. It is now becoming clear that it is absolute motion that causes these effects. This explanation of these effects was first proposed by Lorentz, and is called the Lorentz interpretation. In contrast the Einstein interpretation of special relativistic effects is that they follow from the metric properties of the spacetime construct, and that this spacetime is a real physical phenomenon. A significant outcome of the detection of absolute motion is that the Einstein postulates are simply shown to be wrong - they are refuted by numerous experiments. Of course any discussion or analysis of these experiments is banned in physics, such is the strength of the belief system that has grown around Einstein's ideas. The great successes of the special relativistic effects,

particularly in particle physics, are not in conflict with the various observations of absolute motion, but that the spacetime construct has some ontological significance is refuted.

The first major success of General Relativity was the calculation by Einstein of the known residual precession of the perihelion of mercury of 43" per century, after taking into account the Newtonian gravitational effects of the other planets. However that computation has a manifest error in that it asserts that even a circular orbit would have a precession, which is a patently physically meaningless result. This implies that there is an error in this longstanding and indeed famous result. As reported here results from a numerical solution of the orbit equation do not recover the Einstein result, and lead to a precession for mercury of only 4" per century, and so leaving a residual of 39" per century that now remains to be explained. It is argued that this is caused by the 'dark matter' effect within the solar system, namely that the planets violate the spherical symmetry of the solar system, leading to the manifestation of non-Newtonian and non-General Relativistic spatial self-interaction dynamics, and that the magnitude of this effect is determined by the fine structure constant, together with the mass distribution of the planets and other bodies within the solar system.

A significant outcome of the new theory of gravity is a dynamical explanation of the Lense-Thirring or 'frame-dragging' effect. This is now seen to be caused by vorticity in the velocity flow field. However unlike the case of General Relativity this vorticity may be caused by both absolute rotational motion of matter and *also* by absolute translational motion of matter- this latter effect is necessarily absent from General Relativity because of its assumption of no absolute linear motion. The Gravity Probe B is a satellite experiment launched in April 2004 carrying on board four gyroscopes with the sophisticated technology to observe the extremely small precession of these gyroscopes, with the intention of detecting both the 'frame-dragging' caused by the rotation of the earth, now understood to be a vorticity effect, and also the much larger geodetic precession. However it is now a prediction of the new theory of gravity, discussed in Part II, that a third component to the precession should be detectable, namely the 'frame-dragging' caused by the absolute translational motion of the earth and, associated with that, the fluctuations in this precession caused by the new gravitational wave phenomena. So somewhat unexpectedly we see that the Gravity Probe B mission may play a very significant role in checking the new theory of gravity, and particularly in performing as a gravitational wave detector. Of course detecting absolute motion and the associated wave phenomena by this means is certainly technologically in the extreme, as the same phenomena can and have been observed by the much simpler gas-mode Michelson interferometers, and also by RF co-axial cable experiments. In the Gravity Probe B the same effects will be detected indirectly, namely by means of the extremely small vorticity caused by the motion of the earth. In Part II it is also explained how the operation of the Global Positioning System (GPS) may be understood within the

context of the new theory of gravity.

For their many and varied contributions I thank Christopher Klinger, Kirsty Kitto, Susan Gunner, Katie Pilypas, John Wheldrake, Hank Keeton, Tim Eastwood, Daniel Dombrowski, James DeMeo, Horacio Velasco, Paul Dryga, Peter Morris, Jon Opie, Ron Burman, Igor Bray, Lance McCarthy, Darren Freeman, Pete Brown, Glen Deen, Georg Wikman, Vladimir Hnizdo and Thomas Goodey. Particular thanks to Warren Lawrance for the ongoing exchanges of ideas as we explored new ways to experimentally test the new physics, and to Bill Drury who enthusiastically developed the apparatus. Much inspiration has come from the regular meetings of Pamela Lyon's *Intersections Group* with members Pamela, Theresa Hickey, David Scrimgeour and myself. Over many meetings we have explored the Buddhist and Western Process Philosophy insights into our comprehension of reality and how those insights are manifested not only in the new *Process Physics* but also in various aspects of biological systems. Thanks to Valeri Dvoeglazov as the editor of this book series. Finally a special thanks to my wife Krystyna.

Chapter 2

Non-Process and Process Physics

2.1 Modelling Reality

Physics is the science of modelling and so comprehending reality in terms of the phenomena of space, time and matter, and this task has always been intellectually and experimentally challenging. *Process Physics* is an information-theoretic approach to this task. Not only is this approach generating a new conceptual framework, it has also given rise to various predictions that are testable against existing experimental data, going back to the enormously influential Michelson-Morley experiment of 1887. *Process Physics* is radically different from the current *Non-Process Physics* modelling of reality, and the experimental data analysed herein clearly refutes much of the foundations of *Non-Process Physics*. *Non-Process Physics* is essentially the reality paradigm associated with the names of Galileo, Newton, Einstein and many others. Its most distinctive feature is that it models time by geometry, and although superficially it has been very successful it is demonstrated here that much of the so-called 'experimental confirmation' of its foundational assumptions has in fact been nothing more than a consequence of major misunderstandings in experimental and theoretical physics. *Process Physics* on the other hand is distinguished by modelling time as *process*. It arose from various considerations including:

(i) the belief that the geometrical modelling of time was deficient, that it simply missed most aspects of the phenomena of *time* [1].

(ii) the discovery that 'beneath' the quantum theory of matter known as quantum field theory there were the elements of a stochastic neural-network, that is, a mathematical system that has some resemblance to the mathematical modelling of the neural networks of biological systems. This suggested that reality was probably generating and processing information as patterns, and not as symbols in some axiomatic formal system, and that this was 'semantic information', that is having 'meaning' within the system, and

(iii) the Gödel limitations of formal information systems in which the information is syntactical and so has no 'meaning' within the system. *Non-Process Physics* is such a syntactical system.

Over a number of recent years these ideas were moulded into a new paradigm for reality in which much of the success of the *Non-Process Physics* paradigm was recovered, but most significantly it became apparent for the first time why reality is the way it is, rather than as in the previous paradigm, a mere mimicry of reality encoded in formalisms and 'laws'. It turns out that by taking account of the Gödel limitations we realise the end of an old paradigm and the emergence of a much richer paradigm.

The *Process Physics* paradigm has in fact a long and illustrious history beginning most notably with the ideas of Heraclitus of Ephesus (540-480 BCE) who should perhaps be regarded as the first process physicist. This paradigm has had many supporters and collectively it became known as *Process Philosophy*, as distinct from its non-process competitor *Analytic Philosophy*. Within *Process Philosophy* the most distinguished contributors were Peirce, James, Bergson and Whitehead to name a few. A collection of their writings is available in [2]. Recently Eastman and Keeton [3] have produced a resource guide to work within the general area of process physics and with an emphasis on the work of Whitehead, see also [4].

The successes of *Process Physics* are already impacting on the foundations of physics with much support evident in existing experimental data. The new physics is also already motivating new experiments as would be expected of any new paradigm. It is becoming clear now how to design experiments that can and will distinguish the older *Non-Process Physics* from the new *Process Physics*. As well this new physics will have a major impact outside of the traditional boundaries of science, where it offers particular insights into our attempts to comprehend the phenomena of consciousness, and more broadly the nature of living systems. If these insights are also supported by new scientific endeavours then we can expect significant changes in our appreciation of our own human nature and its many manifestations. Indeed *Process Physics* may unsnarl what Schopenhauer called the *world-knot* [5]. These potential developments will not be canvassed here as this work is focused exclusively on bringing the new paradigm to investigation and acceptance by the traditional-science community. For that reason this work is both theoretically and experimentally detailed for without a penetrating analysis the claims for the new physics could not be sustained.

The collapse of the older non-process paradigm is also exposing dramatic human aspects of the historical development of that paradigm, for the failure of that paradigm is actually traceable to numerous bungles and flawed human behaviour. Indeed some of that history is shockingly scandalous, and in particular the ongoing behaviour of the physics profession is very disturbing - basically the non-process paradigm has acquired the status of a belief system, as distinct from a science, and as such is defended with ruthless and unscrupulous behaviour. For many the

non-process paradigm is now beyond challenge, and both old and new experiments that contradicted that paradigm are simply to be ignored and even suppressed. Indeed the many true successes of the old paradigm have ultimately led to nothing more than stagnation and decay, and much current work in theoretical physics has degenerated to spurious mathematical generalisations of a failed paradigm.

The consolidation so far of the new process physics is evident in the table of contents. In general the work moves from the logic of the limitations of logic to the bootstrapping of a semantic information system. This bootstrapping system possesses none of the known phenomena of current physics, but in later chapters we see the emergence of space and quantum matter in a unified manner. The characteristics of the emergent space are different from that of the modelling of space within the geometrical paradigm and in particular as well as absolute motion, that is motion with respect to space itself, a new and detailed theory of gravity arises. Essentially ever since the Einsteins, referring to Albert Einstein and his then wife Mileva Maric-Einstein, proposed that absolute motion was without meaning and so unobservable, following Poincaré, the physicists have essentially banned the concept, and it remains as such today. This state of affairs can be traced to a key misunderstanding that follows from the Einstein postulates; namely that absolute motion is incompatible with relativistic effects. However there is extensive experimental evidence, which is assembled and analysed here for the first time, that absolute motion has been observed again and again, and was clearly evident even in the seminal Michelson-Morley experiment. Over the years the only experiments that were permitted to be published in the physics literature were those that actually failed to observe absolute motion. Not because they were poorly executed but simply because in principle they were actually unable to detect the phenomenon of absolute motion. The experiments that detected and studied absolute motion, and amongst these the most significant was the impressive series by Miller, now reveal evidence in support of the new theory of gravity. Gravity is neither a force nor a curvature of spacetime, but rather inhomogeneities in the effective in-flow of the quantum foam that is space into matter. This in-flow and even its associated turbulence are manifest in the experimental data from various absolute motion experiments. As a consequence we clearly see that the Einstein curved spacetime construct is without experimental support, that it actually never was confirmed by the key and celebrated experiments, for they were actually confirming another explanation. In the end we see that the Einstein spacetime formalism is demonstrably wrong, and that the evidence against it was available even before the Einsteins put forward their fundamental assumptions that later became the foundations of twentieth century physics. Essentially the whole Einstein formalism has all the hallmarks of another system of 'epicycles' - when finally we understand what is going on the whole construct evaporates, just as Ptolemy's epicycles did when it was realised that they were entirely a consequence of not separating a measurement protocol from the phenomena it was meant to measure. In the case of Ptolemy it was finally realised that the

earth was itself undergoing motion. In the case of the Einstein formalism we finally understand that the rods and clocks used to define and implement measurements of motion are actually affected by motion through the quantum foam that is space, a view that predated the Einsteins and is now seen to be correct.

All of these developments and the clearing away of 'epicycle' descriptions lead us back to very challenging notions about the nature of time and the deep connectivity and processing that is reality, a connectivity that was evident in some aspects of the quantum theory, but which was essentially outside of the non-process paradigm. This new physics is seen to be panexperientialist in character in which a primitive self-awareness or 'consciousness' is foundational to reality in the manner argued by Griffin and others [5], a consciousness that appears to be intrinsic to the semantic nature of the information system that is process physics. Such notions it seems may well be moving into the realm of experimental science and will result in a unification of human knowledge and experience that is beyond our prevailing comprehensions.

2.2 Non-Process Physics

Non-Process Physics had its genesis with the introduction by Galileo of a geometrical modelling of the phenomena of time. At first this seems quite a strange model as geometry has little in common with time. Time has three aspects, and briefly they are (i) that there is a present moment that (ii) separates the past from the future, and (iii) the past is fixed and at best partially recorded, while the future is undecided and certainly not recorded. The only aspect of time that the geometrical model captures is that of order: the sequence of points along a one-dimensional geometrical line have the property that if $A < B$ and $B < C$, then $A < C$, where $A, B, C, ...$ are points on the line, and the relation $A < B$ means "A is to the left of B", as in Fig.2.1. To model time this geometrical order property of points to used to represent the time order of events: $A, B, C....$ now represent events, and $A < B$ means that event A is or was "before" event B. However the model has no means of modelling the present moment effect - there is no moving point on the line that we could identify as *Now*.

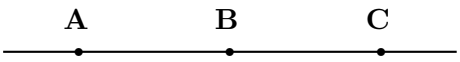

Figure 2.1: Modelling the order aspect of the phenomena of time by the ordering of points along a one-dimensional geometrical line.

As a consequence of that the model is unable to capture the distinction between the past and the future, and even worse the identification of $<$ with time ordering is not unique, as we could also have chosen to use $A < B$ to mean "A was after B".

Despite this mismatching this modelling of time proved to be exceptionally useful, particularly after the metric property of the line was used to quantify time intervals: the distance $d(A, B)$ between A and B along the line is used to represent the time interval $t(A, B)$ between events A and B. The efficacy of this followed when it was demonstrated by Galileo that the quantification of time intervals actually was useful in kinematical observations of pendula and other experimental phenomena, and that regular oscillations of for example a pendulum could be used to measure $t(A, B)$. Newton developed this model much further by showing that it could be used to model the dynamics of motion as well, as for example in the famous equation

$$m\frac{d^2x(t)}{dt^2} = F(t), \tag{2.1}$$

which not only uses the geometrical model of time, as in the symbol t, but also uses the older modelling of space by the Euclidean geometrical model, as in the symbol x (here we show only one of the three dimensions of space). Eqn.(2.1) also illustrates the use of the *calculus* that was independently developed by Leibniz and Newton. As well the symbols m and F refer to the mass of the object undergoing motion and the force acting on that mass, respectively. We offer later an explanation for inertia, as measured by this m.

The overwhelming success of the paradigm of reality encapsulated in (2.1) eventually led most physicists to actually believe that the phenomena of time was *really* nothing more than geometry, just as they had believed that the phenomena of space was *really* geometry. The way physicists got around the obvious lack of the phenomena of the *Now*, the present moment effect, was to imagine that the present moment was thought of as a point moving along the line. This is an example of a metarule, here the *geometrical time* metarule: it plays no part in the analysis of (2.1) but seems to make the model better match up with reality.

One would have expected that the manifest deficiencies of the geometrical *non-processing* model of time would eventually have resulted in extensive research by physicists to develop a better model, and perhaps even one that could mimic all the aspects of the phenomena of time. But this simply did not happen. In the twentieth century we know that this did not happen because of again the influence of the Einsteins. The ill-conceived attempt to formulate a model of reality in which absolute motion was without meaning resulted in the introduction of the spacetime construct. This is a four-dimensional geometrical construct in which the one-dimensional model of time is fused with the three-dimensional model of space, but fused in a special way in that observers in relative motion would identify different foliations of the construct as their geometrical time lines, so that their modellings of time no longer coincided, and as a consequence they could no longer necessarily agree on the time-ordering of events. Rather than being seen as an indicator of something wrong in the model, this aspect of the spacetime model became a celebrated feature, and the whole notion of change, of the evolution of reality from a past state to a future state disappeared, and reality it was claimed was simply

a frozen unchanging four-dimensional block of geometry: when the universe was formed the whole of the *future* of that universe also popped into existence. So what about our experiences of the *present moment* and the distinction between past and future? Well that was dismissed as being some trick of our minds, and a trick that psychologists should investigate, but certainly not physicists. As will become clear later the Einstein postulates that led to this bizarre spacetime construct of reality are simply proven wrong by experiment: absolute motion is an observable feature of reality and experiments that show this have been carried out many times. As a consequence time is an aspect of reality that is distinct from the phenomena of space, and neither are at a deep level geometrical systems.

2.3 Process Physics

Process Physics $[6-20]$ is a radical information-theoretic modelling of reality which arose from analysis of various extant limitations; from the limitations of formal information systems discovered by Gödel, Turing and Chaitin, from the limitations of the geometric modelling of time in the models constructed by Galileo, Newton and Einstein, and by the limitations of the quantum theory and its failure to account for the measurement process. As is usual within physics these limitations were obscured by various metarules and metaphysical constructs. This information-theoretic modelling was also motivated by the discovery that stochastic neural network models are foundational to known quantum field theories [6, 7].

In process physics the fundamental assumption is that reality is to be modelled as self-organising semantic information, that is, information that is 'internally' meaningful, using a self-referentially limited neural network model. Such a system has no *a priori* objects or laws, and is induced using a bootstrap system, so that it is the system itself that 'internally' creates patterns of relationships and their dominant modes of behaviour, and all (sub)systems are fractal in character, that is, relationships within relationships, and so on *ad infinitum*. In this way all emergent phenomena are unified, and it is this key feature that has resulted in an understanding and linking, for the first time, of various phenomena. A key feature of this process-physics is that this fracticality is associated with self-organising criticality.

It will be shown that space and quantum physics are emergent and unified, with time a distinct non-geometric process, that quantum phenomena are caused by fractal topological defects embedded in and forming a growing three-dimensional fractal process-space, which is essentially a quantum foam. Other features of the emergent physics were quantum field theory with emergent flavour and confined colour, limited causality and the Born quantum measurement metarule, inertia, time-dilation effects, gravity and the equivalence principle, a growing universe with a cosmological constant, black holes and event horizons, and the emergence of classicality.

The emergence of a quantum-foam explanation for space is accompanied by the effect in which quantum 'matter' effectively acts as a sink for the quantum foam.

This provides an explanation for the logical necessity of the phenomenon of gravity. Essentially gravity is the loss of relational information during the in-flow to matter. The presently accepted theory of gravity is General Relativity (GR) with its key concept of curved *spacetime*. Here it is shown that GR is a confused amalgam of the Einstein measurement protocol with nothing more than Newtonian Gravity (NG), at least in the case of the external Schwarzschild metric. The quantum foam in-flow effect that is gravity is seen not to be identical to GR for as shown here GR actually is identical to Newtonian gravity in all the cases where it has been tested experimentally. Significantly we reveal strong experimental and theoretical considerations which indicate that the fundamental foundations of GR appear to be erroneous. The Einstein assumptions on which the Special and General Theory of Relativity are based are shown to be in disagreement with numerous experiments. They are demonstrably wrong[1]. Even more surprisingly is that Newtonian Gravity (NG) appears to be valid only in special circumstances, and that the phenomena of gravity is in fact very different from the expectations of NG and GR. It is argued here that the anomalous rotational speed effect in spiral galaxies is a manifestation of the failure of both Newtonian and the Hilbert-Einstein gravity. A new theory of gravity is presented in provisional form. This theory passes all the tests that GR had apparently passed, but predicts other phenomena that are not predicted by GR or even NG. The spacetime construct is shown here to have no ontological significance though it does have technical uses.

The ongoing failure of physics to fully match all the aspects of the phenomena of time, apart from that of order, arises because physics has always used non-process models, as is the nature of formal or syntactical systems. Such systems do not require any notion of process - they are entirely structural and static. The new process physics overcomes these deficiencies by using a non-geometric process model for time, but process physics also argues for the importance of relational or semantic information in modelling reality. Semantic information refers to the notion that reality is a purely informational system where the information is internally meaningful. Hence the information is 'content addressable', rather than is the case in the usual syntactical information modelling where the information is represented by symbols. This symbolic or syntactical mode is only applicable to higher level phenomenological descriptions, and for that reason was discovered first.

A key long-standing goal of physics has been the unification of gravity and the quantum theory. This unification could not be achieved within the old *non-process physics*, but has now been achieved with the new *process physics*. The quantum theory arises from the non-geometric and non-quantum self-referentially-limited neural network model which implements the semantic information approach to compre-

[1]There is considerable debate, discussed later, about who developed the foundational ideas that eventually resulted in the formulation of the spacetime SR and GR. The key new insight offered here is that aside from this historical analysis the resulting SR and GR are actually wrong, and amounted to an obscurification rather than a contribution to the development and understanding of relativistic effects.

hending reality. What has been achieved in process physics is the explanation of why reality must be so, and why the modes of behaviour are encodeable in the syntax of the non-process physics. This older mode of dealing with reality will continue to be used because for many problems it is eminently practical. It will require the continued use of various metarules to overcome its limitations, but we now have an explanation for them as well.

Process Physics shows that there is a Quantum Gravity, but it is unrelated to General Relativity and General Covariance, and essentially describes the emergent quantum phenomena of the process-space or quantum foam, and its response to quantum 'matter', and all this within an information-theoretic framework. This Quantum Gravity is manifested in the emergent Quantum Homotopic Field Theory for the process-space or quantum foam. Clearly it would be absurd to attempt the 'quantisation' of GR, not only because 'quantisation' is a dubious idea at best, but because GR is a fundamentally flawed theory of gravity.

A pure semantic information system must be formed by a subtle bootstrap process. The mathematical model for this has the form of a stochastic neural network (SNN) for the simple reason that neural networks are well known for their pattern or non-symbolic information processing abilities [23, 24]. The stochastic behaviour is related to the limitations of syntactical systems discovered by Gödel [25] and more recently extended by Chaitin [26, 27, 28], but also results in the neural network being innovative in that it creates its own patterns. The neural network is self-referential, and the stochastic input, known as self-referential noise, acts both to limit the depth of the self-referencing and also to generate potential order.

Chapter 3

Syntactical and Semantic Information Systems

3.1 Self-Referential Systems and Gödel's Theorem

In modelling reality with formal or syntactical information systems physicists assume that a full account of reality can be compressed into axioms and rules for the manipulation of symbols. However Gödel discovered that self-referential syntactical systems (and these include basic mathematics) have fundamental limitations which amount to the realisation that not all truths can be compressed into an axiomatic structure, that formal systems are much weaker than previously supposed. In physics such systems have always been used in conjunction with metarules and metaphysical assertions, all being 'outside' the formal system and designed to overcome the limitations of the syntax. Fig.3.1 depicts the current understanding of self-referential syntactical systems. Here the key feature is the Gödel boundary demarcating the provable from the unprovable truths of some system. Chaitin, using Algorithmic Information Theory, has demonstrated that in mathematics the unprovable truths are essentially random in character. This, however, is a structural randomness in the sense that the individual truths do not have any structure to them which could be exploited to condense them down to or be encoded in axioms. This is unlike random physical events which occur in time. Of course syntactical systems are based on the syntax of symbols and this is essentially non-process or non-timelike.

There is an analogy between the structure of self-referential syntactical information systems and the present structure of quantum theory, as depicted in Fig.3.2. There the formal and hence non-process mathematical structure is capable of producing many provable truths, such as the energy levels of the hydrogen atom, and these are also true in the sense that they agree with reality. But from the beginning of quantum theory the Born measurement metarule was introduced to relate this non-process modelling to the actual randomness of quantum measurement events.

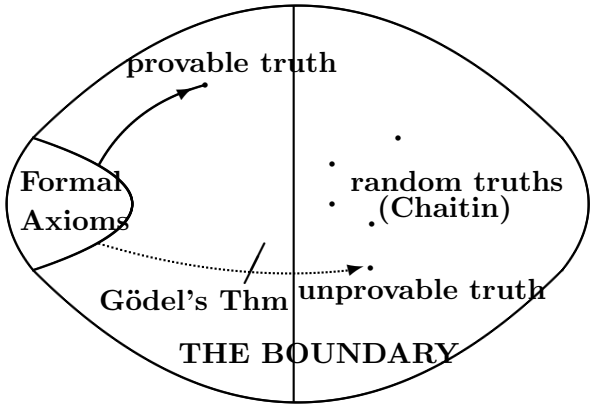

Figure 3.1: Graphical depiction of the 'logic space' of a self-referential syntactical information system, showing the formal system consisting of symbols and rules, and an example of one theorem (a provable truth). Also shown are unprovable truths which in general are random (or unstructured) in character, following the work of Chaitin. The Gödelian boundary is the demarcation between provable and unprovable truths.

The individuality of such random events is not a part of the formal structure of quantum theory. Of course it is well known that the non-process or structural aspects of the probability metarule are consistent with the mathematical formalism, in the form of the usual 'conservation of probability' equation and the like. Further, the quantum theory has always been subject to various metaphysical interpretations, although these have never played a key role for practitioners of the theory. This all suggests that perhaps the Born metarule is bridging a Gödel-type boundary, that there is a bigger system required to fully model quantum aspects of reality, and that the boundary is evidence of self-referencing in that system.

3.2 Semantic Information System

Together the successes and failures of physics suggest that a generalisation beyond the traditional use of syntactical information theory is required to model reality. This has now been identified as a semantic information system which is modelled as a stochastic neural network.

Fig.3.3 shows a graphical depiction of the bootstrapping of a pure semantic information system, showing the stochastic neural network-like process system from which the semantic system is seeded or bootstrapped. Via a Self-Organised Criticality Filter (SOCF) this seeding system is removed or hidden. From the process system, driven by Self-Referential Noise (SRN), there are emergent truths, some of which are generically true (ensemble truths) while others are purely contingent. The

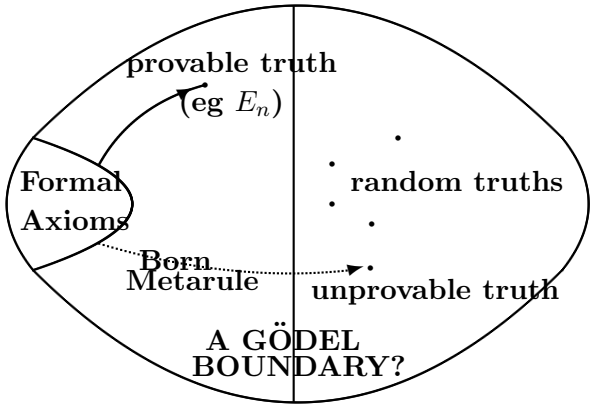

Figure 3.2: Graphical depiction of the syntactical form of conventional quantum theory. The Born measurement metarule appears to bridge a Gödel-like boundary.

ensemble truths are also reachable from the Induced Formal System as theorems, but from which, because of the non-process nature of the Induced Formal System, the contingent truths cannot be reached. In this manner there arises a Gödel-type boundary. The existence of the latter leads to induced metarules that enhance the Induced Formal System, if that is to be used solely in higher order phenomenology. A detailed account of a Semantic Information System is given in Chap.4.

3.3 Process Philosophy

Western science and philosophy have always been dominated by non-process thought. This 'historical record' or *being* model of reality has been with us since Parmenides, and his student Zeno of Elea, and is known as the Eleatic model (c500 BCE). Zeno gave us the first insights into the inherent problems of comprehending motion, a problem long forgotten by conventional non-process physics, but finally explained by process physics. The *becoming* or *processing* model of reality dates back to Heraclitus of Ephesus (540-480 BCE) who argued that common sense is mistaken in thinking that the world consists of stable things; rather the world is in a state of flux. The appearances of 'things' depend upon this flux for their continuity and identity. What needs to be explained, Heraclitus argued, is not change, but the appearance of stability. With process physics western science and philosophy is now able to move beyond the moribund non-process mindset. While it was the work of Gödel who demonstrated beyond any doubt that the non-process system of thought had fundamental limitations; implicit in his work is that the whole reductionist mindset that goes back to Thales of Miletus could not offer, in the end, an effective account

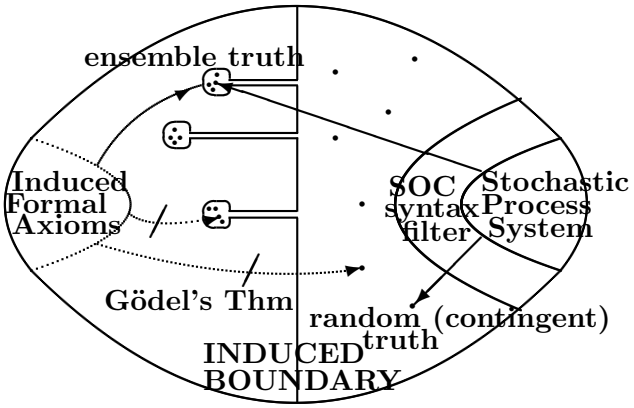

Figure 3.3: Graphical depiction of the bootstrapping of and the emergent structure of a self-organising pure semantic information system. As a high level effect we see the emergence of an induced formal system, corresponding to the current standard syntactical modelling of reality. There is an emergent Gödel-type boundary which represents the inaccessibility of the random or contingent truths from the induced formal or syntactical system. A process of self-organised criticality (SOC) filters out the seeding or bootstrap syntax.

of reality. However the notion that there were limits to syntactical or symbolic encoding is actually very old. Priest [29] has given an account of that history. However in the East the Buddhists in particular were amazingly advanced in their analysis and comprehension of reality. Stcherbatsky [30], writing about the extraordinary achievements of Buddhist logic in the C6 and C7th CE, noted that

> *Reality according to Buddhists is kinetic, not static, but logic, on the other hand, imagines a reality stabilized in concepts and names. The ultimate aim of Buddhist logic is to explain the relation between a moving reality and the static constructions of logic.*

In the West the process system approach to reality was developed, much later, by such *process philosophers* as Charles Peirce, William James, Henri Bergson and Alfred Whitehead to name a few, although their achievements were very limited and substantially flawed, limited as they were by the physical phenomena known to them. A collection of their writings is available in [2]. Perhaps a quote from Charles Peirce [2], writing in 1891, gives the sense of their thinking;

> *The one intelligible theory of the universe is that of objective idealism, that matter is effete mind, inveterate habits becoming physical laws. But before this can be accepted it must show itself capable of explaining the tridimensionalty of space, the laws of motion, and the general characteristics of the universe, with mathematical clearness and precision; for no less should be demanded of every philosophy.*

With process physics we have almost achieved this end, and Wheeler has already expressed this notion of *inveterate habits* as "law without law" [31]. As the reader will note the self-referentially limited neural network model, that underpins process physics, is remarkably akin to Peirce's *effete mind*. It is the limitations of syntax, and the need for intrinsic or semantic information 'within' reality and at all levels, that reality is not imposed, that drives us to this approach. Einstein, the modern day eleatic thinker, realised all too well the limitations of non-process thinking but was unable to move out of the non-process realm that the West had created for itself, for according to Carnap [32];

> *Once Einstein said that the problem of the Now worried him seriously. He explained that the experience of the Now means something special for man, something essentially different from the past and the future, but that this important difference does not and cannot occur within physics. That this experience cannot be grasped by science seems to him a matter of painful but inevitable resignation. I remarked that all that occurs objectively can be described in science: on the one hand the temporal sequence of events is described in physics; and, on the other hand, the peculiarities of man's experiences with respect to time, including his different attitude toward past, present and future, can be described and (in principle) explained in psychology. But Einstein thought that scientific descriptions cannot possibly satisfy our human needs; that there is something essential about the Now which is just outside of the realm of science.*

It was the Einsteins' error in rejecting absolute motion that trapped twentieth century physics in the non-process or no *now* mindset. As is shown here experiments that could detect absolute motion did so, and those that could not not do so in principle of course did not detect absolute motion. Nevertheless all of these latter experiments were claimed to have confirmed the SR and GR spacetime formalism which is fundamentally based an the absence of absolute motion as an aspect of reality.

Chapter 4

Self-Referentially Limited Neural Networks

4.1 Bootstrapping a Semantic Information System

Here we describe a model for a self-referentially limited neural network and then how such a network results in emergent geometry and quantum behaviour, and which, increasingly, appears to be a unification of space and quantum phenomena. Process physics is a semantic information system and is devoid of *a priori* objects and their laws and so it requires a subtle bootstrap mechanism to set it up. We use a stochastic neural network, Fig.4.1a, having the structure of real-number valued connections or relational information strengths B_{ij} (considered as forming a square matrix) between pairs of nodes or pseudo-objects i and j. In standard neural networks [23, 24] the network information resides in both link and node variables, with the semantic information residing in attractors of the iterative network. Such systems are also not pure in that there is an assumed underlying and manifest *a priori* structure.

The nodes and their link variables will be revealed to be themselves sub-networks of informational relations. To avoid explicit self-connections $B_{ii} \neq 0$ which are a part of the sub-network content of i, we use antisymmetry $B_{ij} = -B_{ji}$ to conveniently ensure that $B_{ii} = 0$, see Fig.4.1b.

At this stage we are using a syntactical system with symbols B_{ij} and, later, rules for the changes in the values of these variables. This system is the syntactical *seed* for the pure semantic system. Then to ensure that the nodes and links are not remnant *a priori* objects the system must generate strongly linked nodes (in the sense that the B_{ij} for these nodes are much larger than the B_{ij} values for non- or weakly-linked nodes) forming a fractal network; then self-consistently the start-up nodes and links may themselves be considered as mere names for sub-networks of relations. For a successful suppression the scheme must display self-organised criticality (SOC) [33] which acts as a filter for the start-up syntax. The designation 'pure' refers to the notion that all seeding syntax has been removed.

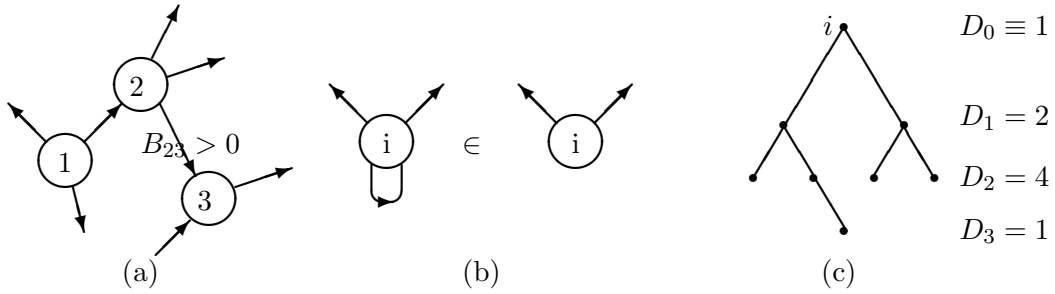

Figure 4.1: (a) Graphical depiction of the neural network with links $B_{ij} \in \mathcal{R}$ between nodes or pseudo-objects. Arrows indicate sign of B_{ij}. (b) Self-links are internal to a node, so $B_{ii} = 0$. (c) An $N = 8$ spanning tree for a random graph (not shown) with $L = 3$. The distance distribution D_k is indicated for node i.

SOC is the process where the emergent behaviour displays universal criticality in that the behaviour is independent of the particular start-up syntax; such a start-up syntax then has no ontological significance.

To generate a fractal structure we must use a non-linear iterative system for the B_{ij} values. These iterations amount to the necessity to introduce a time-like process. Any system possessing *a priori* 'objects' can never be fundamental as the explanation of such objects must be outside the system. Hence in process physics the absence of intrinsic undefined objects is linked with the phenomena of time, involving as it does an ordering of 'states', the present moment effect, and the distinction between past and present. Conversely in non-process physics the necessity for *a priori* objects is related to the use of the non-process geometrical model of time, with this modelling and its geometrical-time metarule being an approximate emergent description from process-time. In this way process physics arrives at a new modelling of time, *process time*, which is much more complex than that introduced by Galileo, developed by Newton, and reaching its so-called high point but deeply flawed Einstein spacetime geometrical model. Unlike these geometrical models process-time does model the *Now* effect. Process physics also shows that time cannot be modelled by any other structure, other than a time-like process, here an iterative scheme. There is nothing *like* time available for its modelling. The near obsession of theoretical physicists with the geometrical modelling of time, and its accompanying notion of *analytical determinism*, has done much to retard the development of physics. The success of process physics implies that time along with self-referencing is in some sense prior to the other phenomena, and certainly prior to space, as will be seen in Chap.6 within the discussion of a multi-component or multi-world universe.

The stochastic neural network so far has been realised with one particular scheme involving a stochastic non-linear matrix iteration, see (4.1). The matrix inversion B^{-1} then models self-referencing in that it requires, in principle, all elements of B to compute any one element of B^{-1}. As well there is the additive Self-Referential

Noise (SRN) w_{ij} which limits the self-referential relational information but, significantly, also acts in such a way that the network is innovative in the sense of generating semantic information, that is relational information which is internally meaningful. The emergent behaviour is believed to be completely generic in that it is not suggested that reality is a computation, rather it appears that reality has the form of a self-referential order-disorder information system. It is important to note that process physics is a non-reductionist modelling of reality; the basic iterator (4.1) is premised on the general assumption that reality is sufficiently complex that self-referencing occurs, and that this has limitations. Eqn.(4.1) is then a minimal bootstrapping implementation of these notions. At higher emergent levels this self-referencing manifests itself as *interactions* between emergent patterns, but other novel effects may also arise.

To be a successful contender for the Theory of Everything (TOE) process physics must ultimately prove the uniqueness conjecture: that the characteristics (but not the contingent details) of the pure semantic information system are unique. This would involve demonstrating both the effectiveness of the SOC filter and the robustness of the emergent phenomenology, and the complete agreement of the latter with observation.

The stochastic neural network is modelled by the iterative process

$$B_{ij} \to B_{ij} - a(B + B^{-1})_{ij} + w_{ij}, \quad i, j = 1, 2, ..., 2N; N \to \infty, \tag{4.1}$$

where $w_{ij} = -w_{ji}$ are independent random variables for each ij pair and for each iteration and chosen from some probability distribution. Here a is a parameter the precise value of which should not be critical but which influences the self-organisational process.

4.2 Stochastic Neural Networks from Quantum Field Theory

It may be helpful to outline the thoughts that led to (4.1), arising as it did from the quantum field theory frontier of quark physics. A highly effective approximation to Quantum Chromodynamics (QCD) was developed that made extensive use of bilocal fields and the functional integral calculus (FIC), see [34] for reviews of this Global Colour Model (GCM). In the GCM the bilocal-field correlators (giving meson and baryon correlators) are given by the generating functional

$$Z[J] = \int \mathcal{D}B^{\theta} \exp(-S[B] + \int dx^4 d^4 y B^{\theta}(x, y) J^{\theta}(x, y)). \tag{4.2}$$

Here $x, y \in E^4$, namely a Euclidean-metric space-time, as the hadronic correlators are required for vacuum-to-vacuum transitions, and as is well known the use of the Euclidean metric picks out the vacuum state of the quantum field theory.

The physical Minkowski-metric correlators are then obtained by analytic continuation $x_4 \to ix_0$. Eqn.(4.2) follows from (approximately) integrating out the gluon variables, and then changing variables from the quark Grassmannian functional integrations to bilocal-field functional integrations. Here the θ index labels generators of flavour, colour and spin. This form is well suited to extracting hadronic phenomena as the vacuum state of QCD corresponds to a BCS-type superconducting state, with the $q\overline{q}$ Cooper pairs described by those non-zero mean-field $\overline{B}^{\theta}(x,y)$ determined by the Euler-Lagrange equations of the action,

$$\frac{\delta S[B]}{\delta B^{\theta}(x,y)}|_{\overline{B}^{\theta}(x,y)} = 0. \tag{4.3}$$

That (4.3) has non-zero solutions is the constituent-quark/BCS-state effect. This is a non-linear equation for those non-zero bilocal fields about which the induced effective action for hadronic fields is to be expanded.

Rather than approximately evaluating (4.2) as a functional integral, as done in [34], we may use the Parisi-Wu [35] stochastic 'quantisation' procedure, which involves the Langevin iterative equation

$$B^{\theta}(x,y) \to B^{\theta}(x,y) - \frac{\delta S[B]}{\delta B^{\theta}(x,y)} + w^{\theta}(x,y), \tag{4.4}$$

where $w^{\theta}(x,y)$ are Gaussian random variables with zero means. After many iterations a statistical equilibrium is achieved, and the required hadronic correlators may be obtained by statistical averaging: $< B^{\theta}(x,y)B^{\phi}(u,v)... >$, but with again analytic continuation back to Minkowski metric required. In particular, writing $B^{\theta}(x,y) = \phi(\frac{x+y}{2})\Gamma(x-y, \frac{x+y}{2})$, then $\phi(x)$ is a meson field, while $\Gamma(x,X)$ is the meson form factor.

That (4.4) leads to quantum behaviour is a remarkable result. The presence of the noise means that the full structure of $S[B]$ is explored during the iterations, whereas in (4.2) this is achieved by integration over all values of the $B^{\theta}(x,y)$ variables. The correlators $< B^{\theta}(x,y)B^{\phi}(u,v)... >$ correspond to complex quantum phenomena involving bound states of constituent quarks embedded in a BCS superconducting state. However the Euclidean-metric E^4-spacetime plays a completely classical and passive background role.

Now (4.4) has the form of a stochastic neural network (see later), with link variables $B^{\theta}(x,y)$, that is, with the nodes being continuously distributed in E^4. An interesting question arises: if we strip away the passive classical E^4 background and the superscript indices , so that $B^{\theta}(x,y) \to B_{ij}$ and we retain only a simple form for $S[B]$, then does this discretised Langevin equation, in (4.1), which now even more so resembles a stochastic neural network, continue to display quantum behaviour? In series of papers [6, 9, 10, 11] it has been found that indeed the SNN in (4.1) does exhibit quantum behaviour, by generating a quantum-foam dynamics for an emergent space, and with quantum -'matter' being topological-defects embedded

in that quantum-foam in a unification of quantum space and matter. Indeed the remarkable discovery is that (4.1) generates a quantum gravity. Note, however, that now the iterations in (4.1) correspond to physical time, and we do not wait for equilibrium behaviour. Indeed the non-equilibrium behaviour manifests as a growing universe. The iterations correspond to a non-geometric modelling of time with an intrinsic *arrow of time*, as the iterations in (4.1) cannot be reversed. Hence the description of this new physics as *Process Physics*.

If (4.1) does in fact lead to a unification of gravity and quantum theory, then the deep question is how should we interpret (4.1)? The stochastic noise has in fact been interpreted as the new intrinsic Self-Referential Noise when the connection with the work of Gödel and Chaitin became apparent, and as discussed above. Hence beneath quantum field theory there is evidence of a self-referential stochastic neural network, and its interpretation as a semantic information system. Only by discarding the spacetime background of Quantum Field Theory (QFT) do we discover the necessity for space and the quantum.

4.3 Neural Networks

We now briefly compare the iteration system in (4.1) to an Attractor Neural Network (ANN) and illustrate its basic mode of operation (see [23, 24] for details of neural networks). An ANN has link $J_{ij} \in \mathcal{R}$ and node $s_i = \pm 1$ variables $(i, j = 1, 2, ...N)$, with $J_{ij} = J_{ji}$ and $J_{ii} = 0$. Here $s = +1$ denotes an active node, while $s = -1$ denotes an inactive node. The time evolution of the nodes is given by, for example,

$$s_i(t) = \text{sign}(\sum_j J_{ij} s_j(t-1)). \tag{4.5}$$

To imprint a pattern its $s_i \propto \xi_i$ values are imposed on the nodes and the Hebbian Rule is used to change the link strengths

$$J_{ij}(t) = J_{ij}(t-1) + c s_i(t-1) s_j(t-1), \tag{4.6}$$

and for p successively stored patterns $(\xi^1, \xi^2, ...\xi^p)$ we end up with

$$J_{ij} = \sum_{\mu=1}^{p} \xi_i^\mu \xi_j^\mu, \quad i \neq j. \tag{4.7}$$

The imprinted patterns correspond to local minima of the 'energy' function

$$E[\{s\}] = -\frac{1}{2} \sum J_{ij} s_i s_j, \tag{4.8}$$

which has basins of attraction when the ANN is 'exposed' to an external input $s_i(0)$. As is well known over iterations of (4.5) the ANN node variables converges to one

of the stored patterns most resembling $s_i(0)$. Hence the network categorises the external input.

The iterator (4.1), however, has no external inputs and its operation is determined by the detailed interplay between the order/disorder terms. As well it has no node variables: whether a node i is active is determined implicitly by $|B_{ij}| > b$, for some j, where b is some minimum value for the link variables. Because B_{ij} is antisymmetric and real its eigenvalues occur in pairs $ib, -ib$ (b real), with a complete set of orthonormal eigenvectors $\xi^\mu, \mu = \pm 1, \pm 2, .., \pm N$, $(\xi^{\mu *} = \xi^{-\mu})$ so that

$$B_{jk} = \sum_{\mu=\pm 1,\pm 2,..} ib_\mu \xi_j^\mu \xi_k^{\mu *}, \quad b_\mu = -b_{-\mu} \in \mathcal{R}, \tag{4.9}$$

where the coefficients must occur in conjugate pairs for real B_{ij}. This corresponds to the form

$$B = MDM^{-1}, \quad D = \begin{pmatrix} 0 & +b_1 & 0 & 0 & & \\ -b_1 & 0 & 0 & 0 & & \\ 0 & 0 & 0 & +b_2 & & \\ 0 & 0 & -b_2 & 0 & & \\ & & & & . & \\ & & & & & . \end{pmatrix} \tag{4.10}$$

where M is a real orthogonal matrix. Both the b_μ and M change with each iteration.

Let us consider, in a very unrealistic situation, how patterns can be imprinted unchanged into the SNN. This will only occur if we drop the B^{-1} term in (1). Suppose the SRN is frozen (artificially) at the same form on iteration after iteration. Then iterations of (4.1) converge to

$$B = \frac{1}{a} w = \sum_\mu i a^{-1} w_\mu \eta_j^\mu \eta_k^{\mu *}, \tag{4.11}$$

where w^μ and η^μ are the eigensystem for w. This is analogous to the Hebbian rule (4.6), and demonstrates the imprinting of w, which is strong for small a. If that 'noise' is now 'turned-off' then this imprinted pattern will decay, but do so slowly if a is small. Hence to maintain an unchanging imprinted pattern it needs to be continually refreshed via a fixed w. However the iterator with the B^{-1} term present has a significantly different and richer mode of behaviour as the system will now generate novel patterns, rather than simply imprinting whatever pattern is present in w. Indeed the system uses special patterns (the gebits) implicit in a random w that are used as a resource with which much more complex patterns are formed.

The task is to determine the nature of the self-generated patterns, and to extract some effective descriptive syntax for that behaviour, remembering that the behaviour is expected to be quantum-like.

4.4 Emergent Geometry in Stochastic Neural Network: Gebits

We start the iterations of (4.1) at $B \approx 0$, representing the absence of information, that is, of patterns. With the noise absent the iterator behaves in a deterministic and reversible manner giving a condensate-like system with a B matrix of the form in (4.10) or (4.12a), but with the matrix M iteration independent and determined uniquely by the start-up B, and each b_μ evolves according to the iterator $b_\mu \to b_\mu - a(b_\mu - b_\mu^{-1})$, which converges to $b_\mu = \pm 1$. The corresponding eigenvectors ξ^μ do not correspond to any meaningful patterns as they are determined entirely by the random values from the start-up $B \approx 0$. However in the presence of the noise the iterator process is non-reversible and non-deterministic and, most importantly, non-trivial in its pattern generation. The iterator is manifestly non-geometric and non-quantum in its structure, and so does not assume any of the standard features of syntax based non-process physics models. Nevertheless, as we shall see, it generates geometric and quantum behaviour. The dominant mode is the formation of an apparently randomised background (in B) but, however, it also manifests a self-organising process which results in non-trivial patterns which have the form of a growing three-dimensional fractal process-space displaying quantum-foam behaviour. These patterns compete with this random background and represent the formation of a 'universe'.

The emergence of order in this system might appear to violate expectations regarding the 2nd Law of Thermodynamics; however because of the SRN the system behaves as an open system and the growth of order arises from the self-referencing term, B^{-1} in (4.1), selecting certain implicit order in the SRN. Hence the SRN acts as a source of negentropy. The term *negentropy* was introduced by E. Schrödinger in 1945 [36], and since then there has been ongoing discussion of its meaning. In process physics it manifests as the SRN.

This growing three-dimensional fractal process-space is an example of a Prigogine far-from-equilibrium dissipative structure [37] driven by the SRN. From each iteration the noise term will additively introduce rare large value w_{ij}. These w_{ij}, which define sets of strongly linked nodes, will persist through more iterations than smaller valued w_{ij} and, as well, they become further linked by the iterator to form a three-dimensional process-space with embedded topological defects. In this way the stochastic neural-network creates stable strange attractors and as well determines their interaction properties. This information is all internal to the system; it is the semantic information within the network.

We introduce, for convenience only, some terminology: we think of B_{ij} as indicating the connectivity or relational strength between two monads i and j. The monads concept was introduced by Leibniz, who espoused the *relational* mode of

thinking in response to and in contrast with Newton's *absolute* space[1].

$$B_c = \begin{pmatrix} 0 & +1 & 0 & 0 & & \\ -1 & 0 & 0 & 0 & & \\ 0 & 0 & 0 & +1 & & \\ 0 & 0 & -1 & 0 & & \\ & & & & . & \\ & & & & & . \end{pmatrix} (a),\ B = \begin{pmatrix} g_1 & & & & & \\ & \bigcirc & & & & \\ & & g_2 & & & \\ & & & g_3 & & \\ & & & & c_1 & \\ & & & & & c_2 \end{pmatrix} (b). \tag{4.12}$$

The monad i has a pattern of dominant (larger valued B_{ij}) connections B_{i1}, $B_{i2}, ...$, where $B_{ij} = -B_{ji}$ avoids self-connection ($B_{ii} = 0$), and real number valued. The self-referential noise $w_{ij} = -w_{ji}$ are independent random variables for each ij and for each iteration, and with variance η. With the noise absent the iterator converges to one of the *condensate* MB_cM^{-1} where the matrix M depends on the initial B. This behaviour is similar to the condensate of Cooper pairs in QFT, but here the condensate (indicating a non-zero dominant configuration) does not have any space-like structure. However in the presence of the noise, after an initial chaotic behaviour when starting the iterator from $B \approx 0$, the dominant mode is the formation of a randomised condensate $C \approx \mu \otimes B_c + B_b$, up to an orthogonality transformation, indicating B_c but with the $\pm 1's$ replaced by $\pm\mu_i$'s (where the μ_i are small and given by a computable iteration-dependent probability distribution $\mathcal{M}(\mu)$) and with a noisy background B_b of very small B_{ij}.

The key discovery is that there is an extremely small self-organising process buried within this condensate and which has the form of a three-dimensional fractal process-space, which we now explain. Consider the connectivity from the point of view of one monad, call it monad i. Monad i is connected via these large B_{ij} to a number of other monads, and the whole set of connected monads forms a tree-graph relationship. This is because the large links are very improbable, and a tree-graph relationship is much more probable than a similar graph involving the same monads but with additional links. The set of all large valued B_{ij} then form tree-graphs disconnected from one-another; see Fig.4.2a. In any one tree-graph the natural 'distance' measure for any two monads within a graph is the smallest number of links connecting them. Let $D_1, D_2, ..., D_L$ be the number of nodes of distance $1, 2, ..., L$ from monad i (define $D_0 = 1$ for convenience), where L is the largest distance from i in a particular tree-graph, and let N be the total number of nodes in the tree. Then $\sum_{k=0}^{L} D_k = N$; see Fig.4.2b for an example.

Now consider the number $\mathcal{N}(D, N)$ of different random N-node trees, with the same distance distribution $\{D_k\}$, to which i can belong. By counting the different

[1]However we see later that these two concepts are indeed compatible, but only by enlarging the meaning of 'absolute space'.

linkage patterns, together with permutations of the monads we obtain

$$\mathcal{N}(D,N) = \frac{(M-1)!D_1^{D_2}D_2^{D_3}...D_{L-1}^{D_L}}{(M-N-2)!D_1!D_2!...D_L!}. \tag{4.13}$$

Here $D_k^{D_{k+1}}$ is the number of different possible linkage patterns between level k and level $k+1$, and $(M-1)!/(M-N-2)!$ is the number of different possible choices for the monads, with i fixed. The denominator accounts for those permutations which have already been accounted for by the $D_k^{D_{k+1}}$ factors. We compute the most likely tree-graph structure by maximising $\ln\mathcal{N}(D,N) + \lambda(\sum_{k=0}^{L} D_k - N)$ where λ is a Lagrange multiplier for the constraint. Using Stirling's approximation for $D_k!$ we obtain

$$D_{k+1} = D_k \ln\frac{D_k}{D_{k-1}} - \lambda D_k + \frac{1}{2}. \tag{4.14}$$

We may compute the most likely tree-graph structure by maximising $\mathcal{N}(D,N)$ with respect to $\{D_k\}$. This equation has an approximate analytic solution [38] $D_k = \frac{2N}{L}\sin^2(\pi k/L)$. These results imply that the most likely tree-graph structure to which a monad can belong has a distance distribution $\{D_k\}$ which indicates that the tree-graph is embeddable in a 3-dimensional hypersphere, S^3.

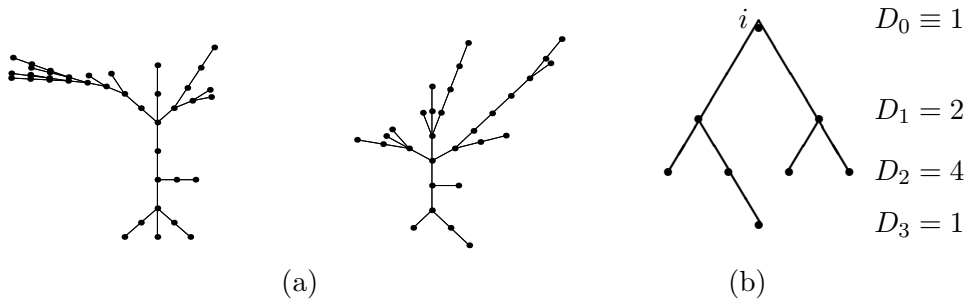

Figure 4.2: (a) Rare and large components of B form disconnected tree-graphs, (b) An $N = 8$ tree-graph with $L = 3$ for monad i, with indicated distance distribution D_k.

We call these tree-graph B-sets *gebits* (geometrical bits). However S^3 embeddability of these gebits is a weaker result than demonstrating the necessary emergence of S^3-spaces, since extra cross-linking connections would be required for this to produce a strong embeddability.

The monads for which the B_{ij} are, from the SRN term, large thus form disconnected gebits, and in (4.12b) we relabel the monads to bring these new gebits $g_1, g_2, g_3, ..$ to block diagonal form, with the remainder indicating the small and growing thermalised condensate, $C = c_1 \oplus c_2 \oplus c_3 \oplus ...$ In (4.12b) the g_i indicate unconnected gebits, while the icon $\bigcirc$ represents older and connected gebits, and suggests a compact 3-space. The remaining very small B_{mn}, not shown in (4.12b), are background noise only.

A key dynamical feature is that most gebit matrices g have $\det(g) = 0$, since most tree-graph connectivity matrices are degenerate. For example in the tree in Fig.4.2b the B matrix has a nullspace, spanned by eigenvectors with eigenvalue zero, of dimension two irrespective of the actual values of the non-zero B_{ij}; for instance the right hand pair ending at the level $D_2 = 4$ are identically connected and this causes two rows (and columns) to be identical up to a multiplicative factor. So the degeneracy of the gebit matrix is entirely structural. For this graph there is also a second set of three monads whose connectivities are linearly dependent. These $\det(g) = 0$ gebits form a *reactive gebits* subclass, i.e. in the presence of background noise $(g_1 \oplus g_2 \oplus g_3 \oplus ..)^{-1}$ is well-defined and has some large elements. These reactive gebits are the building blocks of the dissipative structure. The self-assembly process is as follows: before the formation of the thermalised condensate B^{-1} generates new connections (large B_{ij}) almost exclusively between gebits and the remaining non-gebit sub-block (having det≈ 0 but because here all the involved $B_{ij} \approx 0$), resulting in the decay, without gebit interconnection, of each gebit. However once the condensate has formed (essentially once the system has 'cooled' sufficiently) the condensate $C = c_1 \oplus c_2 \oplus c_3 \oplus ...$ acts as a quasi-stable (i.e. $\det(C) = \prod_i \det(c_i) \neq 0$) sub-block of (4.12b) and the sub-block of gebits may be inverted separately. The gebits are then interconnected (with many gebits present cross-links are more probable than self-links) via new links formed by B^{-1}, resulting in the larger structure indicated by the $\bigcirc$ in (4.12b). Essentially, in the presence of the condensate, the gebits are *sticky*.

Now (4.13) is strictly valid in the limit of vanishingly small probabilities. For a more general analysis of the connectivity of such gebits assume for simplicity that the large w_{ij} arise with fixed but very small probability p, then the emergent geometry of the gebits is revealed by studying the probability distribution for the structure of the random graph units or gebits minimal spanning trees with D_k nodes at k links from node i ($D_0 \equiv 1$), this is given more generally by (see Appendix A for derivation or [38]);

$$\mathcal{P}[D, L, N] \propto \frac{p^{D_1}}{D_1! D_2! .... D_L!} \prod_{i=1}^{L-1} (q^{\sum_{j=0}^{i-1} D_j})^{D_{i+1}} (1 - q^{D_i})^{D_{i+1}}, \tag{4.15}$$

where $q = 1 - p$, N is the total number of nodes in the gebit and L is the maximum depth from node i. In the limit $p \to 0$ (4.15) reduces to (4.13), proportionally. To find the most likely connection pattern we numerically maximise $\mathcal{P}[D, L, N]$ for fixed N with respect to L and the D_k. The resulting L and $\{D_1, D_2, ..., D_L\}$ fit very closely to the form $D_k \propto \sin^{d-1}(\pi k/L)$; see Fig.4.3a for $N = 5000$ and $\text{Log}_{10} p = -6$. The resultant d values for a range of $\text{Log}_{10} p$ and with $N = 5000$ are shown in Fig.4.3b.

This shows, for p below a critical value, that $d = 3$, indicating that the connected nodes have a natural embedding in a 3D hypersphere S^3; call this a base gebit. Above that value of p, the increasing value of d indicates the presence of extra links that, while some conform with the embeddability, others are in the main defects

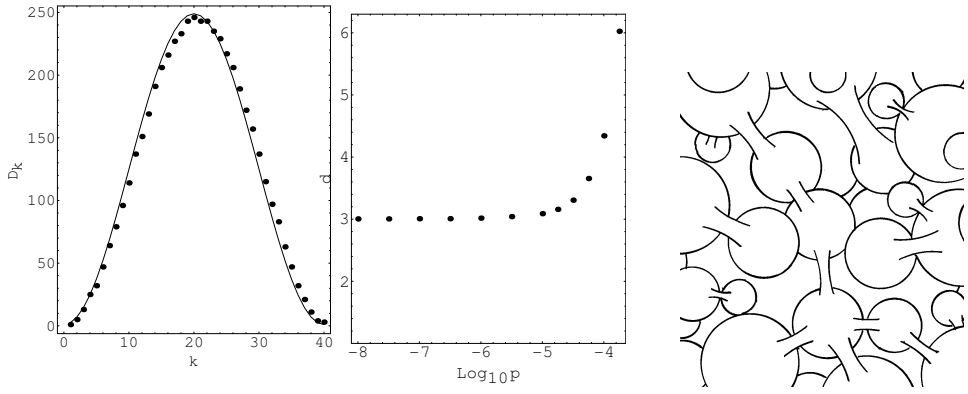

(a) (b) (c)

Figure 4.3: (a) Points show the D_k set and $L = 40$ value found by numerically maximising $\mathcal{P}[D, L, N]$ for $\mathrm{Log}_{10}p = -6$ for fixed $N = 5000$. Curve shows $D_k \propto \sin^{d-1}(\frac{\pi k}{L})$ with best fit $d = 3.16$ and $L = 40$, showing excellent agreement, and indicating embeddability in an S^3 with some topological defects. (b) Dimensionality d of the gebits as a function of the probability p. (c) Graphical depiction of the 'process space' at one stage of the iterative process-time showing a quantum-foam structure formed from embeddings and links of the kind in (a). The linkage connections have the distribution of a 3D space, but the individual gebit components are closed compact spaces and cannot be embedded in a 3D background space. So the drawing is only suggestive. Nevertheless this figure indicates that process physics generates a cellular information system, where the behaviour is determined at all levels by internal information.

with respect to the geometry of the S^3. These extra links act as topological defects. By themselves these extra links will have the connectivity and embedding geometry of numbers of gebits, but these gebits have a 'fuzzy' embedding in the base gebit. This is an indication of fuzzy homotopies (a homotopy is, put simply, an embedding of one space into another). Here we see the emergence of geometry, not only of space but also of the internal flavour symmetry spaces of quantum fields. The nature of the resulting 3D process-space is suggestively indicated in Fig.4.3c, and behaves essentially as a quantum foam [39].

Over ongoing iterations the existing gebits become cross-linked and eventually lose their ability to undergo further linking; they lose their 'stickiness' and decay. The value of the parameter a in (4.1) must be small enough that the 'stickiness' persists over many iterations, that is, it is not quenched too quickly, otherwise the emergent network will not grow. Hence the emergent space is 3D but is continually undergoing replacement of its component gebits; it is an informational process-space, in sharp distinction to the non-process continuum geometrical spaces that have played a dominant role in modelling physical space. If the noise is 'turned off' then this emergent dissipative space will decay and cease to exist. We thus see that the nature of space is deeply related to the logic of the limitations of logic, as

implemented here as a self-referentially limited neural network.

4.5 Gebits as Topological Skyrmions

We need to extract convenient but approximate syntactical descriptions of the semantic information in the network, and these will have the form of a sequence of mathematical constructions, the first being the Quantum Homotopic Field Theory. Importantly they must all retain explicit manifestations of the SRN. To this end first consider the special case of the iterator when the SRN is frozen at a particular w, that is we consider iterations with an artificially fixed SRN term. Then it may be shown that the iterator is equivalent to the minimisation of an 'energy' expression (remember that B and w are antisymmetric)

$$E[B;w] = -\frac{a}{2}\mathrm{Tr}[B^2] - a\mathrm{TrLn}[B] + \mathrm{Tr}[wB]. \tag{4.16}$$

Note that for disconnected gebits g_1 and g_2 this energy is additive, $E[g_1 \oplus g_2] = E[g_1] + E[g_2]$. Now suppose the fixed w has the form of a gebit approximating an S^3 network with one embedded topological defect which is itself an S^3 network, for simplicity. So we are dissecting the gebit into base gebit, defect gebit and linkings or embeddings between the two. We also ignore the rest of the network, which is permissible if our gebit is disconnected from it. Now if $\det(w)$ is not small, then this gebit is non-sticky, and for small a, the iterator converges to $B \approx \frac{1}{a}w$, namely an enhancement only of the gebit. However because the gebits are rare constructs they tend to be composed of larger w_{ij} forming tree structures, linked by smaller valued w_{ij}. The tree components make $\det(w)$ smaller, and then the inverse B^{-1} is activated and generates new links. Hence, in particular, the topological defect relaxes, according to the 'energy' measure, with respect to the base gebit. This relaxation is an example of a 'non-linear elastic' process [40]. The above gebit has the form of a mapping $\pi : S \to \Sigma$ from a base space to a target space. Manton [41, 42, 43] has constructed the continuum form for the 'elastic energy' of such an embedding and for $\pi : S^3 \to S^3$ it is the Skyrme energy

$$E[U] = \int \left[-\frac{1}{2}\mathrm{Tr}(\partial_i U U^{-1} \partial_i U U^{-1}) - \frac{1}{16}\mathrm{Tr}[\partial_i U U^{-1}, \partial_i U U^{-1}]^2 \right], \tag{4.17}$$

where $U(x)$ is an element of $SU(2)$. Via the parametrisation $U(x) = \sigma(x) + i\vec{\pi}(x).\vec{\tau}$, where the τ_i are Pauli matrices, we have $\sigma(x)^2 + \vec{\pi}(x)^2 = 1$, which parametrises an S^3 as a unit hypersphere embedded in E^4 (which has no ontological significance, of course). Non-trivial minima of $E[U]$ are known as Skyrmions (a form of topological soliton), and have $Z = \pm 1, \pm 2, ...$, where Z is the winding number of the map,

$$Z = \frac{1}{24\pi^2} \int \sum \epsilon_{ijk} \mathrm{Tr}(\partial_i U U^{-1} \partial_j U U^{-1} \partial_k U U^{-1}). \tag{4.18}$$

The first key to extracting emergent phenomena from the stochastic neural network is the validity of this continuum analogue, namely that $E[B; w]$ and $E[U]$ are describing essentially the same 'energy' reduction process. This requires detailed analysis.

4.6 Absence of a Cosmic Code

This 'frozen' SRN analysis of course does not match the time-evolution of the full iterator (4.1), for this displays a much richer collection of processes. With ongoing new noise in each iteration and the saturation of the linkage possibilities of the gebits emerging from this noise, there arises a process of ongoing birth, linking and then decay of most patterns. The task is then to identify those particular patterns that survive this flux, even though all components of these patterns eventually disappear, and to attempt a description of their modes of behaviour. This brings out the very biological nature of the information processing in the SNN, and which appears to be characteristic of a 'pure' semantic information system. Kitto [21] has further investigated the analogies between process physics and living systems. The emergent 'laws of physics' are the habitual habits of this system, and it appears that they may be identified. However there is no encoding mechanism for these 'laws', they are continually manifested; there is no *cosmic code*. In contrast living or biological systems could be defined as those emergent patterns which discovered how to encode their 'laws' in a syntactical *genetic code*. Nevertheless such biological systems make extensive use of semantic information at all levels as their genetic code is expressed in the phenotype.

4.7 Entrapped Topological Defects

In general each gebit, as it emerges from the SRN, has active nodes and embedded topological defects, again with active nodes. Further there will be defects embedded in the defects and so on, and so gebits begin to have the appearance of a fractal defect structure, and with all the defects having various classifications and associated winding numbers. The energy analogy above suggests that defects with opposite winding numbers at the same fractal depth may annihilate by drifting together and merging. Furthermore the embedding of the defects is unlikely to be 'classical', in the sense of being described by a mapping $\pi(x)$, but rather would be fuzzy, i.e described by some functional, $F[\pi]$, which would correspond to a classical embedding only if F has a very sharp supremum at one particular $\pi = \pi_{cl}$. As well these gebits are undergoing linking because their active nodes (see [9] for more discussion) activate the B^{-1} new-links process between them, and so by analogy the gebits themselves form larger structures with embedded fuzzy topological defects. This emergent behaviour is suggestive of a quantum space foam, but one containing topological defects which will be preserved by the system, unless annihilation events

occur. If these topological defects are sufficiently rich in fractal structure so as to be preserved, then their initial formation would have occurred as the process-space relaxed out of its initial essentially random form. This phase would correspond to the early stages of the Big-Bang. Once the topological defects are trapped in the process-space they are doomed to meander through that space by essentially self-replicating, i.e. continually having their components die away and be replaced by similar components. These residual topological defects are what we call matter. The behaviour of both the process-space and its defects is clearly determined by the same network processes; we have an essential unification of space and matter phenomena. This emergent quantum foam-like behaviour suggests that the full generic description of the network behaviour is via the Quantum Homotopic Field Theory (QHFT) of the next chapter. We also see that cellular structures are a general feature of semantic information systems, with the information necessarily distributed.

Chapter 5

Quantum Homotopic Field Theory

5.1 Functional Schrödinger Equation

Because of the iterator the resource is the large valued B_{ij} from the SRN because they form the 'sticky' gebits which are self-assembled into the non-flat compact 3D process-space. The accompanying topological defects within these gebits and also the topological defects within the process space require a more subtle description. The key behavioural mode for those defects which are sufficiently large (with respect to the number of component gebits) is that their existence, as identified by their topological properties, will survive the ongoing process of mutation, decay and regeneration; they are topologically self-replicating. Consider the analogy of a closed loop of string containing a knot - if, as the string ages, we replace small sections of the string by new pieces then eventually all of the string will be replaced, however the relational information represented by the knot will remain unaffected as only the topology of the knot is preserved. In the process-space there will be gebits embedded in gebits, and so forth, in topologically non-trivial ways; the topology of these embeddings is all that will be self-replicated in the processing of the dissipative structure.

To analyse and model the 'life' of these topological defects we need to characterise their general behaviour: if sufficiently large (i) they will self-replicate if topological non-trivial, (ii) we may apply continuum homotopy theory to tells us which embeddings are topologically non-trivial, (iii) defects will only dissipate if embeddings of 'opposite winding number' (these classify the topology of the embedding) engage one another, (iv) the embeddings will be in general fractal, and (iv) the embeddings need not be 'classical', ie the embeddings will be fuzzy. To track the coarse-grained behaviour of such a system led to the development of a new form of quantum field theory: Quantum Homotopic Field Theory (QHFT). This models both the process-space and the topological defects.

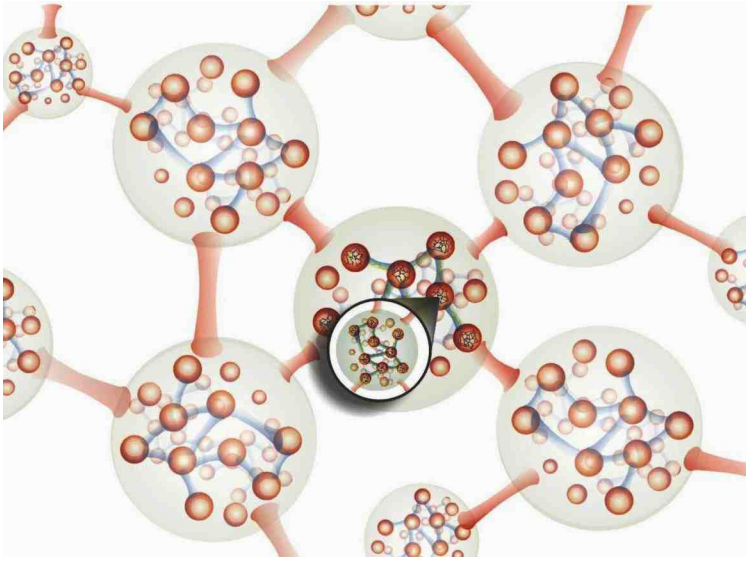

Figure 5.1: An artistic representation of the functional $\Psi[\{\pi\};t]$ showing dominant homotopies. The 'magnifying glass' indicates that these mappings can be nested. Graphic by C. Klinger. First published as the cover graphic of the *The Physicist*, [11].

To construct this QHFT we introduce an appropriate configuration space, namely all the possible homotopic mappings $\pi_{\alpha\beta} : S_\beta \to S_\alpha$, where the $S_1, S_2, ..$, describing 'clean' or topological-defect free gebits, are compact spaces of various types. Then QHFT has the form of an iterative functional Schrödinger equation for the discrete time-evolution of a wave-functional $\Psi[...., \pi_{\alpha\beta}, ...; t]$

$$\Psi[...., \pi_{\alpha\beta}, ...; t+\Delta t] = \Psi[...., \pi_{\alpha\beta}, ...; t] - iH\Psi[...., \pi_{\alpha\beta}, ...; t]\Delta t + \text{QSD terms.} \quad (5.1)$$

This form arises as it is models the preservation of semantic information, by means of a unitary time evolution; even in the presence of the noise in the Quantum State Diffusion (QSD) terms. Because of the QSD noise (5.1) is an irreversible quantum system. The time step Δt in (5.1) is relative to the scale of the fractal processes being explicitly described, as we are using a configuration space of mappings between prescribed gebits. At smaller scales we would need a smaller value for Δt. Clearly this invokes a (finite) renormalisation scheme. We now discuss the form of the hamiltonian and the QSD terms.

First (5.1), without the QSD term, has a form analogous to a 'third quantised' system, in conventional terminology [44]. These systems were considered as perhaps capable of generating a quantum theory of gravity. The argument here is that this is the emergent behaviour of the SNN, and it does indeed lead to quantum gravity, but with quantum matter as well. More importantly we understand the origin of (5.1), and it will lead to quantum and then classical gravity, rather than arise from classical gravity via some *ad hoc* or heuristic quantisation procedure.

Depending on the 'peaks' of Ψ and the connectivity of the resultant dominant mappings such mappings are to be interpreted as either embeddings or links; Fig.5.1 then suggests the dominant process-space form within Ψ showing both links and embeddings. The emergent process-space then has the characteristics of a quantum foam. Note that, as indicated in Fig.5.1, the original start-up links and nodes are now absent. Contrary to the suggestion in Fig.5.1, this process space cannot be embedded in a *finite* dimensional geometric space with the emergent metric preserved, as it is composed of nested finite-dimensional closed spaces.

5.2 Homotopy Hamiltonian

We now consider the form of the hamiltonian H. In the previous chapter it was suggested that Manton's non-linear elasticity interpretation of the Skyrme energy is appropriate to the SNN. This then suggests that H is the functional operator

$$H = \sum_{\alpha \neq \beta} h[\frac{\delta}{\delta \pi_{\alpha\beta}}, \pi_{\alpha\beta}], \tag{5.2}$$

where $h[\frac{\delta}{\delta\pi}, \pi]$ is the (quantum) Skyrme Hamiltonian functional operator for the system based on making fuzzy the mappings $\pi : S \to \Sigma$, by having h act on wave-functionals of the form $\Psi[\pi(x); t]$. Then H is the sum of pairwise embedding or homotopy hamiltonians. The corresponding functional Schrödinger equation would simply describe the time evolution of quantised Skyrmions with the base space fixed, and $\Sigma \in SU(2)$. There have been very few analyses of this class of problem, and then the base space is usually taken to be E^3. We shall not give the explicit form of h as it is complicated, but wait to present the associated action.

In the absence of the QSD terms the time evolution in (5.1) can be formally written as a functional integral

$$\Psi[\{\pi\}; t'] = \int \prod_{\alpha \neq \beta} \mathcal{D}\tilde{\pi}_{\alpha\beta} e^{iS[\{\tilde{\pi}\}]} \Psi[\{\pi\}; t], \tag{5.3}$$

where, using the continuum t limit notation, the action is a sum of pairwise actions,

$$S[\{\tilde{\pi}\}] = \sum_{\alpha \neq \beta} S_{\alpha\beta}[\tilde{\pi}_{\alpha\beta}], \tag{5.4}$$

$$S_{\alpha\beta}[\tilde{\pi}] = \int_t^{t'} dt'' \int d^n x \sqrt{-g} \left[\frac{1}{2} \mathrm{Tr}(\partial_\mu \tilde{U} \tilde{U}^{-1} \partial^\mu \tilde{U} \tilde{U}^{-1}) + \frac{1}{16} \mathrm{Tr}[\partial_\mu \tilde{U} \tilde{U}^{-1}, \partial^\nu \tilde{U} \tilde{U}^{-1}]^2 \right], \tag{5.5}$$

and the now time-dependent (indicated by the tilde symbol) mappings $\tilde{\pi}$ are parametrised by $\tilde{U}(x,t)$, $\tilde{U} \in S_\alpha$. The metric $g_{\mu\nu}$ is that of the n-dimensional base space, S_β, in $\pi_{\alpha,\beta} : S_\beta \to S_\alpha$. As usual in the functional integral formalism the functional derivatives in the quantum hamiltonian, in (5.2), now manifest as the time components ∂_0

in (5.5), so now (5.5) has the form of a 'classical' action, and we see the emergence of 'classical' fields, though the emergence of 'classical' behaviour is a more complex process. Eqns.(5.1) or (5.3) describe an infinite set of quantum skyrme systems, coupled in a pairwise manner. Note that each homotopic mapping appears in both orders; namely $\pi_{\alpha\beta}$ and $\pi_{\beta\alpha}$.

5.3 Quantum State Diffusion

The Quantum State Diffusion (QSD) [45] terms are non-linear and stochastic,

$$\text{QSD} = \sum_j \left(<L_j^\dagger> L_j - \frac{1}{2} L_j^\dagger L_j - <L_j^\dagger><L_j> \right) \Psi \Delta t + \sum_j \left(L_j - <L_j> \right) \Psi \Delta \xi_j, \quad (5.6)$$

which involves summation over the class of Linblad functional operators L_j. The QSD terms are up to 5th order in Ψ, as in general

$$<A>_t \equiv \int \prod_{\alpha \neq \beta} \mathcal{D}\pi_{\alpha\beta} \Psi[\{\pi\}; t]^* A \Psi[\{\pi\}; t] \quad (5.7)$$

and where $\Delta\xi_j$ are complex statistical variables with means $M(\Delta\xi_j) = 0$, $M(\Delta\xi_j \Delta\xi_{j'}) = 0$ and $M(\Delta\xi_j^* \Delta\xi_{j'}) = \delta(j - j')\Delta t$. The remarkable property of this QSD term is that the unitarity of the time evolution in (5.1) is maintained in the mean, as shown in Appendix B.

5.4 Emergent Classicality

These QSD terms are ultimately responsible for the emergence of classicality via an objectification [45], but in particular they produce wave-function(al) collapses during quantum measurements, as the QSD terms tend to 'sharpen' the fuzzy homotopies towards classical or sharp homotopies. So the QSD terms, as residual SRN effects, lead to the Born quantum measurement random behaviour, but here arising from the process physics, and not being invoked as a metarule. Keeping the QSD terms leads to a functional integral representation for a density matrix formalism in place of (5.3), and this amounts to a derivation of the decoherence formalism which is usually arrived at by invoking the Born measurement metarule. Here we see that 'decoherence' arises from the limitations on self-referencing.

In the above we have a deterministic and unitary evolution, tracking and preserving topologically encoded information, together with the stochastic QSD terms, whose form protects that information during localisation events, and which also ensures the full matching in QHFT of process-time to real time: an ordering of events, an intrinsic direction or 'arrow' of time and a modelling of the contingent present moment effect. So we see that process physics generates a complete theory of quantum measurements involving the non-local, non-linear and stochastic QSD

terms. It does this because it generates both the 'objectification' process associated with the classical apparatus and the actual process of (partial) wavefunctional collapse as the quantum modes interact with the measuring apparatus. Indeed many of the mysteries of quantum measurement are resolved when it is realised that it is the measuring apparatus itself that actively provokes the collapse, and it does so because the QSD process is most active when the system deviates strongly from its dominant mode, namely the ongoing relaxation of the system to a 3D process-space, and matter survives only because of its topological form. This is essentially the process that Penrose [46] suggested, namely that the quantum measurement process is essentially a manifestation of quantum gravity. The demonstration of the validity of the Penrose argument of course could only come about when quantum gravity was *derived* from deeper considerations, and not by some *ad hoc* argument such as the *quantisation* of Einstein's classical spacetime model.

That the non-local QSD terms lead to wavefunctional collapse is relevant to the new theory of gravity in Chap.7. This collapse amounts to an ongoing sharpening of the homotopic mappings towards a 'classical' 3D configuration - resulting in essentially the process we have long recognised as 'space'. Being non-local the collapse process does not involve any propagation effects, that is the collapse does not require any effect to propagate *through* the space. For that reason the self-generation of space is in some sense *action-at-a-distance*, and the emergence of such a quantum process underlying reality is, of course, contrary to the long-held belief by physicists that such action is unacceptable, though that belief arose before the quantum collapse was experimentally shown to display *action at a distance* in the Aspect experiment. Hence we begin to appreciate why the new theory of gravity does not involve the maximum speed c of propagation *through* space. and why it does not predict the GR gravitational waves travelling at speed c, of the kind long searched for but not detected.

The mappings $\pi_{\alpha\beta}$ are related to group manifold parameter spaces with the group determined by the dynamical stability of the mappings. This symmetry leads to the flavour symmetry of the standard model of 'particle' physics. Quantum homotopic mappings or skyrmions behave as fermionic or bosonic modes for appropriate winding numbers; so process physics predicts both fermionic and bosonic quantum modes, but with these associated with topologically encoded information and not with objects or 'particles'.

5.5 Emergent Quantum Field Theory

The QHFT is a very complex 'book-keeping' system for the emergent properties of the neural network, and we now sketch how we may extract a more familiar Quantum Field Theory (QFT) that relates to the standard model of 'particle' physics. An effective QFT should reproduce the emergence of the process-space part of the quantum foam, particularly its 3D aspects. The QSD processes play a key role

in this as they tend to enhance classicality. Hence at an appropriate scale QHFT should approximate to a more conventional QFT, namely the emergence of a wavefunctional system $\Psi[U(x);t]$ where the configuration space is that of homotopies from a 3-space to $U(x) \in G$, where G is some group manifold space. This G describes 'flavour' degrees of freedom. So we are coarse-graining out the gebit structure of the quantum-foam. Hence the Schrödinger wavefunctional equation for this QFT will have the form

$$\Psi[U;t+\Delta t] = \Psi[U;t] - iH\Psi[U;t]\Delta t + \text{QSD terms}, \tag{5.8}$$

where the general form of H is known, and where a new residual manifestation of the SRN appears as the new QSD terms. This system describes skyrmions embedded in a continuum space. It is significant that such Skyrmions are only stable, at least in flat space and for static skyrmions, if that space is 3D. This tends to confirm the observation that 3D space is special for the neural network process system.

5.6 Emergent Flavour and Hidden Colour

Again, in the absence of the QSD terms, we may express (5.8) in terms of the functional integral

$$\Psi[U;t'] = \int \mathcal{D}\tilde{U} e^{iS[\tilde{U}]}\Psi[U;t]. \tag{5.9}$$

To gain some insight into the phenomena present in (5.8) or (5.9), it is convenient to use the fact that functional integrals of this Skyrmionic form my be written in terms of Grassmann-variable functional integrals, but only by introducing a fictitious 'metacolour' degree of freedom and associated coloured fictitious vector bosons. This is essentially the reverse of the Functional Integral Calculus (FIC) hadronisation technique in the Global Colour Model (GCM) of QCD [34]. The action for the Grassmann and vector boson part of the system is of the form (written for flat space)

$$S[\overline{p},p,A^a_\mu] = \int d^4x \left(\overline{p}\gamma^\mu(i\partial_\mu + g\frac{\lambda^a}{2}A^a_\mu)p - \frac{1}{4}F^a_{\mu\nu}(A)F^{a\mu\nu}(A)\right), \tag{5.10}$$

where the Grassmann variables $p_{fc}(x)$ and $\overline{p}_{fc}(x)$ have flavour and metacolour labels. The Skyrmions are then re-constructed, in this system, as topological solitons These coloured and flavoured but fictitious fermionic fields $\overline{p}$ and p correspond to the proposed preon system [47, 48]. As they are purely fictitious, in the sense that there are no excitations in the system corresponding to them, the metacolour degree of freedom must be hidden or confined. We thus arrive at the general feature of the standard model of particles with flavour and confined colour degrees of freedom. Then while the QHFT and the QFT represent an induced syntax for the semantic information, the preons may be considered as an induced 'alphabet' for that syntax. The advantage of introducing this preon alphabet is that we can more easily

determine the states of the system by using the more familiar language of fermions and bosons, rather than working with the skyrmionic system, so long as only colour singlet states are finally permitted. In order to establish fermionic behaviour a Wess-Zumino (WZ) process must be extracted from the iterator behaviour or the QHFT. Such a WZ process is time-dependent, and so cannot arise from the frozen SRN argument in Chap.4. It is important to note that (5.10) and the action in (5.9) are certainly not the final forms. Further analysis will be required to fully extract the induced actions for the emergent QFT.

5.7 Hilbert Spaces

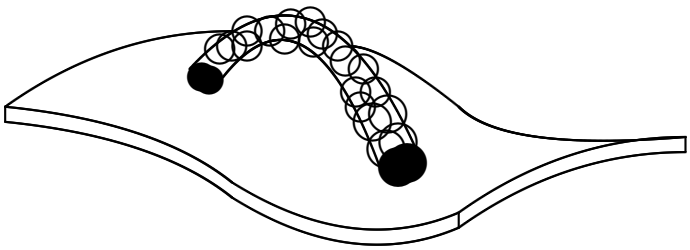

Figure 5.2: The is a representation of the origin of quantum non-locality. An entity is attached at two disjoint regions of the [3]-space, with the gebit structure of that space not shown.

Process Physics has suggested the origin of quantum phenomena and of its Hilbert-space formalism. This phenomena is associated with the time evolution of the conserved topological defects embedded in the process space. However that embedding need not be local, as illustrated in Fig.5.2. This particular situation corresponds to the Hilbert space 'sum'

$$\psi(x) = \psi_1(x) + \psi_2(x), \tag{5.11}$$

where $\psi_1(x)$ and $\psi_2(x)$ are non-zero only in the respective embedding regions. This is how quantum non-locality manifests in conventional quantum theory. So the Hilbert space 'sum' is the representation of the connectivity shown in Fig.5.2. Such a non-local embedding is also responsible for the phenomenon of quantum entanglement.

Chapter 6

Emergent Universe

6.1 Multi-World Universe and the 'Dark Energy' Effect

Process physics predicts that the neural network behaviour will be characterised by a growing 3-dimensional process-space having, at a large scale, the form of a S^3 hypersphere. It is possible to give the dominant rate of growth of this hypersphere. However first, from random graph theory [49], we expect more than one such spatial system, with each having the character of a growing hypersphere, and all embedded in the random background discussed previously. This background has no metric structure, and so these various hyperspheres have no distance measure over them. We have then a multi-world universe (our 'universe' being merely one of these 'worlds'), as represented in Fig.6.1. Being process spaces they compete for new gebits, and so long as we avoid a saturation case, where one 'world' dominates all the others, each will grow according to

$$\frac{dN_i}{dt} = aN_i - bN_i \qquad a > 0, b > 0, \tag{6.1}$$

where the last term describes the decay of gebits at a rate b, while the first describes growth of the i^{th} 'world', this being proportional to the size (as measured by its gebit content number) $N_i(t)$, as success in randomly attaching new gebits is proportional to the number of gebits present (the 'stickiness' effect), so long as we ignore the topological defects (quantum 'matter') as these have a different stickiness, and also affect the decay rate, and so slow down the expansion. Thus $N_i(t)$ will show exponential growth, as appears to be the case as indicated by recent observations of very distant supernovae counts [50]. Hence process physics predicts a positive cosmological constant, now known as the 'dark energy' effect, and that this is unrelated to the phenomenon of gravity. Indeed this multi-world model is incompatible with General Relativity, as it is not capable of even describing the non-geometric background. In this enlarged cosmology each world would have its own independent big-bang beginning, but then it is no longer necessary for this on-going ensemble

of worlds to have had a beginning itself, as we may presumably take the system start-up time to $-\infty$. Hence the observation of the cosmological constant effect is here to be interpreted as arising from the existence of these other worlds, and that this complete system of 'worlds' is without a beginning. This avoids the logical problems associated with the notion of a single world arising spontaneously from 'nothing' - *ex nihilo*.

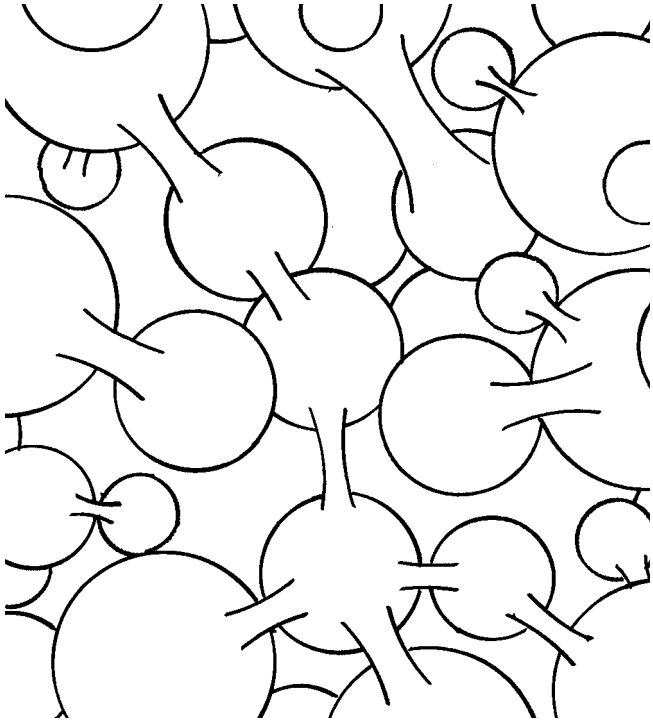

Figure 6.1: A graphical representation of a 'multi-world' universe, with hyperspheres of various sizes and ages embedded in an unstructured non-geometric background, with only minimal linkages between the 'worlds'. This is a reproduction of Fig.4.3(c). This illustrates the notion that reality is fractal.

6.2 Gravity and the Equivalence Principle

One striking outcome of process physics is an explanation for the phenomenon of gravity. First note that matter is merely topological defects embedded in the process space, and we expect such defects to have a larger than usual gebit connectivity; indeed matter is a violation of the 3-D connectivity of this space, and it is for this reason we needed to introduce fields to emulate this extra non-spatial connectivity. One consequence of this is that in the region of these matter fields the gebits decay faster, they are less sticky because of the extra connectivity. Hence in this region,

compared to other nearby matter-free regions the gebits are being 'turned over' more frequently but at the same time are less effective in attracting new gebits. Overall this suggests that matter-occupying-regions act as net sinks for gebits, and there will be a trend for the neighbouring quantum foam to undergo a diffusion/relaxation process in which the foam effectively moves towards the matter: matter acts as a sink for space, but never as a source. Such a process would clearly correspond to gravity. As the effect is described by a net diffusion/relaxation of space which acts equally on all surrounding matter, the in-fall mechanism is independent of the nature of the surrounding matter. This is nothing more than the Equivalence Principle, first noticed by Galileo. As well if the in-fall rate exceeds the rate at which 'motion' through the process-space is possible then an event horizon appears, and this is clearly the black hole scenario. Presumably at the core of a black-hole is a tangle of topological defects, so that the effective dimensionality is very high, and which maintains the in-flow of quantum foam. This in-flow is a loss of information, and so gravity itself is an information-loss process.

6.3 Inertia

One longstanding unsolved problem in physics is the explanation for inertia. This is the effect where objects continue in uniform motion unless acted upon by 'forces', and was first analysed by Galileo in the modern era, but of course Zeno made an early attempt. However there has never been an explanation for this effect. In Newtonian physics it was built into the syntactical description rather than being a prediction of that modelling. Of course current physics is essentially a static modelling of reality, with motion indirectly accessed via the geometrical-time metarule, and so the failure to explain motion is not unexpected. However process physics offers a simple explanation.

The argument for inertia follows from a simple self-consistency argument. Suppose a topological defect, or indeed a vast bound collection of such defects, is indeed 'in motion'. This implies that the gebits are being preferentially replaced in the direction of that 'motion', for motion as such is a self-replication process; there is no mechanism in process physics for a fixed pattern to say 'slide' *through* the quantum-foam. Rather motion is self-replication of the gebit connectivity patterns in a set direction. Since the newest gebits, and hence the stickiest gebits, in each topological defect, are on the side corresponding to the direction of motion, the gebits on that side are preferentially replaced. Hence the motion is self-consistent and self-perpetuating.

An additional effect expected in process physics is that such motion results in a time dilation and length contraction effects; the self-replication effect is to be considered as partly the self-replication associated with any internal oscillations and partly self-replication associated with 'motion'. This 'competition for resources' results in the slowing down of internal oscillations, an idea discussed by Toffoli [51].

Such effects have been seen in a variety of 'non-relativistic' continuum systems [52], and indeed they have a long history. In particular emergent Lorentz relativistic effects have been seen in the modelling of dislocations in crystals [53] where 'breather modes' as solitons arise. Hence the lesson is that emergent Lorentz relativistic effects are generic whenever there is a unification of the substratum system and embedded excitations, here the soliton as a dynamical emergent feature within some dynamical background, rather than being merely 'pasted' onto some *a priori* geometrised and so structureless background. Bell [55] has argued for this dynamical interpretation of Lorentz symmetry, as indeed did Lorentz, until this view was overwhelmed by the Einstein spacetime formalisation of relativistic effects. This is discussed in more detail in the next chapter. More recently similar ideas have emerged [54] in the analysis of the sound waves in classical fluids. In later chapters we assume that the QHFT will also display these generic Lorentzian dynamical effects, namely the time-dilation/length-contraction effects.

Geometry is clearly an emergent but approximate phenomenological language; it is certainly not fundamental, and the implicit assumption in physics that it is fundamental has caused many problems and confusions, in particular the absence of 'structure', and the effect of that structure on 'objects' moving through that structure. In process physics the quantum-foam represents an actual spatial system, and as such amounts to a preferred frame of reference, but one, as we shall see, that is well hidden by the time-dilation and length-contraction effects. Later we show that contrary to popular notions the Michelson interferometer, as one example, can reveal this frame when operated in gas mode, and the data from the 1887 Michelson-Morley and the 1925/26 Miller interferometer experiments are analysed. These data show that evidence of absolute motion relative to this quantum-foam space has been present in the non-vacuum interferometer data for over 100 years. However we shall see that the cosmic speed of the solar system through the quantum foam, though comparable to the speed determined from the dipole-fit to the Cosmic Microwave Background (CMB) radiation, is in quite a different direction. The explanation for this is obvious once we consider in more detail the in-flow explanation of gravity. As well the orbital velocity of the earth about the sun is revealed as well as the quantum-foam in-flow towards the sun, as described above.

Chapter 7

A New Theory of Gravity

Process Physics suggests a new explanation of gravity, but so far the determination of the detailed mathematical description of that explanation from the deeper QHFT is yet to be achieved. As an intermediate and complimentary study here we re-examine the previous two major theories of gravity and find that indeed they do permit a recasting into an 'in-flow' formalism, and which then permits a generalisation that brings about an elegant dynamical explanation for the so-called 'dark matter' effect.

The Newtonian theory of gravity was based on Kepler's Laws of motion for planets in the solar system, which were abstracted from observational data; the most famous being that for circular orbits the orbital speed of a planet is inversely proportional to the inverse of the square root of the orbit radius; $v_O \propto 1/\sqrt{r}$. This led Newton to introduce the 'universal' inverse square law of gravity, namely that the gravitational force between two masses is inversely proportional to the square of the separation,

$$F = \frac{Gm_1m_2}{r^2}, \tag{7.1}$$

which together with the acceleration equation $F = ma$, where here $a = v_O^2/r$ is the centripetal acceleration, explained Kepler's Laws. This led to the introduction of the gravitational acceleration vector field $\mathbf{g}(\mathbf{r})$ as the fundamental dynamical variable for the phenomenon of gravity, and which is determined by (7.2), which relates $\mathbf{g}(\mathbf{r})$ to the matter density $\rho(\mathbf{r})$. Here G is Newton's gravitational constant, the only constant, until recent discoveries in [18, 19] and herein, that is involved in the phenomenon of gravity. Much later Hilbert and Einstein introduced a more general theory of gravity, but which was constrained to agree with this Newtonian theory in the appropriate limits. However while (7.2) for $\mathbf{g}$ is uniquely determined by Kepler's Laws, if we rewrite (7.2) in terms of a velocity field $\mathbf{v}(\mathbf{r}, t)$ then the equation for this vector field is not uniquely determined by Kepler's laws: a new unique 'space' self-interaction dynamical term may be incorporated that does not manifest itself in the planetary motions of the solar system. Numerous major developments then unfold from using this in-flow vector field as the fundamental degree of freedom for the

phenomenon of gravity, foremost being that the new term has a strength determined by a dimensionless constant, a second gravitational constant. Experimental data reveals [18, 19] that this constant is, to within experimental error, none other than the fine structure constant $\alpha = e^2\hbar/c \approx 1/137$. Then the most immediate result is the explanation of the so called 'dark matter' effect in spiral galaxies, though various other gravitational anomalies, as they are known, are also now explainable. So it turns out that the 'dark matter' effect is not caused by a new so-far unidentified form of matter, but is an effect associated with a new feature of the phenomenon of gravity; basically gravity is a much richer and more complex phenomenon than currently appreciated. As argued previously the velocity $\mathbf{v}(\mathbf{r}, t)$ field is associated with a restructuring and effective relative 'flow' of a quantum foam which *is* space; this is *not* a flow of something through space but is a manifestation of a non-geometrical structure to space, with matter effectively acting as a 'sink' for this quantum foam. These deeper insights are based upon the information-theoretic modeling of reality. As well we show that this theory is in agreement with various phenomena of gravity, such as precessing orbits, gravitational lensing etc, which were believed to have suggested that General Relativity was a viable theory of gravity. We show here, of course, that the new dynamics involving the fine structure constant is not contained in General Relativity. It is asserted here that the failure of both the Newtonian theory and General Relativity to account for the 'dark matter' effect, and other gravitational phenomena discussed herein, represents a fatal flaw for both these theories; and that Newton's 'universal' inverse square law (7.1) is not at all 'universal'; it is in fact very restricted in its applicability.

Herein the connection of the new theory of gravity to both the Newtonian theory and to General Relativity is analysed, but the most significant results relate to an analysis of the various phenomena that only this new theory now explains, including the borehole g anomaly effect, the difficulties over the last 60 years in ongoing attempts to increase the accuracy with which G could be measured in Cavendish-type experiments, which are all manifestations of the 'dark matter' effect, but which is, as explained here, most evident in the rotation velocity curves of spiral galaxies [18, 19]. This new theory introduces a new form of quantum-foam black hole, the properties of which are determined by the fine structure constant, and which have either 'minimal' of 'non-minimal' forms. The 'minimal' black holes are mandated by the in-flow into matter, and occur in all forms of matter. In the case of the globular clusters the effective mass of the 'minimal' central black holes are computable and found to be in agreement with recent observations. The 'non-minimal' black holes are not caused by matter and appear to be primordial, namely residual effects of the big bang. They have a non-inverse square law acceleration field, and are the cause of both the rapid formation of galaxies and of the non-Keplerian rotation dynamics of spiral galaxies. They have an effective 'dark matter' density that falls off as almost the inverse of the square of the distance form the black hole, as is indeed observed. The presence of the minimal black holes in stars affects their internal

central dynamics, but the effect of this upon the solar neutrino flux problem has yet to be studied.

As already discussed later the quantum-foam 'in-flow' past the earth towards the sun has already been shown to be present in the data from the Miller interferometer experiment of 1925/1926. That experiment and others have also revealed the existence of gravitational waves, essentially a flow turbulence, predicted by the new theory of gravity, but which are very unlike those predicted, but so far unobserved, by General Relativity.

The new theory also has a 'frame-dragging' effect which is being tested by the Gravity Probe B. This effect is caused by vorticity in the in-flow. As well the new theory has quantum-foam vortex filaments linking, in particular, galactic black holes, and these manifest, via weak gravitational lensing, as the recently observed 'dark matter' networks.

To avoid possible confusion it is important to emphasise that the special relativity effects, such as length contractions, time dilations and mass increases, are very much a part of the new gravity theory, but that it is the Lorentz interpretation of these effects, namely that these effects are real dynamical effects, that is being indicated by experiment and observation to be the correct interpretation, and not the usual non-dynamical spacetime interpretation of these effects. In the same vein it is the failure of the Newtonian theory of gravity that is fatal for General Relativity, and not its connection to these so-called special relativity effects. Finally, while the 'flow equations' are classical equations, the occurrence of α strongly suggests, and as predicted in [6], that this is a manifestation of a quantum-foam substructure to space, and that we have the first experimental evidence of a quantum theory of gravity. As discussed here this leads to relatively easy Cavendish-type laboratory experiments that can explore the α-dependent aspects of gravity - essentially laboratory quantum-gravity experiments. This quantum-foam substructure to space also indicates an explanation of a different effect to that of 'dark matter', namely the so-called 'dark energy' effect, as discussed in Sect.6.1.s

7.1 Gravity as Inhomogeneous In-Flow

Here we show that the Newtonian theory of gravity may be exactly re-written as a 'fluid flow' system, as can General Relativity for a class of metrics. This 'fluid' system is interpreted as a classical description of a quantum foam substructure to space, and the 'flow' describes the relative motion of this quantum foam with, as we now show, gravity arising from inhomogeneities in that flow. These inhomogeneities can be caused by an in-flow into matter, or even as inhomogeneities produced purely by the self-interaction of space itself, as happens for instance for the black holes. The Newtonian theory was originally formulated in terms of a force field, the gravitational acceleration $\mathbf{g}(\mathbf{r}, t)$, which is determined by the matter

density $\rho(\mathbf{r},t)$ according to

$$\nabla.\mathbf{g} = -4\pi G\rho. \tag{7.2}$$

For $\nabla \times \mathbf{g} = 0$ this gravitational acceleration $\mathbf{g}$ may be written as the gradient of the gravitational potential Φ

$$\mathbf{g} = -\nabla\Phi, \tag{7.3}$$

where the gravitational potential is now determined by

$$\nabla^2\Phi = 4\pi G\rho. \tag{7.4}$$

Here, as usual, G is the Newtonian gravitational constant. Now as $\rho \geq 0$ we can choose to have $\Phi \leq 0$ everywhere if $\Phi \to 0$ at infinity. So we can introduce $\mathbf{v}^2 = -2\Phi \geq 0$ where $\mathbf{v}$ is some velocity vector field. Here the value of $\mathbf{v}^2$ is specified, but not the direction of $\mathbf{v}$. Then

$$\mathbf{g} = \frac{1}{2}\nabla(\mathbf{v}^2) = (\mathbf{v}.\nabla)\mathbf{v} + \mathbf{v} \times (\nabla \times \mathbf{v}). \tag{7.5}$$

For zero-vorticity (irrotational) flow $\omega = \nabla \times \mathbf{v} = \mathbf{0}$. Then $\mathbf{g}$ is the usual Euler expression for the acceleration of a fluid element in a time-independent or stationary fluid flow. If the flow is time dependent that expression is expected to become

$$\mathbf{g} = \frac{\partial\mathbf{v}}{\partial t} + (\mathbf{v}.\nabla)\mathbf{v} = \frac{d\mathbf{v}}{dt}, \tag{7.6}$$

which has given rise to the total derivative— of $\mathbf{v}$ familiar from fluid mechanics. This equation is then to be accompanied by the 'Newtonian equation' for the flow field

$$\frac{1}{2}\nabla^2(\mathbf{v}^2) = -4\pi G\rho, \tag{7.7}$$

but to be consistent with (7.6) in the case of a time-dependent matter density this equation should be generalised to

$$\frac{\partial}{\partial t}(\nabla.\mathbf{v}) + \nabla.((\mathbf{v}.\nabla)\mathbf{v}) = -4\pi G\rho. \tag{7.8}$$

This exhibits the fluid flow form of Newtonian gravity in the case of zero vorticity $\nabla \times \mathbf{v} = 0$. For zero vorticity (7.8) determines both the magnitude and direction of the velocity field, for in this case we can write $\mathbf{v} = \nabla u$, where $u(\mathbf{r},t)$ is a scalar velocity potential, and in terms of $u(\mathbf{r},t)$ (7.8) specifies uniquely the time evolution of $u(\mathbf{r},t)$. Note that (7.6) and (7.8) are exactly equivalent to (7.2) for the acceleration field $\mathbf{g}$, and so within the fluid flow formalism (7.6) and (7.8) are together equivalent to the Universal Inverse Square Law for $\mathbf{g}$, and so both are equally valid as regards the numerous experimental and observational checks of the acceleration field $\mathbf{g}$ formalism, particularly the Keplerian rotation velocity law. So we appear

to have two equivalent formalisms for the same phenomenon. Indeed for a stationary spherically symmetric distribution of matter of total mass M the velocity field outside of the matter

$$\mathbf{v}(\mathbf{r}) = -\sqrt{\frac{2GM}{r}}\hat{\mathbf{r}}, \tag{7.9}$$

satisfies (7.8) and reproduces the inverse square law form for $\mathbf{g}$ using (7.6):

$$\mathbf{g} = -\frac{GM}{r^2}\hat{\mathbf{r}}. \tag{7.10}$$

So the immediate questions that arise are (i) can the two formalisms be distinguished experimentally, and (ii) can the velocity field formalism be generalised, leading to new gravitational phenomena? To answer these questions we note that

1. The velocity flow field of some 430km/s in the direction (Right Ascension $= 5.2^{hr}$, Declination$= -67^0$) has been detected in several experiments, as described in considerable detail in [16, 17] and Part III. The major component of that flow is related to a galactic flow, presumably within the Milky Way and the local galactic cluster, but a smaller component of some 50km/s being the flow past the earth towards the sun has also recently been revealed in the data.

2. In terms of the velocity field formalism (7.8) a unique term may be added that does not affect observations within the solar system, such as encoded in Kepler's laws, but outside of that special case the new term causes effects which vary from small to extremely large. This term will be shown herein to cause those effects that have been mistakenly called the 'dark matter' effect.

3. Eqn.(7.8) and its generalisations have time-dependent solutions even when the matter density is not time-dependent. These are a form of flow turbulence, a gravitational wave effect, and they have also been detected, as discussed in [16, 17] and Part III.

4. The need for a further generalisation of the flow equations will be argued for, and this in particular includes flow vorticity that leads to a non-spacetime explanation of the 'frame-dragging' effect, and of the 'dark matter' network observed using the weak gravitational lensing technique.

First let us consider the arguments that lead to a generalisation of (7.8). The simplest generalisation is

$$\frac{\partial}{\partial t}(\nabla.\mathbf{v}) + \nabla.((\mathbf{v}.\nabla)\mathbf{v}) + C(\mathbf{v}) = -4\pi G\rho, \tag{7.11}$$

where

$$C(\mathbf{v}) = \frac{\alpha}{8}((trD)^2 - tr(D^2)), \tag{7.12}$$

and

$$D_{ij} = \frac{1}{2}(\frac{\partial v_i}{\partial x_j} + \frac{\partial v_j}{\partial x_i}) \tag{7.13}$$

is the symmetric part of the rate of strain tensor $\partial v_i/\partial x_j$, and α is a dimensionless constant - a new gravitational constant in addition to G. It is possible to check that for the in-flow in (7.9) $C(\mathbf{v}) = 0$. This is a feature that uniquely determines the form of $C(\mathbf{v})$. This means that effects caused by this new term are not manifest in the planetary motions that formed the basis of Kepler's phenomenological laws and that then lead to Newton's theory of gravity. As we shall see the value of α determined from experimental data is found to be the fine structure constant, to within experimental error. As well, as discussed in Sect.8.1 and extensively after that, (7.11) predicts precisely the so-called 'dark matter' effect, with the effective 'dark matter' density defined by

$$\rho_{DM}(\mathbf{r}) = \frac{\alpha}{32\pi G}((trD)^2 - tr(D^2)). \tag{7.14}$$

So the explanation of the 'dark matter' effect becomes apparent once we use the velocity field formulation of gravity. However (7.11) must be further generalised to include (i) the velocity of absolute motion of the matter components with respect to the local quantum foam system, and (ii) vorticity effects.

For these further generalisations we need to be precise by what is meant by the velocity field $\mathbf{v}(\mathbf{r}, t)$. To be specific and also to define a possible measurement procedure we can choose to use the Cosmic Microwave Background (CMB) frame of reference for that purpose, as this is itself easy to establish. However that does not imply that the CMB frame is the local 'quantum-foam' rest frame. Relative to the CMB frame and using the local absolute motion detection techniques described in [17, 16], or more modern techniques that are under development, $\mathbf{v}(\mathbf{r}, t)$ may be measured in the neighbourhood of the observer. Then an 'object' at location $\mathbf{r}_0(t)$ in the CMB frame has velocity $\mathbf{v}_0(t) = d\mathbf{r}_0(t)/dt$ with respect to that frame. We then define

$$\mathbf{v}_R(\mathbf{r}_0(t), t) = \mathbf{v}_0(t) - \mathbf{v}(\mathbf{r}_0(t), t), \tag{7.15}$$

as the velocity of the object relative to the quantum foam at the location of the object. However this absolute velocity of matter $\mathbf{v}_R(t)$ does not appear in (7.11), and so not only is that equation lacking vorticity effects, it presumably is only an approximation for when the matter has a negligible speed of absolute motion with respect to the local quantum foam. To introduce the vector $\mathbf{v}_R(t)$ we need to construct a 2nd-rank tensor generalisation of (7.11), and the simplest form is, as derived in Appendix C,

$$\frac{dD_{ij}}{dt} + \frac{\delta_{ij}}{3}tr(D^2) + \frac{trD}{2}(D_{ij} - \frac{\delta_{ij}}{3}trD)$$
$$+\frac{\delta_{ij}}{3}\frac{\alpha}{8}((trD)^2 - tr(D^2)) = -4\pi G\rho(\frac{\delta_{ij}}{3} + \frac{v_R^i v_R^j}{2c^2} + ..),\ i, j = 1, 2, 3. \tag{7.16}$$

which uses the total derivative of the D_{ij} tensor in (7.13). Because of its tensor structure we can now include the direction of absolute motion of the matter density with respect to the quantum foam, with the scale of that given by c, which is the speed of light relative to the quantum foam. The superscript notation for the components of $\mathbf{v}_R(t)$ is for convenience only, and has no other significance. The trace of (7.16), using the identity

$$(\mathbf{v}.\nabla)(trD) = \frac{1}{2}\nabla^2(\mathbf{v}^2) - tr(D^2) - \frac{1}{2}(\nabla\times\mathbf{v})^2 + \mathbf{v}.\nabla\times(\nabla\times\mathbf{v}), \tag{7.17}$$

gives, for zero vorticity,

$$\frac{\partial}{\partial t}(\nabla.\mathbf{v}) + \nabla.((\mathbf{v}.\nabla)\mathbf{v}) + C(\mathbf{v}) = -4\pi G\rho(1 + \frac{v_R^2}{2c^2} + ..), \tag{7.18}$$

which is (7.11) in the limit $v_R \to 0$. As well the off-diagonal terms, $i \neq j$, are satisfied, to $O(v_R^i v_R^j/c^2)$, for the in-flow velocity field in (7.9). The conjectured form of the RHS of (7.18) is, to $O(v_R^2/c^2)$, based on the Lorentz contraction effect for the matter density, with ρ defined as the matter density if the matter were at rest with respect to the quantum foam. Hence, because of (7.18), (7.16) is in agreement with Keplerian orbits for the solar system with the velocity field given by (7.9).

We now consider a further generalisation of (7.16) to include vorticity effects, namely

$$\frac{dD_{ij}}{dt} + \frac{\delta_{ij}}{3}tr(D^2) + \frac{trD}{2}(D_{ij} - \frac{\delta_{ij}}{3}trD) + \frac{\delta_{ij}}{3}\frac{\alpha}{8}((trD)^2 - tr(D^2))$$
$$+(\Omega D - D\Omega)_{ij} = -4\pi G\rho(\frac{\delta_{ij}}{3} + \frac{v_R^i v_R^j}{2c^2} + ..),\ i,j = 1,2,3. \tag{7.19}$$

$$\nabla\times(\nabla\times\mathbf{v}) = \frac{8\pi G\rho}{c^2}\mathbf{v}_R, \tag{7.20}$$

where

$$\Omega_{ij} = \frac{1}{2}(\frac{\partial v_i}{\partial x_j} - \frac{\partial v_j}{\partial x_i}) = -\frac{1}{2}\epsilon_{ijk}\omega_k = -\frac{1}{2}\epsilon_{ijk}(\nabla\times\mathbf{v})_k \tag{7.21}$$

is the antisymmetric part of the rate of strain tensor $\partial v_i/\partial x_j$, which is the vorticity vector field ω in tensor form. The term $(D\Omega - \Omega D)_{ij}$ allows the vorticity vector field to be coupled to the symmetric tensor D_{ij} dynamics. Again the vorticity is generated by absolute motion of the matter density with respect to the local quantum foam. Eqns (7.19) and (7.20) now permit the time evolution of the velocity field to be determined. Note that the vorticity equation in (7.20) may be explicitly solved, for it may be written as

$$\nabla(\nabla.\mathbf{v}) - \nabla^2\mathbf{v} = \frac{8\pi G\rho}{c^2}\mathbf{v}_R, \tag{7.22}$$

which gives, using

$$\nabla^2\left(\frac{1}{|\mathbf{r}-\mathbf{r}'|}\right) = -4\pi\delta(\mathbf{r}-\mathbf{r}'), \tag{7.23}$$

$$\mathbf{v}(\mathbf{r},t) = \frac{2G}{c^2}\int d^3r' \frac{\rho(\mathbf{r}',t)}{|\mathbf{r}-\mathbf{r}'|}\mathbf{v}_R(\mathbf{r}',t) - \frac{1}{4\pi}\int d^3r' \frac{1}{|\mathbf{r}-\mathbf{r}'|}\nabla(\nabla.\mathbf{v}(\mathbf{r}',t)). \qquad (7.24)$$

This suggests that $\mathbf{v}(\mathbf{r},t)$ is now determined solely by the vorticity equation. However (7.24) is misleading, as (7.20) only specifies the vorticity, and taking the $\nabla\times$ of (7.24) we obtain

$$\omega(\mathbf{r},t) = \nabla\times\mathbf{v}(\mathbf{r},t) = \frac{2G}{c^2}\int d^3r' \frac{\rho(\mathbf{r}',t)}{|\mathbf{r}-\mathbf{r}'|^3}\mathbf{v}_R(\mathbf{r}',t)\times(\mathbf{r}-\mathbf{r}') + \nabla\psi, \qquad (7.25)$$

which is the Biot-Savart form for the vorticity, with the additional term being the homogeneous solution. Then (7.19) becomes an integro-differential equation for the velocity field, with ψ determined by self-consistency. As we shall see in Sect.7.8 (7.25) explains the so-called 'frame-dragging' effect in terms of this vorticity in the in-flow. Of course (7.19) and (7.25) only make sense if $\mathbf{v}_R(\mathbf{r},t)$ for the matter at location $\mathbf{r}$ is specified. We now consider the special case where the matter is subject only to the effects of motion with respect to the quantum-foam velocity-field inhomogeneities and variations in time, which causes a 'gravitational' acceleration.

We also not that (7.19) and (7.20) need to be further generalised to take account of the cosmological-scale effects, namely that the spatial system is compact and growing.

7.2 Gravitational Waves

Newtonian gravity in its original 'force' formalism (7.2) does not admit any wave phenomena. However the completely equivalent 'in-flow' formalism in (7.6) and (7.8) does admit wave phenomena. For the simpler case of zero vorticity, and so permitting the velocity potential description, and also neglecting the 'dark matter' term $C(\mathbf{v})$, then (8.5) becomes

$$\frac{\partial u}{\partial t} + \frac{1}{2}(\nabla u)^2 = -\Phi. \qquad (7.26)$$

and

$$\mathbf{g} = \frac{\partial\nabla u}{\partial t} + \frac{1}{2}\nabla(\nabla u)^2, \qquad (7.27)$$

which together reproduce (7.3), even when the flow is time-dependent. Suppose that (7.26) has for a static matter density a static solution $u_0(\mathbf{r})$ with corresponding velocity field $\mathbf{v}_0(\mathbf{r})$, and with corresponding acceleration $\mathbf{g}_0(\mathbf{r})$. Then we look for time dependent perturbative solutions of (7.26) with $u = u_0 + \overline{u}$. To first order in $\overline{u}$ we then have

$$\frac{\partial\overline{u}(\mathbf{r},t)}{\partial t} = -\nabla\overline{u}(\mathbf{r},t).\nabla u_0(\mathbf{r}). \qquad (7.28)$$

This equation is easily seen to have wave solutions of the form $\overline{u}(\mathbf{r},t) = A\cos(\mathbf{k}.\mathbf{r} - \omega t + \phi)$ where $\omega(\mathbf{k},\mathbf{r}) = \mathbf{v}_0(\mathbf{r}).\mathbf{k}$, for wavelengths short compared to the scale of

changes in $\mathbf{v}_0(\mathbf{r})$. The phase velocity of these waves is then $\mathbf{v}_\phi = \mathbf{v}_0$, and the group velocity is $\mathbf{v}_g = \nabla_k \omega = \mathbf{v}_0$. Then the velocity field is

$$\mathbf{v}(\mathbf{r}, t) = \mathbf{v}_0(\mathbf{r}) - A\mathbf{k}\sin(\mathbf{k}.\mathbf{r} - w(\mathbf{k}, \mathbf{r})t + \phi). \tag{7.29}$$

In general we have, perturbatively, the superposition of such waves, giving

$$\mathbf{v}(\mathbf{r}, t) = \mathbf{v}_0(\mathbf{r}) - \int d^3k A(\mathbf{k})\mathbf{k}\sin(\mathbf{k}.\mathbf{r} - w(\mathbf{k}, \mathbf{r})t + \phi(\mathbf{k})). \tag{7.30}$$

But are these wave solutions physical, or are they a mere artifact of the inflow formalism? First note that the wave phenomena do not cause any gravitational effects, because the acceleration field is independent of their existence; whether they are present or not does not affect $\mathbf{g}(\mathbf{r})$. This question is equivalent to asking which of the fields $\mathbf{v}$ or $\mathbf{g}$ is the fundamental quantity. As we have already noted the velocity field $\mathbf{v}$ and these wave phenomena have already been observed [17, 16]. Indeed it is even possible that the effects of such waves are present in the Michelson-Morley 1887 fringe shift data. This would imply that the real gravitational waves have actually been observed for over 100 years.

Within the new theory of gravity these waves do affect the acceleration field $\mathbf{g}$, via the new $C(\mathbf{v})$ term. Numerical studies have shown these wave effects, and that even when the 'dark matter' effect is retained this wave phenomena persists. The observational evidence is that these gravitational waves are apparently present in the Milky Way and local galactic cluster, as revealed in the analysis of data from at least three distinct observations of absolute motion effects [16].

7.3 Geodesics

We now define how the trajectory of a point object is determined by the velocity flow field, which manifests via the velocity of absolute motion of the object relative to the local space, namely via $\mathbf{v}_R$. There is a problem with terminology here: what is called absolute motion here is actually motion with respect to the local substratum structure of space, which means that it is a relative motion. However in the language and restrictions of conventional 'special relativity' all velocities are relative, where in this case it means relative to another object and *not* relative to space itself. Most significantly the geodesic equation herein involves *both* (absolute) motion with respect to space and also the relativistic time dilation effect. This latter effect involves the notion that absolute motion, whether linear or rotational, causes, say, a clock moving through space to tick more slowly than one at rest in space. Similarly in the re-analysis of the principles of operation of the Michelson interferometer it was necessary to take account of both absolute linear motion *and* the relativistic length contraction effect upon the arms of the interferometer caused by that absolute linear motion. So again to observe absolute motion we must take account of those relativistic effects which are actually caused by absolute motion.

This is contrary to the postulate by Einstein which asserts that absolute motion has no meaning and so no experimental manifestation. The GP-B experiment will, yet again, show that this key postulate is invalid, but which does not invalidate the phenomena known as 'special relativistic' effects. In terms of the history of physics it implies that we must return to the pre-Einstein ideas of Lorentz and others.

The path $\mathbf{r}_0(t)$ of an object through space is obtained by extremising the relativistic proper time

$$\tau[\mathbf{r}_0] = \int dt \left(1 - \frac{\mathbf{v}_R^2}{c^2}\right)^{1/2} \tag{7.31}$$

This entails the idea that the speed of light c is the maximum speed through the local space. This means that the speed of light is c only with respect to the local space. That it is believed that c is the speed of light for all observers in uniform linear motion, as postulated by Einstein, is an error that follows from not realising that when in motion the observer's clock and rod are affected by that motion. Without correcting for such absolute motion effects the incorrect notion of c being the 'universal speed of light' is not realised.

To extremise τ we use a small deformation of the trajectory

$$\mathbf{r}_0(t) \to \mathbf{r}_0(t) + \delta\mathbf{r}_0(t) \quad \text{giving} \quad \mathbf{v}_0(t) \to \mathbf{v}_0(t) + \frac{d\delta\mathbf{r}_0(t)}{dt}, \tag{7.32}$$

and then we also have

$$\mathbf{v}(\mathbf{r}_0(t) + \delta\mathbf{r}_0(t), t) = \mathbf{v}(\mathbf{r}_0(t), t) + (\delta\mathbf{r}_0(t).\nabla)\mathbf{v}(\mathbf{r}_0(t)) + ... \tag{7.33}$$

Then

$$\begin{aligned}
\delta\tau &= \tau[\mathbf{r}_0 + \delta\mathbf{r}_0] - \tau[\mathbf{r}_0] \\
&= -\int dt\, \frac{1}{c^2}\mathbf{v}_R.\delta\mathbf{v}_R \left(1 - \frac{\mathbf{v}_R^2}{c^2}\right)^{-1/2} + ... \\
&= \int dt \frac{1}{c^2}\left(\mathbf{v}_R.(\delta\mathbf{r}_0.\nabla)\mathbf{v} - \mathbf{v}_R.\frac{d(\delta\mathbf{r}_0)}{dt}\right)\left(1 - \frac{\mathbf{v}_R^2}{c^2}\right)^{-1/2} + ... \\
&= \int dt \frac{1}{c^2}\left(\frac{\mathbf{v}_R.(\delta\mathbf{r}_0.\nabla)\mathbf{v}}{\sqrt{1 - \frac{\mathbf{v}_R^2}{c^2}}} + \delta\mathbf{r}_0.\frac{d}{dt}\frac{\mathbf{v}_R}{\sqrt{1 - \frac{\mathbf{v}_R^2}{c^2}}}\right) + ... \\
&= \int dt\, \frac{1}{c^2}\delta\mathbf{r}_0 \,.\left(\frac{(\mathbf{v}_R.\nabla)\mathbf{v} + \mathbf{v}_R \times (\nabla \times \mathbf{v})}{\sqrt{1 - \frac{\mathbf{v}_R^2}{c^2}}} + \frac{d}{dt}\frac{\mathbf{v}_R}{\sqrt{1 - \frac{\mathbf{v}_R^2}{c^2}}}\right) + ...
\end{aligned} \tag{7.34}$$

Hence a trajectory $\mathbf{r}_0(t)$ determined by $\delta\tau = 0$ to $O(\delta\mathbf{r}_0(t)^2)$ satisfies

$$\frac{d}{dt}\frac{\mathbf{v}_R}{\sqrt{1-\frac{\mathbf{v}_R^2}{c^2}}} = -\frac{(\mathbf{v}_R.\nabla)\mathbf{v} + \mathbf{v}_R \times (\nabla \times \mathbf{v})}{\sqrt{1-\frac{\mathbf{v}_R^2}{c^2}}}. \tag{7.35}$$

Substituting $\mathbf{v}_R(t) = \mathbf{v}_0(t) - \mathbf{v}(\mathbf{r}_0(t), t)$ and using

$$\frac{d\mathbf{v}(\mathbf{r}_0(t), t)}{dt} = (\mathbf{v}_0.\nabla)\mathbf{v} + \frac{\partial \mathbf{v}}{\partial t}, \tag{7.36}$$

and then

$$\frac{d}{dt}\frac{\mathbf{v}_0}{\sqrt{1-\frac{\mathbf{v}_R^2}{c^2}}} = \mathbf{v}\frac{d}{dt}\frac{1}{\sqrt{1-\frac{\mathbf{v}_R^2}{c^2}}} + \frac{\frac{\partial \mathbf{v}}{\partial t} + (\mathbf{v}.\nabla)\mathbf{v} + (\nabla \times \mathbf{v}) \times \mathbf{v}_R}{\sqrt{1-\frac{\mathbf{v}_R^2}{c^2}}}, \tag{7.37}$$

and finally

$$\frac{d\mathbf{v}_0}{dt} = -\frac{\mathbf{v}_R}{1-\frac{\mathbf{v}_R^2}{c^2}}\frac{1}{2}\frac{d}{dt}\left(\frac{\mathbf{v}_R^2}{c^2}\right) + \left(\frac{\partial \mathbf{v}}{\partial t} + (\mathbf{v}.\nabla)\mathbf{v}\right) + (\nabla \times \mathbf{v}) \times \mathbf{v}_R. \tag{7.38}$$

This is a generalisation of the acceleration in (7.5) to include the vorticity effect , as the last term, and the first term which is the resistance to acceleration caused by the relativistic 'mass' increase effect. This term leads to the so-called geodetic effects . The vorticity term causes the GP-B gyroscopes to develop the vorticity induced precession, which is simply the rotation of space carrying the gyroscope along with it, compared to more distant space which is not involved in that rotation. The middle term, namely the acceleration in (7.5), is simply the usual Newtonian gravitational acceleration, but now seen to arise from the inhomogeneity and time-variation of the flow velocity field. As already noted it was this geodesic equation that has been checked in various experiments, but always, except in the case of the binary pulsar slow-down, with the velocity field given by the Newtonian 'inverse square law' equivalent form in (7.9). This flow is exactly equivalent to the external Schwarzschild metric. Eqn.(7.38) is a generalisation of (7.6) to include Lorentzian dynamical effects. Note that the occurrence of $1/\sqrt{1-\frac{\mathbf{v}_R^2}{c^2}}$ will lead to the precession of the perihelion of elliptical planetary orbits, and also to horizon effects wherever $|\mathbf{v}| = c$: the region where $|\mathbf{v}| < c$ is inaccessible from the region where $|\mathbf{v}| > c$. So the fluid flow dynamics in (7.19) and (7.25) and the gravitational dynamics for the matter in (7.38) now form a closed system. This system of equations is a considerable generalisation from that of Newtonian gravity, and would appear to be very different from the curved spacetime formalism of General Relativity. However we now show that General Relativity leads to a very similar system of equations,

but with one important exception, namely that the 'dark matter' 'quantum-foam' dynamics is missing from the Hilbert-Einstein theory of gravity.

The above may be modified when the 'object' is a massless photon, and the corresponding result leads to the gravitational lensing effect. But not only will ordinary matter produce such lensing, but the effective 'dark matter' density will also do so, and that is relevant to the recent observation by the weak lensing technique of the so-called 'dark matter' networks, in Sect.9.8.

7.4 The Einstein Measurement Protocol

The quantum foam, it is argued, induces actual dynamical time dilations and length contractions in agreement with the Lorentz interpretation of special relativistic effects. Then observers in uniform motion 'through' the foam will on measurement of the speed of light obtain always the same numerical value c. To see this explicitly consider how various observers $P, P', ..$ moving with different speeds through the foam, measure the speed of light. They each acquire a standard rod and an accompanying standardised clock. That means that these standard rods would agree if they were brought together, and at rest with respect to the quantum foam they would all have length Δl_0, and similarly for the clocks. Observer P and accompanying rod are both moving at speed v_R relative to the quantum foam, with the rod longitudinal to that motion. P then measures the time Δt_R, with the clock at end A of the rod, for a light pulse to travel from end A to the other end B and back again to A. The light travels at speed c relative to the quantum-foam. Let the time taken for the light pulse to travel from $A \to B$ be t_{AB} and from $B \to A$ be t_{BA}, as measured by a clock at rest with respect to the quantum foam[1]. The length of the rod moving at speed v_R is contracted to

$$\Delta l_R = \Delta l_0 \sqrt{1 - \frac{v_R^2}{c^2}}. \tag{7.39}$$

In moving from A to B the light must travel an extra distance because the end B travels a distance $v_R t_{AB}$ in this time, thus the total distance that must be traversed is

$$ct_{AB} = \Delta l_R + v_R t_{AB}, \tag{7.40}$$

Similarly on returning from B to A the light must travel the distance

$$ct_{BA} = \Delta l_R - v_R t_{BA}. \tag{7.41}$$

Hence the total travel time Δt_0 is

$$\Delta t_0 = t_{AB} + t_{BA} \quad = \quad \frac{\Delta l_R}{c - v_R} + \frac{\Delta l_R}{c + v_R} \tag{7.42}$$

[1]Not all clocks will behave in this same 'ideal' manner.

$$= \frac{2\Delta l_0}{c\sqrt{1-\frac{v_R^2}{c^2}}}. \tag{7.43}$$

Because of the time dilation effect for the moving clock

$$\Delta t_R = \Delta t_0 \sqrt{1-\frac{v_R^2}{c^2}}. \tag{7.44}$$

Then for the moving observer the speed of light is defined as the distance the observer believes the light travelled ($2\Delta l_0$) divided by the travel time according to the accompanying clock (Δt_R), namely $2\Delta l_0/\Delta t_R = c$. So the speed v_R of the observer through the quantum foam is not revealed by this procedure, and the observer is erroneously led to the conclusion that the speed of light is always c. This follows from two or more observers in manifest relative motion all obtaining the same speed c by this procedure. Despite this failure this special effect is actually the basis of the spacetime Einstein measurement protocol. That this protocol is blind to the absolute motion has led to enormous confusion within physics. Later we shall see how to overcome the 'blindness' of this procedure, and so manifestly reveal an observer's v_R.

To be explicit the Einstein measurement protocol actually inadvertently uses this special effect by using the radar method for assigning historical spacetime coordinates to an event: the observer records the time of emission and reception of radar pulses ($t_r > t_e$) travelling through the space of quantum foam, and then retrospectively assigns the time and distance of a distant event B according to (ignoring directional information for simplicity)

$$T_B = \frac{1}{2}(t_r + t_e), \quad D_B = \frac{c}{2}(t_r - t_e), \tag{7.45}$$

where each observer is now using the same numerical value of c. The event B is then plotted as a point in an individual geometrical construct by each observer, known as a spacetime record, with coordinates (D_B, T_B). This is no different to an historian recording events according to some agreed protocol. Unlike historians, who don't confuse history books with reality, physicists do so. We now show that because of this protocol and the quantum foam dynamical effects, observers will discover on comparing their historical records of the same events that the expression

$$\tau_{AB}^2 = T_{AB}^2 - \frac{1}{c^2}D_{AB}^2, \tag{7.46}$$

is an invariant, where $T_{AB} = T_A - T_B$ and $D_{AB} = D_A - D_B$ are the differences in times and distances assigned to events A and B using the Einstein measurement protocol (7.45), so long as both are sufficiently small compared with the scale of inhomogeneities in the velocity field.

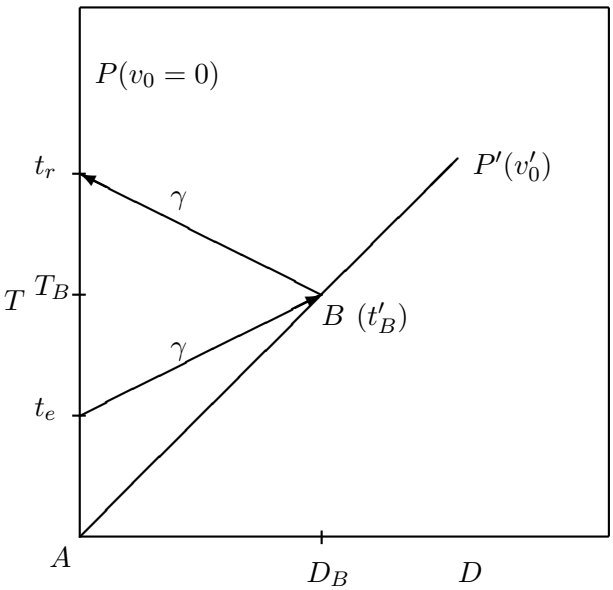

Figure 7.1: Here $T-D$ is the spacetime construct (from the Einstein measurement protocol) of a special observer P *at rest* wrt the quantum foam, so that $v_0 = 0$. Observer P' is moving with speed v'_0 as determined by observer P, and therefore with speed $v'_R = v'_0$ wrt the quantum foam. Two light pulses are shown, each travelling at speed c wrt both P and the quantum foam. As we see later these one-way speeds for light, relative to the quantum foam, are equal by observation. Event A is when the observers pass, and is also used to define zero time for each for convenience.

To confirm the invariant nature of the construct in (7.46) one must pay careful attention to observational times as distinct from protocol times and distances, and this must be done separately for each observer. This can be tedious. We now demonstrate this for the situation illustrated in Fig.7.1.

By definition the speed of P' according to P is $v'_0 = D_B/T_B$ and so $v'_R = v'_0$, where T_B and D_B are the protocol time and distance for event B for observer P according to (7.45). Then using (7.46) P would find that $(\tau^P_{AB})^2 = T^2_B - \frac{1}{c^2}D^2_B$ since both $T_A = 0$ and D_A=0, and whence $(\tau^P_{AB})^2 = (1 - \frac{v'^2_R}{c^2})T^2_B = (t'_B)^2$ where the last equality follows from the time dilation effect on the P' clock, since t'_B is the time of event B according to that clock. Then T_B is also the time that P' would compute for event B when correcting for the time-dilation effect, as the speed v'_R of P' through the quantum foam is observable by P'. Then T_B is the 'common time' for event B assigned by both observers[2]. For P' we obtain directly, also from (7.45) and (7.46), that $(\tau^{P'}_{AB})^2 = (T'_B)^2 - \frac{1}{c^2}(D'_B)^2 = (t'_B)^2$, as $D'_B = 0$ and $T'_B = t'_B$. Whence for this situation

$$(\tau^P_{AB})^2 = (\tau^{P'}_{AB})^2, \tag{7.47}$$

[2]Because of gravitational in-flow effects this 'common time' is not the same as a 'universal' or 'absolute time'; see later.

and so the construction (7.46) is an invariant.

While so far we have only established the invariance of the construct (7.46) when one of the observers is at rest wrt to the quantum foam, it follows that for two observers P' and P'' both in motion wrt the quantum foam it follows that they also agree on the invariance of (7.46). This is easily seen by using the intermediate step of a stationary observer P:

$$(\tau_{AB}^{P'})^2 = (\tau_{AB}^{P})^2 = (\tau_{AB}^{P''})^2. \tag{7.48}$$

Hence the protocol and Lorentzian effects result in the construction in (7.46) being indeed an invariant in general. This is a remarkable and subtle result. For Einstein this invariance was a fundamental assumption, but here it is a derived result, but one which is nevertheless deeply misleading. Explicitly indicating small quantities by Δ prefixes, and on comparing records retrospectively, an ensemble of nearby observers agree on the invariant

$$\Delta\tau^2 = \Delta T^2 - \frac{1}{c^2}\Delta D^2, \tag{7.49}$$

for any two nearby events. This implies that their individual patches of spacetime records may be mapped one into the other merely by a change of coordinates, and that collectively the spacetime patches of all may be represented by one pseudo-Riemannian manifold, where the choice of coordinates for this manifold is arbitrary, and we finally arrive at the invariant

$$\Delta\tau^2 = g_{\mu\nu}(x)\Delta x^\mu \Delta x^\nu, \tag{7.50}$$

with $x^\mu = \{D_1, D_2, D_3, T\}$. Eqn.(7.50) is invariant under the Lorentz transformations

$$x'^\mu = L^\mu{}_\nu x^\nu, \tag{7.51}$$

where, for example for relative motion in the x direction, $L^\mu{}_\nu$ is specified by

$$\begin{aligned} x' &= \frac{x - vt}{\sqrt{1 - v^2/c^2}}, \\ y' &= y, \\ z' &= z, \\ t' &= \frac{t - vx/c^2}{\sqrt{1 - v^2/c^2}}. \end{aligned} \tag{7.52}$$

7.5 Galilean Relativity and Special Relativity

The previous section has resulted in an unusual outcome. Galilean Relativity was the first relativity principle considered in physics, and corresponds to the following

transformation rule relating position and time measurements between observers in relative motion

$$x'^{\mu} = \mathcal{G}^{\mu}{}_{\nu} x^{\nu}, \tag{7.53}$$

where, also for relative motion in the x direction, $\mathcal{G}^{\mu}{}_{\nu}$ is specified by

$$\begin{aligned} x' &= x - vt, \\ y' &= y, \\ z' &= z, \\ t' &= t. \end{aligned} \tag{7.54}$$

In current physics this transformation is regarded as the limiting form of the Lorentz transformation when the speed of relative motion of the two observers v is small compared to the speed of light c. This amounts to the belief that the Galilean transformation is fundamentally incorrect. However it is now becoming clear that this is not the correct interpretation of the relationship between these two relativity principles. The real difference between the Lorentz transformation, as in (7.52), and the corresponding Galilean transformation in (7.54), is that the Lorentz transformation is relating uncorrected or 'raw' observational data, after using only the Einstein measurement protocol, while the Galilean transformation is relating that same data after correcting for the effects of absolute motion on the rods and clocks used in collecting that data. In the Galilean case one must also use a measurement protocol which takes account of the fact that the speed of light is c only with respect to the preferred frame of reference. Then observers must also take measurements of their own absolute velocities with respect to that special frame, before correcting their own 'raw' data. Hence the coordinates x^{μ} in (7.52) and in (7.54) refer to fundamentally different kinds of data. That data becomes the same when $v << c$. Hence the Lorentz transformation and the Galilean are both physically correct, which means that both correctly represent reality. This outcome is of course a radical development. For the Galilean case one must determine motion relative to absolute space which, as discussed extensively throughout this book, has been possible for more than a century, though always denied by physicists. The Lorentz transformation was originally formulated with a special frame of reference in mind, that is that absolute motion was causing length contractions and time dilation effects.

To emphasise the role of the Galilean transformation we not that the (7.19)-(7.20) are covariant with respect to a change of observer, but that they are not covariant with respect to a change in the velocity field of the matter density, measured with respect to the (local) quantum foam state - an absolute quantity. Suppose we have an observer for whom the matter density is $\rho(\mathbf{r}, t)$. Then let (7.19)-(7.20) have solution $\mathbf{v}_0(\mathbf{r}, t)$. Then for a second observer moving at velocity $-\mathbf{V}$ with respect to the first observer, the equations for the velocity field now involve a matter density $\rho(\mathbf{r} + \mathbf{V}t, t)$. Then for the second observer (7.19)-(7.20) has solution

$$\mathbf{v}(\mathbf{r}, t) = \mathbf{v}_0(\mathbf{r} + \mathbf{V}t, t) - \mathbf{V}. \tag{7.55}$$

Note that this change of observer is a manifestly time-dependent process and the time derivatives play an essential role. As well the result is nontrivial as (7.19)-(7.20) is a non-linear system. The solution (7.55) follows from noting that, for example,

$$\begin{aligned}
\mathbf{g}(\mathbf{r},t) &= \frac{\partial \mathbf{v}_0(\mathbf{r}+\mathbf{V}t,t)}{\partial t} + ((\mathbf{v}_0(\mathbf{r}+\mathbf{V}t,t)-\mathbf{V}).\nabla)(\mathbf{v}_0(\mathbf{r}+\mathbf{V}t,t)-\mathbf{V}),\\
&= \left.\frac{\partial \mathbf{v}_0(\mathbf{r}+\mathbf{V}t',t)}{\partial t'}\right|_{t'\to t} + \mathbf{g}_0(\mathbf{r}+\mathbf{V}t,t) - (\mathbf{V}.\nabla)\mathbf{v}_0(\mathbf{r}+\mathbf{V}t,t),\\
&= +(\mathbf{V}.\nabla)\mathbf{v}_0(\mathbf{r}+\mathbf{V}t,t) + \mathbf{g}_0(\mathbf{r}+\mathbf{V}t,t) - (\mathbf{V}.\nabla)\mathbf{v}_0(\mathbf{r}+\mathbf{V}t,t),\\
&= \mathbf{g}_0(\mathbf{r}+\mathbf{V}t,t), \qquad (7.56)
\end{aligned}$$

as there is a key cancellation of two terms in (7.56), and that as well, for example, clearly $C(\mathbf{v}_0(\mathbf{r}+\mathbf{V}t,t)-\mathbf{V}) = C(\mathbf{v}_0(\mathbf{r}+\mathbf{V}t,t))$, and so this term is also simply translated. At the same time $\mathbf{v}_R$ on the RHS of the equations is *unchanged* by a change of observer. Hence the Galilean velocity transformation law (7.55) is appropriate. However the effects associated with, say, a rigid body moving through the quantum foam is a non-trivial problem, as clearly then, for example, additional vorticity effects will arise. In this case the velocity field cannot be obtained by use of the Galilean velocity transformation rule. Hence in the new physics Galilean relativity transformations between different observers measurements coexist with an absolute (local) frame of reference. This is a different scenario from that usually thought of in connection with these transformations. Further discussion is in Sect.7.9.

The restored significance and role for the Galilean transformation raises important questions about the Maxwell theory of electrodynamics. The equations of this theory are covariant under the Lorentz transformation, and the successes of this theory have always been used to argue for the validity of the Special Relativity, and for the invalidity of Galilean Relativity. However the validity of this argument is now suspect. It is almost certainly the case that the Maxwell theory will need to be modified to take account of the effects associated with a preferred frame. This is not discussed in this book except for some special evidence that has emerged. The first evidence is that Michelson interferometers can only act as absolute motion detectors when the light passes through a gas, and fail when the light passes though a vacuum. The original Michelson-Morley experiment used air. A related piece of evidence, reported in Sect.12.2, is that a Michelson interferometer in which the light passes through a transparent solid is unable to detect absolute motion, just as when the light passes through a vacuum[3]. Hence the electromagnetic properties of solids in absolute motion appear to be different to the case of a gas. The most likely explanation is that for a solid a real dynamical length contraction results in a change not only of the length but also of the refractive index in the direction of motion. When the transparent solid is transverse to the direction of motion then there is still a length contraction, but now essentially orthogonal to the light path.

[3]However a combination of one air path and one transparent solid path can be used in an interferometer to detect absolute motion

But of course being a solid, contractions in one direction will have an effect on the lengths in the other two directions. We will also have the corresponding effects on the refractive index in each direction, so that it becomes anisotropic simply because of the absolute motion. As well a new theory of electromagnetism is required to explain the Fresnel drag effect. The important outcome here is that we have *both* Galilean Relativity and Special Relativity.

7.6 The Origins of General Relativity

Above it was seen that the Lorentz symmetry of the spacetime construct would arise if the quantum foam system that forms space affects the rods and clocks used by observers in the manner indicated. The effects of absolute motion with respect to this quantum foam are in fact easily observed, and so the velocity $\mathbf{v}_R$ of each observer is measurable. However if we work only with the spacetime construct then the effects of the absolute motion are hidden. Einstein was very much misled by the reporting of the experiment by Michelson and Morley of 1887, as now (see later) it is apparent that this experiment, and others since then, revealed evidence of absolute motion. The influence of the Michelson-Morley experiment had a major effect on the subsequent development of physics. One such development was the work of Hilbert and Einstein in finding an apparent generalisation of Newtonian gravity to take into account the apparent absence of absolute motion. Despite the deep error in this work the final formulation, known as General Relativity, has had a number of putative successes including the perihelion precession of mercury, the bending of light and gravitational red shift. Hence despite the incorrect treatment of absolute motion the formalism of General Relativity apparently has some validity. In the next chapter we shall *deconstruct* this formalism to discover its underlying physics, but here we first briefly outline the GR formalism.

The spacetime construct is a static geometrical non-processing historical record, and is nothing more than a very refined history book, with the shape of the manifold encoded in a metric tensor $g_{\mu\nu}(x)$. However in a formal treatment by Einstein the SR formalism and later the GR formalism is seen to arise from three fundamental assumptions:

(1) **The laws of physics have the same form in all inertial reference frames.**

(2) **Light propagates through empty space with a definite speed c independent of the speed of the source or observer.**

(3) **In the limit of low speeds the new formalism should agree with Newtonian gravity.** (7.57)

We shall see in later chapters there is strong evidence that all three of these assumptions are in fact wrong, except for the second part of (2). Nevertheless there

is something that is partially correct within the formalism, and that part needs to be extracted and saved, with the rest discarded. From the above assumptions Hilbert and Einstein guessed the equation which specify the metric tensor $g_{\mu\nu}(x)$, namely the geometry of the spacetime construct,

$$G_{\mu\nu} \equiv R_{\mu\nu} - \frac{1}{2}Rg_{\mu\nu} = \frac{8\pi G}{c^2}T_{\mu\nu}, \tag{7.58}$$

where $G_{\mu\nu}$ is the Einstein tensor, $T_{\mu\nu}$ is the energy-momentum tensor, $R_{\mu\nu} = R^{\alpha}_{\mu\alpha\nu}$ and $R = g^{\mu\nu}R_{\mu\nu}$ and $g^{\mu\nu}$ is the matrix inverse of $g_{\mu\nu}$. The curvature tensor is

$$R^{\rho}_{\mu\sigma\nu} = \Gamma^{\rho}_{\mu\nu,\sigma} - \Gamma^{\rho}_{\mu\sigma,\nu} + \Gamma^{\rho}_{\alpha\sigma}\Gamma^{\alpha}_{\mu\nu} - \Gamma^{\rho}_{\alpha\nu}\Gamma^{\alpha}_{\mu\sigma}, \tag{7.59}$$

where $\Gamma^{\alpha}_{\mu\sigma}$ is the affine connection

$$\Gamma^{\alpha}_{\mu\sigma} = \frac{1}{2}g^{\alpha\nu}\left(\frac{\partial g_{\nu\mu}}{\partial x^{\sigma}} + \frac{\partial g_{\nu\sigma}}{\partial x^{\mu}} - \frac{\partial g_{\mu\sigma}}{\partial x^{\nu}}\right). \tag{7.60}$$

In this formalism the trajectories of test objects are determined by

$$\frac{d^2x^{\lambda}}{d\tau^2} + \Gamma^{\lambda}_{\mu\nu}\frac{dx^{\mu}}{d\tau}\frac{dx^{\nu}}{d\tau} = 0, \tag{7.61}$$

which is equivalent to extremising the functional

$$\tau[x] = \int dt\sqrt{g_{\mu\nu}\frac{dx^{\mu}}{dt}\frac{dx^{\nu}}{dt}}, \tag{7.62}$$

with respect to the path $x[t]$. This is precisely equivalent to (7.31).

In the case of a spherically symmetric mass M the well known solution of (7.58) outside of that mass is the external-Schwarzschild metric

$$d\tau^2 = (1 - \frac{2GM}{c^2r})dt^2 - \frac{1}{c^2}r^2(d\theta^2 + \sin^2(\theta)d\phi^2) - \frac{dr^2}{c^2(1 - \frac{2GM}{c^2r})}. \tag{7.63}$$

This solution is the basis of various experimental checks of General Relativity in which the spherically symmetric mass is either the sun or the earth. The four tests are: the gravitational redshift, the bending of light, the precession of the perihelion of Mercury (but see Sect.7.7 for deep problems with this test), and the time delay of radar signals.

However the solution (7.63) is in fact completely equivalent to the in-flow interpretation of Newtonian gravity. Making the change of variables $t \to t'$ and $\mathbf{r} \to \mathbf{r}' = \mathbf{r}$ with

$$t' = t + \frac{2}{c}\sqrt{\frac{2GMr}{c^2}} - \frac{4GM}{c^2}\tanh^{-1}\sqrt{\frac{2GM}{c^2r}}, \tag{7.64}$$

the Schwarzschild solution (7.63) takes the form

$$d\tau^2 = dt'^2 - \frac{1}{c^2}(dr' + \sqrt{\frac{2GM}{r'}}dt')^2 - \frac{1}{c^2}r'^2(d\theta'^2 + \sin^2(\theta')d\phi'), \tag{7.65}$$

which is exactly the Panlevé-Gullstrand form of the metric $g_{\mu\nu}$ [56, 57] with the velocity field given exactly by the Newtonian form in (7.9). In which case the geodesic equation (7.61) of test objects in the Schwarzschild metric is equivalent to solving (7.38). This choice of coordinates corresponds to a particular frame of reference in which the test object has velocity $\mathbf{v}_R = \mathbf{v} - \mathbf{v}_0$ relative to the inflow field $\mathbf{v}$, as seen in (7.31). This results shows that the Schwarzschild metric in GR is completely equivalent to Newton's inverse square law: GR in this case is nothing more than Newtonian gravity in disguise. So the so-called 'tests' of GR were nothing more than a test of the geodesic equation, where most simply this is seen to determine the motion of an object relative to an absolute local frame of reference - the quantum foam frame.

It is conventional wisdom for practitioners in General Relativity to regard the choice of coordinates or frame of reference to be entirely arbitrary and having no physical significance: no observations should be possible that can detect and measure $\mathbf{v}_R$. This 'wisdom' is based on two beliefs (i) that all attempts to detect $\mathbf{v}_R$, namely the detection of absolute motion, have failed, and that (ii) the existence of absolute motion is incompatible with the many successes of both the Special Theory of Relativity and of the General Theory of Relativity. Both of these beliefs are demonstrably false.

The results in this section suggest, just as for Newtonian gravity, that the Einstein General Relativity is nothing more than the dynamical equations for a velocity flow field $\mathbf{v}(\mathbf{r}, t)$. Hence the non-flat spacetime construct appears to be merely an unnecessary artifact of the Einstein measurement protocol, which in turn was motivated by the mis-reporting of the results of the Michelson-Morley experiment [16]. The putative successes of General Relativity should thus be considered as an insight into the fluid flow dynamics of the quantum foam system, rather than any confirmation of the validity of the spacetime formalism, and it was this insight that in [15] led, in part, to the flow dynamics in (7.19) and (7.20). Let us therefore substitute the metric

$$d\tau^2 = g_{\mu\nu}dx^\mu dx^\nu = dt^2 - \frac{1}{c^2}(d\mathbf{r}(t) - \mathbf{v}(\mathbf{r}(t), t)dt)^2, \tag{7.66}$$

into (7.58) using (7.60) and (7.59). This metric involves the arbitrary time-dependent velocity field $\mathbf{v}(\mathbf{r}, t)$. The various components of the Einstein tensor are then found to be

$$\begin{aligned} G_{00} &= \sum_{i,j=1,2,3} v_i \mathcal{G}_{ij} v_j - c^2 \sum_{j=1,2,3} \mathcal{G}_{0j} v_j - c^2 \sum_{i=1,2,3} v_i \mathcal{G}_{i0} + c^2 \mathcal{G}_{00}, \\ G_{i0} &= -\sum_{j=1,2,3} \mathcal{G}_{ij} v_j + c^2 \mathcal{G}_{i0}, \qquad i = 1, 2, 3. \end{aligned}$$

$$G_{ij} \;=\; \mathcal{G}_{ij}, \qquad i,j=1,2,3. \tag{7.67}$$

where the $\mathcal{G}_{\mu\nu}$ are given by

$$\begin{aligned}
\mathcal{G}_{00} &= \frac{1}{2}((trD)^2 - tr(D^2)),\\
\mathcal{G}_{i0} &= \mathcal{G}_{0i} = -\frac{1}{2}(\nabla\times(\nabla\times\mathbf{v}))_i, \qquad i=1,2,3.\\
\mathcal{G}_{ij} &= \frac{d}{dt}(D_{ij}-\delta_{ij}trD) + (D_{ij}-\frac{1}{2}\delta_{ij}trD)trD\\
&\quad -\frac{1}{2}\delta_{ij}tr(D^2) + (\Omega D - D\Omega)_{ij}, \qquad i,j=1,2,3.
\end{aligned} \tag{7.68}$$

In vacuum, with $T_{\mu\nu}=0$, we find from (7.58) and (7.67) that $G_{\mu\nu}=0$ implies that $\mathcal{G}_{\mu\nu}=0$. This system of equations is thus very similar to the in-flow dynamics in (7.19) and (7.20), except that in vacuum GR, for the Panlevé-Gullstrand metric, demands that

$$((trD)^2 - tr(D^2)) = 0. \tag{7.69}$$

This simply corresponds to the fact that GR does not permit the 'dark matter' effect, namely that $\rho_{DM}=0$, according to (7.14), and this happens because GR was forced to agree with Newtonian gravity, in the appropriate limits, and that theory also has no such effect. As well in GR the energy-momentum tensor $T_{\mu\nu}$ is not permitted to make any reference to absolute linear motion of the matter; only the relative motion of matter or absolute rotational motion is permitted.

It is very significant to note that the above exposition of the GR formalism for the Panlevé-Gullstrand metric is exact. Then taking the trace of the $\mathcal{G}_{ij}$ equation in (7.68) we obtain, also exactly, and again using the identity in (7.17), and in the case of zero vorticity, and outside of matter so that $T_{\mu\nu}=0$,

$$\frac{\partial}{\partial t}(\nabla.\mathbf{v}) + \nabla.((\mathbf{v}.\nabla)\mathbf{v}) = 0, \tag{7.70}$$

which is the Newtonian 'velocity field' formulation of Newtonian gravity outside of matter. This should have been expected as it corresponds to the previous observation that 'Newtonian in-flow' velocity field is exactly equivalent to the external Schwarzschild metric. So again we see the extreme paucity of new physics in the GR formalism: all the key tests of GR are now seen to amount to a test *only* of $\delta\tau[x]/\delta x^\mu = 0$, when the in-flow field is given by (7.68), and which is nothing more than Newtonian gravity. Of course Newtonian gravity was itself merely based upon observations within the solar system, and this was too special to have revealed key aspects of gravity. Hence, despite popular opinion, the GR formalism is based upon very poor evidence. Indeed there is only one definitive confirmation of the GR formalism apart from the misleading external-Schwarzschild metric cases, namely the observed decay of the binary pulsar orbital motion, for only in this case is the metric non-Schwarzschild, and therefore non-Newtonian. However the new theory of

gravity also leads to the decay of orbits, and on the grounds of dimensional analysis we would expect comparable predictions. So GR is not unique in predicting orbital decay.

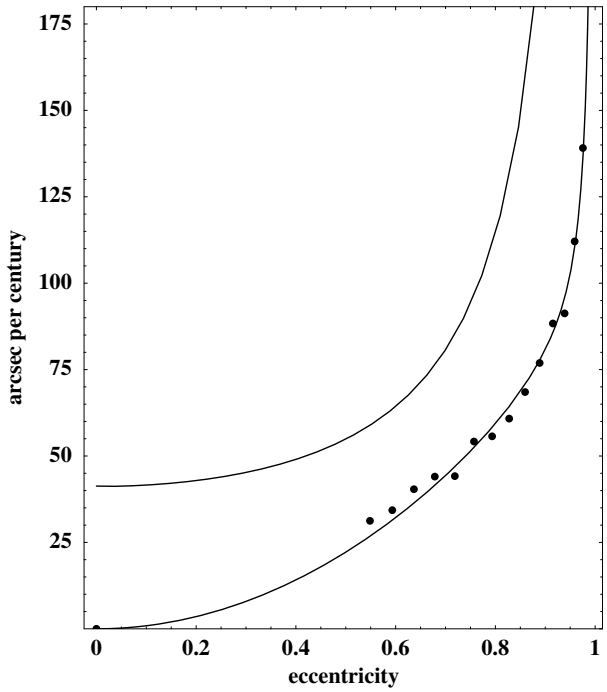

Figure 7.2: Plots of the precession of the perihelion of mercury in arcsec per century versus possible eccentricities, with the semimajor axis of the ellipse fixed at $a = 57.91 \times 10^6$ km. The actual eccentricty is $e = 0.2056$. The upper plot shows the standard result from General Relativity, as in (7.71), which has an unphysical non-zero precession even for a circular orbit, with $e = 0$. This suggests an error in the usual approximate analytic analysis. The data points follow from the numerical solution of (7.72) and (7.73) for various eccentricities. For small eccentricities an extrapolation to zero precession for $e = 0$ is used, using the fitted form in (7.85). This gives a precession of $\Delta\phi = 3.8$ arcsec/century as the corrected prediction from General Relativity, and also from the new theory of gravity in the absence of the 'dark matter' effect. This disagreement with the observed non-Newtonian component of the precession implies that General Relativity actually failed in this test. It is argued that the 'dark matter' effect within the new theory of gravity is required to fully explain this precession.

7.7 Precession of the Perihelion of Mercury

One of the first tests of General Relativity was the computation by Einstein of the precession of the perihelion of mercury. This involved determining the orbit from solving the geodesic equation in (7.61) for the case of the Schwarzschild metric in

(7.63), using approximate analytic methods; see [63] for one of many presentations of that analysis. The result was that the perihelion of mercury should precess in an advancing sense by

$$\Delta\phi = \frac{6\pi GM}{ac^2(1-e^2)} \text{ radians/revolution,} \tag{7.71}$$

where M is the mass of the sun, $a = 57.91 \times 10^6$km is the semimajor axis of the elliptical orbit of mercury, and $e = 0.2056$ is the eccentricity of that ellipse. Then (7.71) gives a rate of precession of 43.03 arcsec/century. Old observations of mercury were re-analysed by Clemence [64] in 1943, giving $\Delta\phi = 43.11 \pm 0.45$ arcsec/century, and so apparently in excellent agreement with General Relativity. However it should be noted that the above 'observed value' is arrived at after accounting for most of the observed precession as being caused by Newtonian gravitational effects of the other planets, and so the residual component of $\Delta\phi = 43.11 \pm 0.45$ arcsec/century is that which could not be explained by Newtonian gravity. Similar and apparently successful agreements were also obtained for other planets and for Icarus. This test of the General Relativity account of the phenomenon of gravity has always been regarded as one of its most well established successes.

However the General Relativity precession result in (7.71) is manifestly incorrect: it predicts that even a circular orbit, with $e = 0$, would precess. But such a precession is unphysical; what observation could be used to observe the precession of a circular orbit? Fig.7.2 shows the precession in (7.71) for mercury as we artificially vary only the eccentricty, and we clearly see the anomalous result for small eccentricities, as we approach the limit of a circular orbit. So clearly there is a fundamental and longstanding error in the usual derivation of orbit precessions from General Relativity, and the famous agreements with the 'observed values' may have been fortuitous and misleading.

To resolve this problem numerical solutions of the geodesic equation will now be given, for by using numerical techniques we of course avoid any subtle errors in the analytic analysis. As already noted the use of the Schwarzschild metric is completely equivalent to solving the geodesic equation (7.38) with the velocity field given in (7.9). For the new theory this involves neglecting any 'dark matter' effects, and also neglecting vorticity effects. As well using this formalism avoids the ontologically invalid introduction of the spacetime metric, particularly as the velocity in-flow has been observed, as discussed in Sect.11.1. To that end we write (7.38) in polar coordinates

$$\ddot{r} - r\dot{\theta}^2 = -\frac{1}{2c^2(1-\mathbf{v}_R^2/c^2)}\frac{d(\mathbf{v}_R{}^2)}{dt}\mathbf{v}_R.\hat{\mathbf{r}} - \frac{GM}{r^2}, \tag{7.72}$$

$$2\dot{r}\dot{\theta} + r\ddot{\theta} = -\frac{1}{2c^2(1-\mathbf{v}_R^2/c^2)}\frac{d(\mathbf{v}_R{}^2)}{dt}\mathbf{v}_R.\hat{\theta} \tag{7.73}$$

and where

$$\mathbf{v}_R = \left(\sqrt{\frac{2GM}{r}} + \dot{r} \right) \hat{\mathbf{r}} + r\dot{\theta}\hat{\theta}, \tag{7.74}$$

is the total velocity of the planet relative to the local substratum, which is in-flowing past the planet towards the sun, which results in a radial outward velocity component of $+\sqrt{\frac{2GM}{r}}$, as the planet is moving against this in-flow; see Fig.10.5. We ignore, for the moment, the effects of the absolute linear motion of the solar system through this substratum. Here $\hat{\mathbf{r}}$ and $\hat{\theta}$ are the usual polar coordinate unit vectors. Eqns.(7.73) and (7.74) give, after keeping terms only to $O(\mathbf{v}_R^2/c^2)$,

$$2\dot{r}\dot{\theta} + r\ddot{\theta} = -\frac{1}{2c^2}\frac{d({\mathbf{v}_R}^2)}{dt} r\dot{\theta} \tag{7.75}$$

or

$$\frac{d\,\ln(r^2\dot{\theta})}{dt} = -\frac{1}{2c^2}\frac{d({\mathbf{v}_R}^2)}{dt} \tag{7.76}$$

giving

$$r^2\dot{\theta} = he^{-\mathbf{v}_R^2/2c^2} \tag{7.77}$$

where h is an integration constant. We can now express $\mathbf{v}_R^2$ in terms of r and $\dot{r}$ to terms of order $1/c^2$. From (7.74) and (7.77) we obtain

$$\mathbf{v}_R^2 = \left(\sqrt{\frac{2GM}{r}} + \dot{r} \right)^2 + \frac{h^2 e^{-\mathbf{v}_R^2/c^2}}{r^2}. \tag{7.78}$$

Solving this to order $O(1/c^2)$ we obtain

$$\mathbf{v}_R^2 = \left(\sqrt{\frac{2GM}{r}} + \dot{r} \right)^2 + \frac{h^2}{r^2} + O(\frac{1}{c^2}). \tag{7.79}$$

Substituting this and (7.77) into (7.72) gives the one uncoupled equation for the radius $r(t)$ of the orbit as a function of time, and to leading order this is

$$\ddot{r} - \frac{h^2}{r^3}(1 - \frac{\mathbf{v}_R^2}{c^2}) = -\frac{1}{2c^2}\frac{d({\mathbf{v}_R}^2)}{dt} \left(\sqrt{\frac{2GM}{r}} + \dot{r} \right) - \frac{GM}{r^2}, \tag{7.80}$$

with ${\mathbf{v}_R}^2$ given by (7.79).

First we need to verify that (7.80) has circular orbit solutions. For such orbits, with $r = a$, $\dot{r} = 0, \ddot{r} = 0$, and (7.73) gives

$$\dot{\theta}(t) = \sqrt{\frac{GM}{a^3}}, \tag{7.81}$$

which gives Kepler's Law for the period of the planet

$$T^2 = \frac{(2\pi)^2 a^3}{GM}. \tag{7.82}$$

We also find that

$$|\mathbf{v}_R| = \sqrt{\frac{3GM}{a}}, \tag{7.83}$$

and

$$h^2 = GMa \exp\left(\frac{3GM}{ac^2}\right). \tag{7.84}$$

We see that of course there is no notion of this circular orbit 'precessing'.

For elliptical orbits we solve (7.80) and (7.79) numerically. This is actually a very difficult numerical problem as the orbit must be computed to very high precision, because the precession per orbit is very small. To achieve this the differential equation solver package **NDSolve** in *Mathematica* v5 was run under Mac OS X on a 64 bit Powerbook G4. Earlier versions of Mathematica and/or 32 bit machines are not capable of the required precision. Even then there was a limit to the smallest eccentricity for which the results were of sufficient accuracy, as shown by the data points in Fig.7.2. The analytic form for the precession

$$\Delta\phi = \frac{6\pi GM(b\, e^2 + d\, e^4)}{ac^2(1-e^2)} \tag{7.85}$$

was fitted to the data points, together with the known solution $\Delta\phi = 0$ at $e = 0$, by choosing values for the parameters b and d, giving the lower curve in Fig.7.2. For the actual eccentricity of mercury this then gives $\Delta\phi = 3.8$ arcsec/century, leaving a residual precession of 39 arcsec/century. So we see that the putative success of General Relativity in explaining the precession of the perihelion of mercury was actually fortuitous. In reality General Relativity failed this test.

A first possible explanation for the above residual precession is that it could be caused by the absolute motion of the solar system. This effect is easily incorporated into the above equations by adding a fixed velocity vector to $\mathbf{v}_R$ in (7.74). However this absolute velocity of the solar system is known to be perpendicular to the plane of the ecliptic, and numerical solutions of the geodesic equation, of the form described above, show that because of this direction there is a negligible effect upon the rate of precession.

Another possible explanation is that the presence of the planets within the solar system breaks the spherical symmetry of the matter distribution, in which case the 'dark matter' effect will have an effect on the in-flow velocity, which will no longer be described by the special form in (7.9). The deviations from this form require the solution of the velocity flow equations, and this requires modelling of the matter distribution of the planets etc. The net effect is an increased in-flow, particularly in the plane of the ecliptic, causing a slightly larger gravitational acceleration towards

the sun. This provides an excellent opportunity to check the new theory of gravity as once the matter distribution is known the magnitude of this effect should be determined by the fine structure constant. Such detailed numerical studies are not reported here. As well this slightly increased gravitational acceleration in the plane of the ecliptic, and directed towards the sun, may also be of the same origin as the inward acceleration known as the Pioneer 10/11 anomalous acceleration. So the precession the perihelion of mercury may finally be understood as an effect of the in-flow of quantum foam past the earth towards the sun, and with such an in-flow affected by the planets in a non-Newtonian manner, that is with a self-interaction of space triggered by the presence of the planets, and with a magnitude set by the fine structure constant.

7.8 Gravity Probe B Gyroscope Experiment

The Stanford University-NASA Gravity Probe B satellite experiment has the capacity to measure the precession of four on-board gyroscopes to unprecedented accuracy [58, 59, 60, 61, 62]. The experiment was proposed independently by George Pugh in 1959 and Leonard Schiff in 1960. Such a precession is predicted by the Einstein theory of gravity, General Relativity (GR), with two components: (i) a geodetic precession, and (ii) a 'frame-dragging' precession known as the Lense-Thirring effect. The latter is a particularly interesting effect induced by the rotation of the earth, and described in GR in terms of a 'gravitomagnetic' field. According to GR this smaller effect will give a precession perpendicular to the plane of the satellite orbit accumulating to 0.042 arcsec per year for the GP-B gyroscopes. However the new theory gives a different account of gravity. Here we show that GR and the new theory make very different predictions for the 'frame-dragging' effect, and so the GP-B experiment will be able to decisively test both theories. While predicting the same earth-rotation induced precession, the new theory has an additional much larger 'frame-dragging' effect caused by the observed translational motion of the earth, and in a different direction to the earth induced rotation induced precession. As well the new non-metric theory explains the 'frame-dragging' effect in terms of vorticity in a 'substratum flow'. This 'flow' exhibits fluctuations or wave effects that have already been seen in at least three experiments. These are the gravitational waves of the new theory of gravity, and are completely different from the gravitational waves predicted by General Relativity. The magnitude and signature of this new component of the gyroscope precession is predicted, which it is predicted will be detectable by the GP-B experiment.

Here we consider one difference between the two theories, namely that associated with the vorticity part of (7.38), leading to the 'frame-dragging' or Lense-Thirring effect. In GR the vorticity field is known as the 'gravitomagnetic' field $\mathbf{B} = -c\vec{\omega}$. In both GR and the new theory the vorticity is given by (7.25) but with a key difference: in GR $\mathbf{v}_R$ is *only* the rotational velocity of the matter in the earth, whereas in (7.19)

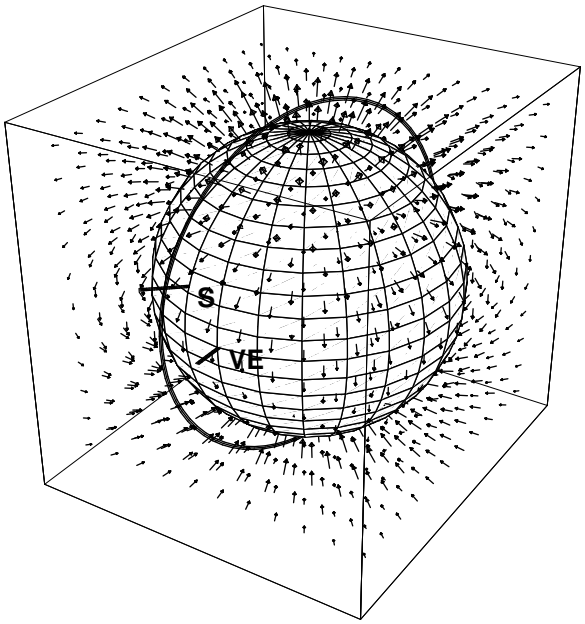

Figure 7.3: Shows the earth (N is up) and vorticity vector field component $\vec{\omega}$ induced by the rotation of the earth, as in (7.86). The polar orbit of the GP-B satellite is shown, **S** is the gyroscope starting spin orientation, directed towards the guide star IM Pegasi, RA = $22^h\ 53'\ 2.26''$, Dec = $16^0\ 50'\ 28.2''$, and **VE** is the vernal equinox.

and (7.20) $\mathbf{v}_R$ is the vector sum of the rotational velocity and the translational velocity of the earth through the substratum. At least seven experiments have detected this translational velocity; some were gas-mode Michelson interferometers and others coaxial cable experiments, as extensively discussed in Part III, and the translational velocity is now known to be approximately 430 km/s in the direction RA = 5.2^h, Dec= -67^0. This direction has been known since the Miller [123] gas-mode interferometer experiment, but the RA was more recently confirmed by the 1991 DeWitte coaxial cable experiment performed in the Brussels laboratories of Belgacom. This flow is related to galactic gravity flow effects, and so is different to that of the velocity of the earth with respect to the Cosmic Microwave Background (CMB), which is 369 km/s in the direction RA $= 11.20^h, \text{Dec} = -7.22^0$.

First consider the common but much smaller rotation induced 'frame-dragging' or vorticity effect. Then $\mathbf{v}_R(\mathbf{r}) = \mathbf{w} \times \mathbf{r}$ in (7.25), where $\mathbf{w}$ is the angular velocity of the earth, giving

$$\vec{\omega}(\mathbf{r}) = 4\frac{G}{c^2}\frac{3(\mathbf{r}.\mathbf{L})\mathbf{r} - r^2\mathbf{L}}{2r^5}, \tag{7.86}$$

where $\mathbf{L}$ is the angular momentum of the earth, and $\mathbf{r}$ is the distance from the centre. This component of the vorticity field is shown in Fig.7.3. Vorticity may be detected by observing the precession of the GP-B gyroscopes. The vorticity term in

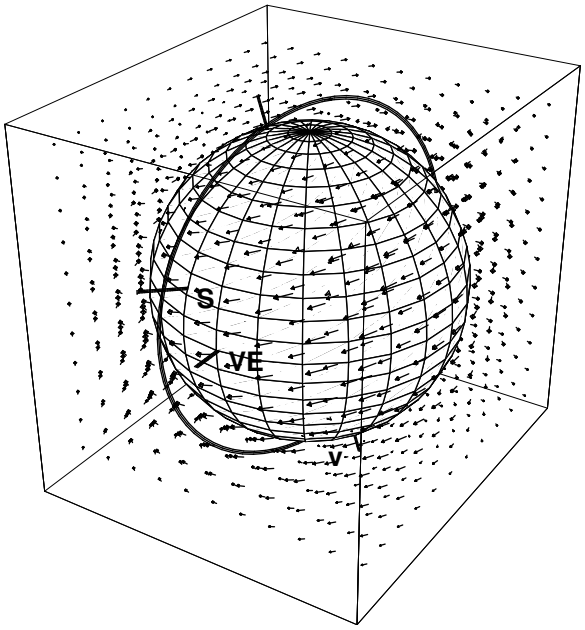

Figure 7.4: Shows the earth (N is up) and the much larger vorticity vector field component $\vec{\omega}$ induced by the translation of the earth, as in (7.89). The polar orbit of the GP-B satellite is shown, and **S** is the gyroscope starting spin orientation, directed towards the guide star IM Pegasi, RA = $22^h\ 53'\ 2.26''$, Dec = $16^0\ 50'\ 28.2''$, **VE** is the vernal equinox, and **V** is the direction RA = 5.2^h, Dec = -67^0 of the translational velocity $\mathbf{v}_c$.

(7.37) leads to a torque on the angular momentum **S** of the gyroscope,

$$\vec{\tau} = \int d^3r\rho(\mathbf{r})\ \mathbf{r} \times (\vec{\omega}(\mathbf{r}) \times \mathbf{v}_R(\mathbf{r})), \tag{7.87}$$

where ρ is its density, and where $\mathbf{v}_R$ is used here to describe the rotation of the gyroscope. Then $d\mathbf{S} = \vec{\tau}dt$ is the change in **S** over the time interval dt. In the above case $\mathbf{v}_R(\mathbf{r}) = \mathbf{s} \times \mathbf{r}$, where **s** is the angular velocity of the gyroscope. This gives

$$\vec{\tau} = \frac{1}{2}\vec{\omega} \times \mathbf{S} \tag{7.88}$$

and so $\vec{\omega}/2$ is the instantaneous angular velocity of precession of the gyroscope. This corresponds to the well known fluid result that the vorticity vector is twice the angular velocity vector. For GP-B the direction of **S** has been chosen so that this precession is cumulative and, on averaging over an orbit, corresponds to some 7.7×10^{-6} arcsec per orbit, or 0.042 arcsec per year. GP-B has been superbly engineered so that measurements to a precision of 0.0005 arcsec are possible.

However for the unique translation-induced precession if we use $v_R \approx v_C = 430$ km/s in the direction RA = 5.2^{hr}, Dec = -67^0, namely ignoring the effects of the

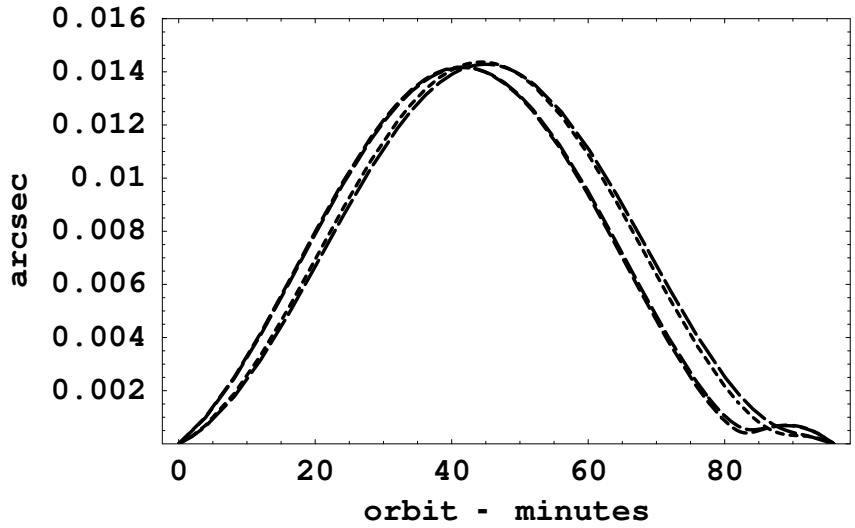

Figure 7.5: Predicted variation of the precession angle $\Delta\Theta = |\Delta\mathbf{S}(t)|/|\mathbf{S}(0)|$, in arcsec, over one 97 minute GP-B orbit, from the vorticity induced by the translation of the earth, as given by (7.90). The orbit time begins at location **S**. Predictions are for the months of April, August, September and February, labeled by increasing dash length. The 'glitches' near 80 minutes are caused by the angle effects in (7.90). These changes arise from the effects of the changing orbital velocity of the earth about the sun. The GP-B expected angle measurement accuracy is 0.0005 arcsec. The gravitational waves will affect these plots, as shown in Fig.7.7 for 40 orbits.

orbital motion of the earth, the observed flow past the earth towards the sun, and the flow into the earth, and effects of the gravitational waves, then (7.25) gives

$$\vec{\omega}(\mathbf{r}) = \frac{2GM}{c^2}\frac{\mathbf{v}_C \times \mathbf{r}}{r^3}. \tag{7.89}$$

This much larger component of the vorticity field is shown in Fig.7.4. The maximum magnitude of the speed of this precession component is $\omega/2 = gv_C/c^2 = 8 \times 10^{-6}$arcsec/s, where here g is the gravitational acceleration at the altitude of the satellite. This precession has a different signature: it is not cumulative, and is detectable by its variation over each single orbit, as its orbital average is zero, to first approximation. Fig.7.5 shows $\Delta\Theta = |\Delta\mathbf{S}(t)|/|\mathbf{S}(0)|$ over one orbit, where, as in general,

$$\Delta\mathbf{S}(t) = \int_0^t dt' \frac{1}{2}\vec{\omega}(\mathbf{r}(t')) \times \mathbf{S}(t') \approx \left(\int_0^t dt' \frac{1}{2}\vec{\omega}(\mathbf{r}(t'))\right) \times \mathbf{S}(0). \tag{7.90}$$

Here $\Delta\mathbf{S}(t)$ is the integrated change in spin, and where the approximation arises because the change in $\mathbf{S}(t')$ on the RHS of (7.90) is negligible. The plot in Fig.7.5 shows this effect to be some $30\times$ larger than the expected GP-B errors, and so easily

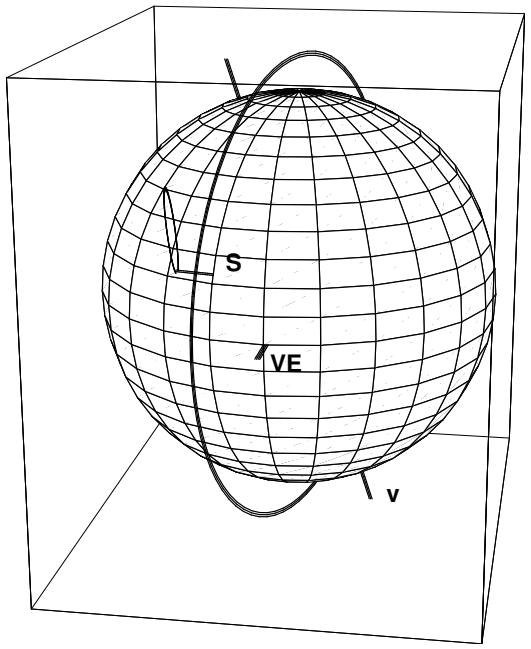

Figure 7.6: Predicted precession of the gyroscope spin axis, over one orbit of the satellite, but greatly exaggerated, directly manifesting the vorticity component of the flow caused by the translation of the earth, as in (7.89) and Fig.7.4. This component of the spin precession forms an elongated ellipse. Gravitational waves will cause changes in the size and orientation of this precession ellipse. The angle $\Delta\Theta$ in Fig.7.5 is the angle subtended at the earth's centre by the starting position at **S** and a point on this ellipse of precession. The precession caused by the vorticity component arising from the rotation of the earth is perpendicular to the plane of the orbit, while the geodetic precession component is in the plane of the orbit. The polar orbit of the GP-B satellite is shown, and **S** is the gyroscope starting spin orientation, directed towards the guide star IM Pegasi, RA = 22^h $53'$ $2.26''$, Dec = 16^0 $50'$ $28.2''$, **VE** is the vernal equinox, and **V** is the direction RA = 5.2^h, Dec = -67^0 of the translational velocity $\mathbf{v}_c$.

detectable. This precession is about the instantaneous direction of the vorticity $\vec{\omega}(\mathbf{r}((t))$ at the location of the satellite, and so is neither in the plane, as for the geodetic precession, nor perpendicular to the plane of the orbit, as for the earth-rotation induced vorticity effect. This absolute motion induced spin precession is shown in Fig.7.6.

Because the yearly orbital rotation of the earth about the sun slightly effects $\mathbf{v}_C$ [16] predictions for four months throughout the year are shown in Fig.7.5. Such yearly effects were first seen in the Miller [123] experiment.

However a significant prediction for the GP-B expeirment is the magnitude and signature of the new gravitational-wave induced spin precessions that GP-B is capable of detecting.

The novel gravitational waves predicted in Sect.7.2 and which have been detected

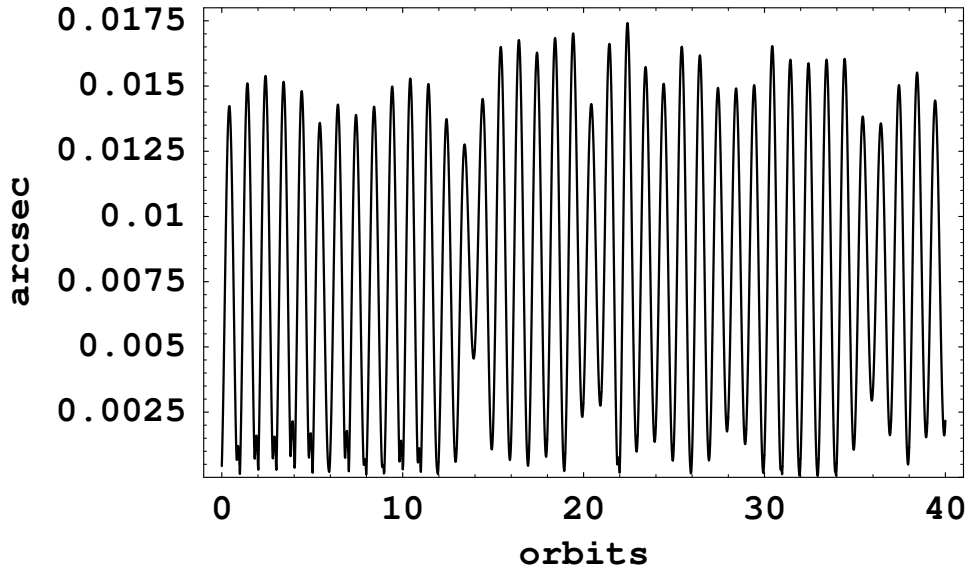

Figure 7.7: Predicted variation of the precession angle $\Delta\Theta = |\Delta\mathbf{S}(t)|/|\mathbf{S}(0)|$, in arcsec, as given by (7.90), over 40 GP-B orbits, from the vorticity induced by the absolute linear motion of the earth, and with the mainly galactic gravitational waves now included by means of the simulation described in the text. This plot shows the expected magnitude and signature of the effects of the gravitational waves. The corresponding prediction for one orbit, but without the gravitational wave effect, is shown in Fig.7.5. The main signature of the gravitational waves for GP-B is the variation, from orbit to orbit, of the maximum precession angle, as shown in this plot. The orbit time begins at location **S** in Fig.7.5. Predictions are for the month of September. The GP-B expected angle measurement accuracy is 0.0005 arcsec.

in various experiments, as discussed in Sect.11.3, are significant in magnitude compared to the average absolute motion speed of some 430 km/s. For that reason they have a significant effect upon the vorticity field, and consequently of the GP-B spin precessions. To give a first indication of the expected size of these wave induced spin precessions we have used the speed magnitude fluctuations in Fig.11.2 by simply adding these fluctuations to the speed of 430 km/s in the direction RA $= 5.2^h$, Dec$= -67^0$, but without allowing for any fluctuation in direction. Then the spin precession in (7.90) was integrated over 40 orbits of the satellite, with the results shown in Fig.7.7 for September. This figure should be compared with the form in Fig.7.5 for only one orbit, and without the gravitational wave effect. We see the magnitude and signature of the gravitational wave induced spin precessions, including the effect that the absolute motion induced precessions now no longer return to zero after each orbit. Whether this effect persists over many months is not possible to predict, but if it did persist then it would seriously interfere with, in particular, the observation of the earth-rotation induced spin precession, which is cumulative

but very small.

There is a technical difficulty in observing the effects shown in Figs.7.5 and 7.7, namely that the guide star is not visible to the on-board GP-B telescope during the 'mid-part' of each orbit, as is apparent from Fig.7.4.

7.9 Velocity Superposition Effect

Despite being non-linear (7.19)-(7.20) possess an approximate superposition effect, which explains why the existence of absolute motion and as well the presence of the $C(\mathbf{v})$ term appear to have almost escaped attention in the case of gravitational experiments near the earth.

First note that in analysing (7.19)-(7.20) we need to recognise two distinct effects: (i) the effect of a change of description of the flow when changing between observers, and (ii) the effects of absolute motion of the matter with respect to the quantum foam substratum. Whether the matter is at rest or in absolute motion with respect to this substratum does have a dynamical effect, and this paper is primarily about understanding this effect. While the Newtonian theory and GR both offer an account of the first effect, and different accounts at that, neither have the second dynamical effect, as this is a unique feature of the new theory of gravity. Let us consider the first effect, as this is somewhat standard. It basically comes down to noting that under a change of observer (7.19)-(7.20) transform covariantly under a Galilean transformation. Suppose that according to one observer O the matter density is specified by a form $\rho_O(\mathbf{r},t)$, and that (7.19)-(7.20) has a solution $\mathbf{v}_O(\mathbf{r},t)$, and then with acceleration $\mathbf{g}_O(\mathbf{r},t)$ given by (7.38)[4]. Then for another observer O' (and for simplicity we assume that the observers use coordinate axes that have the same orientation, and that at time $t=0$ they coincide), moving with uniform velocity $\mathbf{V}$ relative to observer O, observer O' describes the matter density with the form $\rho_{O'}(\mathbf{r},t) = \rho_O(\mathbf{r}+\mathbf{V}t,t)$. Then, as we now show, the corresponding solution to (7.19)-(7.20) for O' is *exactly*

$$\mathbf{v}_{O'}(\mathbf{r},t) = \mathbf{v}_O(\mathbf{r}+\mathbf{V}t,t) - \mathbf{V}. \tag{7.91}$$

This is easily established by substitution of (7.91) into (7.19)-(7.20), and noting that the LHS leads to a RHS where the density has the different form noted above, but that $\mathbf{v}_R$ is *invariant* under this change of observer, for each observer agrees on the absolute velocity of each piece of matter with respect to the local quantum foam. Under the change of observers, from O to O', (7.91) gives

$$D_{ij}(\mathbf{r},t) \to D_{ij}(\mathbf{r}+\mathbf{V}t,t) \quad \text{and} \quad \Omega_{ij}(\mathbf{r},t) \to \Omega_{ij}(\mathbf{r}+\mathbf{V}t,t). \tag{7.92}$$

Then for the total or Euler fluid derivative in (7.5) we have for observer O'

$$\frac{dD_{ij}(\mathbf{r}+\mathbf{V}t,t)}{dt} \equiv \frac{\partial D_{ij}(\mathbf{r}+\mathbf{V}t,t)}{\partial t} + (\mathbf{v}_O(\mathbf{r}+\mathbf{V}t,t)-\mathbf{V}).\nabla D_{ij}(\mathbf{r}+\mathbf{V}t,t),$$

[4]Note that here and in the following, except where indicated, the subscripts are O and not 0.

$$
\begin{aligned}
&= \left.\frac{\partial D_{ij}(\mathbf{r}+\mathbf{V}t',t)}{\partial t'}\right|_{t'\to t} + \left.\frac{\partial D_{ij}(\mathbf{r}+\mathbf{V}t,t''))}{\partial t''}\right|_{t''\to t} + \\
&\qquad (\mathbf{v}_O(\mathbf{r}+\mathbf{V}t,t)-\mathbf{V}).\nabla D_{ij}(\mathbf{r}+\mathbf{V}t,t), \\
&= (\mathbf{V}.\nabla)D_{ij}(\mathbf{r}+\mathbf{V}t,t) + \left.\frac{\partial D_{ij}(\mathbf{r}+\mathbf{V}t,t''))}{\partial t''}\right|_{t''\to t} + \\
&\qquad (\mathbf{v}_O(\mathbf{r}+\mathbf{V}t,t)-\mathbf{V}).\nabla D_{ij}(\mathbf{r}+\mathbf{V}t,t), \\
&= \left.\frac{\partial D_{ij}(\mathbf{r}+\mathbf{V}t,t''))}{\partial t''}\right|_{t''\to t} + \mathbf{v}_O(\mathbf{r}+\mathbf{V}t,t).\nabla D_{ij}(\mathbf{r}+\mathbf{V}t,t), \\
&= \left.\frac{dD_{ij}(\mathbf{r},t))}{dt}\right|_{\mathbf{r}\to\mathbf{r}+\mathbf{V}t}
\end{aligned}
\tag{7.93}
$$

as there is a key cancellation of two terms in (7.93). Clearly then all the terms on the LHS of (7.19)-(7.20) have the same transformation property. Then, finally, from the form of the LHS, both equations give the density dependent RHS, but which now involves the form $\rho_O(\mathbf{r},t)|_{\mathbf{r}\to\mathbf{r}+\mathbf{V}t}$, and this is simply $\rho_{O'}(\mathbf{r},t)$ given above. If the observers coordinate axes do not have the same orientation then a time-independent orthogonal similarity transformation $D \to SDS^T$, $\Omega \to S\Omega S^T$, and $v_R^i \to \sum_j S_{ij}v_R^j$ arises as well. Hence the description of the flow dynamics for observers in uniform relative motion is Galilean covariant. While this transformation rule for the Euler derivative is not a new result, there are some subtleties in the analysis, as seen above. The subtlety arises because the change of coordinate variables necessarily introduces a time dependence in the observer descriptions, even if the flow is inherently stationary.

Finally, using an analogous argument to that in (7.93), we see explicitly that the acceleration in (7.38) is also Galilean covariant under the above change of observer with transformation (7.91), and indeed each of the three terms is separately covariant, with again the time derivative part of the middle term playing a key role, and then $\mathbf{g}(\mathbf{r},t) \to \mathbf{g}(\mathbf{r}+\mathbf{V}t,t)$ (in the case of observer axes with the same orientation). This simply asserts that all observers actually agree on the gravitational acceleration, up to the indicated trivial translation effect caused by the motion of the observer.

We now come to item (ii) above, namely the more subtle but experimentally significant *approximate* velocity superposition effect. This approximate effect relates to the change in the form of the solutions of (7.19)-(7.20) when the matter density is in motion, as a whole, with respect to the quantum-foam substratum, as compared to the solutions when the matter is, as a whole, at rest. Already even these descriptions involve a subtlety. Consider the case when a star, say, is 'at rest' with respect to the substratum. Then the flow dynamics in (7.19)-(7.20) will lead to a position and time dependent flow solution $\mathbf{v}(\mathbf{r},t)$. But that flow leads to a position and time dependent $\mathbf{v}_R(\mathbf{r},t) = \mathbf{v}_0(\mathbf{r},t) - \mathbf{v}(\mathbf{r},t)$ on the RHS of (7.19)-(7.20), where $\mathbf{v}_0(\mathbf{r},t)$ is the velocity of the matter at position $\mathbf{r}$ and time t according to some

specific observer's frame of reference[5]. Hence the description of the matter being 'at rest' or 'in motion' relative to the substratum is far from simple. In general, with time-dependent flows, none of the matter will ever be 'at rest' with respect to the substratum, and this description is covariant under a change of observer. In the case of a well isolated star existing in a non-turbulent substratum we could give the terms 'at rest as a whole' or 'moving as whole' a well defined meaning by deciding how the star as a whole, considered as a rigid body, was moving relative to the more distant unperturbed substratum. Despite these complexities the solutions of (7.19)-(7.20) have, under certain special conditions, an approximate dynamical velocity superposition effect, and these conditions actually occur for the earth, and have played a key role in observations of absolute motion. To see this effect we need to make some approximations in considering the form of the solutions of (7.19)-(7.20). First we note that the vorticity from (7.20) is small, $\nabla \times \mathbf{v} \approx \mathbf{0}$, as it is a 'relativistic effect'. So for simplicity we shall assume zero vorticity, and also neglect on the RHS the $(\mathbf{v}_R/c)^2$ terms. We may then write $\mathbf{v} = \nabla u$, and then (7.19) reduces to

$$\frac{\partial u}{\partial t} = -\frac{1}{2}(\nabla u)^2 - \Phi - \Phi_{DM}, \tag{7.94}$$

where Φ is the Newtonian gravitational potential, and Φ_{DM} is an effective 'gravitational potential' that describes the dynamical 'dark matter' effect,

$$\nabla^2 \Phi_{DM}(\mathbf{r}, t) = 4\pi G \rho_{DM}(\mathbf{r}, t), \tag{7.95}$$

with ρ_{DM} defined in (9.4), and so $\Phi_{DM}[\mathbf{v}]$ depends functionally on $\nabla u(\mathbf{r}, t)$. Of course Φ, like Φ_{DM}, has the form

$$\Phi(\mathbf{r}, t) = -G \int d^3 r' \frac{\rho(\mathbf{r}', t)}{|\mathbf{r} - \mathbf{r}'|}. \tag{7.96}$$

Eqn.(7.94) is then an integro-differential equation determining the time evolution of $u(\mathbf{r}, t)$ from any given initial flow state $u(\mathbf{r}, t_0)$. The Φ_{DM} term is an important non-Newtonian dynamical feature of gravity, and leads to, for example, the bore hole g anomaly, the phenomenon of black holes, and the non-Keplerian rotation of spiral galaxies.

Eqn.(7.94) gives for the time-evolution of the velocity field

$$\mathbf{v}(\mathbf{r}, t) = \mathbf{v}(\mathbf{r}) - \nabla \int_0^t dt' \left(\frac{1}{2} |\mathbf{v}(\mathbf{r}, t')|^2 + \Phi + \Phi_{DM}[\mathbf{v}] \right), \tag{7.97}$$

where clearly $\mathbf{v}(\mathbf{r})$ is that flow at $t = 0$.

The flow fields have wavelike substructure. To see this suppose that (7.94) has a time evolution $u_0(\mathbf{r}, t)$ with corresponding velocity field $\mathbf{v}_0(\mathbf{r}, t)$. Then we look for

[5]Here the subscript is 0 and not an O. $\mathbf{v}_R(\mathbf{r}, t)$ was defined in (**??**). For matter described by a density distribution it is appropriate to introduce the field $\mathbf{v}_0(\mathbf{r}, t)$.

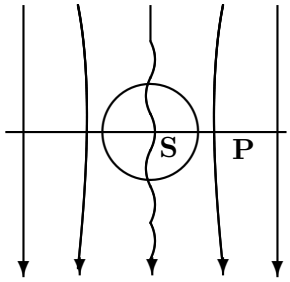

Figure 7.8: Velocity field $\mathbf{v}$, with asymptotic flow $\mathbf{V}$, expected from (7.97) showing greatest turbulence effects along the direction parallel to $\mathbf{V}$ and through the bulk of the sun S. Flow described by network of observers co-moving with the sun. On and near the plane P, with normal $\mathbf{V}$, we have $\mathbf{v}_{in}.\mathbf{V} \approx \mathbf{0}$. The direction of absolute motion $\mathbf{V}$ of the solar system is such that P is very accurately the plane of the ecliptic.

time-dependent perturbative solutions of (7.94) with $u = u_0 + \overline{u}$. To first order in $\overline{u}$ we then have

$$\frac{\partial \overline{u}(\mathbf{r},t)}{\partial t} = -\nabla \overline{u}(\mathbf{r},t).\nabla u_0(\mathbf{r},t). \tag{7.98}$$

This equation has wave solutions of the form $\overline{u}(\mathbf{r},t) = A\cos(\mathbf{k}.\mathbf{r} - \omega t + \phi)$ where $\omega(\mathbf{k},\mathbf{r},t) = \mathbf{v}_0(\mathbf{r},t).\mathbf{k}$, for wavelengths and time-scales short compared to the scale of changes in $\mathbf{v}_0(\mathbf{r},t)$. The local phase velocity of these waves is then $\mathbf{v}_\phi = \mathbf{v}_0$, and the local group velocity is $\mathbf{v}_g = \nabla_k \omega = \mathbf{v}_0$. Then the velocity field is

$$\mathbf{v}(\mathbf{r},t) = \mathbf{v}_0(\mathbf{r}) - A\mathbf{k}\sin(\mathbf{k}.\mathbf{r} - w(\mathbf{k},\mathbf{r},t)t + \phi). \tag{7.99}$$

In general we have, perturbatively, the superposition of such waves, giving

$$\mathbf{v}(\mathbf{r},t) = \mathbf{v}_0(\mathbf{r},t) - \int d^3k A(\mathbf{k})\mathbf{k}\sin(\mathbf{k}.\mathbf{r} - w(\mathbf{k},\mathbf{r},t)t + \phi(\mathbf{k})). \tag{7.100}$$

This perturbative analysis then suggests waves within waves, and with these waves interacting according to the non-linear terms neglected in (7.98), that is a turbulent fractal structure, where the equipotential surfaces for u have dimples upon dimples etc. Such wave effects have been detected [17, 19].

Let us first consider the time evolution from (7.97) for the case of the sun undergoing an absolute linear motion with absolute velocity $-\mathbf{V}$ (with respect to the substratum). This motion would be a consequence of galactic in-flows and the galactic orbital velocity of the solar system. We shall neglect here any time-dependence or inhomogeneity in $\mathbf{V}$, as we are interested here in the local effects caused by the absolute motion of the sun through space. Let us start (7.97) with

$$\mathbf{v}(\mathbf{r}) = \mathbf{v}_{in}(\mathbf{r}) + \mathbf{V}, \tag{7.101}$$

where $\mathbf{v}_{in}(\mathbf{r})$ is a radial in-flow which is an exact time-independent solution of (7.97) when $\mathbf{V} = \mathbf{0}$, which exists if the matter density of the sun is taken to be spherically symmetric [19]. This $\mathbf{v}(\mathbf{r})$ has the asymptotic limit of $+\mathbf{V}$, appropriate to the above absolute motion of the sun, and where in (7.101) we are using a network of observers co-moving with the sun. We can easily see how this absolute motion of the sun affects the flow. For a small time interval the change in $\mathbf{v}(\mathbf{r}, t)$ from (7.97) is

$$\Delta\mathbf{v}(\mathbf{r}, t) = -\nabla(\mathbf{v}_{in}(\mathbf{r}).\mathbf{V})\Delta t + ... \tag{7.102}$$

This gives a growing change in $\mathbf{v}(\mathbf{r}, t)$, which to a first approximation is a non-uniform displacement of the in-flow. This is smallest in those regions where $\mathbf{v}_{in}.\mathbf{V} \approx \mathbf{0}$, which is near the plane P in Fig.7.8. The flow is thus expected to be most affected along the direction parallel to $\mathbf{V}$ and through the bulk of the sun S. The change in (7.102) cannot continue indefinitely, and a better *ansatz* is to begin with a displaced in-flow as in

$$\mathbf{v}(\mathbf{r}) = \mathbf{v}_{in}(\mathbf{r} - \mathbf{a}) + \mathbf{V}, \tag{7.103}$$

where $\mathbf{a}$ parametrises a uniform displacement to be estimated from the dynamics. This corresponds to the notion that the in-flow is somewhat 'dragged' or displaced by the absolute motion[6]. Using (7.103) in (7.97) gives, exactly,

$$\frac{\partial\mathbf{v}}{\partial t} = \nabla\left(-\mathbf{v}_{in}(\mathbf{r} - \mathbf{a}).\mathbf{V} + \Phi(\mathbf{r} - \mathbf{a}) - \Phi(\mathbf{r}) + \Phi_{DM}(\mathbf{r} - \mathbf{a}) - \Phi_{DM}(\mathbf{r})\right), \tag{7.104}$$

where we have used the equation satisfied by the displaced in-flow $\mathbf{v}_{in}(\mathbf{r} - \mathbf{a})$. Then the displacement $\mathbf{a}$ is to be determined by demanding that the time and spatial average $<\frac{\partial\mathbf{v}}{\partial t}>_{t,\mathbf{r}}$ is minimised. Then the time-dependence is reduced to that only of the necessary turbulence induced by the absolute motion of the matter through space. Starting the time-evolution with the flow in (7.101) will result in a relaxation to something like the flow in (7.103) accompanied by excessive turbulence initially. To do better than (7.103) will require numerical modelling. The approximate flow in (7.103) has an important property, namely that the so-called 'dark-matter' density is unchanged by a non-zero $\mathbf{V}$, except for the displacement $\rho_{DM}(\mathbf{r}) \to \rho_{DM}(\mathbf{r} - \mathbf{a})$. As well in the limit $\Phi_{DM} \to 0$ this flow gives exactly the same $\mathbf{g}$, up to the translation effect, because of the time-derivative term in (7.6), as when the sun is not in absolute motion, for the reasons discussed above.

Hence the time-averaged flow is approximately $\mathbf{v}(\mathbf{r}) = \mathbf{v}_{in}(\mathbf{r}) + \mathbf{V}$, where well away from the sun we can ignore any displacement effect, with measure $\mathbf{a}$. This is even more accurate in the plane P. This is the dynamical superposition effect. Now

[6]This is completely different to the old idea by Stokes of 'entrainment', wherein the flow is supposed to have no $\mathbf{V}$ component in and near the earth. This outdated idea arose from the erroneous conclusion that the Michelson-Morley 1887 experiment had failed to detect absolute motion.

for the solar system, and thus the sun, the observed direction of $\mathbf{V}$ is such that P is the plane of the ecliptic[7].

For the earth we may in the first instance ignore the mass of the earth, and treat it as a test particle in motion through the above superposed flow determined by the flow into the sun and the absolute linear motion of the sun. Then for observers co-moving with the earth the observed velocity is the vector sum of the cosmic velocity of the solar system, the in-flow of space past the earth into the sun, and the orbital velocity of the earth about the sun (which enters with a minus sign for a co-moving observer). Then, as in Fig.10.5,

$$\mathbf{v} \approx \mathbf{V} + \mathbf{v}_{in} - \mathbf{v}_{tangent}. \tag{7.105}$$

This neglects the flow component $\mathbf{v}_E$ caused by the matter of the earth. In the absence of absolute motion of the earth this has a value of 11km/s near the surface, and so is much smaller than the observed speed of absolute motion of the earth. To include at first approximation $\mathbf{v}_E$ we can again use the displacement *ansatz*, namely $\mathbf{v}_E(\mathbf{r}) \to \mathbf{v}_E(\mathbf{r} - \mathbf{b})$, where here $\mathbf{b}$ is the displacement vector for the earth in-flow. Then (7.105) becomes

$$\mathbf{v}(\mathbf{r}) \approx \mathbf{V} + \mathbf{v}_{in} - \mathbf{v}_{tangent} - \mathbf{v}_E(\mathbf{r} - \mathbf{b}). \tag{7.106}$$

For the earth this means also that to this degree of approximation the earth's absolute motion does not affect the magnitude of the 'dark-matter' effect within the earth, causing only a displacement. This is important as in [19] the effects of absolute motion of the earth were neglected in analysing the bore-hole g anomaly data, from which the parameter α was found to be equal to the value of the fine structure constant, to within errors. That analysis thus effectively assumed that the displacement effect was sufficiently small.

The velocity superposition effect in (7.105) was assumed in [16], but it was also assumed implicitly by Miller [123] in the analysis of his data, but there Miller did not include the $\mathbf{v}_{in}$ component as Miller was of course unaware of the flow theory of gravity. For that reason a re-analysis of the Miller scaling argument was required in [16], and only then did the corrected Miller's scaling argument results for the cosmic velocity of the solar system come into agreement with the new velocity from analysis of the Miller data using the refractive index effect.

For circular orbits of the earth about the sun $v_{tangent}$ and v_{in} are given by

$$v_{tangent} = \sqrt{\frac{GM}{R}}, \tag{7.107}$$

$$v_{in} = \sqrt{\frac{2GM}{R}}, \tag{7.108}$$

[7]That the direction of absolute motion of the solar system is almost exactly normal to the plane of the ecliptic was discovered by Miller [123]. This is probably not a coincidence as only then is the relativistic acceleration term in (7.38) a minimum.

while the net speed v_R of the earth from the vector sum $\mathbf{v}_R = \mathbf{v}_{tangent} - \mathbf{v}_{in}$ is

$$v_N = \sqrt{\frac{3GM}{R}}, \tag{7.109}$$

where M is the mass of the sun, R is the distance of the earth from the sun, and G is Newton's gravitational constant. The gravitational acceleration of the earth towards the sun arises from inhomogeneities in the v_{in} flow component. These expressions give $v_{tangent} = 30$km/s, $v_{in} = 42.4$km/s (at the earth distance) and $v_N = 52$km/s. As discussed in [16] $\mathbf{v}_{in}$ is extractable from Miller's 1925/26 air-mode Michelson interferometer experiment because Miller took data during four separate months of the year, and over a year the vector sum of the three velocities varies. The extraction of v_{in} from the Miller data provided, some 80 years after that most significant experiment, the first experimental confirmation of the new 'in-flow' theory of gravity.

This approximate velocity superposition principle is the key to understanding the operation of the earth based detections of absolute motion in Part III.

7.10 Gravitational In-Flow and the GPS

We show here that the new in-flow theory of gravity and the observed absolute velocity of motion of the solar system through space are compatible with the operation of the Global Positioning System (GPS), and that the new theory of gravity finally provides a theory for the operation of the GPS, that is, that the account given by General Relativity was actually only fortuitously correct. Given the developments above this turns out to be an almost trivial exercise. As usual in this system the effects of the sun and moon are neglected. Various effects need to be included as the system relies upon extremely accurate atomic clocks in the satellites forming the GPS constellation. Within both the new theory and General Relativity these clocks are affected by both their speed and the gravitational effects of the earth. As well the orbits of these satellites and the critical time delays of radio signals from the satellites need to be computed. For the moment we assume spherical symmetry for the earth. The effects of non-sphericity will be discussed below. In General Relativity the orbits and signalling time delays are determined by the use of the geodesic equation (7.61) and the Schwarzschild metric (7.63). However these two equations are equivalent to the orbital equation (7.38) and the velocity field (7.91), with a velocity $\mathbf{V}$ of absolute motion, and with the in-flow given by (7.9), noting the result in Sect.7.9. For EM signalling the elapsed time in (7.31) requires careful treatment. Hence the two systems are mathematically completely equivalent: the computations within the new system may most easily be considered by relating them to the mathematically equivalent General Relativity formalism. We can also see this by explicitly changing from the CMB frame to a non-rotating frame co-moving with

the earth by means of the change of variables

$$\begin{aligned} \mathbf{r} &= \mathbf{r}' + \mathbf{V}t, \\ t &= t', \\ \mathbf{v} &= \mathbf{v}' + \mathbf{V}, \end{aligned} \tag{7.110}$$

which lead to the relationships of differentials

$$\begin{aligned} \nabla' &= \nabla, \\ \frac{\partial}{\partial t'} &= \frac{\partial}{\partial t} + \mathbf{V}.\nabla \end{aligned} \tag{7.111}$$

These expressions then lead to the demonstration of the covariance of (7.19)-(7.20). Then in the earth co-moving frame the absolute cosmic velocity $\mathbf{V}$ only appears on the RHS of these equations, and as noted in the previous section, has an extremely small dynamical effect.

There are nevertheless two differences between the two theories. One is their different treatment of the non-sphericity of the earth via the $C(\mathbf{v})$ term, and the second difference is the effects of the in-flow turbulence. In the operation of the GPS the density $\rho(\mathbf{r})$ of the earth is not used. Rather the gravitational potential $\Phi(\mathbf{r})$ is determined observationally. In the new gravity theory the determination of such a gravitational potential via (7.19)-(7.20) and $\Phi(\mathbf{r}) = -\frac{1}{2}\mathbf{v}^2(\mathbf{r})$ would involve the extra $C(\mathbf{v})$ term. Hence because of this phenomenological treatment the effects of the $C(\mathbf{v})$ term are not checkable. However the gravitational wave effect is expected to affect the operation of the GPS, and the GPS constellation would offer a worldwide network which would enable the investigation of the spatial and temporal correlations of these gravitational waves.

There is also a significant interpretational difference between the two theories. For example in General Relativity the relativistic effects involve both the 'special relativity' orbital speed effect via time dilations of the satellite clocks together with the General Relativity 'gravitational potential energy' effect on the satellite clocks. In the new theory there is only one effect, namely the time dilation effect produced by the motion of the clocks through the quantum foam, and the speeds of these clocks involves the vector sum of the orbital velocity and the velocity caused by the in-flow of the quantum foam into the earth. This is illustrated by Fig.10.5, where now the orbit refers to that of a satellite about the earth.

As well as providing a platform for studying the new gravitational waves, the GPS is already used for accurate time transfers. But because General Relativity and the new theory of gravity are fundamentally different there will be differences at higher orders in v_R/c. A systematic study of these corrections should be undertaken with the possibility that they will permit the establishment of more accurate global time standards.

7.11 Gravity and Quantum Non-Locality

The new theory of gravity, as expressed in (7.19)-(7.20) and the corresponding expression for the gravitational acceleration, has a remarkable property, namely that it is invariant under a Galilean transformation, as explicitly discussed in the following two sections. But most importantly this implies that gravitational effects are instantaneous, that is, that there are no time delays in the 'propagation' of gravitational effects. In fact to be more accurate these effects do not propagate. This is not to be confused with the gravitational wave effects which do propagate with finite speeds. Hence the new theory shares with the Newtonian theory of gravity the notion of 'action at a distance'. The explanation for this is that space is a quantum system that is continually undergoing quantum collapse into a classical state. Like other quantum collapse processes this quantum space collapse is non-local, because at a deep level the universe is intrinsically connected and non-local, as illustrated in Fig.5.2.

Chapter 8

The 'Dark Matter' Effect and the Fine Structure Constant

The 'dark matter' effect first came to notice some 60 years ago from observations of a mass paradox in galaxies and galactic clusters by Oort (1932) [67]; the dynamical estimates of the local density differed from that determined from the luminosity. Zwicky (1933) [69] measured the radial velocities of galaxies in the Coma cluster and also found that there was a mass discrepancy, with the required mass, based on the Newtonian theory of gravity, being ten-fold greater than that deduced from the luminosities. This supposedly extra 'mass' was called 'dark matter' because it produced no luminosity. In 1959 Kahn and Woltjer [68] noticed that the relative motion of the Andromeda galaxy and the Milky Way galaxy suggested again a ten-fold mass discrepancy. Then Einasto [70], Sizikov [71] and Freeman [72] realised that the rotation velocities in the outer regions of spiral galaxies were again much greater than expected from the luminosity. So it began to be realised that this 'dark matter' effect was a general property of galaxies and clusters of galaxies. Possible 'matter' interpretations for this effect have been numerous. Here we argue that it is simply a failure of Newtonian gravity, a failure 'inherited' by General Relativity. In a major development it is shown that this galactic 'dark matter' effect is related to the borehole g anomalies noticed in the 1980's by geophysicists. The new theory of gravity has two fundamental constants, the well-known Newtonian constant G, and a new constant which the Greenland borehole data shows is none other than the fine structure constant. The new 'quantum-foam' effects responsible for the 'dark matter' effect may be easily investigated in laboratory quantum-gravity Cavendish-type experiments.

8.1 'Dark Matter' as a Quantum Foam Dynamical Effect

We now make more explicit the 'dark matter' effect in a form that will be extensively analysed in the following sections. Restricting the flow dynamics to that of a matter system approximately at rest with respect to the quantum foam system, and also neglecting vorticity effects, (7.19) and (7.20) simplify to (7.11), with the key $C(\mathbf{v})$ term defined in (7.12). In this case we have

$$\mathbf{g} = \frac{\partial \mathbf{v}}{\partial t} + (\mathbf{v}.\nabla)\mathbf{v}, \tag{8.1}$$

and then (7.11) gives

$$\nabla.\mathbf{g} = -4\pi G\rho - C(\mathbf{v}) = -4\pi G\rho - 4\pi G\rho_{DM}, \tag{8.2}$$

after writing the new term as $C(\mathbf{v}) = 4\pi G\rho_{DM}$, with

$$\rho_{DM}(\mathbf{r}) = \frac{\alpha}{32\pi G}((trD)^2 - tr(D^2)). \tag{8.3}$$

So we see that ρ_{DM} would act as an effective matter density, and it is demonstrated later that it is the consequences of this term which have been misinterpreted as 'dark matter'. Note however ρ_{DM} is not positive definite. We see that this effect is actually the consequence of quantum foam effects within the new proposed dynamics for gravity, and which becomes apparent particularly in spiral galaxies. With $\nabla \times \mathbf{v} = 0$ we can write $\mathbf{v} = \nabla u$, and (7.11) has the form

$$\nabla^2 \left(\frac{\partial u}{\partial t} + \frac{1}{2}(\nabla u)^2 \right) = -4\pi G\rho - C(\nabla u(\mathbf{r})). \tag{8.4}$$

Then noting (7.23) we see that (8.4) has the non-linear integro-differential equation form

$$\frac{\partial u(\mathbf{r},t)}{\partial t} = -\frac{1}{2}(\nabla u(\mathbf{r},t))^2 + \frac{1}{4\pi}\int d^3r' \frac{C(\nabla u(\mathbf{r}',t))}{|\mathbf{r}-\mathbf{r}'|} - \Phi(\mathbf{r},t), \tag{8.5}$$

where Φ is the Newtonian gravitational potential

$$\Phi(\mathbf{r},t) = -G\int d^3r' \frac{\rho(\mathbf{r}',t)}{|\mathbf{r}-\mathbf{r}'|}. \tag{8.6}$$

Hence the Φ field acts as the source term for the velocity potential. Note that in the Newtonian theory of gravity one has the choice of using either the acceleration field $\mathbf{g}$ or the velocity field $\mathbf{v}$. However in the new theory of gravity this choice is no longer available: the fundamental dynamical degree of freedom is necessarily the $\mathbf{v}$ field, again because of the presence of the $C(\mathbf{v})$ term, which obviously cannot be written in terms of $\mathbf{g}$. If we were to ignore time-dependent behaviour (8.5) gives

$$|\mathbf{v}(\mathbf{r})|^2 = \frac{2}{4\pi}\int d^3r' \frac{C(\mathbf{v}(\mathbf{r}'))}{|\mathbf{r}-\mathbf{r}'|} - 2\Phi(\mathbf{r}). \tag{8.7}$$

This non-linear equation clearly cannot be solved for $\mathbf{v}(\mathbf{r})$ as its direction is not specified. This form makes it clear that we should expect gravitational waves, but certainly not waves travelling at the speed of light as c does not appear in (8.5). Note that (8.5) involves 'action-at-a-distance' effects, as there is no time-delay in the denominators. This was a feature of Newton's original theory of gravity. Here it is understood to be caused by the underlying quantum-foam dynamics (QHFT) which reaches this classical 'flow' description by ongoing non-local and instantaneous wavefunctional collapses. Contrary to popular belief even GR has this 'action-at-a-distance' feature, as the reformulation of GR via the Panlevé-Gullstrand metric leads also to an equation of the form in (8.4), but with the $C(\mathbf{v})$ term absent.

The new flow dynamics encompassed in (7.19)-(7.20) thus accounts for most of the known gravitational phenomena, but will lead to some very clear cut experiments that will distinguish it from the two previous attempts to model gravitation. It turns out that these two attempts were based on some key 'accidents' of history. In the case of the Newtonian modelling of gravity the prime 'accident' was of course the solar system with its high degree of spherical symmetry[1]. In each case we had test objects, namely the planets, in orbit about the sun, or we had test object in orbit about the earth. In the case of the General Relativity modelling the prime 'accident' was the mis-reporting of the Michelson-Morley experiment, and the ongoing belief that the so called 'relativistic effects' are incompatible with absolute motion, and of course that GR was constructed to agree with Newtonian gravity in the 'non-relativistic' limit, and so 'inherited' the flaws of that theory. We shall consider in detail later some further anomalies that might be appropriately explained by this new modelling of gravity. Of course that the in-flow has been present in various experimental data is also a significant argument for something like (7.19)-(7.20) to model gravity.

8.2 Gravitational Anomalies

There are numerous gravitational anomalies, including not only the spiral-galaxy 'dark matter' effect and problems in measuring G, but as well there are others that are not well-known in physics, presumably because their existence is incompatible with the Newtonian or the Hilbert-Einstein gravity theories.

The most significant of these anomalies is the Allais effect [73]. In the 1950's Allais conducted a long series of experiments using a paraconical pendulum, which can be thought of as a Foucault pendulum with a short arm length and a special pivot mechanism. These observations revealed pendulum precession effects that are distinct from the Foucault pendulum precession, which mainly manifests in the case of a very long pendulum, associated with the position of the moon, but with a magnitude very much larger than the well-known tidal effects. However in June 1954 Allais reported that the paraconical pendulum exhibited peculiar movements

[1] And that the sun has only a minimal gravitational attractor

at the time of a solar eclipse. Allais was recording the precession of the pendulum in Paris. Coincidentally during the 30 day observation period a partial solar eclipse occurred at Paris on June 30. During the eclipse the precession of the pendulum was seen to be disturbed. Similar results were obtained during another solar eclipse on October 29 1959. There have been other repeats of the Allais experiment with varying results.

Another anomaly was reported by Saxl and Allen [74] during the solar eclipse of March 7 1970. Significant variations in the period of a torsional pendulum were observed both during the eclipse and as well in the hours just preceding and just following the eclipse. The effects seem to suggest that an "apparent wavelike structure has been observed over the course of many years at our Harvard laboratory", where the wavelike structure is present and reproducible even in the absence of an eclipse.

Again Zhou and Huang [75] report various clock anomalies occurring during the solar eclipses of September 23 1987, March 18 1988 and July 22 1990 observed using atomic clocks.

Another anomaly is the Shnoll effect [76] which has been under extensive study for nearly 50 years. Here the rates of various biological and chemical reactions, and also nuclear decays, show non-random short-time effects in the rate fluctuations, and which exhibit correlations between these different processes, where the correlations also manifest over large distances. As well the non-random effects have a characterisable structure which reoccurs with the periodicity of 24 hours (most likely to be a sidereal day), 27 days and 365 days. This most startling effect would appear to be indicating the existence of a structure to space that displays variations over large length scales, and with time variations that relate these structures to the absolute motion and gravitational wave effects discussed later.

The most significant anomaly is of course the 'dark matter' effect associated with the rotational velocities of objects in spiral galaxies. This anomaly led to the introduction of the 'dark matter' concept - but with no such matter ever having been detected, despite extensive searches. This anomaly was compounded when recently observations of the rotational velocities of objects within elliptical galaxies was seen to require very little 'dark matter'. Of course this is a simple consequence of the new theory of gravity, as we shall see.

All these anomalies, including the g anomaly in Sect.8.3 and others such as the the solar neutrino flux deficiency problem were clearly indicating that gravity has aspects to it that are not within the prevailing theories.

8.3 The Borehole g Anomaly

Stacey and others [77, 78, 79, 80] have found evidence for non-Newtonian gravitation from gravimetric measurements (Airy experiments) in mines and boreholes. The discovery was that the measured value of g down mines and boreholes became greater

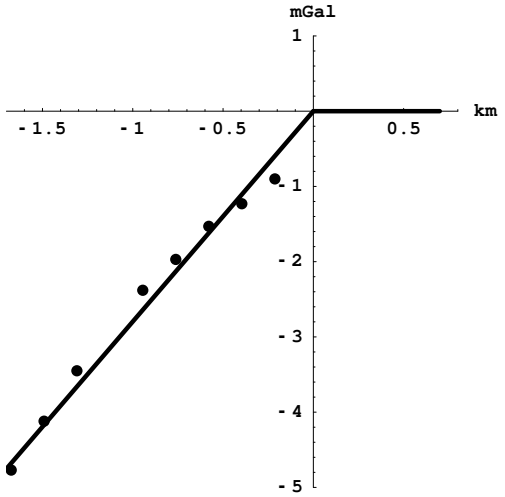

Figure 8.1: The data shows the gravity residuals for the Greenland Ice Cap [81] Airy measurements of the $g(r)$ profile, defined as $\Delta g(r) = g_{Newton} - g_{observed}$, and measured in mGal (1mGal = 10^{-3} cm/s^2), plotted against depth in km. Using (8.18) we obtain $\alpha^{-1} = 139 \pm 5$ from fitting the slope of the data, as shown.

than that predicted by the Newtonian theory, given the density profile $\rho(r)$ implied by sampling, and so implying a defect in Newtonian gravity, as shown in Fig.8.1 for the Greenland Ice shelf borehole measurements. The results were interpreted and analysed using either a value of G different to but larger than that found in laboratory experiments or by assuming a short range Yukawa type force in addition to the Newtonian 'inverse-square law'. Numerous experiments were carried out in which g was measured as a function of depth, and also as a function of height above ground level using towers. The tower experiments [82, 83] did not indicate any non-Newtonian effect, and so implied that the extra Yukawa force explanation was not viable. The combined results appeared to have resulted in confusion and eventually the experimental effect was dismissed as being caused by erroneous density sampling. However the new theory of gravity predicts such an effect, and in particular that the effect should manifest within the earth but not above it, as was in fact observed. That is $d\Delta g(r)/dr$ should be discontinuous at the boundary, as shown in Fig.8.1. Essentially this effect is caused by the new $C(\mathbf{v})$ term in the in-flow theory of gravity which, as we have noted earlier, is active whenever there is a lack of complete spherical symmetry, or even within matter when there is spherical symmetry.

When the matter density and the flow are both spherically symmetric and stationary in time, and assuming no vorticity, and neglecting the velocity field $\mathbf{v}_R$, the flow equations (7.19)-(7.20) become (7.11), which then has the radial form, with $v' \equiv dv/dr$,

$$2\frac{vv'}{r} + (v')^2 + vv'' = -4\pi G\rho(r) - 4\pi G\rho_{DM}(r), \tag{8.8}$$

and then

$$\rho_{DM}(r) = \frac{\alpha}{32\pi G}\left(\frac{v^2}{2r^2} + \frac{vv'}{r}\right). \tag{8.9}$$

Eqn.(8.8) may be written in a non-linear integral form

$$v^2(r) = \frac{8\pi G}{r}\int_0^r s^2\left[\rho(s) + \rho_{DM}(s)\right]ds + 8\pi G\int_r^\infty s\left[\rho(s) + \rho_{DM}(s)\right]ds, \tag{8.10}$$

which follows from evaluating

$$|\mathbf{v}(\mathbf{r})|^2 = 2G\int d^3r'\frac{\rho(r) + \rho_{DM}(r)}{|\mathbf{r} - \mathbf{r}'|}. \tag{8.11}$$

in the case of spherical symmetry and a radial in-flow.

First consider solutions to (8.10) in the perturbative regime, and iterating once we find

$$\rho_{DM}(r) = \frac{\alpha}{2r^2}\int_r^\infty s\rho(s)ds + O(\alpha^2), \tag{8.12}$$

so that in spherical systems the 'dark matter' effect is concentrated near the centre, and we find that the total 'dark matter'

$$M_{DM} \equiv 4\pi\int_0^\infty r^2\rho_{DM}(r)dr = \frac{4\pi\alpha}{2}\int_0^\infty r^2\rho(r)dr + O(\alpha^2) = \frac{\alpha}{2}M + O(\alpha^2), \tag{8.13}$$

where M is the total amount of (actual) matter. Hence to $O(\alpha)$ $M_{DM}/M = \alpha/2$ independently of the matter density profile.

When the matter density $\rho(r) = 0$ for $r \geq R$, as for the earth, then we also obtain, to $O(\alpha)$, from (7.6) and (8.10) Newton's 'inverse square law' for $r > R$

$$g(r) = \begin{cases} -\dfrac{(1+\frac{\alpha}{2})GM}{r^2}, & r > R, \\ -\dfrac{4\pi G}{r^2}\displaystyle\int_0^r s^2\rho(s)ds - \frac{2\pi\alpha G}{r^2}\int_0^r\left(\int_s^R s'\rho(s')ds'\right)ds, & r < R, \end{cases} \tag{8.14}$$

and we see that the effective Newtonian gravitational constant in (8.14) is $G_N = (1 + \frac{\alpha}{2})G$ which is different to the fundamental gravitational constant G in (7.19)-(7.20). The result in (8.14), which is different from that of the Newtonian theory ($\alpha = 0$) has actually been observed in mine/borehole measurements [77, 78, 81] of $g(r)$, though of course there had been no explanation for the effect, and indeed the reality of the effect was eventually doubted. The gravity residual [77, 78, 81] is defined as

$$\Delta g(r) \equiv g(r)_{Newton} - g(r)_{observed} \tag{8.15}$$

$$= g(r)_{Newton} - g(r). \tag{8.16}$$

The 'Newtonian theory' assumed in the determination of the gravity residuals is, in the present context,

$$g(r)_{Newton} = \begin{cases} -\dfrac{G_N M}{r^2}, & r > R, \\ -\dfrac{4\pi G_N}{r^2}\displaystyle\int_0^r s^2\rho(s)ds, & r < R, \end{cases} \tag{8.17}$$

with $G_N = (1 + \frac{\alpha}{2})G$. Then $\Delta g(r)$ is found to be, to 1st order in α and in $R - r$, i.e. near the surface,

$$\Delta g(r) = \begin{cases} 0, & r > R, \\ -2\pi\alpha G_N \rho(R)(R - r), & r < R. \end{cases} \tag{8.18}$$

which is the form actually observed [77, 78, 81]. So outside of the spherical earth the Newtonian theory and the in-flow theory are indistinguishable, as indicated by the horizontal line, for $r > R$, in Fig.8.1. However inside the earth the two theories give a different dependence on r, due to the 'dark matter' effect within the earth.

Gravity residuals from a borehole into the Greenland Ice Cap were determined down to a depth of 1.5km [81]. The ice had a density of $\rho(R) = 930$ kg/m^3, and from (8.18), using $G_N = 6.6742 \times 10^{-11}$ m^{3}s^{-2}kg^{-1}, we obtain from a linear fit to the slope of the data points in Fig.8.1 that $\alpha^{-1} = 139 \pm 5$, which equals the value of the fine structure constant $\alpha^{-1} = 137.036$ to within the errors, and for this reason we identify the α constant in (7.19)-(7.20) as being the fine structure constant.

8.4 The Fine Structure Constant

The so called fine structure constant α was introduced into physics by Sommerfeld in 1916. Sommerfeld extended the Bohr theory of atoms to include elliptical orbits and the relativistic dependence of mass on speed. The result for a typical energy difference is

$$E_{nk} = -\frac{mc^2\alpha^2 k}{2n^2}\left(1 + \frac{\alpha^2}{n^2}\left(\frac{n}{k} - \frac{3}{4}\right)\right). \tag{8.19}$$

We see that the leading term contains α^2, as well as the second term which introduces another α^2. It is because of its presence in this second order term that α is called the fine structure constant, though that is really a misnomer, for α determines also the Bohr energies, as is seen once we compare the atomic energy levels with the rest mass energy of the electron, as in (8.19).

8.5 Measurements of G and the Fine Structure Constant

As already noted Newton's Inverse Square Law of Gravitation may only be strictly valid in special cases. The theory that gravitational effects arise from inhomo-

geneities in the quantum foam flow implies that there is no 'universal law of gravitation' because the inhomogeneities are determined by non-linear 'fluid equations' and the solutions have no form which could be described by a 'universal law'. Fundamentally there is no generic fluid flow behaviour. The Inverse Square Law is then only an approximation, with large deviations seen in the case of spiral galaxies. Nevertheless Newton's gravitational constant G will have a definite value as it quantifies the effective rate at which matter dissipates the information content of space.

From these considerations it follows that the measurement of the value of G will be difficult as the measurement of the forces between two of more objects, which is the usual method of measuring G, will depend on the geometry of the spatial positioning of these objects in a way not previously accounted for because the Newtonian Inverse Square Law has always been assumed, or in some case a specified change in the form of the law has been used. But in all cases a 'law' has been assumed, and this may have been the flaw in the analysis of data from such experiments. This implies that the value of G from such experiments will show some variability as a systematic effect has been neglected in analysing the experimental data. So experimental measurements of G should show an unexpected contextuality. As well the influence of surrounding matter has also not been properly accounted for. Of course any effects of turbulence in the inhomogeneities of the flow has presumably also never even been contemplated. The first measurement of G was in 1798 by Cavendish using a torsional balance. As the precision of experiments increased over the years and a variety of techniques used the disparity between the values of G has actually increased [108]. Fig.8.2 shows the results from precision measurements of G over the last 60 years. As can be seen one indication of the contextuality is that measurements of G produce values that differ by nearly 40 times their individual error estimates. In 1998 CODATA increased the uncertainty in G, shown by the dotted line in 8.2, from 0.013% to 0.15%.

Note that the relative spread $\Delta G_N/G_N \approx O(\alpha)$, as we would now expect. Essentially the different Cavendish-type laboratory experiments used different matter geometries and, as we have seen, the geometry of the masses has an effect on the in-flow, and so on the measured force between the masses. Only for the borehole-type experiments do we have a complete analytic analysis, in Sect.8.3, and an ocean measurement is of that type, and experiment [84] gives a $G_N = (6.677 \pm 0.013) \times 10^{-11}$ $\mathrm{m^2 s^{-2} kg^{-1}}$, shown by the upper horizontal line in Fig.8.2. From that value we may extract the value of the 'fundamental gravitational constant' G by removing the 'dark matter' effect: $G \approx (1 - \frac{\alpha}{2})G_N = (6.6526 \pm 0.013) \times 10^{-11}$ $\mathrm{m^2 s^{-2} kg^{-1}}$, shown by the lower horizontal line in Fig.8.2, compared to the current CODATA value of $G_N = (6.6742 \pm 0.001) \times 10^{-11}$ $\mathrm{m^2 s^{-2} kg^{-1}}$, which is contaminated with 'dark matter' effects. Then in the various experiments, without explicitly computing the 'dark matter' effect, one will find an 'effective' value of $G_N > G$ that depends on the geometry of the masses. A re-analysis of the data in Fig.8.2 using the in-flow theory is predicted to resolve these apparent discrepancies. Examples of how the quantum-

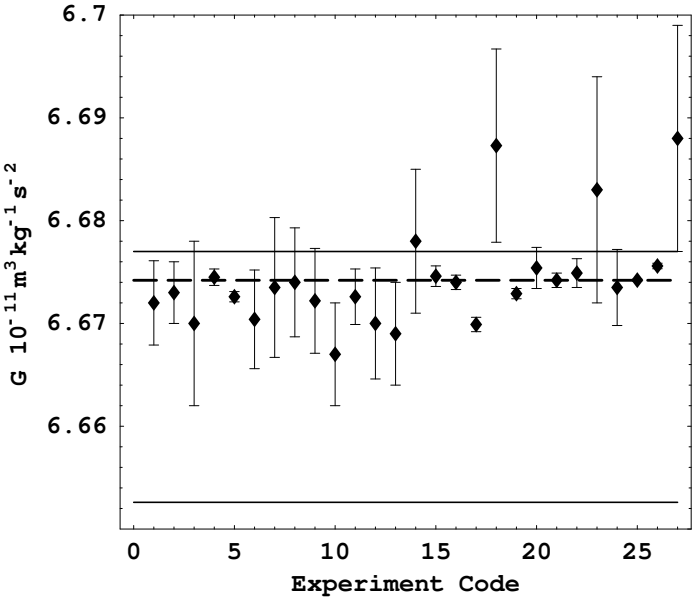

Figure 8.2: Results of precision measurements of G published in the last sixty years in which the Newtonian theory was used to analyse the data. These results show the presence of a systematic effect, not in the Newtonian theory, of fractional size $\Delta G/G \approx \alpha/4$. The upper horizontal line shows the value of G from ocean Airy measurements [84], while the dotted line shows the current CODATA G value. The lower horizontal line shows the value of G after removing the 'dark matter' effects from the [84] G value.
Experiment Codes: 1: Gaithersburg 1942 [85], **2:** Magny-les-Hameaux 1971 [86], **3:** Budapest 1974 [87], **4;** Moscow 1979 [88], **5:** Gaithersburg 1982 [89], **6-19:** Fribourg Oct 84, Nov 84, Dec 84, Feb 85 [90], **10:** Braunschweig 1987 [91], **11:** Dye 3 Greenland 1995 [92], **12:** Gigerwald Lake 1994 [93], **13-14:** Gigerwald lake19 95 112m, 88m [94], **15:** Lower Hutt 1995 MSL [95], **16:** Los Alamos 1997 [96], **17:** Wuhan 1998 [97], **18:** Boulder JILA 1998 [98], **19:** Moscow 1998 [99], **20:** Zurich 1998 [100], **21:** Lower Hutt MSL 1999 [101], **22:** Zurich 1999 [102], **23:** Sevres 1999 [103], **24:** Wuppertal 1999 [104], **25:** Seattle 2000 [105], **26:** Sevres 2001 [106], **27:** Lake Brasimone 2001 [107].

foam fluid-flow theory of gravity alters the analysis of data from Cavendish-type experiments are given in Sect.9.10, and in general the 'dark matter' effects are of order α.

Chapter 9

Gravitational Attractors as Black Holes

Here we consider a new phenomena which is not in either the Newtonian or Einsteinian theories of gravity, namely the existence of gravitational attractors. Such an attractor may exist by itself or it may be accompanied by matter, as in the case of planets, stars, globular clusters and galaxies, both elliptical and spiral. As we have seen in Sect.8.3 the existence of such an attractor at the centre of the earth is suggested by the borehole g anomaly data. Here we develop the general theory of these attractors. Indeed they are apparently a common occurrence. Up to now the effects of these 'attractors' in globular clusters, quasistellar objects (QSO) and galaxies have been interpreted by astronomers as General Relativity 'black holes', but only by default as no other phenomenon was until now known which could account for the strong gravitational effects observed at the centres of these systems. These attractors are self-sustaining quantum foam in-flows, and their behaviour is determined solely by the fine structure constant. They are quantum foam in-flow singularities. So to that extent they are classical manifestations of quantum gravity. These attractors have an event horizon where the in-flow speed reaches the speed of light, and within this horizon the speed increases without limit to an infinite speed at a singular point. In-falling matter can produce radiation from the heating effects associated with this in-fall.

However the existence of these in-flow singularities does not require that they be formed by the collapse of matter, and they need not have matter at their centres, so in many respects they differ from the 'black holes' of General Relativity. They also differ from these 'black holes' in that their gravitational acceleration $g(r)$ is not given by Newton's inverse square law. It is suggested here that along with matter and radiation, that they formed the third component of the universe, apart from space itself. And that they played a key role in the formation of gravitationally collapsed systems, such as stars and galaxies, and that the long range nature of their acceleration field $g(r)$ explains the apparent relatively rapid formation of such

structures in the early universe.

Here we first consider the special case of a one-parameter class of matter-free spherical attractors, and then the case when the attractor is associated with matter. In this case the attractor may be minimal or non-minimal, with the distinction determined by whether or not the attractor produces a long-range acceleration field, as for the non-minimal attractors. We also consider a class of non-spherical attractors, but the non-sphericity produce only short range effects. For the case of spherical attractors we determine the size of the event horizon. For globular clusters we can then predict the minimum mass of the central attractor and compare that with the total mass of the cluster. This ratio is shown to be equal to $\alpha/2$, and this prediction is in agreement with the observations of the M15 and G1 globular clusters. Hence the globular clusters supply a striking confirmation of the new theory of gravity and its attractors. In Chap.9.10 we show that these attractors may be experimentally studied in Cavendish-style laboratory gravitational experiments, and so provide the opportunity for the first laboratory quantum gravity experiments.

There will be at least a minimal attractor within the sun which scan also be detected by analysing the neutrino flux and its energy spectrum, as these attractors produce central gravitational forces very different from the Newtonian theory, which is an essential input into current stellar dynamics.

9.1 Spherical Gravitational Attractors

Here we reveal the one-parameter class of spherical attractors in the absence of matter. For a spherically symmetric in-flow $v(r,t)$ the simplified in-flow equation (7.11), in the case of zero vorticity and neglecting the velocity field $\mathbf{v}_R$, has the form

$$\frac{\partial v'}{\partial t} + vv'' + \frac{vv'}{r} + (v')^2 + \frac{\alpha}{2}\left(\frac{v^2}{2r^2} + \frac{vv'}{r}\right) = 0, \tag{9.1}$$

where $v' = \partial v(r)/\partial r$. For a stationary flow this equation becomes linear in $f(r)$ where $v(r) = \sqrt{f(r)}$

$$\frac{f''}{2} + \frac{f'}{r} + \frac{\alpha}{2}(\frac{f}{2r^2} + \frac{f'}{2r}) = 0. \tag{9.2}$$

The general solution of this homogeneous equation is

$$f(r) = \frac{K}{r} + \frac{\beta}{r^{\alpha/2}}, \tag{9.3}$$

where K and β are arbitrary constants. The effective 'dark matter' density (8.9) is then

$$\rho_{DM}(r) = \frac{\alpha\beta}{16\pi G}(1 - \frac{\alpha}{2})\frac{1}{r^{2+\alpha/2}}, \tag{9.4}$$

which essentially has the $1/r^2$ dependence, as seen in spiral galaxies and discussed later. Note that the K term does not contribute to ρ_{DM}. However the K term is

not a solution of (7.19)-(7.20) for a stationary flow. The reason for this is somewhat subtle. By direct computation we would appear to obtain that

$$\nabla^2 \frac{1}{|\mathbf{r}|} = \frac{1}{2}\frac{d^2}{dr^2}\frac{1}{r} + \frac{1}{r}\frac{d}{dr}\frac{1}{r} = 0, \tag{9.5}$$

which is used in finding the K term part of (9.3). But in fact the correct result is

$$\nabla^2 \frac{1}{|\mathbf{r}|} = -4\pi\delta^{(3)}(\mathbf{r}). \tag{9.6}$$

This is confirmed by applying the divergence theorem

$$\int dV \nabla.\mathbf{w} = \int d\mathbf{A}.\mathbf{w} \tag{9.7}$$

with $\mathbf{w} = \nabla(1|/\mathbf{r}|)$ for a spherical region. The RHS of (9.7) gives -4π independent of the radius of the sphere. So the LHS must have a delta function distribution at $\mathbf{r} = \mathbf{0}$, as in (9.6). Hence the K term should not be present in (9.3). Essentially for this term to appear the RHS of (7.19)-(7.20) would have to have a $-4\pi\delta^{(3)}(\mathbf{r})$ term corresponding to a point mass. However by definition all of the matter density is included in $\rho(\mathbf{r})$, and in the present case there is no matter present at all. However for the β term the result is different. By direct computation we find that

$$\nabla^2 \frac{1}{|\mathbf{r}|^\alpha} = -\frac{\alpha(1-\alpha)}{r^{2+2\alpha}}. \tag{9.8}$$

Using the divergence theorem again but now with $\mathbf{w} = \nabla(1/|\mathbf{r}|^\alpha)$ we find that (9.7) is satisfied, and so no delta-function distribution is needed on the RHS of (9.8). Hence the correct general solution of (9.2) is

$$f(r) = \frac{\beta}{r^{\alpha/2}}, \tag{9.9}$$

which defines a one-parameter class of spherically symmetric attractors. The gravitational acceleration produced by this in-flow is

$$g(r) = \frac{1}{2}\frac{df(r)}{dr} = -\frac{\alpha\beta}{4r^{1+\alpha/2}}, \tag{9.10}$$

which decreases slowly with distance, compared to Newton's inverse square law. Because these attractors can be independent of matter they would have arisen in the early universe during the formation of space itself. Once matter had cooled to the recombination temperature of about 3000^oK, these attractors would have played a key role in the formation of the first stars and the galaxies. This attractor has a spatial in-flow with a speed singularity at $r = 0$. There is a spherical event horizon, where $v = c$, at $r_H = (\frac{\beta}{c^2})^{2/\alpha}$. Hence the attractor acts as a 'black hole', but very much unlike the 'black hole' in General Relativity, and so the universe would have had primordial black holes from the very beginning.

9.2 Minimal Attractor for a Uniform Density Sphere

Now consider the gravitational attractors that are formed by the presence of matter. Here the quantum foam in-flow associated with the matter appears to trigger a non-Newtonian in-flow at the centre of the matter distribution. Now for a spherically symmetric matter density and a spherically symmetric in-flow $v(r,t)$ the basic in-flow equation (7.19)-(7.20) has the form

$$\frac{\partial v'}{\partial t} + vv'' + \frac{vv'}{r} + (v')^2 + \frac{\alpha}{2}\left(\frac{v^2}{2r^2} + \frac{vv'}{r}\right) = -4\pi G\rho(r), \tag{9.11}$$

Again for a stationary in-flow this equation becomes linear in $f(r)$ where $v(r) = \sqrt{f(r)}$

$$\frac{f''}{2} + \frac{f'}{r} + \frac{\alpha}{2}(\frac{f}{2r^2} + \frac{f'}{2r}) = -4\pi G\rho(r). \tag{9.12}$$

Define the particular 'matter dependent' solution of this inhomogeneous equation to be $f_m(r)$. Then the general solution of (9.1) is the sum of this particular solution and the solutions of the homogeneous equation,

$$f(r) = \frac{\beta}{r^{\alpha/2}} + f_m(r), \tag{9.13}$$

where β is again an arbitrary constant. The effective 'dark matter' density (8.9) is now

$$\rho_{DM}(r) = \frac{\alpha\beta}{16\pi G}(1 - \frac{\alpha}{2})\frac{1}{r^{2+\alpha/2}} + \frac{\alpha}{2}(\frac{f_m}{2r^2} + \frac{f_m'}{2r}). \tag{9.14}$$

Let us now consider the solution of (9.12) for a piece-wise constant matter density, in particular for a sphere of radius R of uniform density ρ:

$$\rho(r) = \rho, \quad 0 < r < R; \quad \rho(r) = 0, \quad r > R. \tag{9.15}$$

The solution of (9.12) is then found to be, in each region,

$$f(r) = \begin{cases} \dfrac{\beta}{r^{\alpha/2}} - \dfrac{16\pi\rho G r^2}{3(4+\alpha)}, & 0 < r < R, \\ \dfrac{K}{r} + \dfrac{\overline{\beta}}{r^{\alpha/2}}, & r > R, \end{cases} \tag{9.16}$$

where in general β and $\overline{\beta}$ have different values. As well the K term is permitted in the external region. Indeed for a non-stepwise density the K term would arise as the asymptotic or the 'matter dependent' solution $f_m(r)$. The complete solution is obtained by ensuring that $f(r)$ and $f'(r)$ are continuous at $r = R$, which is required of the 2nd order differential equation. Let us first consider the critical case where

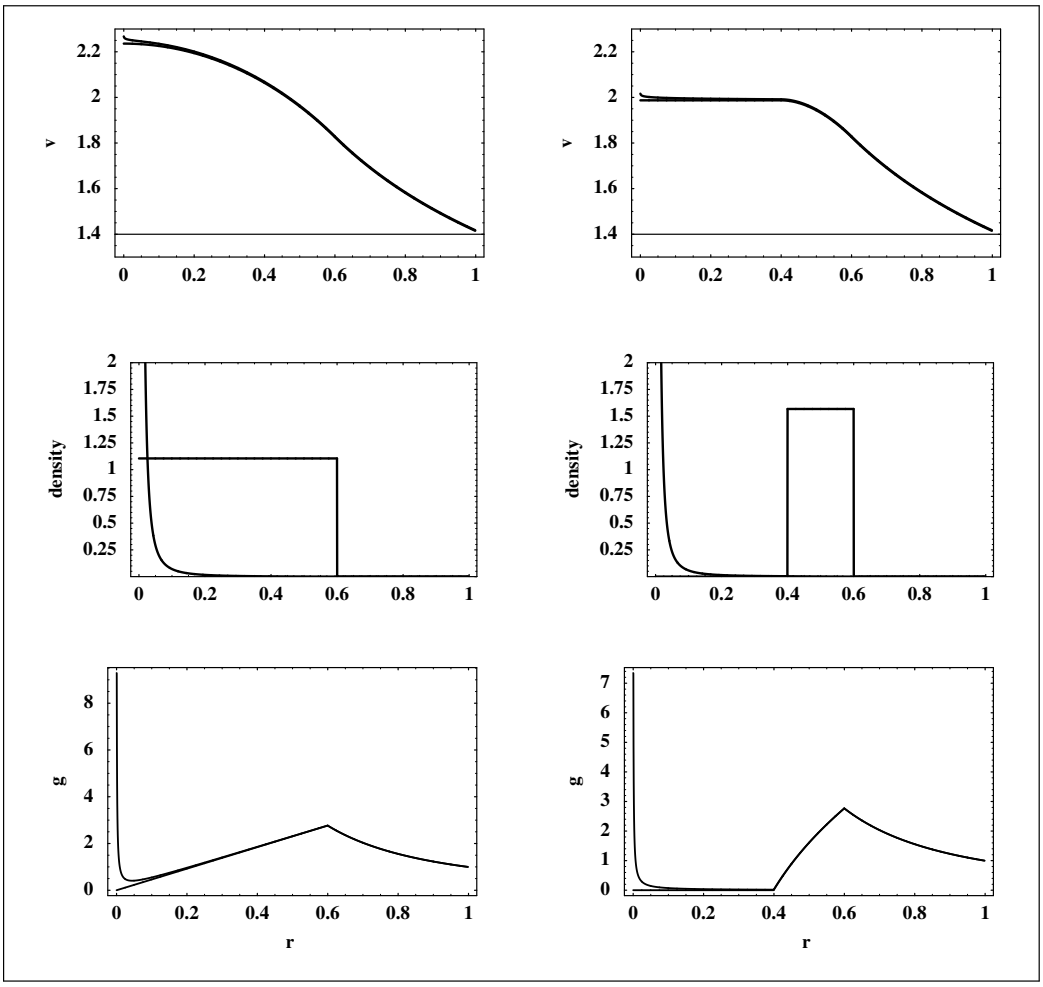

Figure 9.1: Solutions of (9.11) for a uniform density sphere (on the left), and for a spherical shell (on the right). The upper plots show the in-flow speeds for both Newtonian gravity and for the new theory of gravity, which displays the increase in speed near the attractor at $r = 0$. The middle plots are the matter density profiles, with the 'dark matter' density peaking at $r = 0$. The lower plots show the gravitational acceleration $|g(r)|$, with again a comparison of the Newtonian gravity and the new theory, which shows large accelerations near the attractor at $r = 0$.

the gravitational attractor does not extend beyond the sphere, i.e. $\overline{\beta} = 0$. This shall result in what is defined here to be a 'minimal attractor'. Then we find that

$$\beta = \frac{16\pi\rho G R^{2+\alpha/2}}{(1-\alpha/2)(4+\alpha)}, \tag{9.17}$$

$$K = 16\pi\rho G R^3 \frac{2+\alpha/2}{3(1-\alpha/2)(4+\alpha)} = 2(1+\frac{\alpha}{2}+O(\alpha^2)\ )MG, \tag{9.18}$$

where M is the total matter content of the sphere. Then for the 'dark matter' density we obtain

$$\rho_{DM}(r) = \begin{cases} \frac{\alpha\beta}{16\pi G}(1-\frac{\alpha}{2})\frac{1}{r^{2+\alpha/2}} - \frac{\alpha\rho}{4+\alpha} = \frac{\alpha\rho}{4}\left(\left(\frac{R}{r}\right)^{2+\alpha/2} - 1\right), & 0 < r < R, \\ 0, \quad r > R. \end{cases} \tag{9.19}$$

which agrees with (8.12), to $O(\alpha)$, for a uniform matter density. Eqn.(9.18) gives the external gravitational acceleration

$$g(r) = -\frac{(1+\frac{\alpha}{2}+O(\alpha^2)\ )MG}{r^2}, \quad r > R, \tag{9.20}$$

in agreement with (8.14). So for this case the system would produce Keplerian orbits for small test objects in orbit about this sphere. So the perturbative analysis in Sect.8.3 gave rise to a minimal attractor. For such a uniform density sphere the in-flow speed $v(r)$, matter density $\rho(r)$ and 'dark matter' density $\rho_{DM}(r)$, and the acceleration $-g(r)$ are plotted in the left column of Fig.9.1, including the special case $\alpha = 0$ which gives the Newtonian gravity results. Shown in the right hand column of Fig.9.1 are the corresponding results for a spherical shell with the same total mass M, as the sphere. In general the new theory predicts a gravitational attractor at the centre of all spherical matter distributions. Then the effective mass of the attractor is $M_{DM} = \alpha M/2$, as measured by the external gravitational acceleration in (9.20). Note that for the minimal attractor the in-flow is uniquely determined by the matter density, apart of course from time-dependent behaviour. The minimal attractor is caused by the matter induced in-flow, and as such is not the result of a primordial attractor.

9.3 Non-Minimal Attractor for a Uniform Density Sphere

Now consider the more general case of a non-minimal attractor for which the non-Newtonian acceleration field (9.10) extends beyond the matter density. These attractors have a primordial origin, and would have played a critical role in the formation of the matter system from a gas cloud. In the non-minimal case with $\overline{\beta} > 0$, we

find solutions parametrised by M and an arbitrary valued $\overline{\beta}$. Again for a sphere of uniform density as in (9.15) and with regional solutions as in (9.16), matching $f(r)$ and $f'(r)$ at $r = R$ gives

$$\beta = \overline{\beta} + \frac{16\pi\rho G R^{2+\alpha/2}}{(1-\alpha/2)(4+\alpha)}, \tag{9.21}$$

$$K = 16\pi\rho G R^3 \frac{2+\alpha/2}{3(1-\alpha/2)(4+\alpha)} = 2(1+\frac{\alpha}{2}+O(\alpha^2)\ )MG. \tag{9.22}$$

Hence the value of K is unchanged from the minimal case, while the value of β is simply increased by $\overline{\beta}$ from the minimal case. Then for the 'dark matter' density we obtain

$$\rho_{DM}(r) = \begin{cases} \frac{\alpha\overline{\beta}}{16\pi G}(1-\frac{\alpha}{2})\frac{1}{r^{2+\alpha/2}} + \frac{\alpha\rho}{4}\left(\left(\frac{R}{r}\right)^{2+\alpha/2} - 1\right), & 0 < r < R, \\ \frac{\alpha\overline{\beta}}{16\pi G}(1-\frac{\alpha}{2})\frac{1}{r^{2+\alpha/2}}, & r > R. \end{cases} \tag{9.23}$$

Then the external gravitational acceleration is given by

$$g(r) = -\frac{(1+\frac{\alpha}{2}+O(\alpha^2)\ )MG}{r^2} - \frac{\alpha\overline{\beta}}{4r^{1+\alpha/2}}, \quad r > R, \tag{9.24}$$

which asymptotically is dominated by the non-Newtonian second term, which essentially decreases like $1/r$. The first term is of course Newton's Inverse Square Law. In this non-minimal attractor case we have a superposition of a minimal attractor, with its strength given by the results in Sect.9.2, and an independent vacuum attractor with strength $\overline{\beta}$. This happens because in the case of a static spherically symmetric system the flow equation is linear. Of course in a physical situation these two components would interact because the matter density would respond to the total gravitational acceleration. Here we have ignored this dynamical effect.

One important consequence of this form for $g(r)$ is that asymptotically Kepler's orbital laws are violated. For circular orbits the centripetal acceleration relation $v_O(r) = \sqrt{rg(r)}$ gives the orbital speed to be

$$v_O(r) = \left(\frac{M + M_{DM}}{r} + \frac{\alpha\beta}{4r^{\alpha/2}}\right)^{1/2}, \tag{9.25}$$

which gives an extremely flat rotation curve. Such rotation curves are well known from observations of spiral galaxies.

9.4 Non-Spherical Gravitational Attractors

The in-flow equation (7.19)-(7.20) also has non-spherical attractors of the form

$$\mathbf{v}(\mathbf{r}) = \frac{\mathbf{r}}{r}\left(\frac{\beta}{r^{\alpha/2}} + \frac{q}{r^{\gamma}}\cos(\theta) + ...\right)^{1/2}, \tag{9.26}$$

where θ is the angle measured from some fixed direction, and where

$$\gamma = \frac{2 + \alpha + \sqrt{36 - 4\alpha + \alpha^2}}{4} \approx 2 + \frac{\alpha}{6}. \tag{9.27}$$

So the non-spherical term falls off quickly with distance.

9.5 Fractal Attractors

In the early universe there would have been primordial gravitational attractors of various strengths, as defined by their β values. It is unknown what spectrum of β values would have occurred. These would initially have all been devoid of matter agglomerations, that is they would be 'bare' attractors, because of the high temperatures. Each such attractor represents an in-flow of space which would have been in competition with the overall growth of space, as described previously. Each such attractor would have a region of influence, beyond which its flow field and consequently its gravitational field would be cancelled by that of other attractors. That is, the in-flow would be confined to that region. Clearly attractors with larger β values would have larger regions of influence. Hence space would be demarcated into a cellular form. However within each such cellular region there would be smaller attractors, and within their regions, further smaller attractors. We would then expect a fractal cellular structure: cells within cells and so on. This form is predicted by the emergent geometry of the gebit structure, as discussed in Sect.4.4, and so we appear to be seeing the linking of the bottom-up approach, from the information theoretic ideas, with the top-down phenomenological description of space and gravity, that has arisen from generalising the flow formalism of both Newtonian gravity and General Relativity. This fractal cellular structure is consistent with the in-flow equation. Each cell would respond gravitationally to the gravitational field of the cell in which it is effectively embedded. Presumably attractors can merge, though this has not been analysed so far. Over time one would then expect that over time extremely strong and spatially extended attractors would arise. As the universe cooled and the plasma recombined to form a neutral gas, that gas would have been rapidly attracted by the long range gravitational fields. Detailed studies of the dynamics of this system of fractal attractors is required, as it is this system that determined the matter distribution.

9.6 Globular Clusters

Astronomers using the Hubble Space Telescope announced [109, 110] that they had discovered evidence for intermediate mass black holes (IMBH), with masses from 100 to tens of thousands of solar masses. They believed that they had already established the existence of stellar black holes with masses from a few to ten solar masses. Stellar black holes were believed to be formed by the collapse of the cores

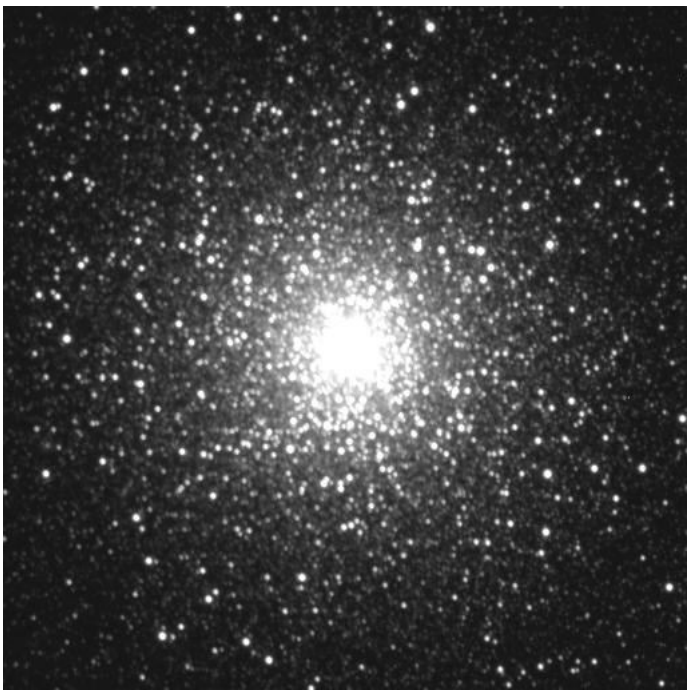

Figure 9.2: Globular cluster M15 in the constellation Pegasus, about 40,000 light years away, contains some 30,000 stars. M15 is one of some 150 known globular clusters that from a halo surrounding the Milky Way. The core is tightly packed.

of giant stars. But M15 and G1 suggested the existence of medium sized black holes. M15, Fig.9.2, is in the constellation Pegasus, while G1 is near the Andromeda Galaxy. These clusters are some of the nearly 150 known globular clusters that form a halo surrounding the Milky Way. It is believed that the rising density of stars towards the centre had resulted in a collapse of the core, leaving an IMBH. Using the motion of stars within the clusters the mass of the cluster and of the 'black hole' were determined. In General Relativity the mass of such a black hole would depend on how many stars had been drawn into the black hole, and that is not predictable without generating some dynamical history for the globular cluster. However in the new theory of gravity we must have at least a minimal gravitational attractor, whose mass is computable, and is given to sufficient accuracy by the perturbative result. So the globular clusters M15 and G1 give an excellent opportunity to test the presence of the attractor and its effective mass.

Numerical solutions of (8.8) for a typical cluster density profile are shown in Fig.9.3 and revealed that indeed the central 'dark matter' attractor has a mass accurately given by the perturbative result $M_{DM}/M = \alpha/2 = 0.00365$. For M15 the mass of the central 'black hole' was found to be [109] $M_{DM} = 1.7^{+2.7}_{-1.7} \times 10^3 \mathrm{M}_\odot$,

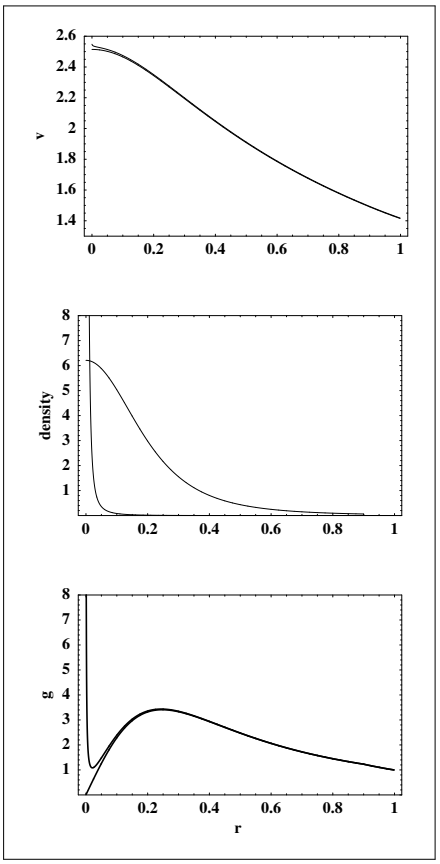

Figure 9.3: Assuming a matter density profile falling off like $1/(r^2 + b^2)^2$, appropriate for a globular cluster, the in-flow speed was computed from the in-flow equation, as shown in the upper plot, which is larger than the 'Newtonian in-flow' speed near $r = 0$, as also shown in the plot. The difference becomes very large for small r, but this is not shown in the plot. The matter density and the effective 'dark matter' density are shown in the middle plot. The lower plot shows the gravitational acceleration, with the strong peak at $r = 0$ caused by the induced minimal attractor. The effective mass of the attractor is given by $M_{DM} = \alpha M/2$ to good accuracy. A non-minimal attractor would give even larger effects near $r = 0$.

and the total mass of M15 was determined [111] to be $4.9 \times 10^5 \mathrm{M}_\odot$. Then these results together give $M_{DM}/M = 0.0035^{+0.011}_{-0.0035}$ which is in excellent agreement with the above prediction. For G1 we have [110] $M_{DM} = 2.0^{+1.4}_{-0.8} \times 10^4 \mathrm{M}_\odot$, and $M = (7-17) \times 10^6 \mathrm{M}_\odot$. These values give $M_{MD}/M = 0.0006 - 0.0049$, which is also consistent with the above $\alpha/2$ prediction.

However there is one complication in this analysis. The determination of the 'black hole' mass followed from stochastic modelling of the motion of the inner stars, which was compared with the motion of those stars as revealed by the HST. In that modelling the gravitational acceleration caused by the 'black hole' would have been described by Newton's inverse square law form: $g(r) \sim 1/r^2$. However the attractor produces a gravitational acceleration of the form: $g(r) \sim 1/r^{1+\alpha/2}$. Hence to test the attractor explanation it is necessary for the stochastic modelling to be repeated using this modified force law. Nevertheless that the attractor explanation gives masses consistent with the observations and modelling is very encouraging. The attractor explanation is independent of the dynamical history of the globular cluster. Observations of other clusters should confirm that they all have the same mass ratio $M_{DM}/M = \alpha/2$. Of course there is an event horizon associated with the attractor, and to that extent we can continue to describe the attractor as a 'black hole', though one very different from that of General Relativity.

9.7 Spiral and Elliptical Galaxies

Consider the non-perturbative solution of (7.19)-(7.20), say for a galaxy with a non-spherical matter distribution. Then numerical techniques are necessary, but beyond a sufficiently large distance the in-flow will have spherical symmetry, and in that region we may use (8.8) and (8.9) with $\rho(r) = 0$. Then this pair has an exact non-perturbative analytic solution which we write in the form

$$v(r) = \overline{K} \left(\frac{1}{r} + \frac{1}{R_S} \left(\frac{R_S}{r} \right)^{\frac{\alpha}{2}} \right)^{1/2} , \tag{9.28}$$

where $\overline{K}$ and R_S are arbitrary constants in the $\rho = 0$ region, but where the value of $\overline{K}$ is determined by matching to the solution in the matter region. Here R_S characterises the length scale of the non-perturbative non-minimal attractor part of this expression, and $\overline{K}$ depends on α and G and details of the matter distribution. The galactic circular orbital velocities of stars etc may be used to observe this process in a spiral galaxy and from (8.1) and (9.28) we obtain a replacement for the Newtonian 'inverse square law',

$$g(r) = \frac{\overline{K}^2}{2} \left(\frac{1}{r^2} + \frac{\alpha}{2 r R_S} \left(\frac{R_S}{r} \right)^{\frac{\alpha}{2}} \right) , \tag{9.29}$$

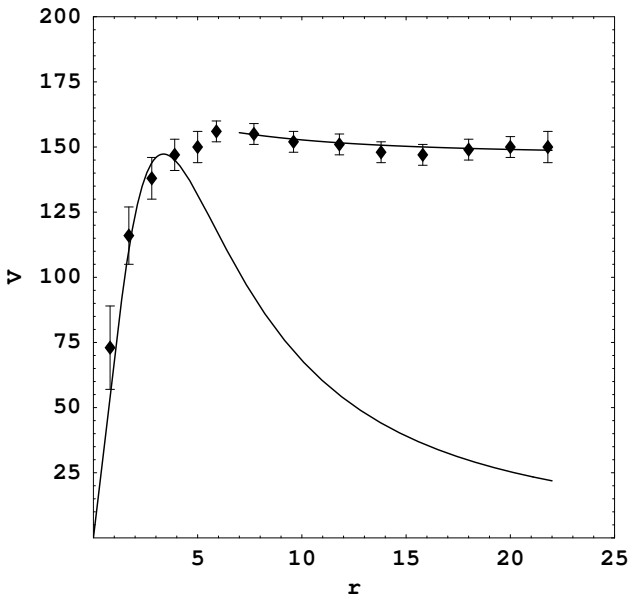

Figure 9.4: Rotation-velocity curve plot for the spiral galaxy NGC3198, with v in km/s, and r in kpc/h. Complete curve is rotation curve expected from Newtonian theory of gravity or the General Theory of Relativity for an exponential disk, which decreases asymptotically like $1/\sqrt{r}$. The incomplete curve shows the asymptotic form from (9.30).

in the asymptotic limit. From (9.29) the centripetal acceleration relation $v_O(r) = \sqrt{rg(r)}$ gives a 'universal rotation curve'

$$v_O(r) = \frac{\overline{K}}{2}\left(\frac{1}{r} + \frac{\alpha}{2R_S}\left(\frac{R_S}{r}\right)\frac{\alpha}{2}\right)^{1/2} \quad . \tag{9.30}$$

Because of the α dependent part this rotation-velocity curve falls off extremely slowly with r, as is indeed observed for spiral galaxies. Of course it was the inability of the Newtonian and Einsteinian gravity theories to explain these observations that led to the notion of 'dark matter'. It is possible to illustrate the form in (9.30) by comparing it with rotation curves of spiral galaxies. Persic, Salucci and Stel [112] analysed some 1100 optical and radio rotation curves, and demonstrated that they are describable by the empirical universal rotation curve (URC)

$$\begin{aligned} v_O(x) &= v(R_{opt})\left[\left(0.72 + 0.44\mathrm{Log}\frac{L}{L_*}\right)\frac{1.97x^{1.22}}{(x^2+0.78^2)^{1.43}}\right. \\ &\qquad \left. +1.6\mathrm{e}^{-0.4(L/L_*)}\frac{x^2}{x^2+1.5^2(\frac{L}{L_*})^{0.4}}\right]^{1/2} \end{aligned} \tag{9.31}$$

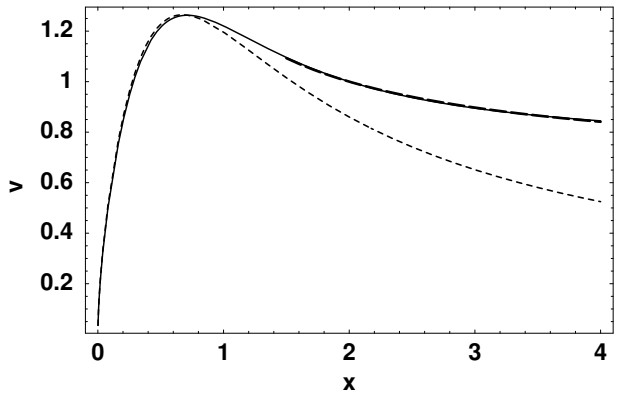

Figure 9.5: Spiral galaxy rotation velocity curve plots, with $x = r/R_{opt}$. Solid line is the Universal Rotation Curve (URC) for luminosity $L/L_* = 3$, using the URC in (9.31), Ref.[112]. Short dashes line is URC with only the matter exponential-disk contribution, and re-fitted to the full URC at low x. Long dashes line is the form in (9.30), for $\alpha = 1/137$ and $R_S = 0.01R_{opt}$.

where $x = r/R_{opt}$, and where R_{opt} is the optical radius, or 85% matter limit. The first term is the Newtonian contribution from an exponential matter disk, and the 2nd term is the 'dark matter' contribution. This two-term form also arises from the in-flow theory, as follows from (8.7). The form in (9.30) with $\alpha = 1/137$ fits, for example, the high luminosity URC, for a suitable value of R_S, which depends on the luminosity, as shown by one example in Fig.9.5. For low luminosity data the observations do not appear to extend far enough to reveal the asymptotic form of the rotation curve, predicted by (9.30).

But the general form in (9.28) leads to a key question. Why is it that R_S is essentially very large for the earth, as shown by the borehole data, and also for elliptical galaxies as shown by the recent discovery [113] that planetary nebulae in ordinary elliptical galaxies, serving as observable 'test objects', have Keplerian or Newtonian rotation curves, whereas spiral galaxies have small values of R_S compared to their R_{opt} values, and that furthermore their R_S values are related to their luminosity. The answer to this question is that the in-flow equation actually has a one-parameter class of matter-free non-perturbative non-minimal gravitational attractor exact solutions of the form

$$v(r) = \frac{\beta}{r^{\alpha/4}}, \tag{9.32}$$

These solutions correspond to a novel feature of the new theory of gravity, namely the occurrence of these gravitational attractors. These attractors presumably were produced during the big-bang, and since they can coalesce to form larger attractors, it is most likely that it is such an attractor that leads to the formation of galaxies. As already noted in (9.23) the effective 'dark matter' density for these attractors

falls off, essentially, like $1/r^2$, as astronomers had deduced from observations of the rotation curves of spiral galaxies. This leads to the following expression for the total 'dark matter' within radius R

$$M_{r<R} = 4\pi \int_0^R \rho_{DM}(r) r^2 dr = \frac{\alpha\beta R^{1-\alpha/2}}{4G}, \tag{9.33}$$

which increases almost linearly with R. It is this expression that explains the observations that the total amount of 'dark matter' exceeds the real amount of matter, as revealed by its luminosity, by often an order of magnitude. As R is made larger this 'dark matter' mass increases without limit. Attractors appear to form a cellular network, with the attractor form in (9.32) only valid for a single attractor. Attractors with large β values, and so large regions of influence, will attract greater quantities of the original post-big-bang gas. As well because these have large in-flow velocities the matter will end up with high angular momentum, resulting in a spiral galaxy and/or a cluster of galaxies. Then the magnitude of β is related to the total amount of matter in the galaxy, which manifests eventually as its luminosity. Smaller attractors will form galaxies with lower in-flow speeds and so are less likely to have large amounts of angular momentum. This case seems to explain the elliptical galaxies. We would also expect the effective mass of the supermassive black holes at the centre of galaxies to be related to the total mass $M_{r<R}$, as has been noted. The distribution of the 'dark matter' effective density may be observed by gravitational lensing, because the geodesic equation actually determines the effect of the quantum-foam in-flow on light. Such observations have already become available from microlensing observations and analysis [116, 117].

9.8 'Dark Matter' Vortex Filaments

We consider here a possible generalisation of the vorticity equation in (7.20), by including on the RHS a contribution form the effective 'dark matter' density, so that it becomes

$$\nabla \times (\nabla \times \mathbf{v}) = \frac{8\pi G\rho}{c^2}\mathbf{v}_R + \frac{8\pi G\rho_{DM}}{c^2}\mathbf{v}. \tag{9.34}$$

Using the definition of ρ_{DM}, and away from actual matter, this becomes

$$\nabla \times (\nabla \times \mathbf{v}) = \frac{\alpha}{4c^2}((trD)^2 - tr(D^2))\mathbf{v}. \tag{9.35}$$

This equation has vortex filament solutions. Writing $\mathbf{v}(\mathbf{r}) = (+y, -x, 0)h(r)$ for a vortex in the z-direction, where $h(r)$ is the vortex profile, and where coordinates are used where $r = \sqrt{x^2 + y^2}$ is the perpendicular distance from the axis of the vortex, (9.35) gives the non-linear differential equation for $h(r)$,

$$\frac{3h'}{r} + h'' + \frac{\alpha}{2c^2}(h + rh')h^2 = 0. \tag{9.36}$$

Although no analytic solutions are known, numerical studies reveal that this equation has non-trivial vortex profiles. These vortices can only end on a black hole singularity, and so these vortices provide a possible explanation for the so-called 'dark matter' networks which have been detected using weak gravitational lensing [116, 117], for the 'dark-matter' density associated with these vortices lenses light, via the geodesic equation, as if there were real matter present. At the galactic scale these vortex filaments then link the black holes which are necessarily present in galaxies. As well they provide a possible explanation for the Allais solar eclipse effect, in that the anomalous precession of the paraconical pendulum during a solar eclipse appears to indicated the presence of at least a vortex filament linking the minimal black hole within the sun with the corresponding minimal black hole within the earth, with the moon and its black hole disturbing the earth-sun vortex filament during a solar eclipse. More complicated scenarios could have an earth-moon vortex as well as a sun-moon vortex.

9.9 Stellar Structure

The structure of stars is very much based on the assumption that the Newtonian theory of gravity is sufficiently accurate. This leads to the Solar Standard Model (SSM) in the case of the sun. However the new theory of gravity predicts at least a minimal gravitational attractor at the centres of stars, with an associated event horizon. This quantum-foam in-flow singularity causes the gravitational acceleration to be very different to that from the Newtonian theory, as already illustrated by a number of cases. Bahcall and Davis started an exploration of the sun by means of neutrinos [114, 115], with that work resulting in the solar neutrino anomaly, namely that all experiments, exploring different portions of the solar neutrino spectrum, reported a flux less than that predicted. The solar neutrino flux is determined by the physical and chemical properties of the sun, such as density, temperature, composition and so on. The current interpretation of the solar neutrino anomaly is in terms of the neutrino masses and mixing leading to oscillations of ν_e into active (ν_μ and/or ν_τ) or sterile neutrino, ν_s.

Because of the gravitational attractor effect one of the key equations in the SSM, the equation for hydrostatic equilibrium,

$$\frac{dP(r)}{dr} = -\rho(r)g(r) = -\frac{G\rho(r)m(r)}{r^2}, \tag{9.37}$$

where $P(r)$ is the hydrostatic pressure, $\rho(r)$ is the matter density and $m(r)$ is the matter within radius r, must be changed to

$$\frac{dP(r)}{dr} = -\frac{G\rho(r)m(r)}{r^2} - \frac{2\pi\alpha\rho(r)G}{r^2}\int_0^r \left(\int_s^R s'\rho(s')ds'\right) ds, \tag{9.38}$$

from (8.14) to $O(\alpha)$ terms. Towards the centre of the star this equation is dominated by the α dependent term. We can illustrate this for the simple case of uniform density. In this case (9.37) gives

$$P(r) = \frac{2\pi G\rho^2(R^2 - r^2)}{3}, \tag{9.39}$$

where R is the radius of the star, and where $P(R) = 0$, giving a finite pressure at the centre $r = 0$. However (9.38) becomes

$$\frac{dP(r)}{dr} = -\frac{4}{3}\pi G\rho^2 r - \pi\alpha\rho^2 G(\frac{R^2}{r} - \frac{r}{3}), \tag{9.40}$$

with solution

$$P(r) = \frac{2\pi(1 + \alpha/4)G\rho^2(R^2 - r^2)}{3} + \pi\alpha G\rho^2 R^2 \ln(\frac{R}{r}), \tag{9.41}$$

which reveals a logarithmic pressure singularity at the centre. In a more realistic modelling this effect would probably be even more pronounced, as the density would increase there as a consequence of such a pressure increase. Existing stellar structure codes need modification in order for this effect to be explored, and for any signature of the effect on the neutrino flux revealed. Because there is an event horizon at the centre of stars, essentially a black hole effect, though one very different from that of General Relativity, an additional source of energy, and hence heating is available, namely the radiation from matter falling into this black hole. This would, even by itself, increase the temperature of the central region of stars.

Radiometric data from the Pioneer 10/11, Galileo, and Ulysses spacecraft indicated an apparent anomalous, constant, acceleration acting on the spacecraft with a magnitude of $\sim 8.5 \times 10^{-8}$ cm/s^2 directed towards the sun [118]. For Pioneer 10/11 the acceleration was 8.56×10^{-8} cm/s^2 at 30 AU, while at 60 AU it was 8.09×10^{-8} cm/s^2. If there was a non-minimal gravitational attractor associated with the sun, we would expect an anomalous acceleration directed towards the sun, but decreasing like $1/r$. However the Pioneer 10/11 data does not indicate any such decrease, and so we conclude that (i) there is no evidence yet for such a non-minimal attractor, and (ii) that the new theory of gravity does not offer an explanation for this anomalous acceleration.

9.10 Laboratory Quantum Gravity Experiments

Quantum gravity effects are really just quantum-foam in-flow effects. As discussed in Sect.8.5 such effects have been manifest in ongoing attempts to measure G over the last 60 years. There they showed up as $O(\alpha)$ unexplained systematic effects. The new theory of gravity has two fundamental constants α and G, and clearly one cannot measure one of these alone. These G measurement experiments basically

measure the force between two test masses as a function of separation distance. Using the linearity of the Newtonian theory of gravity the computation of these forces involves a vector sum of the forces between the individual mass points in the different test masses. However in the new theory there is a non-linearity whose magnitude is determined by α. Assuming a stationary in-flow the velocity field is given by the simplified flow equation (7.11), neglecting vorticity and the velocity field $\mathbf{v}_R$, which gives

$$|\mathbf{v}(\mathbf{r})|^2 = \frac{2}{4\pi}\int d^3r' \frac{C(\mathbf{v}(\mathbf{r}'))}{|\mathbf{r}-\mathbf{r}'|} - 2\Phi(\mathbf{r}). \tag{9.42}$$

with the *ansatz* that the direction of $\mathbf{v}(\mathbf{r})$ is the same as the direction of $\mathbf{g}(\mathbf{r})$, where this gravitational acceleration is given by

$$\mathbf{g}(\mathbf{r}) = \frac{\mathbf{1}}{\mathbf{2}}\nabla(\mathbf{v^2}(\mathbf{r})). \tag{9.43}$$

A more complete analysis, which avoids the directional *ansatz*, involves computing the time-dependent solutions of the velocity potential equation (8.5). Here $\Phi(\mathbf{r})$ is the Newtonian gravity potential caused by the matter density, while the α dependent term is

$$C(\mathbf{v}) = \frac{\alpha}{8}((trD)^2 - tr(D^2)), \tag{9.44}$$

and where

$$D_{ij} = \frac{1}{2}(\frac{\partial v_i}{\partial x_j} + \frac{\partial v_j}{\partial x_i}). \tag{9.45}$$

Clearly the first term of the RHS of (9.42) is a contribution to the Newtonian potential from the 'dark matter' effect. As we have already noted this effect permits the introduction of an effective 'dark matter' density of the form

$$\rho_{DM}(\mathbf{r}) = \frac{\alpha}{32\pi G}((trD)^2 - tr(D^2). \tag{9.46}$$

It is easier to see the effects of the non-linearity of this term by computing and displaying this matter density in those cases relevant to a Cavendish-type laboratory experiment in which both α and G are measured together. In Fig.9.6 is shown the 'dark matter' density for two spheres for the cases of two separation distances. When the sphere are well separated the 'dark matter' effect occurs at the centre of each sphere, but as they are brought together the non-linearity of the effect causes the 'dark matter' density to become essentially polarised, that is, in each mass it moves away from the centre, and there is also a small region of 'dark matter' that forms outside and between the two spheres. Because of this non-linear polarisation effect the net force between the two spheres is not describable by the Newtonian theory. The deviations from the Newtonian theory then permitting the experimental determination of α from such an experiment. This effect is a key prediction and provides a critical test of the new theory. An analysis of the data requires

numerical solutions of the flow fields for each configuration of the masses in such an experiment. To show how a change in matter distribution can effect the results in Fig.9.7 the 'dark matter' density distribution for the case of an elliptical mass is shown for three different eccentricities. Here we see that as the matter distribution becomes more eccentric, approaching that of a thin disk, the 'dark matter' density becomes negative, except near the edges of the disk, and extends beyond the disk, unlike the case of a spherical matter distribution. The magnitude of these effects is $O(\alpha)$, i.e. 1%, and so easily detectable with existing Cavendish-type experimental rigs. The effects of this 'dark matter' polarisation are evident in Figs.9.6 and 9.7. However it should be noted that in doing these computations we have assumed zero vorticity, which may have introduced some anomalous aspects to the flow. Also by neglecting the $\mathbf{v}_R$ field we have certainly neglected the effect upon these flows of the gravitational effect of the earth, when Cavendish experiments are performed upon the surface of the earth.

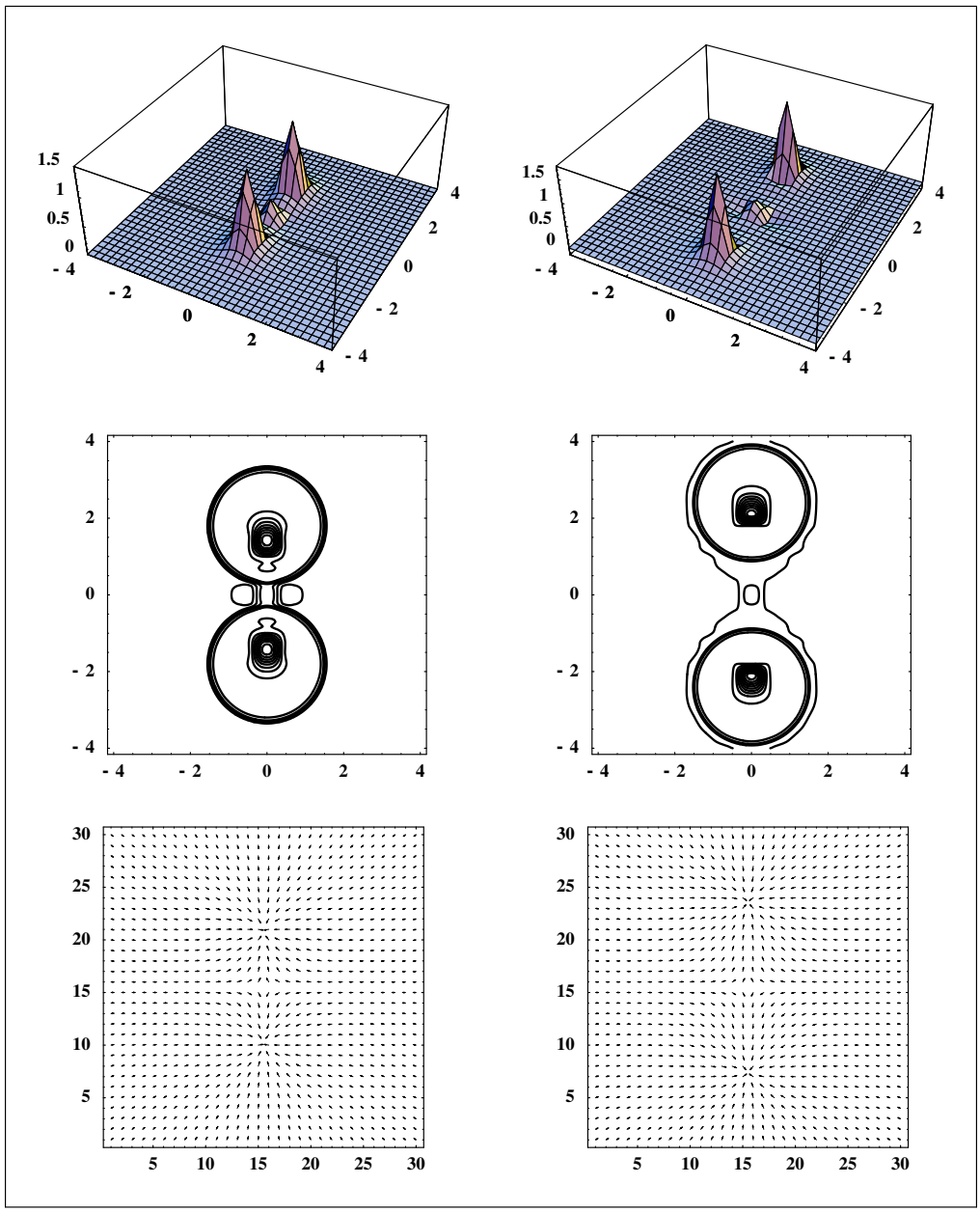

Figure 9.6: Cavendish experiment with two spheres, each of radius 1.5, and with uniform density. On the left the separation of the centres is 3.6, while on the right the separation is 4.8. The upper plots show the 'dark matter' density distributions of the gravitational attractors, as also shown in the middle contour plots. The contour plots clearly reveal the 'polarisation' effect of the 'dark matter' density, which is greater for smaller separations. In each case the ratio of the total 'dark matter' to the total mass is 0.0045. The lower plots show the in-flow velocity fields. These are quantum gravity effects that are detectable in laboratory experiments.

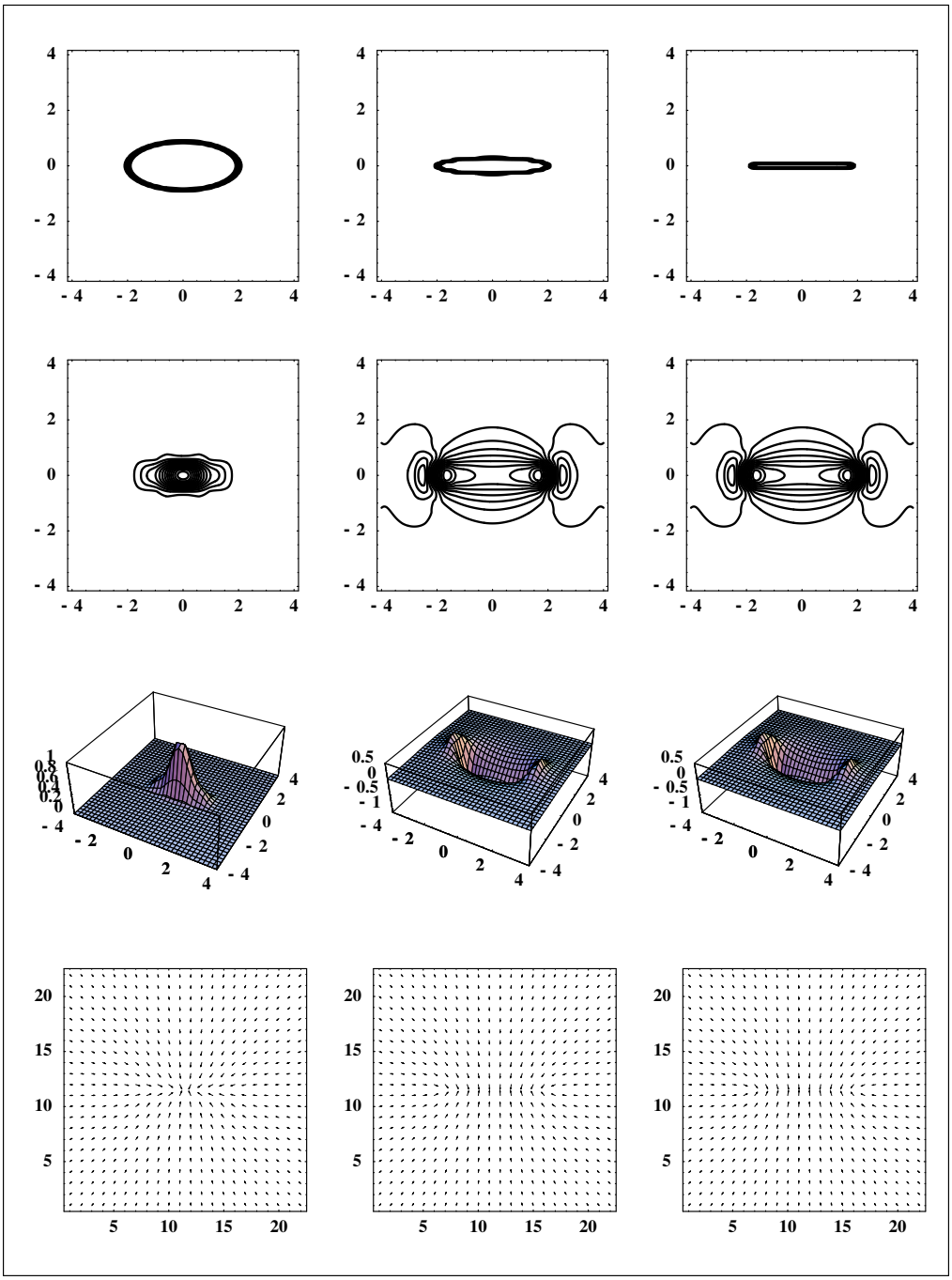

Figure 9.7: Dark matter densities, middle two rows, for solid elliptical masses with cylindrical symmetry, top row, of different eccentricities; $e = 0.9, 0.99$ and 0.999. Velocity flow fields shown in bottom row.

Chapter 10

Detection of Absolute Motion

10.1 Space and Absolute Motion

The phenomena of space has resisted understanding for thousands of years. Properties of space were observed and used by the Babylonians and Egyptians, apparently in the latter case to enable the agricultural boundaries to be re-established after flooding of the Nile Valley. Eventually these properties of space were encoded and formalised in the mathematics of geometry with its abstract notions of a *geometrical space*, *points*, *lines* etc. A major compilation of the results was written by Euclid in 300 BCE. This was the first major modelling of physical phenomena by a mathematical system, and gave us the mindset of syntactical formalism that prevails in physics to this day. Eventually the mathematical model became identified with the phenomena itself, that is, physical space was understood to be a geometrical space. And so the distinction between physical space and geometrical space disappeared. This confusion of a phenomena with its mathematical modelling is a re-occurring problem in physics. Given that now physical space was considered to be a Euclidean geometrical system, and as such devoid of structure, thinkers like Descartes and Newton appreciated that such a modelling appeared to be deficient. To improve the modelling they embellished the old Aristotelian notion that space was occupied by an *aether*. This dualism with both *space* and *aether* became a major concept in physics. It does not appear to have occurred to the early investigators that something other than *geometrical space* could underpin the phenomena of physical space. In the same era Galileo introduced the modelling of time by the geometrical one-dimensional space, and Newton made extensive use of this modelling in his development of dynamics. Like space the phenomena of time eventually became synonymous with its geometrical model until today most physicists regard time as a 'geometrical phenomenon', which is actually an oxymoron, which of course necessitates the denial of any aspects of time that the geometrical model cannot accommodate. Of course that is how *non-process* physics was arrived at.

Descartes considered the aether to have the structure of whirling large and small

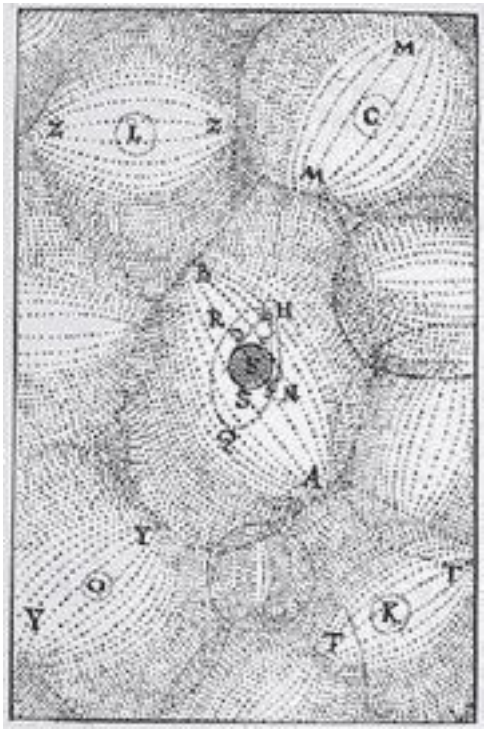

Figure 10.1: Descartes' vortices carry the planets about the sun. Plate VI from [119].

vortices, and that the motion of these vortices, for instance, carried the planets in their orbits about the sun, as illustrated in Fig.10.1.

Newton in a letter in 1675 to Oldenburg, Secretary of the Royal Society, and later to Robert Boyl, used the *aether* to offer a different explanation of planetary motion, namely that the gravitational theory he had developed was to be explained as being the result of a

> *condensation causing a flow of an ether with a corresponding thinning of the ether density associated with the increased velocity of flow*

though Newton was of the opinion that this aether flow was undetectable.

The concept of the aether was generally accepted, and following Maxwell's successful development of the unifying theory for electromagnetic phenomena which predicted a unique speed c for light, the need for the aether became even greater as it was believed that this speed referred to the motion of light relative to the aether. It was the argued by Maxwell that the motion of the earth through the aether should be measurable by means of the change in speed of the light as measured by an observer travelling with the earth. This is the concept of absolute motion, namely that motion with respect to space itself is meaningful and measurable. The size of this effect is $v/c = 1/10,000$, where $v = 30$km/s is the orbital speed of the

earth, and $c = 300,000$km/s. Maxwell appreciated that an experiment that utilised a ray of light going outward and then returning would result in the effect becoming only second order in v/c, and since $(v/c)^2 = 10^{-8}$ it was thought to be too small for measurement.

Michelson responded to Maxwell's challenge and in 1880-1881 he devised the instrument now known as the Michelson interferometer to detect this absolute motion [121]. The dualism of space and aether was still favoured, so such experiments became known as *aether drift* experiments. As explained in detail later a beam of light is split into two, sent in orthogonal directions, and reflected back to a common place. Differences in travel times for the two beams were expected to result in interference fringes being formed, as was seen. However the key operational effect is that the fringes should drift across the field of view as the interferometer is rotated, if absolute motion existed as a phenomenon. The magnitude of the maximum fringe shift is then a measure of the absolute speed of the earth. An interferometer with arms of length $L = 1.2$m was built and operated in Germany by Michelson, but the effects of vibrations made the results inconclusive. In 1887 Michelson and Morley, having constructed a new interferometer with arms with an effective length of $L = 11$m, achieved by the use of multiple reflections from mirrors, performed their key experiment in the Main Building of Adelbert College in Cleveland. No other experiment in the history of physics has ever acquired the significance and consequences of this one experiment.

The experiment involved observations over brief periods over four days in July 1887, and involved in all only 36 turns of the interferometer. Remarkably the results [122] showed the shift of the interference fringes characteristic of absolute motion, and analysis of the results using Newtonian physics gave a speed of approximately 8km/s, which is certainly a very high speed, but significantly less than the orbital speed of the earth. Absolute motion had been discovered, but clearly there was a problem with the magnitude of the effect according to the prevailing theory of the interferometer. How could the interferometer determined speed be less than the orbital speed? It could have just been the bad luck of the month of July when perhaps the solar system and the earth had a net vectorially summed speed of 8km/s. Michelson could easily have resolved this possibility be repeating the experiment over a year, during which time the vectorial sum of the two velocities would have changed and the vector sum effect would have been observable. It would be over 100 years before the smallness of this interferometer determined speed was finally understood. Indeed the Michelson-Morley data corresponds to an actual absolute speed of some 400km/s. The analysis by Michelson of the experimental data thus turned out to be totally flawed. Michelson had placed total faith in Newtonian physics, and in particular in Galilean Relativity, and never countenanced the possibility that it could require revision, that his experiment was in fact revealing not the absence of absolute motion but the very failure of Newtonian physics. The failure by Michelson to understand this point had disastrous consequences for the development of physics

throughout the twentieth century. Physics has yet to recover from the misreporting and misinterpretation of this experiment.

Dayton Miller knew that the Michelson-Morley experiment had in fact detected absolute motion and set out to build even larger Michelson interferometers. Miller also understood that the physical principles involved in the interferometer were not understood, and he introduced the k parameter to allow for this. In one of the greatest experiments ever in physics Miller successfully operated his interferometer over many years taking detailed data from thousands of rotations at all times of the day and throughout the year. As Miller argued an understanding of the value of the k parameter would have to wait further developments in physics, but in the meantime he could determine the magnitude and direction of the absolute speed of the solar system by using the modulating effect of the earth's yearly rotation about the sun. The same analysis also permitted the effective value of k to be determined. Miller's analysis, published [123] in 1933, resulted in an absolute speed of some 200km/s in a direction near to the South Celestial Pole.

Miller's discovery was ignored and after his death his experiments were attacked for being poorly executed. Why was this? And why were the many successful repetitions of the detection of absolute motion ignored? Michelson himself was devoted to the task of detecting absolute motion and repeatedly built and operated new interferometers until his death in 1941. Each one of these interferometers did in fact reveal the effects of absolute motion, but Michelson's method of analysis had remained flawed as he had ignored Miller's treatment of the problem of an inadequate understanding of actually how an interferometer operated. Michelson died not realising that he had again and again observed absolute motion. Ironically during his life he had been richly rewarded by a Nobel prize for reporting that the effects of absolute motion had not been observed. Miller who had perfected the Michelson interferometer and who had worked around the theoretical limitations on the understanding of its operation and who had correctly analysed the vast amount of his data to reveal the magnitude and direction of motion of the solar system, and who had detected the rotational motion of the earth in its orbit about the sun via a purely laboratory based experiment was completely castigated by the physics community.

The operation of the Michelson interferometer was not finally understood until 2002 when the theoretical explanation for Miller's k parameter was finally discovered [12]. Briefly the interferometer involves three key physical effects (i) a change in the difference of the geometrical path length of the two light beams when the interferometer is in absolute motion and (ii) a Fitzgerald-Lorentz real physical contraction of the arm parallel to the direction of motion. The final third and last effect is critical: (iii) the first two effects cancel if the interferometer is operated in vacuum, but do not cancel if the light passes through air or some other gas, and only then is absolute motion detectable by the interferometer. Both the Michelson-Morley and Miller experiments were done in air. It turns out that Miller's k parameter

is determined by the refractive index n of the gas according to $k = \sqrt{n(n^2-1)}$. Finally after over 100 years the diverse gas-mode interferometer data could be analysed and understood. One of the most significant discoveries [14] to come from that re-analysis is that as well as detecting the absolute motion of the solar system through space and the orbital speed of the earth in its orbit about the sun the data also reveals an inflow past the earth towards the sun. This is the very in-flow that Newton had contemplated. It is observable and it is the explanation for gravity. As well the interferometer data shows that the direction of absolute motion relative to local space, after taking account of the in-flow towards the sun, is different to the direction of motion relative to the universe as a whole. This is because of the gravitational quantum-foam in-flow into the Milky Way galaxy and Local Cluster.

But why had all these discoveries not emerged at the beginning of the twentieth century when all the clues and theoretical insights had begun to emerge? The explanation is clear in the history books. In response to Michelson's bungled analysis and building upon the many theoretical insights by Fitzgerald, Lorentz, Larmor and others the Einsteins usurped and formalised the work of all these physicists by asserting that absolute motion was without meaning and consequently not observable. The formalism introduced the geometrical *spacetime* construct which amounted to a truly bizarre reinterpretation of the relativistic effects that Fitzgerald [124], Lorentz [125] and Larmor [126] had introduced. Eventually the Einstein interpretation came to be accepted over the more physical interpretation that the effects on clocks and rods were real physical effects caused by absolute motion. Indeed in an even more bizarre turn of events it became accepted within physics, as a direct consequence of the Einstein postulates, that the relativistic effects were incompatible with absolute motion. Within a decade or so of the introduction of the Einstein re-interpretation absolute motion had become a banned concept in physics, and still is to this day. By the time Miller's extraordinary interferometer experiments began to produce such dazzling evidence of absolute motion effects the prevailing belief in physics was that absolute motion was mutually exclusive to the various experimentally confirmed relativistic effects. So Miller had to be proved wrong. In one of the most perverse papers ever published Shankland and others [127] set out to do just that[1], and after Miller had died. This was despite the fact that Shankland had been a research associate of Miller and had participated in the final determination of the absolute motion of the solar system.

The operation of the Michelson interferometer is analysed in the following chapters, and the various results that follow from analysis of the data are presented. As well other experiments that confirm the Miller results are introduced including in particular a recent 1991 first-order experiment by Roland DeWitte. It is now clear that first-order devices that are far superior to the Michelson interferometer will greatly simplify the experimental study of various physical phenomena that are

[1]Einstein had been very concerned about the results that Miller was obtaining and in a number of letters to Shankland he expressed his gratitude to Shankland for dealing with them.

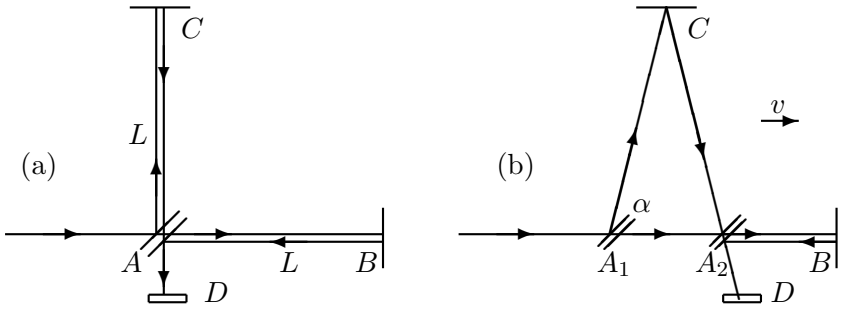

Figure 10.2: Schematic diagrams of the Michelson Interferometer, with beamsplitter/mirror at A and mirrors at B and C on arms from A, with the arms of equal length L when at rest. D is a quantum detector that causes localisation of the photon state by a collapse process. In (a) the interferometer is at rest in space. In (b) the interferometer is moving with speed v relative to space in the direction indicated. Interference fringes are observed at the quantum detector D. If the interferometer is rotated in the plane through 90^o, the roles of arms AC and AB are interchanged, and during the rotation shifts of the fringes are seen in the case of absolute motion, but only if the apparatus operates in a gas. By counting fringe changes the speed v may be determined.

manifest in the absolute motion effects. In particular the gravitationally related in-flow past the earth towards the sun and the turbulence that appears to be present in that in-flow will be studied. As explained earlier the in-flow effect is essentially related to quantum gravity effects, and so the first-order devices gives us for the first time techniques for investigating quantum gravity. Of particular significance is that the direction of the absolute motion of the solar system as determined by the Miller interferometer studies is in a direction different to that of the motion of the solar system with respect to the Cosmic Microwave Background (CMB) defined frame of reference. This again is a manifestation of gravitational in-flows, this time into the Milky Way galaxy and Local Cluster.

10.2 Theory of the Michelson Interferometer

We now show for the first time in over 100 years how the three key effects together permit the Michelson interferometer [121] to reveal the phenomenon of absolute motion when operating in the presence of a gas, with the third effect only discovered in 2002 [12]. The main outcome is the derivation of the origin of the Miller k^2 factor in the expression for the time difference for light travelling via the orthogonal arms,

$$\Delta t = k^2 \frac{L|\mathbf{v}_P|^2}{c^3} \cos(2(\theta - \psi)). \tag{10.1}$$

Here $\mathbf{v}_P$ is the projection of the absolute velocity $\mathbf{v}$ of the interferometer through the quantum-foam onto the plane of the interferometer, where the projected velocity

vector $\mathbf{v}_P$ has azimuth angle ψ relative to the local meridian, and θ is the angle of one arm from that meridian. The k^2 factor is $k^2 = n(n^2 - 1)$ where n is the refractive index of the gas through which the light passes, L is the length of each arm and c is the speed of light relative to the quantum foam. This expression follows from three key effects: (i) the difference in geometrical length of the two paths when the interferometer is in absolute motion, as first realised by Michelson, (ii) the Fitzgerald-Lorentz contraction of the arms along the direction of motion, and (iii) that these two effects precisely cancel in vacuum, but leave a residual effect if operated in a gas, because the speed of light through the gas is reduced to $V = c/n$, ignoring here for simplicity any Fresnel-drag effects, Appendix.E, which are analysed in Appendix.G. This is one of the aspects of the quantum foam physics that distinguishes it from the Einstein formalism. The time difference Δt is revealed by the fringe shifts on rotating the interferometer. In Newtonian physics, that is with no Fitzgerald-Lorentz contraction, $k^2 = n^3$, while in Einsteinian physics $k = 0$ reflecting the fundamental assumption that absolute motion is not measurable and indeed has no meaning. The Special Relativity null effect for the interferometer is explicitly derived in Appendix H. So the experimentally determined value of k is a key test of fundamental physics. Table 1 summarises the differences between the three fundamental theories in their modelling of time, space, gravity and the quantum, together with their distinctive values for the interferometer parameter k^2. For air $n = 1.00029$, and so for process physics $k = 0.0241$ and $k^2 = 0.00058$, which is close to the Einsteinian value of $k = 0$, particularly in comparison to the Newtonian value of $k = 1.0$. This small but non-zero k value explains why the Michelson interferometer experiments gave such small fringe shifts. Fortunately it is possible to check the n dependence of k as two experiments Illingworth [128] and Joos [129] were done in helium gas, and this has an n^2-1 value significantly different from that of air.

Theory	Time	Space	Gravity	Quantum	k^2
Newton	geometry	geometry	force	Quantum Theory	n^3
Einstein	curved geometry		curvature	Quantum Field Theory	0
Process	process	quantum foam	inhomogeneous flow	Quantum Homotopic Field Theory	$n(n^2-1)$

Table 1: Comparisons of Newtonian, Einsteinian and Process Physics.

In deriving (10.2) in the new physics it is essential to note that space is a quantum-foam system which exhibits various subtle features. In particular it exhibits real dynamical effects on clocks and rods. In this physics the speed of light is only c relative to the quantum-foam, but to observers moving with respect to this quantum-foam the speed appears to be still c, but only because their clocks and rods are affected by the quantum-foam. As shown in Sect.7.4 such observers will find that records of observations of distant events will be described by the Einstein spacetime formalism, but only if they restrict measurements to those achieved by using clocks, rods and light pulses, that is using the Einstein measurement protocol.

However if they use an absolute motion detector then such observers can correct for these effects.

It is simplest in the new physics to work in the quantum-foam frame of reference. If there is a gas present at rest in this frame, such as air, then the speed of light in this frame is $V = c/n$. If the interferometer and gas are moving with respect to the quantum foam, as in the case of an interferometer attached to the earth, then the speed of light relative to the quantum-foam is still $V = c/n$ up to corrections due to drag effects. Hence this new physics requires a different method of analysis from that of the Einstein physics. With these cautions we now describe the operation of a Michelson interferometer in this new physics, and show that it makes predictions different to that of the Einstein physics. Of course experimental evidence is the final arbiter in this conflict of theories.

As shown in Fig.10.3 the beamsplitter/mirror when at A sends a photon $\psi(t)$ into a superposition $\psi(t) = \psi_1(t)+\psi_2(t)$, with each component travelling in different arms of the interferometer, until they are recombined in the quantum detector which results in a localisation process, and one spot in the detector is produced[2]. Repeating with many photons reveals that the interference between ψ_1 and ψ_2 at the detector results in fringes. These fringes actually only appear if the mirrors are not quite orthogonal, otherwise the screen has a uniform intensity and this intensity changes as the interferometer is rotated, as shown in the analysis by Hicks [130]. To simplify the analysis here assume that the two arms are constructed to have the same lengths L when they are physically parallel to each other and perpendicular to v, so that the distance BB' is $L\sin(\theta)$. The Fitzgerald-Lorentz effect in the new physics is that the distance SB' is $\gamma^{-1}L\cos(\theta)$ where $\gamma = 1/\sqrt{1-v^2/c^2}$. The various other distances are $AB = Vt_{AB}$, $BC = Vt_{BC}$, $AS = vt_{AB}$ and $SC = vt_{BC}$, where t_{AB} and t_{BC} are the travel times. Applying the Pythagoras theorem to triangle ABB' we obtain

$$t_{AB} = \frac{2v\gamma^{-1}L\cos(\theta) + \sqrt{4v^2\gamma^{-2}L^2\cos^2(\theta) + 4L^2(1-\frac{v^2}{c^2}\cos^2(\theta))(V^2-v^2)}}{2(V^2-v^2)}. \tag{10.2}$$

The expression for t_{BC} is the same except for a change of sign of the $2v\gamma^{-1}L\cos(\theta)$ term, then

$$t_{ABC} = t_{AB} + t_{BC} = \frac{\sqrt{4v^2\gamma^{-2}L^2\cos^2(\theta) + 4L^2(1-\frac{v^2}{c^2}\cos^2(\theta))(V^2-v^2)}}{(V^2-v^2)}. \tag{10.3}$$

The corresponding travel time t'_{ABC} for the orthogonal arm is obtained from (10.3) by the substitution $\cos(\theta) \to \cos(\theta + 90^0) = -\sin(\theta)$. The difference in travel times between the two arms is then $\Delta t = t_{ABC} - t'_{ABC}$. Now trivially $\Delta t = 0$ if $v = 0$,

[2]A simplified analysis when the arms are parallel/orthogonal to the direction of motion is given in Appendix.F.

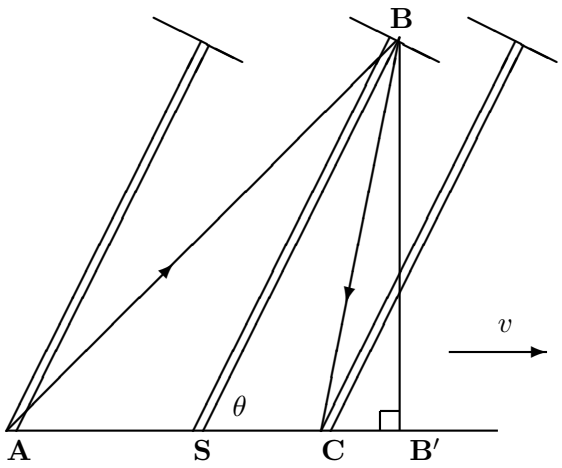

Figure 10.3: One arm of a Michelson Interferometer travelling at angle θ and velocity $\mathbf{v}$, and shown at three successive times: (i) when photon leaves beamsplitter at A, (ii) when photon is reflected at mirror B, and (iii) when photon returns to beamsplitter at C. The line BB' defines right angle triangles ABB' and SBB'. The second arm is not shown but has angle $\theta + 90^o$ to $\mathbf{v}$. Here $\mathbf{v}$ is in the plane of the interferometer for simplicity, and the azimuth angle $\psi = 0$.

but also $\Delta t = 0$ when $v \neq 0$ but only if $V = c$. This then would result in a null result on rotating the apparatus. Hence the null result of Michelson interferometer experiments in the new physics is only for the special case of photons travelling in vacuum for which $V = c$. However if the interferometer is immersed in a gas then $V < c$ and a non-null effect is expected on rotating the apparatus, since now $\Delta t \neq 0$. It is essential then in analysing data to correct for this refractive index effect. The above Δt is the change in travel time when one arm is moved through angle θ. The interferometer operates by comparing the change in the difference of the travel times between the arms, and this introduces a factor of 2. Then for $V = c/n$ we find for $v << V$ that

$$\Delta t = Ln(n^2 - 1)\frac{v^2}{c^3}\cos(2\theta) + \mathrm{O}(v^4), \tag{10.4}$$

that is $k^2 = n(n^2 - 1)$, which gives $k = 0$ for vacuum experiments ($n = 1$). So the Miller phenomenological parameter k is seen to accommodate both the Fitzgerald-Lorentz contraction effect and the dielectric effect, at least for gases[3]. This is very fortunate since being a multiplicative parameter a re-scaling of old analyses is all that is required. Δt is non-zero when $n \neq 1$ because the refractive index effect results in incomplete cancellation of the geometrical effect and the Fitzgerald-Lorentz contraction effect. Of course it was this cancellation effect that Fitzgerald and Lorentz

[3]For Michelson interferometers using light propagation through solids such as plastic or optical fibres there is evidence, discussed in Chap.12.2, that another effect comes into operation, namely a non-isotropic change of refractive index that causes absolute motion effects to be completely cancelled.

actually used to arrive at the length contraction hypothesis, but they failed to take the next step and note that the cancellation would be incomplete in the air operated Michelson-Morley experiment. In a bizarre development modern Michelson interferometer experiments, which use resonant cavities rather than interference effects, but for which the analysis here is easily adapted, and with the same consequences, are operated in vacuum mode. That denies these experiments the opportunity to see absolute motion effects. Nevertheless the experimentalists continue to misinterpret their null results as evidence against absolute motion. Of course these experiments are therefore restricted to merely checking the Fitzgerald-Lorentz contraction effect, and this is itself of some interest.

All data from gas-mode interferometer experiments, except for that of Miller, has been incorrectly analysed using only the first effect as in Michelson's initial theoretical treatment, and so the consequences of the other two effects have been absent. Repeating the above analysis without these two effects we arrive at the Newtonian-physics time difference which, for $v << V$, is

$$\Delta t = Ln^3 \frac{v^2}{c^3} \cos(2\theta) + \mathrm{O}(v^4), \tag{10.5}$$

that is $k^2 = n^3$. The value of Δt, which is typically of order $10^{-17}s$ in gas-mode interferometers corresponding to a fractional fringe shift, is deduced from analysing the fringe shifts, and then the speed v_M has been extracted using (10.5), instead of the correct form (10.4) or more generally (10.2). However it is very easy to correct for this oversight. From (10.4) and (10.5) we obtain for the corrected absolute (projected) speed v_P through space, and for $n \approx 1^+$,

$$v_P = \frac{v_M}{\sqrt{n^2 - 1}}. \tag{10.6}$$

For air the correction factor in (10.6) is significant, and even more so for helium.

10.3 The Michelson-Morley Experiment: 1887

Michelson and Morley reported that their interferometer experiment in 1887 gave a 'null-result' which since then, with rare exceptions, has been claimed to support the Einstein assumption that absolute motion has no meaning. However to the contrary the Michelson-Morley published data [122] shows non-null effects, but much smaller than they expected. They made observations of thirty-six 360^0 turns using an $L = 11$ meter length interferometer operating in air in Cleveland (Latitude $41^0 30'$N) with six turns near 12 :00 hrs (7:00 hrs ST) on each day of July 8, 9 and 11, 1887 and similarly near 18 :00 hrs (13:00 hrs ST) on July 8, 9 and 12, 1887. Each turn took approximately 6 minutes as the interferometer slowly rotated floating on a tank of mercury. They published and analysed the average of each of the 6 data sets. The fringe shifts were extremely small but within their observational capabilities.

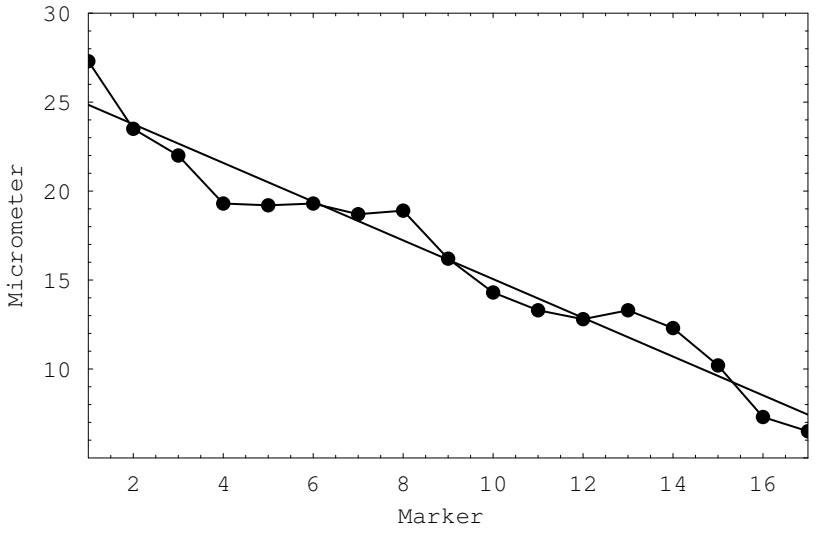

Figure 10.4: Plot of micrometer readings for July 11 12:00 hr (7:00 ST) showing the absolute motion induced fringe shifts superimposed on the uniform temperature induced fringe drift.

local	16	1	2	3	4	5	6	7	
time	8	9	10	11	12	13	14	15	16
12:00hr	27.3	23.5	22.0	19.3	19.2	19.3	18.7	18.9	
July 11	16.2	14.3	13.3	12.8	13.3	12.3	10.2	7.3	6.5
18:00hr	26.0	26.0	28.2	29.2	31.5	32.0	31.3	31.7	
July 9	33.0	35.8	36.5	37.3	38.8	41.0	42.7	43.7	44.0

Table 2. Examples of Michelson-Morley fringe-shift micrometer readings. The readings for July 11 12:00 hr are plotted in Fig.10.4.

Table 2 shows examples of the averaged fringe shift micrometer readings every 22.5^0 of rotation of the Michelson-Morley interferometer [122] for July 11 12:00 hr local time and also for July 9 18:00 hr local time. The orientation of the stone slab base is indicated by the marks $16, 1, 2, ...$ North is mark 16. The dominant effect was a uniform fringe drift caused by temporal temperature effects on the length of the arms, and imposed upon that are the fringe shifts corresponding to the effects of absolute motion, as shown in Fig.10.4.

This temperature effect can be removed by subtracting from the data in each case a best fit to the data of $a + bk$, $\{k = 0, 1, 2, .., 8\}$ for the first 0^0 to 180^0 part of each rotation data set. Then multiplying by 0.02 for the micrometer thread calibration gives the fringe-shift data points in Fig.10.6. This factor of 0.02 converts the micrometer readings to fringe shifts expressed as fractions of a wavelength. Similarly a linear fit has been made to the data from the 180^0 to 360^0 part of each rotation data set. Separating the full 360^0 rotation into two 180^0 parts reduces the effect of the temperature drift not being perfectly linear in time.

In the new physics there are four main velocities that contribute to the total velocity and, as discussed in Sect.7.9, there is an approximate dynamical velocity superposition effect so that these four velocities may be added vectorially, as in

$$\mathbf{v} = \mathbf{v}_{cosmic} + \mathbf{v}_{tangent} - \mathbf{v}_{in} - \mathbf{v}_E. \tag{10.7}$$

Here $\mathbf{v}_{cosmic}$ is the velocity of the solar system, relative to some cosmologically defined frame of reference such as the CMB frame, while the other three are local effects: (i) $\mathbf{v}_{tangent}$ is the tangential orbital velocity of the earth about the sun, (ii) $\mathbf{v}_{in}$ is a quantum-gravity radial in-flow of the quantum foam past the earth towards the sun, and (iii) the corresponding quantum-foam in-flow into the earth is $\mathbf{v}_E$ and makes no contribution to a horizontally operated interferometer, assuming the a velocity superposition approximation, and so that the vorticity and turbulence associated with that flow is not significant. The minus signs in (10.7) arise because, for example, the in-flow towards the sun requires the earth to have an outward directed velocity against that in-flow in order to maintain a fixed distance from the sun, as shown in Fig.10.5. For circular orbits and using in-flow form of Newtonian gravity the speeds $v_{tangent}$ and v_{in} are given by

$$v_{tangent} = \sqrt{\frac{GM}{R}}, \tag{10.8}$$

$$v_{in} = \sqrt{\frac{2GM}{R}}, \tag{10.9}$$

while the net speed v_R of the earth from the vector sum $\mathbf{v}_R = \mathbf{v}_{tangent} - \mathbf{v}_{in}$ is

$$v_R = \sqrt{\frac{3GM}{R}}, \tag{10.10}$$

where M is the mass of the sun, R is the distance of the earth from the sun, and G is Newton's gravitational constant. G is essentially a measure of the rate at which matter effectively 'dissipates' the quantum-foam. The gravitational acceleration arises from inhomogeneities in the flow. These expressions give $v_{tangent} = 30$km/s, $v_{in} = 42.4$km/s and $v_R = 52$km/s.

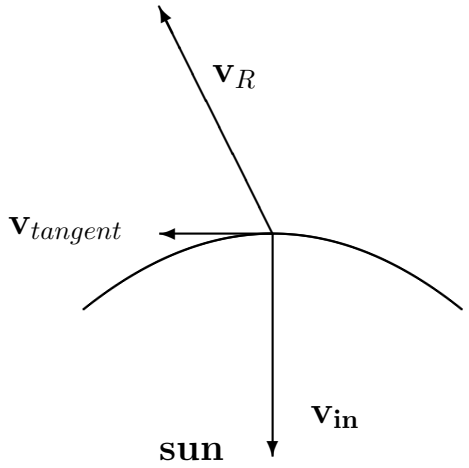

Figure 10.5: Orbit of earth about the sun defining the plane of the ecliptic with tangential orbital velocity $\mathbf{v}_{tangent}$ and quantum-foam in-flow velocity $\mathbf{v}_{in}$. Then $\mathbf{v}_R = \mathbf{v}_{tangent} - \mathbf{v}_{in}$ is the velocity of the earth relative to the quantum foam, after subtracting $\mathbf{v}_{cosmic}$.

Fig.10.6 shows all the data for the 1887 Michelson-Morley experiment for the fringe shifts after removal of the temperature drift effect for each averaged 180 degree rotation. The dotted curves come from the best fit of $\frac{0.4}{30^2} k_{air}^2 v_P^2 \cos(2(\theta - \psi))$ to the data. The coefficient $0.4/30^2$ arises as the apparatus would give a 0.4 fringe shift, as a fraction of a wavelength, with $k = 1$ if $v_P = 30$ km/s [122]. Shown in each figure is the resulting value of v_P. In some cases the data does not have the expected $\cos(2(\theta - \psi))$ form, and so the corresponding values for v_P are not meaningful. The remaining fits give $v_P = 331 \pm 30$ km/s for the 7:00 hr (ST) data, and $v_P = 328 \pm 50$ km/s for the 13:00 hr (ST) data. For comparison the full curves show the predicted form for the Michelson-Morley data, computed for the latitude of Cleveland, using the Miller direction (see later) for $\mathbf{v}_{cosmic}$ of Right Ascension and Declination ($\alpha = 4^{hr}54', \delta = -70^0 30'$) and incorporating the tangential and in-flow velocity effects for July. The magnitude of the theoretical curves are in general in good agreement with the magnitudes of the experimental data, excluding those cases where the data does not have the sinusoidal form. However there are significant fluctuations in the azimuth angle. These fluctuations are also present in the Miller data, and together suggest that this is a real physical phenomenon, and not solely due to difficulties with the operation of the interferometer.

The Michelson-Morley interferometer data clearly shows the characteristic sinusoidal form with period 180^0 together with a large speed. Ignoring the effect of the

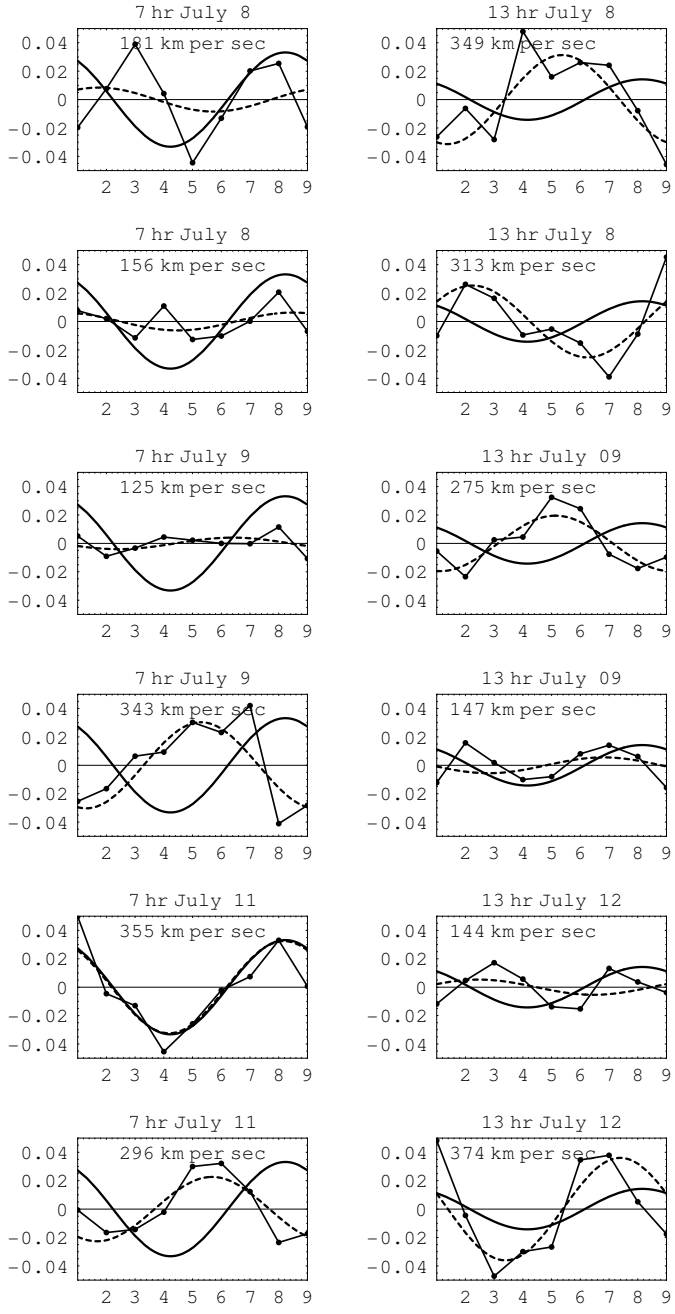

Figure 10.6: Shows all the Michelson-Morley 1887 data after removal of the temperature induced fringe drifts. The data for each 360^0 full turn (the average of 6 individual turns) is divided into the 1st and 2nd 180^0 parts and plotted one above the other. The dotted curve shows a best fit to the data, while the full curves show the expected forms using the Miller direction for $\mathbf{v}_{cosmic}$.

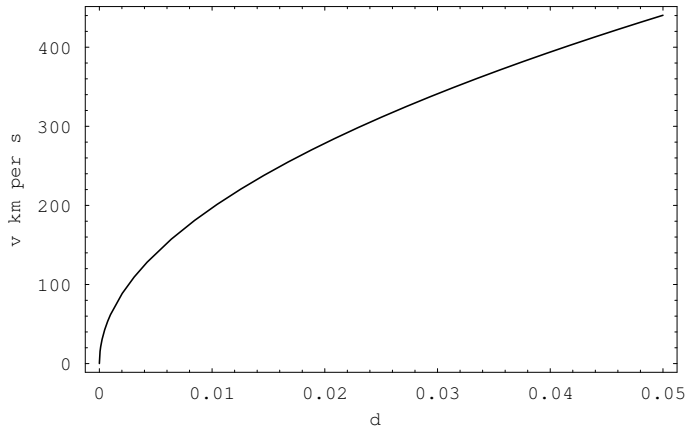

Figure 10.7: Speed calibration for Michelson-Morley experiment. This shows the value of v_P in km/s for values of the fringe shifts, d, expressed as a fraction of one wavelength of the light used, as shown in Fig.10.6

refractive index, namely using the Newtonian value of $k = 1$, gives speeds reduced by the factor k_{air}, namely $k_{air}v_P = 0.0241 \times 330\text{km/s} = 7.9$ km/s. Michelson and Morley reported speeds in the range 5km/s - 7.5km/s. These slightly smaller speeds arise because they averaged all the 7:00 hr (ST) data, and separately all the 13:00 hr (ST) data, whereas here some of the lower quality data has not been used. Michelson was led to the false conclusion that because this speed of some 8 km/s was considerably less than the orbital speed of 30 km/s the interferometer must have failed to have detected absolute motion, and that the data was merely caused by experimental imperfections. This was the flawed analysis that led to the incorrect conclusion by Michelson and Morley that the experiment had failed to detect absolute motion. The consequences for physics were extremely damaging, and are only now being rectified after some 115 years.

10.4 The Miller Interferometer Experiment: 1925-1926

Dayton Miller developed and operated a Michelson interferometer for over twenty years, see Fig.10.8, with the main sequence of observations being on Mt.Wilson in the years 1925-1926, with the results reported in 1933 by Miller [123]. Accounts of the Miller experiments are available in Swenson [131] and DeMeo[4] [132]. Miller developed his huge interferometer over the years, from 1902 to 1906 in collaboration with Morley, and later at Mt.Wilson where the most extensive interferometer observations were carried out. Miller was meticulous in perfecting the operation of

[4]Note however that DeMeo interprets Miller's 'small' speeds, that is some 10km/s, as being a result of entrainment, and not as herein a consequence of the misunderstanding of the physics involved in the operation of the interferometer.

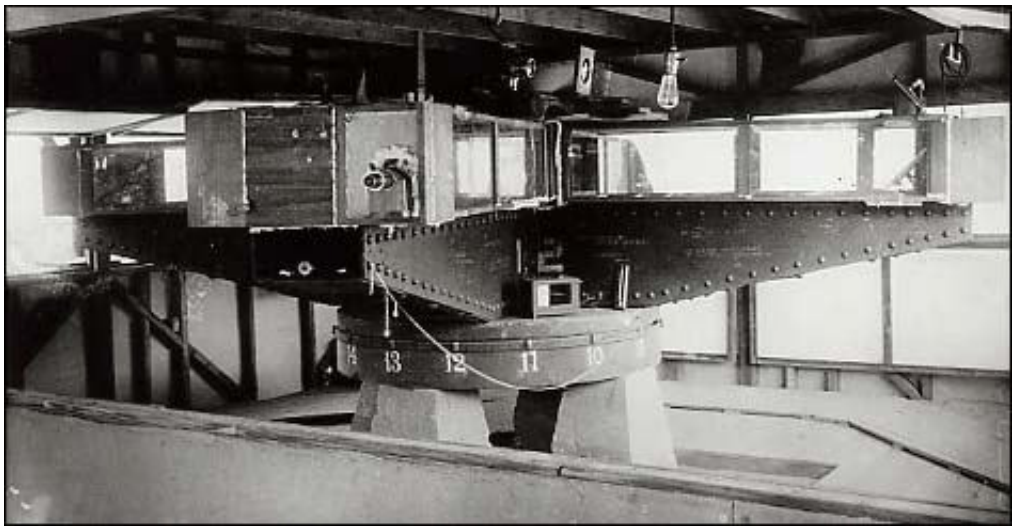

Figure 10.8: Miller's interferometer with an effective arm length of $L = 32$m achieved by multiple reflections, as shown in Fig.10.9. Used by Miller on Mt.Wilson to perform the 1925-1926 observations of absolute motion. The steel arms weighed 1200 kilograms and floated in a tank of 275 kilograms of Mercury. From Case Western Reserve University Archives.

the interferometer and performed many control experiments. The biggest problem to be controlled was the effect of temperature changes on the lengths of the arms. It was essential that the temperature effects were kept as small as possible, but so long as each turn was performed sufficiently quickly, any temperature effect could be assumed to have been linear with respect to the angle of rotation. Then a uniform background fringe drift could be removed, as in the Michelson-Morley data analysis (see Fig.10.4).

In all some 200,000 readings were taken during some 12,000 turns of the interferometer[5]. Analysis of the data requires the extraction of the speed v_M and the azimuth angle ψ by effectively fitting the observed time differences, obtained from the observed fringe shifts, using (10.2), but with $k = 1$. Miller was of course unaware of the full theory of the interferometer and so he assumed the Newtonian theory, which neglected both the Fitzgerald-Lorentz contraction and air effects.

Miller performed this analysis of his data by hand, and the results for April, August and September 1925 and February 1926 are shown in Fig.10.10. The speeds shown are the Michelson speeds v_M, and these are easily corrected for the two neglected effects by dividing these v_M by $k_{air} = \sqrt{(n^2 - 1)} = 0.0241$, as in (10.6).

[5]In a remarkable development in 2002 as a result of a visit by James DeMeo to Case Western Reserve University the original Miller data was located, some 61 years after Miller's death in 1941. Until then it was thought that the data had been destroyed. Analysis of that data by the author of this article has confirmed the accuracy of Miller's analysis. Using more thorough computer based techniques the data is now being re-analysed

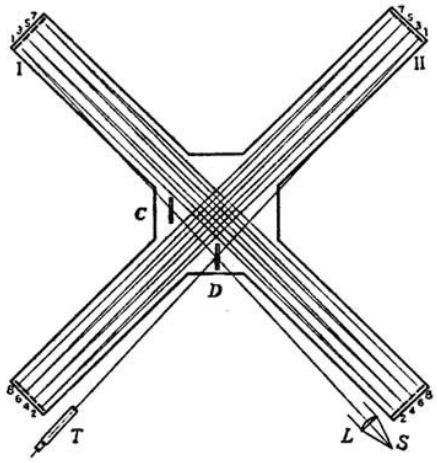

Figure 10.9: The effective arm length of $L = 32$m was achieved by multiple reflections.

Then for example a speed of $v_M = 10km/s$ gives $v_P = v_M/k_{air} = 415$km/s. However this correction procedure was not available to Miller. He understood that the theory of the Michelson interferometer was not complete, and so he introduced the phenomenological parameter k in (10.2). We shall denote his values by $\overline{k}$. Miller noted, in fact, that $\overline{k}^2 << 1$, as we would now expect. Miller then proceeded on the assumption that $\mathbf{v}$ should have only two components: (i) a cosmic velocity of the solar system through space, and (ii) the orbital velocity of the earth about the sun. Over a year this vector sum would result in a changing $\mathbf{v}$, as was in fact observed, see Fig.10.10. Further, since the orbital speed was known, Miller was able to extract from the data the magnitude and direction of $\mathbf{v}$ as the orbital speed offered an absolute scale. For example the dip in the v_M plots for sidereal times $\tau \approx 16^{hr}$ is a clear indication of the direction of $\mathbf{v}$, as the dip arises at those sidereal times when the projection v_P of $\mathbf{v}$ onto the plane of the interferometer is at a minimum. During a 24hr period the value of v_P varies due to the earth's rotation. As well the v_M plots vary throughout the year because the vectorial sum of the earth's orbital velocity $\mathbf{v}_{tangent}$ and the cosmic velocity $\mathbf{v}_{cosmic}$ changes. There are two effects here as the direction of $\mathbf{v}_{tangent}$ is determined by both the yearly progression of the earth in its orbit about the sun, and also because the plane of the ecliptic is inclined at 23.5^0 to the celestial plane. Figs. 10.12 and 10.14 show the expected theoretical variation of both v_P and the azimuth ψ during one sidereal day in the months of April, August, September and February. These plots show the clear signature of absolute motion effects as seen in the actual interferometer data of Fig.10.10.

Note that the above corrected Miller projected absolute speed of approximately $v_P = 415$km/s is completely consistent with the corrected projected absolute speed of some 330km/s from the Michelson-Morley experiment, though neither Michelson nor Miller were able to apply this correction. The difference in magnitude is

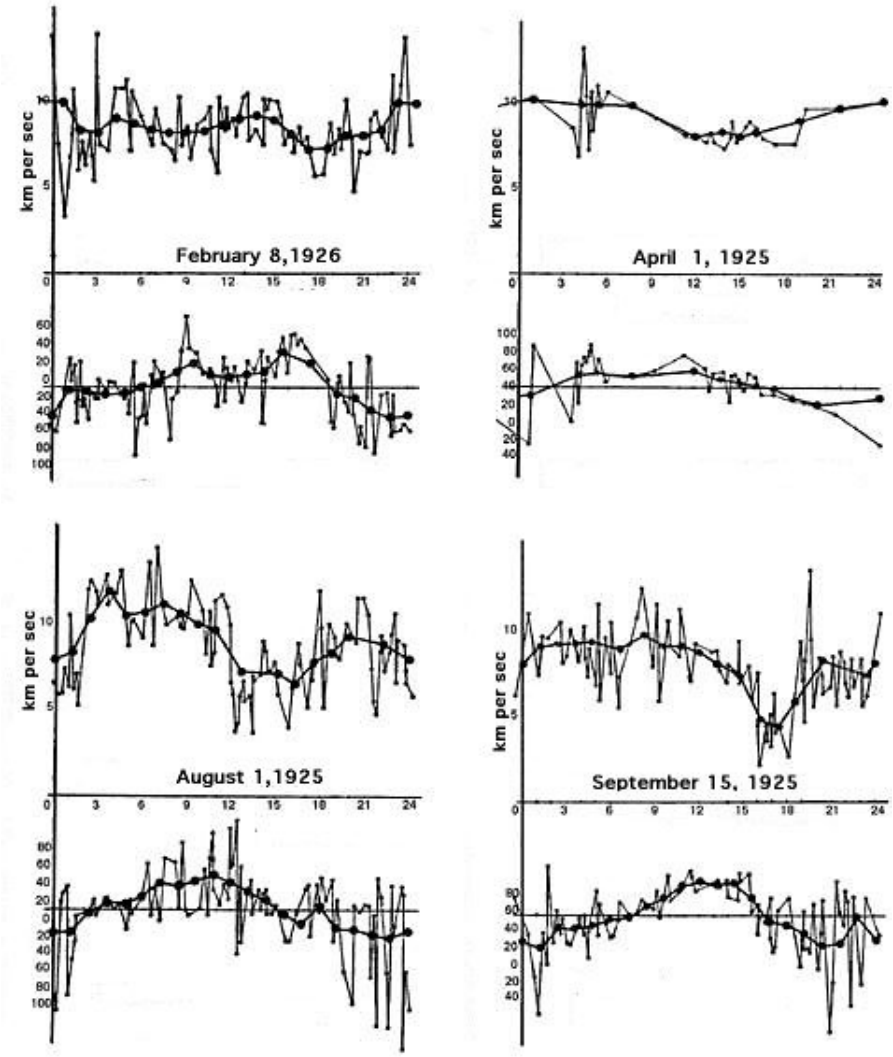

Figure 10.10: Miller's results from the 1925-1926 observations of absolute motion showing the projected 'Michelson' speed v_M in km/s and azimuth angle ψ in degrees plotted against sidereal time in hours. The results are for April, August and September 1925 and February 1926. In most cases the results arise from observations extending over much of each month, i.e not from a single day in each month. Therefore the data points are not strictly in chronological order. The lines joining the data points are merely to make the data points clearer. The smoother line is a running time average computed by Miller. The fluctuations in both v_M and ψ appear to be a combination of apparatus effects and genuine physical phenomena caused by turbulence in the gravitational in-flow of space. Each data point arises from analysis of the average of twenty full rotations of the interferometer.

completely explained by Cleveland having a higher latitude than Mt. Wilson, and also by the only two sidereal times of the Michelson-Morley observations. So from his 1925-1926 observations Miller had completely confirmed the true validity of the Michelson-Morley observations and was able to conclude, contrary to their published conclusions, that the 1887 experiment had in fact detected absolute motion. But it was too late. By then the physicists had incorrectly come to believe that absolute motion was inconsistent with various 'relativistic effects' that had by then been observed. This was because the Einstein formalism had been 'derived' from the assumption that absolute motion was without meaning and so unobservable in principle. Of course the earlier interpretation of relativistic effects by Lorentz had by then lost out to the Einstein interpretation.

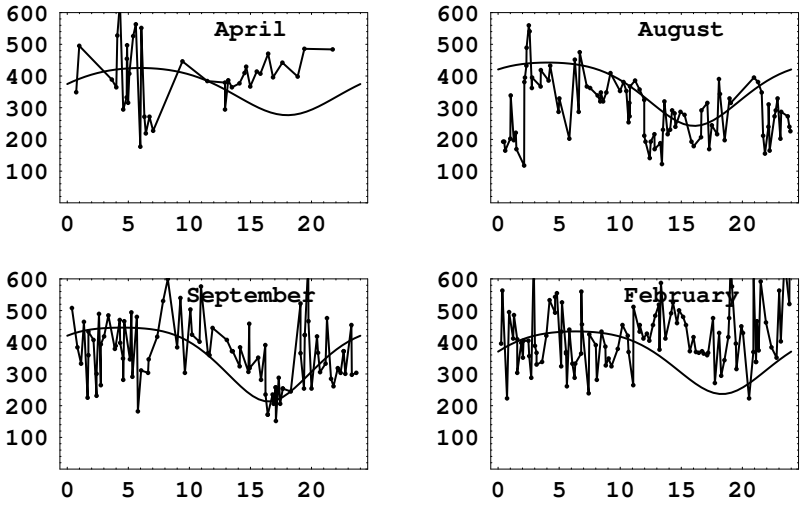

Figure 10.11: Miller interferometer projected speeds v_P in km/s, plotted against sidereal time in hrs, showing both data and best fit of theory giving $v_{cosmic} = 433$ km/s in the direction $(\alpha = 5.2^{hr}, \delta = -67^0)$, and using $n = 1.000226$ appropriate for the altitude of Mt. Wilson. For clarity the theory curves are plotted together in Fig.10.12.

10.5 The Illingworth Experiment: 1927

In 1927 Illingworth [128] performed a Michelson interferometer experiment in which the light beams passed through the gas helium,

> *...as it has such a low index of refraction that variations due to temperature changes are reduced to a negligible quantity.*

For helium at STP $n = 1.000036$ and so $k^2_{He} = 0.00007$, which results in an enormous reduction in sensitivity of the interferometer. Nevertheless this experiment

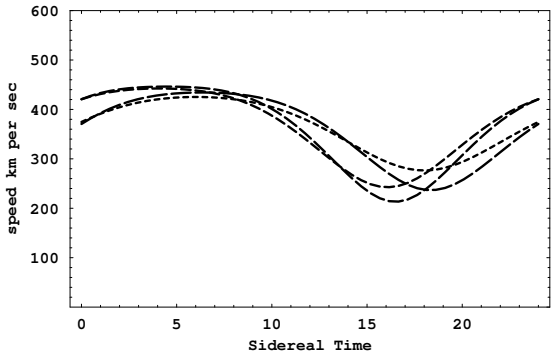

Figure 10.12: Expected theoretical variation of the projected velocity v_P during one sidereal day in the months of April, August, September and February, labelled by increasing dash length for cosmic speed of 433km/s in the direction $(\alpha = 5.2^{hr}, \delta = -67^0)$. This shows how the signature of the effect changes over a year.

gives an excellent opportunity to check the n dependence in (10.6). Illingworth, not surprisingly, reported no "ether drift to an accuracy of about one kilometer per second". Múnera [134] re-analysed the Illingworth data to obtain a speed $v_M = 3.13 \pm 1.04$km/s. The correction factor in (10.6), $1/\sqrt{n_{He}^2 - 1} = 118$, is large for helium and gives $v = 368 \pm 123$km/s. As shown in Fig.10.15 the Illingworth observations now agree with those of Michelson-Morley and Miller, though they would certainly be inconsistent without the $n-$dependent correction, as shown in the lower data points (shown at $5\times$ scale).

So the use by Illingworth of helium gas has turned out have offered a fortuitous opportunity to confirm the validity of the refractive index effect, though because of the insensitivity of this experiment the resulting error range is significantly larger than those of the other interferometer observations. So finally it is seen that the Illingworth experiment detected absolute motion with a speed consistent with all other observations.

10.6 The Joos Experiment: 1930

Joos set out to construct and operate a large vacuum Michelson interferometer in at the Zeiss Works in Jena, Germany [129]. This interferometer had an effective arm length of 21m achieved using multiple reflections in each arm. The vacuum sealing was ineffective and the penetration of air into the vacuum vessel caused problematic vibrations. Subsequently Joos used helium, assuming apparently that helium could be considered as a substitute for a true vacuum[6]. The use of helium is not mentioned in the Joos paper [129], but is mentioned by Swenson [131]. Joos

[6]Thanks to Dr Lance McCarthy for pointing out the use of helium in this experiment and in extracting the data from the Joos paper.

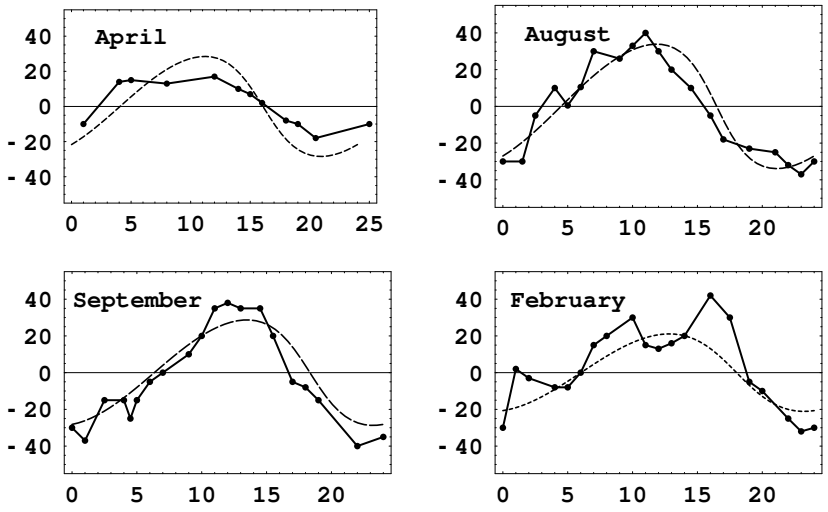

Figure 10.13: Miller azimuths ψ, measured from south and plotted against sidereal time in hrs, showing both data and best fit of theory giving $v_{cosmic} = 433$ km/s in the direction $(\alpha = 5.2^{hr}, \delta = -67^0)$, and using $n = 1.000226$ appropriate for the altitude of Mt. Wilson. The azimuth data gives a clearer signal than the speed data in Fig.10.11. For clarity the theory curves are plotted together in Fig.10.14.

recorded the fringe shifts photographically, and subsequently analysed the images using a photometer. The data for 22 rotations throughout the day of May 30, 1930 are shown in Fig.10.16, and are reproduced from Fig.11 of [129]. From that data Joos concluded, using an analysis that did not take account of the special relativistic length contraction effect, that the fringe shifts corresponded to a speed of only 1.5 km/s. However as previously noted such an analysis is completely flawed. As well the data in Fig.10.16 shows that for all but one of the rotations the fringe shifts were poorly recorded. Only in the one rotation, at 11 23^{58}, does the data actually look like the form expected. In Fig.10.17 that one rotation data is compared with the form expected for Jena on May 30 using the Miller speed and direction together with the new refractive index effect, and using the refractive index of helium. The agreement is quite remarkable. So again contrary the Joos paper and to subsequent history Joos did in fact detect a very large velocity of absolute motion.

10.7 The New Bedford Experiment: 1963

In 1964 from an absolute motion detector experiment at New Bedford, latitude 42^0N, Jaseja *et al.* [136] reported yet another 'null result'. In this experiment two He-Ne masers were mounted with axes perpendicular on a rotating table, see Fig.10.18. Rotation of the table through 90^0 produced repeatable variations in the frequency

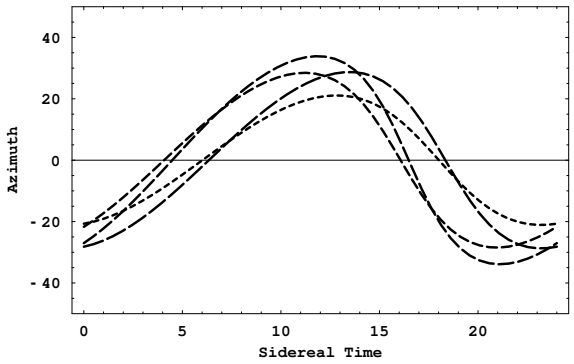

Figure 10.14: Expected theoretical variation of the azimuths ψ, measured from south, during one sidereal day in the months of April, August, September and February, labelled by increasing dash length, for a cosmic speed of 433km/s in the direction $(\alpha = 5.2^{hr}, \delta = -67^0)$. This shows how the signature of the effect changes over a year.

difference of about 275kHz, an effect attributed to magnetorestriction in the Invar spacers due to the earth's magnetic field. Observations over some six consecutive hours on January 20, 1963 from 6:00 am to 12:00 noon local time did produce a 'dip' in the frequency difference of some 3kHz superimposed on the 275kHz effect, as shown in Fig.10.19 in which the local times have been converted to sidereal times. The most noticeable feature is that the dip occurs at approximately $17 - 18{:}00^{hr}$ sidereal time (or $9 - 10:00$ hrs local time), which agrees with the direction of absolute motion observed by Miller and also by DeWitte (see Sect.10.8). It was most fortunate that this particular time period was chosen as at other times the effect is much smaller. The February data in Fig.10.10 shows the minimum at $18{:}00^{hr}$ sidereal time. The local times were chosen by Jaseja *et al* such that if the only motion was due to the earth's orbital speed the maximum frequency difference, on rotation, should have occurred at 12:00hr local time, and the minimum frequency difference at 6:00 hr local time, whereas in fact the minimum frequency difference occurred at 9:00 hr local time.

As for the Michelson-Morley experiment the analysis of the New Bedford experiment was also bungled. Again this apparatus can only detect the effects of absolute motion if the cancellation between the geometrical effects and Fitzgerald-Lorentz length contraction effects is incomplete as occurs only when the radiation travels in a gas, here the He-Ne gas present in the maser.

This double maser apparatus is essentially equivalent to a Michelson interferometer, and so the simple analysis of Appendix F is appropriate. Then the resonant frequency ν of each maser is proportional to the reciprocal of the out-and-back travel

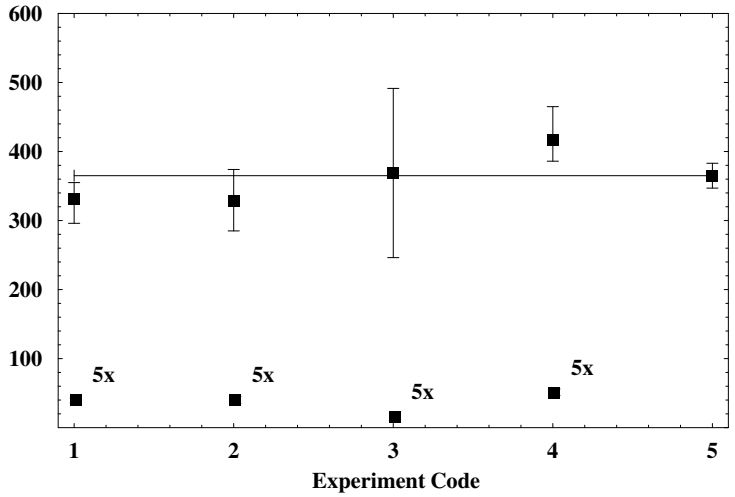

Figure 10.15: Speeds v in km/s determined from various Michelson interferometer experiments (**1**)-(**4**) and CMB (**5**): (**1**) Michelson-Morley (noon observations) and (**2**) (18^h observations) see Chap.10.3, (**3**) Illingworth [128], (**4**) Miller, Mt.Wilson [123], and finally in (**5**) the speed from observations of the CMB spectrum dipole term [135]. The results (**1**)-(**3**) are not corrected for the ±30km/s of the orbital motion of the earth about the sun or for the gravitational in-flow speed, though these correction were made for (**4**) with the speeds from Table 3. The horizontal line at $v = 369$km/s is to aid comparisons with the CMB frame speed data. The Miller direction is different to the CMB direction. Due to the angle between the velocity vector and the plane of interferometer the results (**1**)-(**3**) are less than or equal to the true speed, while the result for (**4**) is the true speed as this projection effect was included in the analysis. These results demonstrate the remarkable consistency between these three interferometer experiments. The Miller speed agrees with the speed from the DeWitte non-interferometer experiment, in Sect.10.8. The lower data, magnified by a factor of 5, are the original speeds v_M determined from fringe shifts using (10.1) with $k = 1$. This figure updates the corresponding figure in Ref.[12].

time. For maser 1

$$\nu_1 = m\frac{V^2 - v^2}{2LV\sqrt{1 - \dfrac{v^2}{c^2}}}, \tag{10.11}$$

for which a Fitzgerald-Lorentz contraction occurs, while for maser 2

$$\nu_2 = m\frac{\sqrt{V^2 - v^2}}{2L}. \tag{10.12}$$

Here m refers to the mode number of the masers. When the apparatus is rotated the net observed frequency difference is $\delta\nu = 2(\nu_2 - \nu_1)$, where the factor of '2' arises as the roles of the two masers are reversed after a 90^0 rotation. Putting $V = c/n$

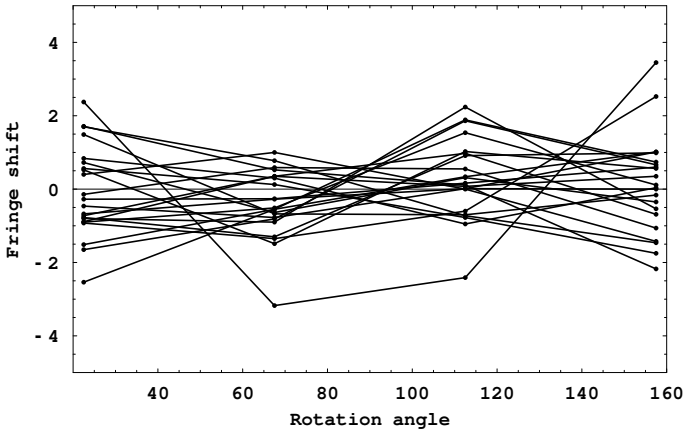

Figure 10.16: The Joos fringes shifts in $\lambda/1000$ recorded on May 30, 1930 from a Michelson interferometer using helium. Only one of the rotations produced a clean signal of the form expected, as shown in Fig.10.17

we find for $v << V$ and with ν_0 the at-rest resonant frequency, that

$$\delta\nu = (n^2 - 1)\nu_0 \frac{v^2}{c^2} + O(\frac{v^4}{c^4}). \tag{10.13}$$

If we use the Newtonian physics analysis, as in Jaseja *et al* [136], which neglects both the Fitzgerald-Lorentz contraction and the refractive index effect, then we obtain $\delta\nu = \nu_0 v^2/c^2$, that is without the $n^2 - 1$ term, just as for the Newtonian analysis of the Michelson interferometer itself. Of course the very small magnitude of the absolute motion effect, which was approximately 1/1000 that expected assuming only an orbital speed of $v = 30$ km/s in the Newtonian analysis, occurs simply because the refractive index of the He-Ne gas is very close to one[7]. Nevertheless given that it is small the sidereal time of the obvious 'dip' coincides almost exactly with that of the other observations of absolute motion.

The New Bedford experiment was yet another missed opportunity to have revealed the existence of absolute motion. Again the spurious argument was that because the Newtonian physics analysis gave the wrong prediction then Einstein relativity must be correct. But the analysis simply failed to take account of the Fitzgerald-Lorentz contraction, which had been known since the end of the 19^{th} century, and the refractive index effect which had an even longer history. As well the authors failed to convert their local times to sidereal times and compare the time for the 'dip' with Miller's time[8].

[7]It is possible to compare the refractive index of the He-Ne gas mixture in the maser with the value extractable from this data: $n^2 = 1 + 30^2/(1000 \times 400^2)$, or $n = 1.0000028$.

[8]There is no reference to Miller's 1933 paper in Ref.[136].

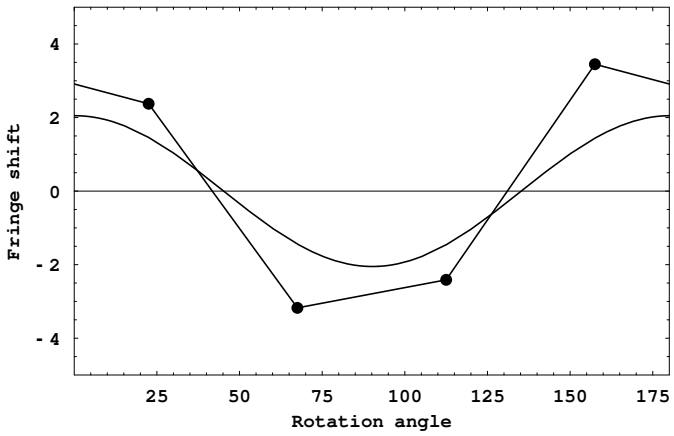

Figure 10.17: Comparison of the Joos data for the one good rotation at 11 23^{58} with the theoretical prediction using the speed and direction from the Miller experiment, together with the length contraction and refractive index effects.

10.8 The DeWitte Experiment: 1991

The Michelson-Morley, Illingworth, Miller and New Bedford experiments all used Michelson interferometers or its equivalent in gas mode, and all revealed absolute motion. The Michelson interferometer is a 2nd-order device meaning that the time difference between the 'arms' is proportional to $(v/c)^2$. There is also a factor of $n^2 - 1$ and for gases like air and particularly helium or helium-Neon mixes this results in very small time differences and so these experiments were always very difficult. Of course without the gas the Michelson interferometer is incapable of detecting absolute motion[9], and so there are fundamental limitations to the use of this interferometer in the study of absolute motion and related effects.

In a remarkable development in 1991 a research project within Belgacom, the Belgium telecommunications company, stumbled across yet another detection of absolute motion, and one which turned out to be 1st-order in v/c. The study was undertaken by Roland DeWitte [137]. This organisation had two sets of atomic clocks in two buildings in Brussels separated by 1.5 km and the research project was an investigation of the task of synchronising these two clusters of atomic clocks. To that end 5MHz radiofrequency signals were sent in both directions through two buried coaxial cables linking the two clusters. The atomic clocks were cesium beam atomic clocks, and there were three in each cluster. In that way the stability of the clocks could be established and monitored. One cluster was in a building on Rue du Marais and the second cluster was due south in a building on Rue de la Paille. Digital phase comparators were used to measure changes in times between clocks within the same cluster and also in the propagation times of the RF signals. Time

[9]So why not use a transparent solid in place of the gas? See Sect.12.2 for the discussion.

Figure 10.18: Schematic diagram for recording the variations in beat frequency between two optical masers: (a) when at absolute rest, (b) when in absolute motion at velocity **v**. PM is the photomultiplier detector. The apparatus was rotated back and forth through 90^0.

differences between clocks within the same cluster showed a linear phase drift caused by the clocks not having exactly the same frequency together with short term and long term noise. However the long term drift was very linear and reproducible, and that drift could be allowed for in analysing time differences in the propagation times between the clusters.

Changes in propagation times were observed and eventually observations over 178 days were recorded. A sample of the data, plotted against sidereal time for just three days, is shown in Fig.10.20. DeWitte recognised that the data was evidence of absolute motion but he was unaware of the Miller experiment and did not realise that the Right Ascension for minimum/maximum propagation time agreed almost exactly with Miller's direction ($\alpha = 5.2^{hr}, \delta = -67^0$). In fact DeWitte expected that the direction of absolute motion should have been in the CMB direction, but that would have given the data a totally different sidereal time signature, namely the times for maximum/minimum would have been shifted by 6 hrs. The declination of the velocity observed in this DeWitte experiment cannot be determined from the data as only three days of data are available. However assuming exactly the same declination as Miller the speed observed by DeWitte appears to be also in excellent agreement with the Miller speed, which in turn is in agreement with that from the Michelson-Morley and Illingworth experiments, as shown in Fig.10.15.

Being 1st-order in v/c the Belgacom experiment is easily analysed to sufficient accuracy by ignoring relativistic effects, which are 2nd-order in v/c. Let the projection of the absolute velocity vector **v** onto the direction of the coaxial cable be v_P as before. Then the phase comparators reveal the difference[10] between the propagation times in NS and SN directions. First consider the analysis with no Fresnel

[10]The measurement protocol in Chap.7.4 uses the sum of the travel times.

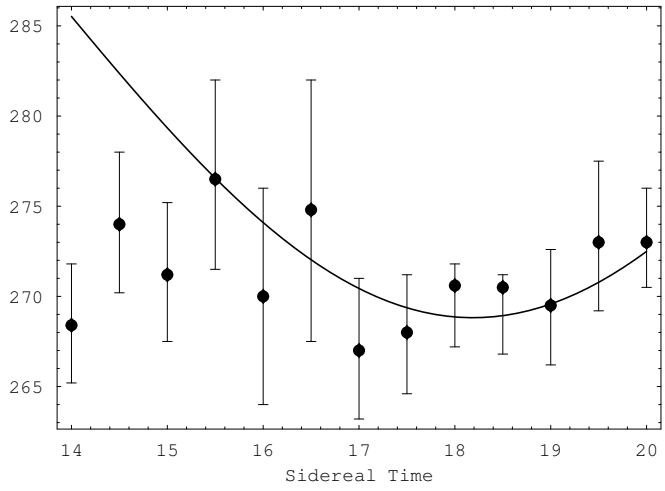

Figure 10.19: Frequency difference in kHz between the two masers in the 1963 New Bedford experiment after a 90^0 rotation. The 275kHz difference is a systematic repeatable apparatus effect, whereas the superimposed 'dip' at $17-18:00^{hr}$ sidereal time of approximately 3kHz is a real time dependent frequency difference. The full curve shows the theoretical prediction for the time of the 'dip' for this experiment using the Miller direction for $\hat{\mathbf{v}}$ ($\alpha = 4^{hr}54^m, \delta = -70^0 33'$) with $|\mathbf{v}| = 417$km/s and including the earth's orbital velocity and sun gravitational in-flow velocity effects for January 20, 1963. The absolute scale of this theoretical prediction was not possible to compute as the refractive index of the He-Ne gas mixture was unknown.

drag effect, Appendix.E,

$$\begin{aligned} \Delta t &= \frac{L}{\frac{c}{n} - v_P} - \frac{L}{\frac{c}{n} + v_P}, \\ &= 2\frac{L}{c/n} n\frac{v_P}{c} + O(\frac{v_P^2}{c^2}) \approx 2t_0 n\frac{v_P}{c}. \end{aligned} \tag{10.14}$$

Here $L = 1.5$ km is the length of the coaxial cable, $n = 1.5$ is the refractive index of the insulator within the coaxial cable, so that the speed of the RF signals is approximately $c/n = 200,000$km/s, and so $t_0 = nL/c = 7.5 \times 10^{-6}$ sec is the one-way RF travel time when $v_P = 0$. Then, for example, a value of $v_P = 400$km/s would give $\Delta t = 30$ns. Because Brussels has a latitude of 51^0 N then for the Miller direction the projection effect is such that v_P almost varies from zero to a maximum value of $|\mathbf{v}|$. The DeWitte data in Fig.10.20 shows Δt plotted with a false zero, but shows a variation of some 28 ns. So the DeWitte data is in excellent agreement with the Miller's data[11]. The Miller experiment has thus been confirmed by a non-interferometer experiment if we ignore a Fresnel drag.

[11]There is ambiguity in Ref.[137] as to whether the time variations in Fig.10.20 include the factor of 2 or not, as defined in (10.14). It is assumed here that a factor of 2 is included.

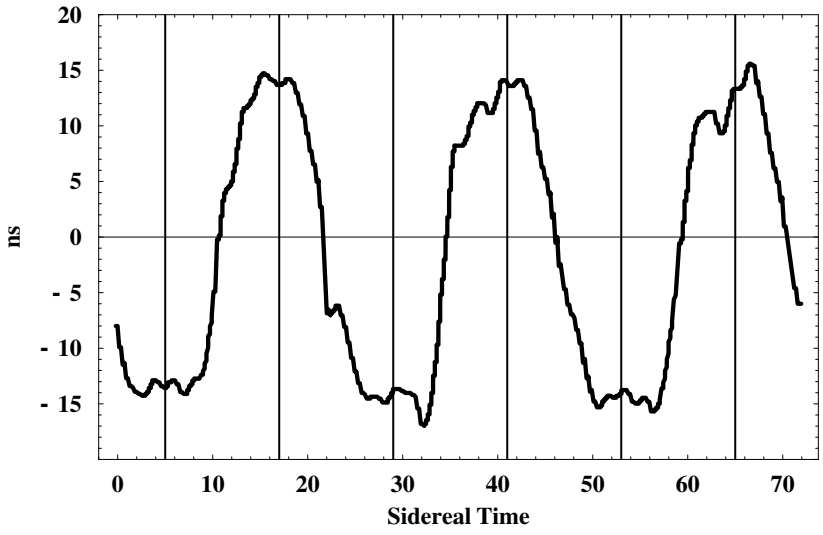

Figure 10.20: Variations in twice the one-way travel time, in ns, for an RF signal to travel 1.5 km through a coaxial cable between Rue du Marais and Rue de la Paille, Brussels. An offset has been used such that the average is zero. The definition of the sign convention for Δt used by DeWitte is unclear. The cable has a North-South orientation, and the data is $\pm$ difference of the travel times for NS and SN propagation. The sidereal time for maximum effect of $\sim$17hr (or $\sim$5hr) (indicated by vertical lines) agrees with the direction found by Miller and also by Jaseja *et al*, but because of the ambiguity in the definition of Δt the opposite direction would also be consistent with this data. Plot shows data over 3 sidereal days and is plotted against sidereal time. See Fig.10.21b for theoretical predictions for one sidereal day. The time of the year of the data is not identified. The fluctuations are evidence of turbulence associated with the gravitational in-flow towards the sun. Adapted from DeWitte [137].

But if we include a Fresnel drag effect then the change in travel time Δt_F becomes

$$\begin{aligned} \Delta t_F &= \frac{L}{\frac{c}{n} + bv_P - v_P} - \frac{L}{\frac{c}{n} - bv_P + v_P}, \\ &= 2\frac{L}{c}\frac{v_P}{c} + O(\frac{v_P^2}{c^2}), \\ &= \frac{1}{n^2}\Delta t, \end{aligned} \tag{10.15}$$

where $b = 1 - 1/n^2$ is the Fresnel drag coefficient, see Appendix.E. Then Δt_F is smaller than Δt by a factor of $n^2 = 1.5^2 = 2.25$, and so a speed of $v_P = 2.25 \times 400 =$ 900 km/s would be required to produce a $\Delta t_F = 30$ ns. This speed is inconsistent with the results from gas-mode interferometer experiments, and also inconsistent with the data from the Torr-Kolen gas-mode coaxial cable experiment, Sect.10.9. This raises the question as to whether the Fresnel effect is present in transparent

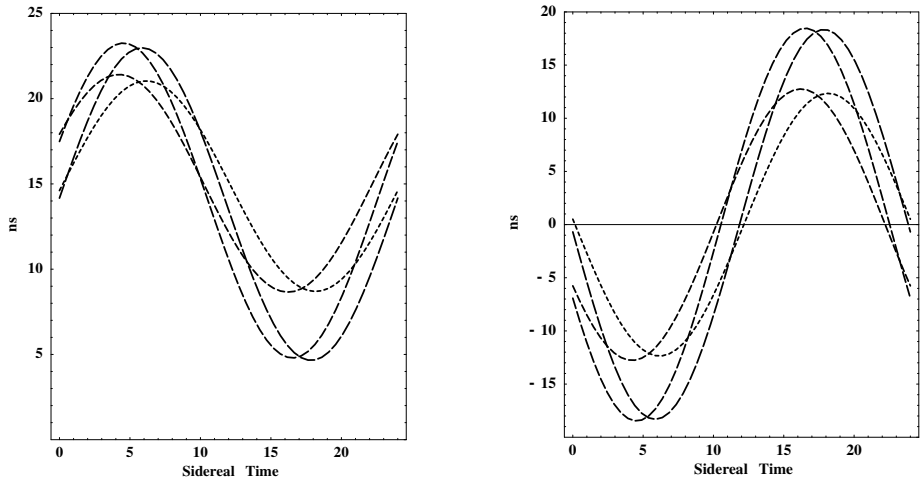

(a) (b)

Figure 10.21: Theoretical predictions for the variations in travel time, in ns, for one sidereal day, in the DeWitte Brussels coaxial cable experiment for $\mathbf{v}_{cosmic}$ in the direction $(\alpha = 5.2^{hr}, \delta = -67^0)$ and with the Miller magnitude of 417 km/s, and including orbital and in-flow effects (but without turbulence). Shown are the results for four days: for the Vernal Equinox, March 21 (shortest dashes), and for 90, 180 and 270 days later (shown with increasing dash length). Figure (a) Shows change in one-way travel time $t_0 n v_P/c$ for signal travelling from N to S. Figure (b) shows Δt, as defined in (10.14), with an offset such that the average is zero so as to enable comparison with the data in Fig.10.20. Δt is twice the one-way travel time. For the direction opposite to $(\alpha = 5.2^{hr}, \delta = -67^0)$ the same curves arise except that the identification of the months is different and the sign of Δt also changes. The sign of Δt determines which of the two directions is the actual direction of absolute motion. However the definition of the sign convention for Δt used by DeWitte is unclear.

solids, and indeed whether it has ever been studied? As well we are assuming the conventional electromagnetic theory for the RF fields in the coaxial cable. An experiment to investigate this is underway at Flinders university, as discussed in Sect.12.3.

The actual days of the data in Fig.10.20 are not revealed in Ref.[137] so a detailed analysis of the DeWitte data is not possible. Nevertheless theoretical predictions for various days in a year are shown in Fig.10.21 using the Miller speed of $v_{cosmic} = 417$ km/s (from Table 3) and where the diurnal effects of the earth's orbital velocity and the gravitational in-flow cause the range of variation of Δt and sidereal time of maximum effect to vary throughout the year. The predictions give $\Delta t = 30 \pm 4$ ns over a year compared to the DeWitte value of 28 ns in Fig.10.20. If all of DeWitte's 178 days of data were available then a detailed analysis would be possible.

Ref.[137] does however reveal the sidereal time of the cross-over time, that is a 'zero' time in Fig.10.20, for all 178 days of data. This is plotted in Fig.10.22 and demonstrates that the time variations are correlated with sidereal time and not local

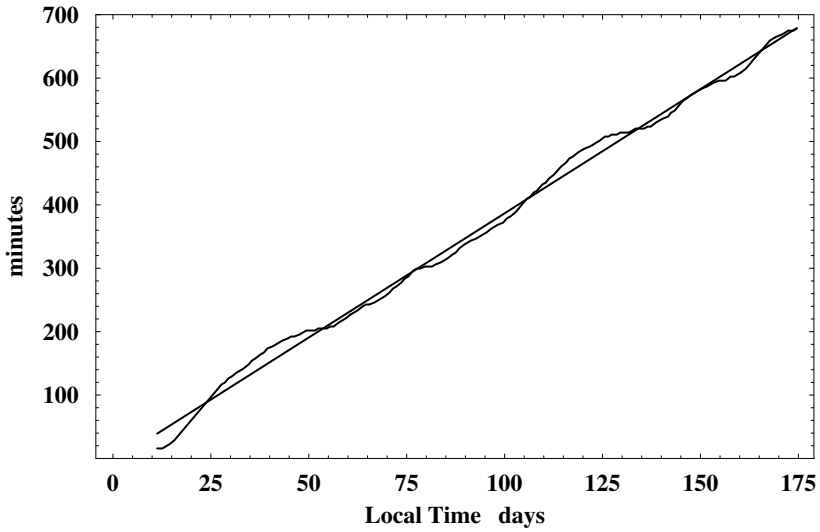

Figure 10.22: Plot of the negative of the drift of the cross-over time between minimum and maximum travel-time variation each day (at $\sim 10^h \pm 1^h$ ST) versus local solar time for some 180 days. The straight line plot is the least squares fit to the experimental data, giving an average slope of 3.92 minutes/day. The time difference between a sidereal day and a solar day is 3.93 minutes/day. This demonstrates that the effect is related to sidereal time and not local solar time. The actual days of the year are not identified in Ref.[137]. Adapted from DeWitte [137].

solar time. A least squares best fit of a linear relation to that data gives that the cross-over time is retarded, on average, by 3.92 minutes per solar day. This is to be compared with the fact that a sidereal day is 3.93 minutes shorter than a solar day. So the effect is certainly cosmological and not associated with any daily thermal effects, which in any case would be very small as the cable is buried. Miller had also compared his data against sidereal time and established the same property, namely that up to small diurnal effects identifiable with the earth's orbital motion, features in the data tracked sidereal time and not solar time; see Ref.[123] for a detailed analysis.

The DeWitte data is also capable of resolving the question of the absolute direction of motion found by Miller. Is the direction $(\alpha = 5.2^{hr}, \delta = -67^0)$ or the opposite direction? Being a 2nd-order Michelson interferometer experiment Miller had to rely on the earth's diurnal effects in order to resolve this ambiguity, but his analysis of course did not take account of the gravitational in-flow effect, and so until a re-analysis of his data his preferred choice of direction must remain to be confirmed. The DeWitte experiment could easily resolve this ambiguity by simply noting the sign of Δt. Unfortunately it is unclear in Ref.[137] as to how the sign in Fig.10.20 is actually defined, and DeWitte does not report a direction expecting, as he did, that the direction should have been the same as the CMB direction.

The DeWitte observations were truly remarkable considering that initially they were serendipitous. They demonstrated yet again that the Einstein postulates were in contradiction with experiment. To my knowledge no physics journal[12] has published a report of the DeWitte experiment and DeWitte himself reports [137] that he was dismissed from Belgacom. DeWiite's data like that of Miller is extremely valuable and needs to be made available for detailed analysis. Regrettably I have received a report that he died, and that the data was lost when he left Belgacom.

That the DeWitte experiment is not a gas-mode Michelson interferometer experiment is very significant. The value of the speed of absolute motion revealed by the DeWitte experiment of some 400 km/s is in agreement with the speeds revealed by the new analysis of various Michelson interferometer data which uses the recently discovered refractive index effect, see Fig.10.15. Not only was this effect confirmed by comparing results for different gases, but the re-scaling of the older v_M speeds to $v = v_M/\sqrt{n^2 - 1}$ speeds resulting from this effect are now confirmed. A new and much simpler 1st-order experiment is discussed in Chap.12.3 which avoids the use of atomic clocks.

10.9 The Torr-Kolen Experiment: 1981

A coaxial cable experiment similar to but before the DeWitte experiment was performed at the Utah University in 1981 by Torr and Kolen [138]. This involved two rubidium vapor clocks placed approximately 500m apart with a 5 MHz sinewave RF signal propagating between the clocks via a nitrogen filled coaxial cable maintained at a constant pressure of $\sim$2 psi. This means that the Fresnel drag effect is not important in this experiment. Unfortunately the cable was orientated in an East-West direction which is not a favourable orientation for observing absolute motion in the Miller direction, unlike the Brussels North-South cable orientation. There is no reference to Miller's result in the Torr and Kolen paper, otherwise they would presumably not have used this orientation. Nevertheless there is a small projection of the absolute motion velocity onto the East-West cable and Torr and Kolen did observe an effect in that, while the round speed time remained constant within 0.0001%c, typical variations in the one-way travel time were observed, as shown in Fig.10.23 by the data points. The theoretical predictions for the Torr-Kolen experiment for a cosmic speed of 433 km/s in the direction $(\alpha = 5.2^{hr}, \delta = -67^0)$, and including orbital and in-flow velocities, are shown in Fig.10.23. As well the maximum effect occurred, typically, at the predicted times. So the results of this experiment are also in remarkable agreement with the Miller direction, and the speed of 417 km/s which of course only arises after re-scaling the Miller speeds for the effects of the gravitational in-flow. As well Torr and Kolen reported fluctuations in both the

[12]Papers reporting or analysing absolute motion and related effects are banned from physics journals. This appears to be based on the almost universal misunderstanding by physicists that absolute motion is incompatible with the many confirmed relativistic effects.

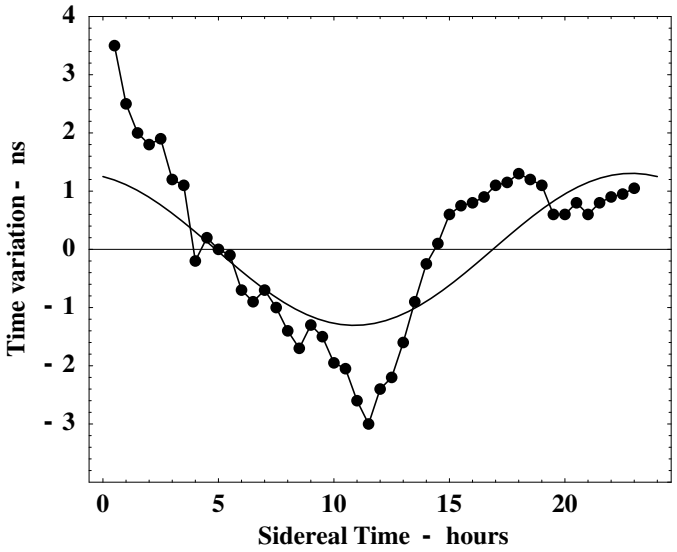

Figure 10.23: Data from the 1981 Torr-Kolen experiment at Logan, Utah [138]. The data shows variations in travel times (ns), for local times, of an RF signal travelling through 500m of coaxial cable orientated in an E-W direction. Actual days are not indicated but the experiment was done during February-June 1981. Results are for a typical day. For the 1st of February the local time of 12:00 corresponds to 13:00 sidereal time. The predictions are for February, for a cosmic speed of 433 km/s in the direction $(\alpha = 5.2^{hr}, \delta = -67^0)$, and including orbital and in-flow velocities but without theoretical turbulence.

magnitude, from 1 - 3 ns, and time of the maximum variations in travel time just as DeWitte observed some 10 years later. Again we argue that these fluctuations are evidence of genuine turbulence in the in-flow as discussed in Sect.11.3. So the Torr-Kolen experiment again shows strong evidence for the new theory of gravity, and which is over and above its confirmation of the various observations of absolute motion.

10.10 Stellar Aberration

James Bradley discovered the aberration of light from stars in 1727. This is the seasonal change in apparent position of the stars, with the effect largest in the direction perpendicular to the plane of the ecliptic. The obvious explanation is that this is caused by the change in velocity of the earth due to its orbital motion about the sun. Despite the simplicity of this phenomenon it has caused considerable misunderstanding after the misreporting of the Michelson-Morley experiment and the adoption by Einstein that absolute motion was unobservable and meaningless. However now that it is clear that a number of experiments have indeed detected absolute motion, and that the Einstein's ideas about the unobservability of absolute motion

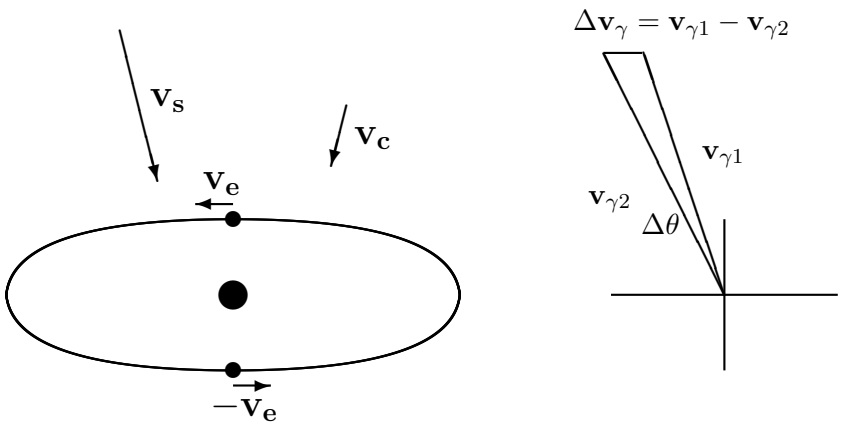

(a) (b)

Figure 10.24: (a) Orbit of the earth about the sun defining the plane of the ecliptic with tangential orbital velocity $\mathbf{v}_e$ at one epoch, and $-\mathbf{v}_e$ six months later. The earth's orbit is shown in the rest frame of the sun. The absolute velocity of the solar system through space is $\mathbf{v}_c$, and $\mathbf{v}_s$ is the velocity of light from a distant star, with $|\mathbf{v}_s| = c$, both relative to absolute space. Vectors not drawn to scale. (b) Shows change in direction of star light over the six months. The angle $\Delta\theta$ between the velocity of the star light $\mathbf{v}_{\gamma 1}$ and $\mathbf{v}_{\gamma 2}$ at the two epochs, both defined in the reference frame of the earth, is the observed aberration.

are incorrect, it is now possible to give a sensible analysis of stellar aberration, which is essentially in accord with the much older explanation using the principles of Galilean Relativity. However now that we know that the solar system has an absolute speed though space of some 420 km/s, the question arises as to why that absolute motion was not apparent in stellar aberrations?

Fig.10.24a shows the orbit of the earth about the sun, defining the plane of the ecliptic with tangential orbital velocity $\mathbf{v}_e$ at one epoch, and $-\mathbf{v}_e$ six months later. The earth's orbit is shown in the rest frame of the sun. The absolute velocity of the solar system through space is $\mathbf{v}_c$, and $\mathbf{v}_s$ is the velocity of light from a distant star, with $|\mathbf{v}_s| = c$, both relative to absolute space. Then

$$\begin{aligned} \mathbf{v}_{\gamma 1} &= \mathbf{v}_s - (\mathbf{v}_c + \mathbf{v}_e), \\ \mathbf{v}_{\gamma 2} &= \mathbf{v}_s - (\mathbf{v}_c - \mathbf{v}_e), \end{aligned} \tag{10.16}$$

is the velocity of light relative to an earth based observer, at the two epochs. This follows using the Galilean Relativity addition rule for velocities. Now we understand that the speed of light $|\mathbf{v}_s| = c$, that is, it has speed c relative to absolute space, in the case of a vacuum. Then the change in the velocity of light from a given star, over the two epochs, for an earth based observer is

$$\Delta v_\gamma = \mathbf{v}_{\gamma 1} - \mathbf{v}_{\gamma 2} = -2\mathbf{v}_e. \tag{10.17}$$

The observable is the change in direction $\Delta\theta$ shown in Fig.10.24b. From the triangle formed by the two vectors, and since the effect is small, we get for the maximum effect to $O(v_e)$, that

$$\Delta\theta \approx \frac{\Delta v_\gamma}{|\mathbf{v}_s - \mathbf{v}_c|} \approx 2\frac{v_e}{c} + O(v_e), \tag{10.18}$$

when $\mathbf{v}_s - \mathbf{v}_c$ is perpendicular to the plane of the ecliptic, and in the second part of the equation we have neglected v_c in comparison with $v_s = c$. This last result corresponds to the older explanations of stellar aberration. Notice that the condition for maximum effect refers now to the vector difference of the stellar light velocity and the velocity of absolute motion of the solar system, and not merely to the stellar light velocity, as in the original analysis. However this distinction is not observable with stellar aberrations. Note however that the magnitude of $|\mathbf{v}_s - \mathbf{v}_c|/c$ does depend of the stellar direction relative to the absolute motion direction, and this changes by approximately ± 0.001 over the full sky. Hence if stellar aberration angles can be measured to better than one part in a thousand the absolute motion of the solar system could be observed by yet another method. Here the maximum northern aberration should be different to the maximum southern aberration. However the Gravity Probe B will be detecting stellar aberration to an extremely high accuracy, and so may be able to confirm the above effects.

Chapter 11

Gravitational In-Flow and Gravitational Waves

11.1 Gravitational In-Flows and the Miller Data

As already noted Miller was led to the conclusion that for reasons unknown the existing theory of the Michelson interferometer did not reveal true values of v_P, and for this reason he introduced the parameter k, with $\overline{k}$ indicating his numerical values. Miller had reasoned that he could determine both $\mathbf{v}_{cosmic}$ and $\overline{k}$ by observing the interferometer determined v_P and ψ over a year because the known orbital velocity of the earth about the sun would modulate both of these observables, and by a scaling argument he could determine the absolute velocity of the solar system. In this manner he finally determined that $|\mathbf{v}_{cosmic}| = 208$ km/s in the direction ($\alpha = 4^{hr}54^{m}, \delta = -70^{0}33'$). However now that the theory of the Michelson interferometer has been revealed an anomaly becomes apparent. Table 3 shows $v = v_M/k_{air}$ for each of the four epochs, giving speeds consistent with the revised Michelson-Morley data. However Table 3 also shows that $\overline{k}$ and the speeds $\overline{v} = v_M/\overline{k}$ determined by the scaling argument are considerably different. Here the v_M values arise after taking account of the projection effect. That $\overline{k}$ is considerably larger than the value of k_{air} indicates that another velocity component has been overlooked. Miller of course only knew of the tangential orbital speed of the earth, whereas the new physics predicts that as-well there is a quantum-gravity radial in-flow $\mathbf{v}_{in}$ of the quantum foam. We can re-analyse Miller's data to extract a first approximation to the speed of this in-flow component. Clearly it is $v_R = \sqrt{v_{in}^2 + v_{tangent}^2}$ that sets the scale and not $v_{tangent}$, and because $\overline{k} = v_M/v_{tangent}$ and $k_{air} = v_M/v_R$ are the scaling relations, then

$$v_{in} \quad = \quad v_{tangent}\sqrt{\frac{v_R^2}{v_{tangent}^2} - 1},$$

$$= \quad v_{tangent}\sqrt{\frac{\overline{k}^2}{k_{air}^2} - 1}. \tag{11.1}$$

Using the $\overline{k}$ values in Table 3 and the value[1] of k_{air} we obtain the v_{in} speeds shown in Table 3, which give an average speed of 54 km/s, compared to the 'Newtonian' in-flow speed of 42 km/s. Note that the in-flow interpretation of the anomaly predicts that $\overline{k} = (v_R/v_{tangent})\, k_{air} = \sqrt{3}\, k_{air} = 0.042$. Alternatively one can simply rescale $\overline{v}$ by $\sqrt{3}$ because $v_R = \sqrt{3}v_{in}$ instead of v_{in} sets the scale. Of course this simple re-scaling of the Miller results is not completely valid because (i) the direction of $\mathbf{v}_R$ is of course different to that of $\mathbf{v}_{tangent}$, and also not necessarily orthogonal to $\mathbf{v}_{tangent}$ because of turbulence, and (ii) also because of turbulence we would expect some contribution from the in-flow effect of the earth itself, namely that it is not always perpendicular to the earth's surface, and so would give a contribution to a horizontally operated interferometer.

Epoch	v_M	$\overline{k}$	$v = v_M/k_{air}$	$\overline{v} = v_M/\overline{k}$	$v = \sqrt{3}\overline{v}$	v_{in}
February 8	9.3 km/s	0.048	385.9 km/s	193.8 km/s	335.7 km/s	51.7 km/s
April 1	10.1	0.051	419.1	198.0	342.9	56.0
August 1	11.2	0.053	464.7	211.3	366.0	58.8
September 15	9.6	0.046	398.3	208.7	361.5	48.8

Table 3. The $\overline{k}$ anomaly, $\overline{k} \gg k_{air} = 0.0241$, as the gravitational in-flow effect. Here v_M and $\overline{k}$ come from fitting the interferometer data (using v_{in} to determine $\overline{k}$), while v and $\overline{v}$ are computed speeds using the indicated scaling. The average of the in-flow speeds is $v_{in} = 54 \pm 5$ km/s, compared to the 'Newtonian' in-flow speed of 42 km/s. From column 4 we obtain the average $v = 417 \pm 40$km/s.

An analysis that properly searches for the in-flow velocity effect clearly requires a complete re-analysis of the Miller data, and this is now possible and underway at Flinders University as the original data sheets have been found. It should be noted that the direction essentially diametrically opposite ($\alpha = 5.2^{hr}, \delta = -67^0$), namely ($\alpha = 17^{hr}, \delta = +68'$) was at one stage considered by Miller as being possible. This is because the Michelson interferometer, being a 2nd-order device, has a directional ambiguity which can only be resolved by using the diurnal motion of the earth. However as Miller did not include the in-flow velocity effect in his analysis it is possible that a re-analysis might give this northerly direction as the direction of absolute motion of the solar system.

Fig.11.1 shows the so called 'aberration orbit' which indicates the change in direction of absolute motion at various epochs due to the vector sum of the three main contributions $\mathbf{v}_{cosmic} + \mathbf{v}_{tangent} - \mathbf{v}_{in}$, with the latter two components having

[1]We have not modified this value to take account of the altitude effect or temperatures atop Mt.Wilson. This weather information was not recorded by Miller. The temperature and pressure effect is that $n = 1.0 + 0.00029\frac{P}{P_0}\frac{T_0}{T}$, where T is the temperature in ^{0}K and P is the pressure in atmospheres. $T_0 = 273$K and $P_0 =$1atm.

a diurnal time-dependence. Note that Miller's data points, in an analogous plot in Fig.28 in Ref.[123], involved for February the average of 8080 single interferometer observations, and for the others 7680 for August, 6640 for September and 3208 for April. So Miller's observations were very thorough.

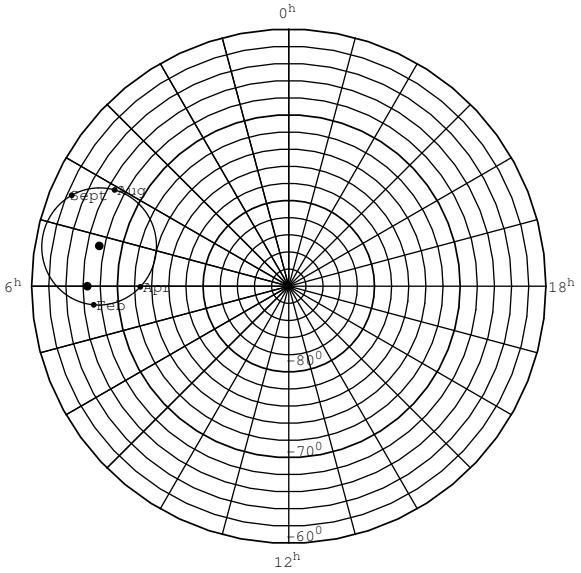

Figure 11.1: The 'Aberration Orbit' shows the net direction of absolute motion at various epochs. The plot shows the south circumpolar region of the celestial sphere. The direction $(\alpha = 6^{hr}, \delta = -66.5^0)$ is the pole of the ecliptic. At the centre of the aberration orbit is the direction $(\alpha = 5.2^{hr}, \delta = -67^0)$. Compared to Miller's analogous plot, Fig.28 in Ref.[123], the inclusion of the in-flow effect has caused the epoch points to be rotated around the aberration orbit.

Hence not only did Miller observe absolute motion, as he claimed, but the quality and quantity of his data has also enabled the confirmation of the existence of the gravitational in-flow effect [13, 14]. This is a manifestation of a new theory of gravity and one which relates to quantum gravitational effects via the unification of matter and space developed in previous chapters. As well the persistent evidence that this in-flow is turbulent indicates that this theory of gravity involves self-interaction of space itself.

11.2 Galactic In-flow and the CMB Frame

Absolute motion (AM) of the solar system has been observed in the direction $(\alpha = 5.2^{hr}, \delta = -67^0)$, up to an overall sign to be sorted out, with a speed of 417 ± 40 km/s. This is the velocity after removing the contribution of the earth's orbital speed and the sun in-flow effect. It is significant that this velocity is different to that associated

with the Cosmic Microwave Background [2] (CMB) relative to which the solar system has a speed of 369 km/s in the direction ($\alpha = 11.20^h, \delta = -7.22^0$), see [135]. This CMB velocity is obtained by finding the preferred frame in which this thermalised 3^0K radiation is isotropic, that is by removing the dipole component. The CMB velocity is a measure of the motion of the solar system relative to the universe as a whole, or aleast a shell of the universe some 14Gyrs away, and indeed the near uniformity of that radiation in all directions demonstrates that we may meaningfully refer to the spatial structure of the universe. The concept here is that at the time of decoupling of this radiation from matter that matter was on the whole, apart from small observable fluctuations, at rest with respect to the quantum-foam system that is space. So the CMB velocity is the motion of the solar system with respect to space *universally*, but not necessarily with respect to the *local* space. Contributions to this velocity would arise from the orbital motion of the solar system within the Milky Way galaxy, which has a speed of some 250 km/s, and contributions from the motion of the Milky Way within the local cluster, and so on to perhaps larger clusters.

On the other hand the AM velocity is a vector sum of this *universal* CMB velocity and the net velocity associated with the *local* gravitational in-flows into the Milky Way and the local cluster. If the CMB velocity had been identical to the AM velocity then the in-flow interpretation of gravity would have been proven wrong. We therefore have three pieces of experimental evidence for this interpretation (i) the refractive index anomaly discussed previously in connection with the Miller data, (ii) the turbulence seen in all detections of absolute motion, and now (iii) that the AM velocity is different in both magnitude and direction from that of the CMB velocity, and that this velocity does not display the turbulence seen in the AM velocity.

That the AM and CMB velocities are different amounts to the discovery of the resolution to the 'dark matter' conjecture. Rather than the galactic velocity anomalies being caused by such undiscovered 'dark matter' we see that the in-flow into non-spherical galaxies, such as the spiral Milky Way, will be non-Newtonian, that is (7.9) is not appropriate to such highly non-spherical systems. When solutions to (7.19)-(7.20) are determined for such systems it will be possible to map out the predicted AM velocity and compare with the observed velocity. As well it will be interesting to determine, at least theoretically, the scale of turbulence expected in galactic systems, particularly as the magnitude of the turbulence seen in the AM velocity is somewhat larger than might be expected from the sun in-flow alone. Any theory for the turbulence effect will certainly be checkable within the solar system

[2] The understanding of the galactic in-flow effect was not immediate: In [12] the direction was not determined, though the speed was found to be comparable to the CMB determined speed. In [13] that the directions were very different was noted but not appreciated, and in fact thought to be due to experimental error. In [14] an analysis of some of the 'smoother' Michelson-Morley data resulted in an incorrect direction. At that stage it was not understood that the data showed large fluctuations in the azimuth apparently caused by the turbulence. Here the issue is hopefully finally resolved.

as the time scale of this is suitable for detailed observation.

It is also clear that the time of observers at rest with respect to the CMB frame is absolute or universal time. This interpretation of the CMB frame has of course always been rejected by supporters of the SR/GR formalism. As for space we note that it has a differential structure, in that different regions are in relative motion. This is caused by the gravitational in-flow effect locally, and as well by the growth of the universe.

11.3 In-Flow Turbulence and Gravitational Waves

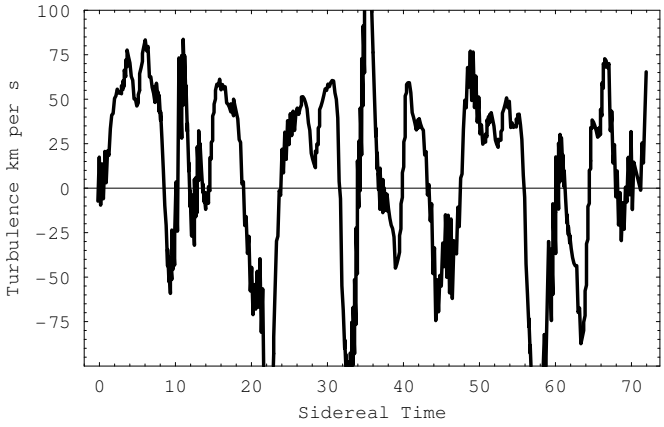

Figure 11.2: Speed fluctuations determined from Fig.10.20 by subtracting a least squares best fit of the forms shown in Fig.10.21b. A 1ns variation in travel time corresponds approximately to a speed variation of 27km/s. The larger speed fluctuations actually arise from a fluctuation in the cross-over time, that is, a fluctuation in the direction of the velocity. This plot implies that the velocity flow-field is turbulent. The scale of this turbulence is comparable to that evident in the Miller data, as shown in Fig.10.10 and Fig.11.3.

The velocity flow-field equation, suggested to have the form (7.19)-(7.20), is expected to have solutions possessing turbulence, that is, fluctuations in both the magnitude and direction of the gravitational in-flow component of the velocity flow-field. Indeed all the Michelson interferometer experiments showed evidence of such turbulence. The first clear evidence was from the Miller experiment, as shown in Fig.10.10 and Fig.11.3. Miller offered no explanation for these fluctuations but in his analysis of that data he did running time averages, as shown by the smoother curves in Fig.10.10. Miller may have in fact have simply interpreted these fluctuations as purely instrumental effects. While some of these fluctuations may be partially caused by weather related temperature and pressure variations, the bulk of the fluctuations appear to be larger than expected from that cause alone. Even the original Michelson-Morley data in Fig.10.6 shows variations in the velocity field and

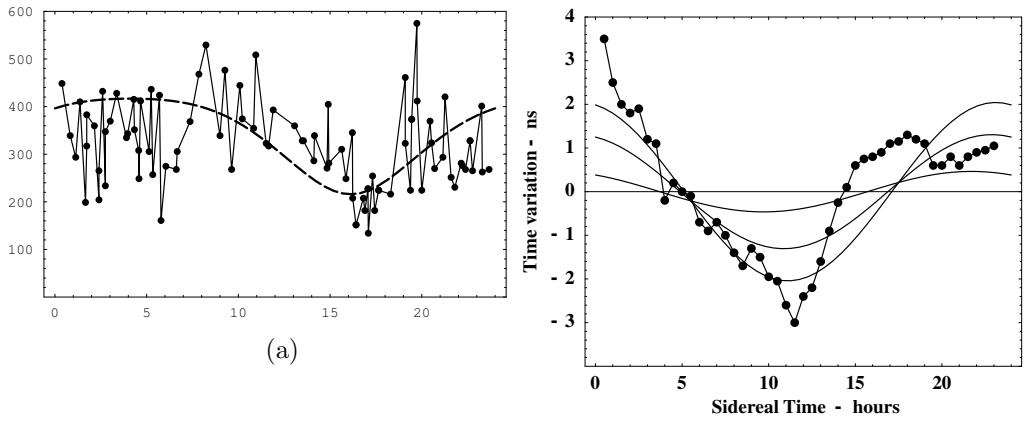

(a) (b)

Figure 11.3: (a) The absolute projected speeds v_P in the Miller experiment plotted against sidereal time in hours for September 1925, showing the variations in speed caused by the gravitational wave turbulence. and (b) similar variations in travel times when the declination is varied by $\pm 10^0$ about the direction $(\alpha = 5.2^{hr}, \delta = -67^0)$, for a cosmic speed of 433 km/s in the Torr-Kolen experiment.

supports this interpretation. However it is significant that the non-interferometer DeWitte data also shows evidence of turbulence in both the magnitude and direction of the velocity flow field, as shown in Fig.11.2. Just as the DeWitte data agrees with the Miller data for speeds and directions the magnitude fluctuations, shown in Fig.11.2, are very similar in absolute magnitude to, for example, the speed turbulence shown in Fig.11.3.

It therefore becomes clear that there is strong evidence for these fluctuations being evidence of physical turbulence in the flow field. The magnitude of this turbulence appears to be somewhat larger than that which would be caused by the in-flow of quantum foam towards the sun, and indeed following on from Sect.11.2 some of this turbulence may be associated with galactic in-flow into the Milky Way. This in-flow turbulence is a form of gravitational wave and the ability of gas-mode Michelson interferometers to detect absolute motion means that experimental evidence of such a wave phenomena has been available for a considerable period of time, but suppressed along with the detection of absolute motion itself. Of course flow equations of the form in (7.19)-(7.20) do not exhibit those gravitational waves of the form that have been predicted to exist based on the Einstein equations, and which are supposed to propagate at the speed of light. All this means that gravitational wave phenomena is very easy to detect and amounts to new physics that can be studied in much detail, particularly using the new 1st-order interferometer discussed in Sect.12.3.

In Sect.7.2 we considered gravitational waves within the in-flow formalism of Newtonian gravity. In the new theory of gravity (7.19)-(7.20) we have the addi-

tional $C(\mathbf{v})$ term. It may be checked that again this equation has perturbative wave solutions where again using the perturbative velocity potential field $\overline{u}(\mathbf{r},t) = A\cos(\mathbf{k}.\mathbf{r}-\omega t)$ where $\omega(\mathbf{k},\mathbf{r}) = \mathbf{v}_0(\mathbf{r}).\mathbf{k}$, for wavelengths short compared to the scale of changes in $\mathbf{v}_0(\mathbf{r})$, and again the velocity field is

$$\mathbf{v}(\mathbf{r},t) = \overline{\mathbf{v}}_0(\mathbf{r}) - A\mathbf{k}\sin(\mathbf{k}.\mathbf{r} - w(\mathbf{k},\mathbf{r})t). \tag{11.2}$$

The same perturbative solutions arise because the new term only contributes terms involving spatial derivatives of $\overline{\mathbf{v}}_0(\mathbf{r})$, and as before we have ignored these.

11.4 Absolute Motion and Quantum Gravity

Absolute rotational motion had been recognised as a meaningful and observable phenomena from the very beginning of physics. Newton had used his rotating bucket experiment to illustrate the reality of absolute rotational motion, and later Foucault and Sagnac provided further experimental proof. But for absolute linear motion the history would turn out to be completely different. It was generally thought that absolute linear motion was undetectable, at least until Maxwell's electromagnetic theory appeared to require it. In perhaps the most bizarre sequence of events in modern science it turns out that absolute linear motion has been apparent within experimental data for over 100 years. It was missed in the first experiment designed to detect it and from then on for a variety of sociological reasons it became a concept rejected by physicists and banned from their journals despite continuing new experimental evidence. Those who pursued the scientific evidence were treated with scorn and ridicule. Even worse was the impasse that this obstruction of the scientific process resulted in, namely the halting of nearly all progress in furthering our understanding of the phenomena of gravity. For it is clear from all the experiments that were capable of detecting absolute motion that there is present in that data evidence of turbulence within the velocity field. Both the in-flow itself and the turbulence are manifestations at a classical level of what is essentially quantum gravity processes.

Process Physics has given a unification of explanation and description of physical phenomena based upon the limitations of formal syntactical systems which had nevertheless achieved a remarkable encapsulation of many phenomena, albeit in a disjointed and confused manner, and with a dysfunctional ontology attached for good measure. As argued in early chapters space is a quantum system continually classicalised by on-going non-local collapse processes. The emergent phenomena is foundational to existence and experientialism. Gravity in this system is caused by differences in the rate of processing of the cellular information within the network which we experience as space, and consequentially there is a differential flow of information which can be affected by the presence of matter or even by space itself. Of course the motion of matter including photons with respect to that spatial information content is detectable because it affects the geometrical and chronological

attributes of that matter, and the experimental evidence for this will be exhaustively discussed in this chapter. What has become very clear is that the phenomena of gravity is only understandable once we have this unification of the quantum phenomena of matter and the quantum phenomena of space itself. In Process Physics the difference between matter and space is subtle. It comes down to the difference between informational patterns that are topologically preserved and those information patterns that are not. One outcome of this unification is that as a consequence of having a quantum phenomena of space itself we obtain an informational explanation for gravity, and which at a suitable level has an emergent quantum description. In this sense we have an emergent quantum theory of gravity. Of course no such quantum description of gravity is derivable from quantising Einsteinian gravity itself. This follows on two counts, one is that the Einstein gravity formalism fails on several levels, as discussed previously, and second that quantisation has no validity as a means of uncovering deeper physics. Most surprising of all is that having uncovered the logical necessity for gravitational phenomena it also appears that even the seemingly well-founded Newtonian account of gravity has major failings. The denial of this possibility has resulted in an unproductive search for dark matter. Indeed like dark matter and spacetime much of present day physics has all the hallmarks of another episode of Ptolemy's epicycles, namely concepts that appear to be well founded but in the end turn out to be illusions, and ones that have acquired the status of dogma.

If the Michelson-Morley experiment had been properly analysed and the phenomena revealed by the data exposed, and this would have required in 1887 that Newtonian physics be altered, then as well as the subsequent path of physics being very different, physicists would almost certainly have discovered both the gravitational in-flow effect and associated turbulence. It is not beyond expectation that a modification of Newtonian gravity in terms of a velocity field and the extra term in (7.19)-(7.20) would have been quickly developed. Even Newton had speculated about an in-flow explanation for gravity.

It is clear then that observation and measurement of absolute motion leads directly to a changed paradigm regarding the nature and manifestations of gravitational phenomena, and that the new 1st-order interferometer described in Chap.12.3 will provide an extremely simple device to uncover aspects of gravity previously denied by current physics. There are two aspects of such an experimental program. One is the characterisation of the turbulence and its linking to the new non-linear term in the velocity field theory (7.19)-(7.20). This is a top down program. The second aspect is a bottom-up approach where the form of (7.19)-(7.20), or its modification, is derived from the deeper informational process physics. This is essentially the quantum gravity route. The turbulence is of course essentially a gravitational wave phenomenon and networks of 1st-order interferometers will permit spatial and time series analysis. There are a number of other gravitational anomalies which may also now be studied using such an interferometer network, and so much new

physics can be expected to be uncovered.

Chapter 12

Modern Interferometers

12.1 Vacuum Michelson Interferometers

Over the years vacuum-mode Michelson interferometer experiments have become increasing popular, although the motivation for such experiments appears to be increasingly unclear. The first vacuum interferometer experiment was planned by Joos [129] in 1930, but because of technical problems helium was actually used, as discussed in Sect.10.6. The first actual vacuum experiment was by Kennedy and Thorndike [139]. Their result was actually unclear but was consistent with a null effect as predicted by both the quantum-foam physics and the Einstein physics. Only Newtonian physics is disproved by such experiments. These vacuum interferometer experiments do give null results, with increasing confidence level, as for example in Refs.[139, 140, 141, 142], but they only check that the Lorentz contraction effect completely cancels the geometrical path-length effect in vacuum experiments, and this is common to both theories. So they are unable to distinguish the new physics from the Einstein physics. Nevertheless recent works [141, 142] continue to claim that the experiment had been motivated by the desire to look for evidence of absolute motion[1], despite effects of absolute motion having been discovered as long ago as 1887. The 'null results' are always reported as proof of the Einstein formalism. Of course all the vacuum experiments can do is check the Lorentz contraction effect, and this in itself is valuable. Unfortunately the analysis of the data from such experiments is always by means of the Robertson [143] and Mansouri and Sexl formalism [144], which purports to be a generalisation of the Lorentz transformation if there is a preferred frame. However in Chap.7.4 we have already noted that absolute motion effects, that is the existence of a preferred frame, are consistent with the usual Lorentz transformation, based as it is on the restricted Einstein measurement protocol. A preferred frame is revealed by gas-mode Michelson inter-

[1]The Journal *Physical Review Letters* has a particular penchant for publishing such works and a total aversion to works reporting experimental data giving evidence for absolute motion and its related gravitational in-flow effects.

ferometer experiments, and then the refractive index of the gas plays a critical role in interpreting the data. The Robertson and Mansouri-Sexl formalism contains no contextual aspects such as a refractive index effect and is thus totally inappropriate to the analysis of so called 'preferred frame' experiments.

It is a curious feature of the history of Michelson interferometer experiments that it went unnoticed that the results fell into two distinct classes, namely vacuum and gas-mode, with recurring non-null results from gas-mode interferometers. The science historian Swenson [131] p243 noted in 1972 that

> *the comparisons of expected to observed fringe shifts over the years of increasing optical sophistication still left little, though something, to be explained.*

History will I think show that the physicists went to great lengths to hide that 'something', and still do so.

12.2 Solid-State Michelson Interferometers

The gas-mode Michelson interferometer has its sensitivity to absolute motion effects greatly reduced by the refractive index effect, namely the $k^2 = n^2 - 1$ factor in (10.1), and for gases with n only slightly greater than one this factor has caused much confusion over the last 115 years. So it would be expected that passing the light beams through a transparent solid with $n \approx 1.5$ rather than through a gas would greatly increase the sensitivity. Such an Michelson interferometer experiment was performed by Shamir and Fox [145] in Haifa in 1969. This interferometer used light from a He-Ne laser and used perspex rods with $L = 0.26$m. The experiment was interpreted in terms of the supposed Fresnel drag effect, which has a drag coefficient given by $b = 1 - 1/n^2$. The light passing through the solid was supposed to be 'dragged' along in the direction of motion of the solid with a velocity $\Delta\mathbf{V} = b\mathbf{v}$ additional to the usual c/n speed. As well the Michelson geometrical path difference and the Lorentz contraction effects were incorporated into the analysis. The outcome was that no fringe shifts were seen on rotation of the interferometer, and Shamir and Fox concluded that this negative result *"enhances the experimental basis of special relativity"*.

The Shamir-Fox experiment was unknown to us[2] at Flinders university when in 2002 several meters of optical fibre were used in a Michelson interferometer experiment which also used a He-Ne laser light source. Again because of the $n^2 - 1$ factor, and even ignoring the Fresnel drag effect, one would have expected large fringe shifts on rotation of the interferometer, but none were observed. As well in a repeat of the experiment single-mode optical fibres were also used and again with no rotation

[2]This experiment was performed by Professor Warren Lawrance, an experimental physical chemist with considerable laser experience.

Figure 12.1: Schematic form of a possible 1st-order interferometer showing laser source (L), glass rod (G), screen (S), mirrors (M) and beam-splitters (BS). The axis of the laser should ideally be orthogonal to the plane of the interferometer.

effect seen. So this experiment is consistent with the Shamir-Fox experiment. Redoing the analysis by including the supposed Fresnel drag effect, as Shamir and Fox did, makes no material difference to the expected outcome. In combination with the non-null results from the gas-mode interferometer experiments along with the non-interferometer experiment of DeWitte it is clear that transparent solids behave differently to a gas when undergoing absolute motion through the quantum foam. Indeed this in itself is a discovery of a new phenomena.

The most likely explanation is that the physical Fitzgerald-Lorentz contraction effect has a anisotropic effect on the refractive index of the transparent solid, and this is such as to cause a cancellation of any differences in travel time between the two arms on rotation of the interferometer. In this sense a transparent solid medium shares this outcome with the vacuum itself.

12.3 New Absolute Motion and Gravitational Wave Detectors

It would appear so far that either very difficult gas-mode Michelson 2nd-order interferometers, perhaps using gases with anomalously large values of n [3], or time-of-flight 1st-order experiments using atomic clocks are required to study absolute motion and related effects. Here the possibility of constructing 1st-order devices is considered. Consider first the interferometer design shown schematically in Fig.12.1. Fringes are produced by the interference of two beams of coherent laser light that are brought together on a screen after having passed through different media of different refractive indices, such as glass and air. If there is no Fresnel drag effect in the glass then on rotation of the device the fringes shift by an amount that is 1st order in v/c

Consider a simplified analysis for which 2nd-order Fitzgerald-Lorentz contraction

[3]The gas Perfluorobutane has $n = 1.0014$ and is particularly suited to this task.

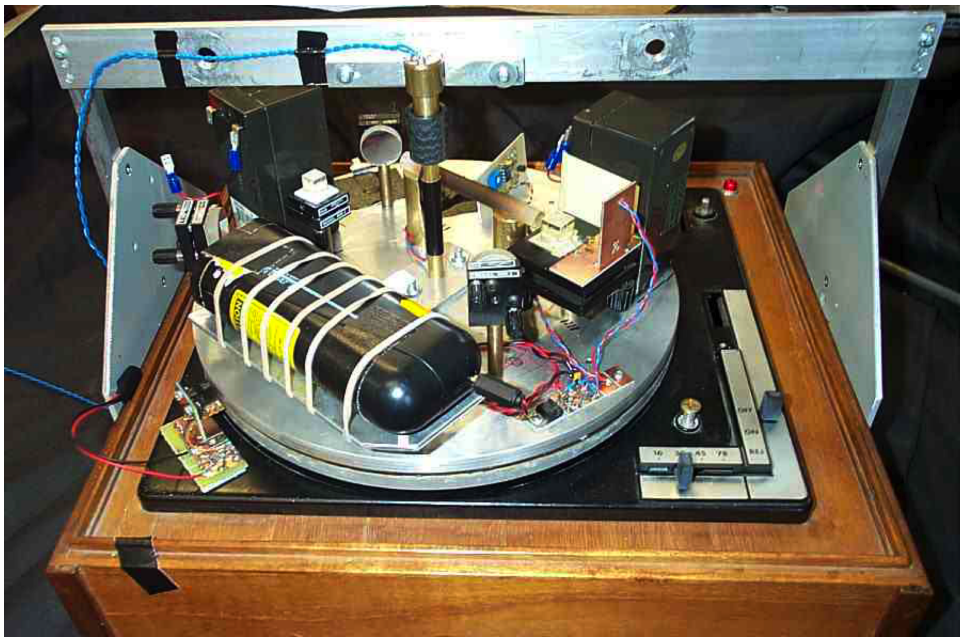

Figure 12.2: The Flinders experiment. The He-Ne laser is in the lower left hand corner. This should be mounted vertically, as is now the case, otherwise rotations effect the laser frequency. The glass rod is orientated from upper left to lower right. Rotations are achieved by means of the record turntable. The two rectangular black boxes are batteries.

effects are ignored. Let the length of the glass rod have refractive index n_2 and length L and the air refractive index n_1 and let the transverse distance be d. Then the difference in travel time for the glass and air paths is

$$\begin{aligned}\Delta t &= \frac{L}{\frac{c}{n_1} - v_P} - \frac{L}{\frac{c}{n_2} - v_P} + \frac{d}{\frac{c}{n_1} - v_T} + \frac{d}{\frac{c}{n_1} + v_T}, \\ &= (\frac{n_1 L}{c} - \frac{n_2 L}{c}) + (\frac{n_2^2 L}{c} - \frac{n_1^2 L}{c})\frac{v_P}{c} + O(\frac{v_P^2}{c^2}) + O(\frac{v_T^2}{c^2}), \qquad (12.1)\end{aligned}$$

where v_P is the projection of the absolute velocity $\mathbf{v}$ onto the axis of the interferometer, and v_T is the projection onto the transverse paths. Here the first bracket is the fixed difference in travel times when $v_P = 0$. The required effect follows from the second term, which gives the change $\delta\Delta t$ in time-difference on rotation of the device,

$$\delta\Delta t = (n_2^2 - n_1^2) t_0 \frac{v_P}{c} \qquad (12.2)$$

where $t_0 = L/c$ is the vacuum travel time for the distance L. Hence $\delta\Delta t$ is the change in the difference of travel times upon rotation, in which v_P changes due to the projection effect. Hence this interferometer is a differential time-of-flight device,

and essentially uses one of the beams as a timing reference beam, and so avoids the need for atomic clocks. This device can be very small. Using $n_2 = 1.5$ for the glass, $n_1 = 1$ for air, $L = 0.1$m and a He-Ne laser, then for $v_P = 400$ km/s we obtain $2\delta\Delta t = 0.011$ns corresponding to some 524 fringe shifts on a 180^0 rotation, that is when $v_P \to -v_P$. This device is sufficiently sensitive that speed measurements accurate to ± 1 km should be possible. This single arm interferometer requires rotation, and this will always complicate its operation. However a static device may be constructed based on three orthogonally orientated arms. Then the fringe shifts in each arm give $\delta\Delta t_x, ..$ and we have from (12.2)

$$\mathbf{v} = (v_x, v_y, v_z) = \frac{c}{t_0(n_2^2 - n_1^2)}(\delta\Delta t_x, \delta\Delta t_y, \delta\Delta t_z), \tag{12.3}$$

which gives the velocity vector of absolute motion relative to the coordinate system defined by the arms. This velocity is then transformed to celestial coordinates. Such a device is ideal to study and characterise the in-flow turbulence which is an aspect of quantum gravity phenomena.

However if there is a Fresnel drag effect in transparent solids then the above analysis is changed significantly, for we then have, again ignoring 2nd order effects,

$$\begin{aligned} \Delta t &= \frac{L}{\frac{c}{n_1} + b_1 v_P - v_P} - \frac{L}{\frac{c}{n_2} + b_2 v_P - v_P} + \frac{d}{\frac{c}{n_1} - v_T} + \frac{d}{\frac{c}{n_1} + v_T}, \\ &= (\frac{n_1 L}{c} - \frac{n_2 L}{c}) + O(\frac{v_P^2}{c^2}) + O(\frac{v_T^2}{c^2}), \end{aligned} \tag{12.4}$$

where $b_i = 1 - 1/n_i^2$ are the Fresnel drag coefficients, and so there is no 1st-order term in v_P/c. Then this arrangement would fail as a 1st-order detector of absolute motion. An experiment to investigate the presence or otherwise of the Fresnel drag effect in transparent solids is underway at Flinders University[4], see Fig.12.2.

Figure 12.3: A 1st-order device for detecting absolute motion. Light from two identical lasers is combined and their beat frequency is detected at D.

If the Fresnel drag effect does occur in solids, and that would cause problems in understanding the DeWitte data, then a different 1st-order device is possible,

[4]Being carried out by Warren Lawrance and Bill Drury.

as shown in Fig.12.3. This involves two identical antiparallel lasers. Then, as in (10.14), the difference in travel time to the detector is given by

$$\Delta t_F = 2\frac{L}{c}\frac{v_P}{c}, \tag{12.5}$$

which is a 1st-order effect. The main difficulty is in the frequency stability of the two lasers. Again to avoid the need for rotations three such devices arranged orthogonally as above would be very effective.

Chapter 13

Looking Back

13.1 The Failure of the Einstein Postulates

Physics is experiment based and so its theoretical proposals must be exposed to ongoing experimental challenge, although many editors of physics and other science journals don't appear to accept this notion[1]. The Einstein interpretation of relativistic effects was from the beginning based on a false conclusion from the now *infamous* Michelson-Morley experiment. That this interpretation has survived for so long and had so much influence requires careful analysis, for there have been many contributing factors apart from the politics of physics and the spurious influences of a few individuals. The psychological and sociological aspects of the creation, promotion and adoption by the physics community of the Einstein postulates and General

[1]For example the paper Ref.[12] reporting the re-analysis of Michelson interferometer experiments with the inclusion, for the first time, of the refractive index effect and so evidence for absolute motion, and paper Ref.[13] reporting the discovery of the evidence for the gravitational in-flow effect in Miller's data and its connection to quantum gravity, were both summarily rejected by an editor of *Physical Review Letters* without even allowing the papers to be peer reviewed. A similar response came from editors of *Science* and then *Nature* in summarily rejecting the discovery of the new role of the fine structure constant in Ref.[18, 19]. But the most extreme response was from the physics arXiv, an electronic archive system. Paper [12] was successfully submitted to the gr-qc arXiv, the section dealing with gravity. Within hours of that submission it was manually removed, with the explanation that this paper dealing with absolute motion was not acceptable. Subsequently all e-mail announcements of recent arXiv submissions, and further submissions to all but the general-physics arXiv were banned, as were all cross-listings. When the explanation for the 'dark matter' effect was discovered the paper [18, 19] was banned from cross-listing to the astronomers arXiv, astro-ph, and to the gravity arXiv gr-qc, desipte a formal request pointing out the obvious interest that astronomers would have in this discovery, presumably because it was not consistent with General Relativity. Simply put a person was deciding that the astronomers would not be permitted to learn about this discovery. There are many more disturbing examples of how the physics community and science journals have responded to these discoveries. In 2002 the editor of a well known science journal imposed a total ban on reporting the discovery of absolute motion. It appears that for many physicists and editors the Einstein postulates, as distinct from special relativity effects, and General Relativity are beyond experimental checking. They are now true by belief. So 400 years after Galileo's similar experiences such unscientific attitudes are still the norm.

Theory of Relativity is in itself a subject that will attract great attention from the historians of science, particularly when it is realised that the history written up to now has missed the most dramatic insight of all, namely that the postulates and that theory of gravity are actually falsified by experimental data, and that the evidence for the invalidity of the postulates had been present in diversified experimental data from the very beginning. Here I will briefly layout the amazing sequence of events that resulted in the Einstein formalism slipping through the checks of experiment, until finally it had become an unassailable edifice of theoretical physics and in popular culture a metaphor for the brilliance of the human mind. Sadly it is actually a metaphor for the exact opposite.

The search for an understanding of reality has been long and arduous. The history of this endeavour is replete with examples of the tortuous nature of this, but none more so than the confusion surrounding the explication of the nature of space and time. The Michelson-Morley experiment actually plays a key role here for it led not only to a genuine discovery, but also to much obscurification. The experiment was conceived as a technique for observing absolute motion, which is motion relative to some structural elements of or within space itself. On the basis of Galilean Relativity[2] the theory of the Michelson interferometer was layed out by Michelson, although only with the assistance of Lorentz who had to correct Michelson's analysis[3]. The fringe shifts seen in the experiment in 1887 were smaller than expected and so the appropriate conclusion should have been that (i) absolute motion had been detected, but (ii) that Galilean Relativity in its present form was wrong as it had predicted too large an effect. From here on and for the next 100 or so years the story becomes ever more murky.

One possible interpretation was based on the aether entrainment ideas of Stokes [146] that arose in order to explain the stellar aberration. This explanation was that the observed absolute motion of some 8 km/s, according to Galilean Relativity and for which this speed is less than the orbital speed of the earth[4], was actually relative to some aetherial matter within space and which was being entrained by the motion of the earth itself through space. This explanation then had the dualism of two velocities, one of the earth's motion with respect to space and the other of the earth's motion with respect to an aether residing in space. It was this interpretation that caused Miller to do his experiment up on Mt.Wilson, the idea being that the entrainment effect would be less at higher altitudes. However the entrainment theory has never amounted to more than a distraction to the main theme and its subsequent

[2]That is, without as well the Fitzgerald-Lorentz contraction.

[3]Michelson had neglected that in Galilean Relativity the propagation times in the transverse arm, as well as the longitudinal arm, is affected by absolute motion.

[4]As well the magnitude of the fringe shifts at 12 noon and 6 pm had the wrong dependence on solar time in order to be explained as being caused by the orbital motion of the earth about the sun, see Fig.10.6. This meant of course that the fringe shifts were caused by an absolute motion in a direction different to the orbital velocity direction.

history will not be followed here[5].

On the incorrect basis that there had been no fringe shifts Fitzgerald and Lorentz independently offered the explanation that the arm parallel to the direction of absolute motion had been shortened as a physical effect of the motion, and that the amount of contraction was such as to exactly cancel the geometrical effect that Michelson and Lorentz had shown was expected on the basis of Galilean Relativity. So we have here another error, as the actual fringe shifts were not null, only small. Nevertheless this contraction effect turned out to be fundamentally correct, although Einstein was to put a different and now incorrect interpretation upon it. At the same time Larmor suggested that a time dilation effect would occur for actual physical clocks. In 1887 Voigt [147] had already proposed what is now known as the Lorentz transformation[6]. This is now understood to be a mapping between measurements made by observers using rods and clocks for which the corrections for the length contraction and time dilation effects have not been made. In essence the Lorentz transformation deals with 'raw' observational data. Of course these two effects are real and as such represent a significant discovery about the dynamics of space itself, although following Einstein this was not the way they were finally seen. Of course it would be bizarre if, for example, a physicist did not correct for temperature effects on a measuring rod in measuring lengths, but this is exactly what has happened to length and time measurements within the Einstein formalism: the physical effects are asserted to be in principle not correctable.

As a consequence of these developments there emerged the Lorentzian interpretation of these *relativistic effects*. Lorentzian Relativity (LR) asserts that motion through space causes physical effects upon rods and clocks, and that measurements with these by observers in different states of absolute motion could be related by means of a linear mapping - the Lorentz transformation. What was to cause much confusion later was that the Lorentz transformation made no mention of the absolute velocity of the two observers, it only contains reference to their relative velocity, and so the effects of the absolute motion had become hidden as far as this mapping is concerned. However it remains valid that one of the possible observers is actually at rest with respect to the actual physical space, and that the Lorentz transformation is not the full story.

It is at this stage that Albert Einstein and his wife Mileva Maric-Einstein[7] enter the story, and their individual roles in that story has never been resolved. Essentially their contribution was to formalise some of what had been discovered by the earlier investigators. Rather than acknowledging and building upon that work the relativistic effects were to be explained by the postulates (1) and (2) of (7.57). This is the Einsteinian Relativity (ER) formalism. In this the history of

[5]In searching for evidence to support this entrainment explanation James DeMeo travelled to Cleveland in 2002 in an attempt to locate the Miller interferometer data, and succeeded!

[6]Later Lorentz suggested that the 'Lorentz Transformation' be called the 'Transformation of Relativity'.

[7]Mileva studied physics and mathematics at the ETH in Switzerland.

the subject until then was completely turned around and from the postulates the Lorentz transformation was derived. This had a disastrous effect on the future of physics as from then on physicists, with sloppy thinking, were led to believe that since the Lorentz transformation had been derived from the postulate that denied the existence of absolute motion, then absolute motion must necessarily be incompatible with relativistic effects. It must be the case that we have one or the other. Both of these postulates were already in conflict with the actual data of the Michelson-Morley experiment. Although the Einstein's were aware of this experiment[8] it is not clear whether they were aware that fringe shifts of the correct form had in fact been observed.

The major and fundamental difference between LR and ER is that in LR absolute motion is meaningful and measurable, while in ER it is not meaningful and hence not measurable. The ER formalism is based on axiomatising the feature of the Lorentz transformation that the absolute velocities of each observer do not play a role. Of course it is simple to experimentally distinguish between LR and ER as they have opposite predictions regarding the detection of absolute motion. Unfortunately for the history of physics the Michelson interferometer is not very sensitive to the effects of absolute motion as discussed elsewhere in this work. Indeed the Michelson interferometer is unsuited to this task. Its major use is actually in checking the accuracy of the Fitzgerald-Lorentz contraction effect, and to do this it must operate in vacuum mode. To detect absolute motion it must operate in gas mode. Because this was not understood right through the twentieth century it was assumed that as better and better vacuum Michelson interferometers were developed and that no evidence of absolute motion was forthcoming then the ER formalism must be the correct one. In fact there had been gas-mode interferometer experiments such as Miller's that had most clearly detected the effects of absolute motion, but they were rejected for totally spurious arguments.

One consequence of the Einstein postulates and the ER formalism was the introduction and acceptance of the spacetime construct, and the assertion that only this had physical or ontological significance and that the older separate concepts of time as process and space as an entity of some sort were abandoned. In the spacetime construct the notion of change is removed. All that remained was a bizarre geometrical modelling of time. The spacetime construct is an artifact of the Lorentz transformation and as such lacks the dynamics that the effects of absolute motion revealed. Spacetime is itself a totally static geometrical structure upon which the whole edifice of twentieth century physics was built. It certainly contains some truth as the Lorentz transformation upon which it is founded does encode the consequences of actual physical effects, and so the validity of much of twentieth century theoretical physics is limited to that which is compatible with these effects but which explicitly denies the underlying dynamics.

The ongoing confusion in physics has led to the belief that the small effects of

[8] As revealed in the letters A. Einstein later wrote to Shankland.

absolute motion seen in interferometer experiments are incompatible with relativistic effects and so the effects must be caused by spurious experimental imperfections and hence the ER formalism is confirmed. Indeed most so-called experimental *confirmations* of the ER formalism are really nothing more than demonstrations of relativistic effects, and as such are equally compatible with LR.

However worse was to come. Eventually through the work of Hilbert and Einstein a mathematical generalisation of the ER formalism to include gravitational effects was produced. In this gravity is understood to be a curvature of the previously flat spacetime construct. This generalisation was designed to reduce to the flat spacetime construct in the absence of matter, while in the case of low velocities it was meant to reduce to Newtonian gravity, at least as far as its predictions went, although it clearly had a different ontology. There are now various experimental and observational demonstrations of the supposed efficacy of this generalised spacetime formalism, but as noted previously none of these actually support the formalism. In the only cases where the formalism has been checked the metric of the curved spacetime turns out to be flat and identically equivalent to the in-flow formulation of Newtonian gravity. So to this extent the generalisation is actually untested. The so called *demonstrations* amount to nothing more than relativistic effects, using (7.31), where the absolute velocity of the object's motion relative to absolute space is manifest, and which may possess an inhomogeneous flow as a manifestation of gravity.

13.2 The Shankland Paper: 1955

As previously discussed the Miller experiment has now been strongly confirmed by other experiments, including two which were not even interferometer experiments. All agree on the direction and speed of absolute motion that Miller was the first to discover. As well his data now provides experimental evidence for an explanation of gravity different from those of both Newton and Einstein. So the Miller experiment was one of the most significant physics experiments done in the twentieth century. We know that Einstein was very concerned about the Miller experiments for as he noted in a letter to Robert Millikan in June 1921,

> *I believe that I have really found the relationship between gravitation and electricity, assuming that the Miller experiments are based on a fundamental error. Otherwise, the whole relativity theory collapses like a house of cards.*
> (in Clark[133] 1971, p.328)

So why were Miller's experiments rejected? Part of the answer is that by the time Miller began reporting his results the Einstein interpretation that the Michelson-Morley experiment had indeed shown a 'null effect' had been accepted. As well no

one had noticed that the small effect actually present in these gas-mode interferometer experiments was related to the type of gas present, and that furthermore if the gas was removed only then did the small effect truly go away. That was all bad enough showing as it did a disregard for the scientific method. Miller's data was clearly revealing the failure of the Einstein formalism, as Einstein was himself very much aware. Suggestions that the effects were temperature effects had of course led to intensive investigation by Miller over many years, and even Einstein had been pressing this explanation. In a responding to Einstein Miller wrote that

> *The trouble with Professor Einstein is that he knows nothing about my results...He ought to give me credit for knowing that temperature differences would affect the results. He wrote to me in November suggesting this. I am not so simple as to make no allowance for temperature.*
> (Cleveland Plain Dealer January 27, 1926)

However worse was to come for Shankland, who had assisted Miller in the analysis of his data, and after prior consultations with Einstein, produced a critique [127] of the Miller results in which Shankland claimed, 14 years after Miller's death, that the Miller fringe shifts were due to statistical fluctuations in the readings of the fringe positions, and other systematic effects were ascribed to local temperature conditions. Shankland wrote [127] that

> *Miller's extensive Mt.Wilson data contained no effect of the kind predicted by the aether theory and, within the limitations imposed by the local disturbances, are entirely consistent with a null result at all epochs during a year.*

Miller however had already noted that at no time did he ever observe any periodic effects related to local civil time as would be the case if the sun's heating effect were present. On the contrary Miller's results show very clearly that the features in the data correlate with sidereal time.

An extensive review of the Shankland paper has recently been written by DeMeo [132] where various deficiencies of that paper are noted. The claim by Shankland that the periodic effects were temperature effects caused by the heating of the sun had been thoroughly investigated by Miller, and are known to be invalid. Shankland also dismissed Miller's results on the grounds that there were significant fluctuations present in the data. Of course Shankland was assuming, without investigation, that these fluctuations were not evidence of a real physical effect. We now believe that these fluctuations are in fact evidence of turbulence in the gravitational in-flow. So Shankland's dismissal of the Miller experiment was an enormous blow to the progress of physics in the twentieth century.

Einstein was deeply appreciative of Shankland's paper and its rebuttal of the effects that Miller had reported. In 1954 Einstein wrote to Shankland:

> *I thank you very much for sending me your careful study about the Miller experiments. Those experiments, conducted with so much care, merit, of course, a very careful statistical investigation. This is more so as the existence of a not trivial positive effect would affect very deeply the fundament of theoretical physics as it is presently accepted. You have shown convincingly that the observed effect is outside the range of accidental deviations and must, therefore, have a systematic cause having nothing to do with 'ether wind', but with differences of temperature of the air traversed by the two light bundles which produce the bands of interference.* (Shankland [148], p.2283)

13.3 The Demise of Spacetime

The geometric construct of spacetime introduced by Minkowski and Einstein has become one of the bedrock concepts in physics, and has even entered popular culture. It was based on the putative successes of the Special Relativity and the General Relativity, but in particular it was based on the belief that a preferred frame of reference did not exist, had no meaning, and was unobservable. We were then left with this four dimensional spacetime construct, which then acquired the status of an actual existing entity, despite all of the peculiarities that have previously been discussed. However there is abundant evidence that the principles on which these two relativity theories are based have been experimentally falsified. Indeed their whole history has been a sad saga of one blunder after another. There was never any evidence for the absence of absolute motion with respect to a physically existing space. Even the first search for such an effect by Michelson and Morley in 1887 found very good evidence for absolute motion, as evidenced herein. Subsequent searches by various experimentalists were also successful in another six experiments, and perhaps even more will emerge. Regrettably, in current physics, the rewards are for those who do ever more sophisticated absolute motion experiments and find a 'null' result, as *expected*. Non-null results are simply not acceptable. Editors of science journals automatically reject any experimental evidence of absolute motion or even analysis or discussion of existing data that indicates absolute motion. This all indicates a collapse of the principles of science and physics in particular: science by its very nature must be evidence based. Editors who reject out of hand, particularly denying even peer review, have corrupted the science by their actions. And the impact on the science is extremely damaging. Much effort in recent years has gone into perfecting vacuum Michelson interferometers. Some use the resonant cavity technology. That these experiments see no evidence of absolute motion continues to be quoted as "best evidence" for there being no absolute motion. The most appalling consequence of this continued blinkered view has been the building at enormous cost of the long baseline fixed Michelson interferometers. The belief is that gravitational waves of the type predicted by General Relativity will be found, if not by these then by the next

generation which are already in planning. Had the evidence for absolute motion not been suppressed, as it still is to this day, and if the various gravitational anomalies had not been dealt with by either denial or ad hoc explanations, then it is very probable that these particular interferometers would not have been built. They are really little more than a monuments to corrupt practices in physics over most of the last century, despite the ingenious technological developments that have been made to increase their sensitivities. Their sole existence is to observe waves associated with the warping of the spacetime manifold, a concept that has no ontological significance or meaning.

This does not deny the existence of the so called relativistic effects, such as the length contraction effect, the time dilation effect, the increase of mass of moving objects. But all these effects now have a much simpler explanation within the Lorentzian interpretation of relativity. Indeed we see that both the Galilean transformation and the Lorentz transformation of data for different observers now have true physical but different meanings. We also see that the speed of light in vacuum is only $c \approx 300,000$ km/s relative to the local space, which evidence suggests has quantum structure. So the whole story of the absolute nature of the speed of light and of the ontological significance of spacetime collapses, just like Ptolemy's epicycles.

13.4 Absolute Space and Universal Time

Having dispensed with spacetime it is important to understand what we have replaced it with. For the case of space we have a physical system with a quantum substructure, apparently undergoing continual quantum state collapse to a classical configuration, at least at the higher levels. This system is a dynamical process and different regions of that space are in relative motion, and as well the whole system continues to grow and does so at an accelerating rate. The relative motion is associated with both that growth as well as with the gravitational in-flows into either matter or into the new gravitational attractors. To an observer this gravitational effect is only evident via observations of tidal processes. This means in the case of observers on earth we can see this relative in-flow effect by observing, say, the in-flow of space past the earth into the sun and noting that the direction as observed at various times of the year remains directed towards the sun. This effect is now evident in Miller's 1925/26 data. With new benchtop interferometers now under construction these gravitational in-flows will come under intense study, particularly the turbulence or gravitational waves that they are already known to exist. So we have an absolute space as a local ontologically meaningful entity: an observer may be moving locally with respect to that local space, and that motion is measureable. But whether or not that same observer is moving relative to another region of space is not directly observable, unless some form of matter is present at that distant location, and can be used to indicate the local state of rest. So absolute space must not

be thought of in the Newtonian sense as being unchanging and having no relative motion with respect to itself.

At the core of the new *Process Physics* is that space and time are completely different. While spacetime is being dispensed with, it is not by deconstruction back to a separate geometrical model of time and a geometrical model of space. Rather time is a fundamental process without geometrical properties, although of course historical records may be coordinatised by using the geometrical construct as a pagination technique, and as has been done here in various theoretical analyses. But is time universal? A more explicit form for this question is: is there a means for all observers to agree on a unique time to categorise events? A weaker version of the same questions is: can all observers agree on the rate of time? The fundamental iterator equation of Part I invoked an single iteration process, which does suggest a universal time. But is that time rate meaningful and observable, or is it merely an artifact of the bootstrapping of the semantic information system? An observer can correct her local standards of length and time by compensating for absolute motion through space. That removes the special relativity effects. But what about the effect of the local flow into matter or into an attractor?. As it is only motion relative to the local space that causes these effects then, for example, an observer moving with the local flow, and that is detectable, will experience no length contractions or time dilation effects, at least according to the formalism proposed in Chapters 7 and 7. On a cosmological scale we have the cosmologically preferred frame defined by the CMB, but that is not in general the same as the local preferred frame. Rather the CMB provides a cosmologically averaged frame, but then that frame defines motion relative to a section of space that existed long ago. Another aspect to these questions is the suggestion, also from the present level of development of the new theory of gravity, that gravitational effects are instantaneous because they involve quantum collapse processes. If correct then this suggests that the gravitational quantum collapse process could in principle supply a phenomenon that could be used for defining absolute time.

Chapter 14

Conclusions

Process Physics has been shown to be a major development in the modelling of reality. After some 400 years, during which physics was founded on a geometrical model of time, we now have a new non-geometrical process modelling of time that matches all the aspects of the phenomena of time. This model of time is part of a pre-geometric information-theoretic approach to comprehending reality. It was inspired by the logic of the limitations of the logic of formal syntactical information systems discovered by Gödel. The structural randomness, discovered by Chaitin, beyond the Gödel boundary in such systems was generalised to randomness in a time-like processing system by introducing the concept of self-referential noise. In this way we model the idea that there are limits to the information content within the processing information-theoretic system and in reality itself. Most significant is that this system entails the idea of *semantic* information, which is information that is generated and recognised within the system itself. This is in sharp contrast to the syntactical information-theoretic approach that has been the core concept in the traditional modelling of reality from its beginnings, though rarely acknowledged as such. As well evidence of a processing information-theoretic system was exposed as being at the base of the quantum field theory modelling of quantum matter, by means of the stochastic 'quantisation' formalism.

Having set up a processing information-theoretic system in which all information is internally generated and recognised we have explored in considerable detail the nature of the emergent information and shown that, to the extent currently available, the system generates *phenomena* that exhibit a remarkable likeness to those aspects of reality that physicists have so carefully revealed over past centuries. These include:

1. The emergence of elements of geometry by way of the gebits.

2. The self-linking of these gebits to form a fractal processing system displaying quantum-foam behaviour that entails both space and quantum matter embedded in that space. So we have a quantum behaviour emergent within a

system in which no quantum behaviour had been present. Thus we have a derivation of the logical necessity of quantum behaviour from the processing information-theoretic system. The key concept of self-referential noise is central to this emergence.

3. The quantum description of space displays ongoing non-local collapse of its quantum structure so that a classical 3D-space is effectively present at a higher level. This space is growing in size over time and this matches the observed behaviour of our universe.

4. A formalism to encode the emergent behaviour of the quantum 'matter' within the system was developed. Here 'matter' corresponds to topologically stabilised defects within the spatial network, and it was argued that these topological defects display flavour and hidden colour degrees of freedom. The spin 1/2 formalism is also emergent.

5. The quantum 'matter', like space itself, is fundamentally non-local, and the collapse mechanism that is known to happen within quantum system upon measurements is now explained, and the randomness of that collapse is seen to be yet another manifestation of the self-referential noise. This ongoing and internal collapse process is responsible for the emergence of classical behaviour, which explains why at a macroscopic level our reality is *discrete* and *hard*, and very different to the underlying information-theoretic substratum.

6. The unification of space and quantum in a process system led to an explanation of inertia and gravity, with the latter displaying the equivalence principle. It was argued that matter effectively acts as a sink for the information patterns in the quantum foam that forms the spatial degrees of freedom. Then gravity manifests as a net in-flow or relaxation of that spatial information into matter.

7. The *motion* of matter through this spatial system is expected to display the relativistic effects of length contractions and time dilations. As well, because space is fundamentally different from time, absolute motion is a key prediction of process physics. It was shown that the spacetime construct is not an aspect of reality, but at best only a useful mathematical tool. Fundamentally the Lorentz interpretation of relativistic effects is seen to arise within process physics.

8. The new theory of space and gravity was investigated in considerable detail. It was shown that Newtonian gravity could be written in the mathematical language of a fluid flow system. The Hilbert-Einstein General Relativity spacetime formalism was shown to be completely equivalent to this Newtonian flow mathematics in all cases where the spacetime formalism had been checked, namely the external Schwarzschild metric for spherically symmetric

systems. So the famous tests of General Relativity had in fact not tested the GR formalism, but merely the Newtonian gravitational formalism.

9. A generalisation of the Newtonian gravitational in-flow formalism was proposed. This offers an explanation for the effects seen in spiral galaxies which have been misinterpreted as being caused by *dark matter*. Rather these effects are seen as an indicator of the failure of Newtonian gravity, a formalism that had been inspired by the overly special nature of the solar system. The new theory of gravity involves two fundamental constant, the familiar G, and a new dimensionless constant. Analysis of the Greenland borehole g anomaly showed that this constant is the fine structure constant α. This amounted to the discovery of quantum aspects to gravity, and indeed quantum gravity.

10. The failure of Newtonian gravity caused difficulties in measuring G. It is now seen that the presence of an unknown systematic effect of relative magnitude α was present in these measurements. Cavendish-type laboratory experiments now give the opportunity to study quantum gravity.

11. It was shown that the famous derivation of the observed residual perihelion precession of 43" per century for mercury was in fact based upon an error in the analysis within General Relativity, and that General Relativity predicts only 4" per century, leaving a residue of 39" per century, and that this is probably explainable in terms of the 'dark matter' effect induced by the lack of perfect spherical symmetry caused by the presence of the planets.

12. The 'dark matter' effect, as quantum-foam in-flow, leads to a new phenomenon of gravitational attractors, a new form of black hole, which may exist in relation to matter, or without matter. They would have come into existence during the big-bang. They form, particularly after coalescing into stronger and larger attractors, the mechanism for the rapid formation of galaxies in the early universe. The variation in magnitude of these attractors explains why the rotation curves of spiral galaxies is very flat at the outer limits, and why this asymptotic form is related to the luminosity of such galaxies.

13. The distinction between minimal and non-minimal attractors was introduced, and it appears that the globular clusters M15 and G1 have minimal attractors, as the effective mass of these attractors was determined, and shown to agree with the 'black hole' masses determined from observations and analysis. This effect, and the related effect of non-minimal attractors in galaxies, opens up a new field of astronomy, in which fundamental quantum process are now manifesting in large scale phenomena, such as the intermediate mass and supermassive black hole phenomena.

14. The 'dark matter' effect also changes the theory of stellar structure as stars must have at least a minimal gravitational attractor at their centres. This

is expected to affect the neutrino production rate, and may help explain the solar neutrino flux anomaly. Indeed solar neutrinos may be used as a probe of the sun's attractor. There is also, necessarily, an attractor at the centre of planets, and of course it was the earth's attractor that was unknowingly detected by geophysicists when they observed the g anomaly in mine shafts and boreholes.

15. *Process Physics* predicts that absolute motion is meaningful and measureable, in sharp contrast to the Einstein assumptions. A detailed investigation of absolute motion experiments revealed that for over 100 years many of these experiments had indeed detected absolute motion. These include the original experiment by Michelson and Morley. The interpretation and reporting of the *non-null* results from this influential experiment were totally bungled.

16. By the time Miller, some 40 years later, had figured out how to avoid a repetition of the Michelson-Moley errors and had convincingly established the existence of absolute motion effects and had determined a speed and direction of motion of the solar system, the physics community was firmly in the erroneous mindset that Einstein had promulgated. One consequential devastating misunderstanding, which is still prevalent, is that absolute motion is totally incompatible with relativistic effects. This arose from Einstein's derivation of these relativistic effects by denying absolute motion. The error in logic here is simple: if one assumes the absence of absolute motion, and then deduces the special relativistic effects, then the observation of those special relativistic effects does not imply the truth of the original assumptions. To do so would be to confuse an *if* relationship with an *if and only if* relationship. So most physicists are of the belief that the many examples of relativistic effects imply that absolute motion is impossible. Consequentially any experimental evidence to the contrary has been suppressed over the last 100 years. This has had a devastating effect on physics.

17. It was shown that the Michelson interferometer can detect absolute motion when operated in gas mode, and many examples of such experiments were given. All these experiments are in agreement.

18. Several non-interferometer experiments were also analysed and the remarkable coaxial cable experiment by DeWitte in 1991 was shown to be in agreement with the interferometer experiments.

19. A feature of the Miller interferometer data was that with the new gas-mode effects now understood a re-analysis of the Miller data revealed the in-flow of space past the earth towards the sun. So this old and ridiculed experiment was seen to provide evidence in support of the new theory of gravity. This data as well as that of the DeWitte experiment suggested that the in-flow

displayed turbulence, as expected of the new theory. This turbulence is a gravitational wave effect. So the existence of gravitational waves has been in the experimental data from at least the 1920's, but unrecognised as such.

20. The direction of motion of the solar system through space is distinctly different to the direction of motion of the solar system with respect to the Cosmic Microwave Background. This is interpreted as evidence for the in-flow of space into the Milky Way and Local Cluster, and is further evidence in support of the new theory of gravity.

21. Various bench-top interferometer devices for detecting absolute motion effects and the new gravitational waves were discussed.

22. The various observations of absolute motion over the last 115 years prove conclusively that the Einstein formalism is incorrect. The belief that vacuum resonant-cavity experiments have confirmed that formalism are based on ongoing misunderstandings. In all cases the experiments were confirming relativistic effects that have nothing to do with the Einstein formalism, and which predated that formalism. It is the original Lorentz Relativity that experiments have been confirming.

23. The emergent unification within *process physics* of quantum behaviour for both 'matter' and space, and displaying gravitational phenomena, means that we have a quantum theory of gravity.

24. The velocity field turbulence present in the Miller, DeWitte and Torr-Kolen data clearly amount to the observation of gravitational waves. But this observed phenomenon is very different to those gravitational waves predicted by the Hilbert-Einstein GR formalism. As that formalism is now demonstrably falsified by experiment there is no reason to believe that these *spacetime* gravitational waves exist. The long-baseline static vacuum Michelson interferometers that have been constructed to observe these waves were built only because the observations of absolute motion had been suppressed.

25. The new theory of gravity gave a simple dynamical explanation for the Lense-Thirring or 'frame-dragging' effect, as being caused by vorticity induced by the motion, say, of the earth. In particular a novel vorticity caused by the absolute linear motion of the earth is predicted to be observable using the Gravity Probe B. This experiment is also predicted to be able to detect the new gravitational waves.

Finally the successes of *process physics* imply that we should give consideration to its foundational assumptions, and one is that reality is a non-local experiential information system. One way to interpret this is that reality has a primitive form of self awareness. In increasingly more complex systems such as biological systems

this self awareness may manifest as consciousness. This is a conjecture for further careful consideration.

Process Physics is clearly a model of reality that implements many of the ideas that have been considered within *Process Philosophy*, which dates back to at least Heraclitus of Ephesus. The convergence of this physics and this philosophy represents an exciting development and a unification of not only various areas of physics but also of many other areas of human intellectual endeavours. This all points to an exciting future.

Chapter 15

Appendices

Appendix A

Gebit Connectivity

The probability that a connected random graph with N vertices has a depth structure $D_0, D_1, ..., D_L$ was given in (4.15) and there it was shown that it leads to the concept of emergent geometry via the *gebit* concept. Eqn.(4.15) was first derived by Nagels [38]. The notes here are adapted from those by Christopher Klinger.

Consider a set of M nodes with pairwise links arising with probability $p \ll 1$. The probability of nonlinking is then $q = 1 - p$. We shall term linked nodes as being 'adjacent', though the use of this geometric language is to be justified and its limitations determined. The set M will be partitioned into finite subsets of mutually disconnected components, each having N_i nodes which are at least simply connected - that is, each N_i may be described by a non-directed graph.

Consider one of these components, with $N = N_i \gg 1$, and choose one vertex to be the 'origin'. We will determine the probable distribution of vertices in this component as measured by the depth structure of a minimal spanning tree. See Fig.A.1 for the definition of depth structure. Let D_k be the number of vertices at a distance k from the origin then $D_0 = 1$ is the origin, D_1 is the number of adjacent vertices or nearest neighbours to the origin, and D_2 is the number of next nearest neighbours and so on. Then, since N is finite, there is a maximum distance L on the graph and D_L is the number of vertices at this maximum distance from the origin.

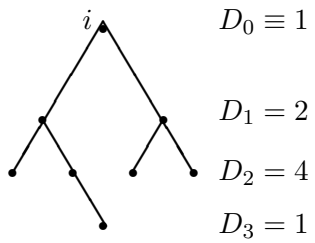

Figure A.1: An $N = 8$ tree-graph with $L = 3$ for monad i, with indicated distance distribution D_k.

There is then the constraint

$$\sum_{k=0}^{L} D_k = N, \tag{A.1}$$

and also

$$\begin{cases} D_0 = 1, \\ D_k > 0, \quad 0 \leq k \leq L, \\ D_k = 0, \quad k > L. \end{cases} \tag{A.2}$$

To calculate the probability for the distribution $\{D_k : 0 \leq k \leq N,\ \sum_{k=0}^{N-1} D_k = N\}$ we require:

1. the probability for the number D_1 of nearest neighbours (i.e. those vertices at unit distance from the origin) is p^{D_1}, which may be written as $(1-q)^{D_1} = (1-q_0^{D_0})^{D_1}$, since $D_0 = 1$;

2. the probability for the next nearest neighbours, D_2, is obtained by considering that any vertex at this level is

   (a) adjacent to at least one point at unit distance from the origin;

   (b) not adjacent to the origin itself.

   Condition (b) is easily obtained since it occurs with probability $q = 1 - p$ so there is a factor of q^{D_2} for this.

   Condition (a) may be obtained by first considering the counter argument ie that the vertex is *not* adjacent to any of the D_1. This has probability q^{D_1}. Thus the probability that it *is* adjacent to at least one of the D_1 is just $1-q^{D_1}$. So there is an overall factor of $(1-q^{D_1})^{D_2}$ for this condition.

   Hence, the probability of obtaining D_2 is the product of these two factors ie

   $$\text{prob}\,(D_2) = \left(1 - q^{D_1}\right)^{D_2}\ q^{D_2}; \tag{A.3}$$

3. the probability for D_3, those vertices at distance $k = 3$ from the origin, is similarly defined by the requirements that a vertex in D_3 is

   (a) adjacent to least one vertex in D_2;

   (b) not adjacent to any vertex in D_1;

   (c) not adjacent to the origin.

   Condition (a) is argued precisely as the corresponding condition in item 2 above, ie it provides a factor $(1-q^{D_2})^{D_3}$.

Condition (b) is expressed as q^{D_1}, thus providing the factor $(q^{D_1})^{D_3}$.

Conditioned (c) is satisfied simply by the factor q^{D_3}, which may be written as $(q^{D_0})^{D_3}$ since $D_0 \equiv 1$. Hence the probability of obtaining D_3 is

$$\left(1-q^{D_2}\right)^{D_3}\left(q^{D_1}\right)^{D_3}\left(q^{D_0}\right)^{D_3} = \left(q^{D_0+D_1}\right)^{D_3}\left(1-q^{D_2}\right)^{D_3}; \tag{A.4}$$

4. for vertices at a distance $i+1$ from the origin, induction on the previous results gives

$$\text{prob}\,(D_{i+1}) = \left(q^{\sum_{j=0}^{i-1} D_j}\right)^{D_{i+1}}\left(1-q^{D_i}\right)^{D_{i+1}}. \tag{A.5}$$

So the probability P for the depth distribution is the probability of obtaining a particular set $(D_1,\ D_2,\ \cdots,\ D_L)$ which is

$$P = p^{D_1}\prod_{i=1}^{L-1}\left(q^{\sum_{j=0}^{i-1} D_j}\right)^{D_{i+1}}\left(1-q^{D_i}\right)^{D_{i+1}}. \tag{A.6}$$

Note that vertices may be permuted between the *sets* of vertices at different distances. That is, the same magnitudes for each D_k could be obtained by many other possible configurations which result from a relabelling of the graph. First, there are $(N-1)!$ ways of relabelling the graph once the choice of origin has been fixed so there are $(N-1)!$ ways of obtaining the same P, where the depth structure given by $(D_1,\ D_2,\ \cdots,\ D_L)$ is identical. Second, the number of instances of a particular shape irrespective of labelling (beyond the choice of origin) is given by the product $D_1!D_2!\ \cdots\ D_L!$.

Hence there are $\frac{(N-1)!}{D_1!D_2!\,\cdots\,D_L!}$ ways of obtaining a graph (from a fixed origin) with a particular depth structure and therefore, the probability for a specified shape with N given and the origin arbitrarily chosen, that is, the probability distribution, is

$$\mathcal{P} = \frac{(N-1)!}{D_1!D_2!\ \cdots\ D_L!}\,p^{D_1}\prod_{i=1}^{L-1}\left(q^{\sum_{j=0}^{i-1} D_j}\right)^{D_{i+1}}\left(1-q^{D_i}\right)^{D_{i+1}}. \tag{A.7}$$

which is (4.15).

Appendix B

Quantum State Diffusion

Here[1] we show that despite the stochasticity in the QSD terms unitarity is preserved in the mean by the Quantum Homotopic Field Theory (QHFT) in (5.1). The QSD term is

$$\begin{aligned} QSD = & \sum_j \Big(\langle L_j^\dagger \rangle L_j - \frac{1}{2} L_j^\dagger L_j - \langle L_j^\dagger \rangle \langle L_j \rangle \Big) \Psi(\ldots, \pi_{\alpha\beta}, \ldots, t) \Delta t \\ & + \sum_j \Big(L_j - \langle L_j \rangle \Big) \Psi(\ldots, \pi_{\alpha\beta}, \ldots, t) d\xi_j \end{aligned} \tag{B.1}$$

where the $\Delta\xi_j$ are complex statistical variables with means

$$\begin{aligned} \mathrm{M}(\Delta\xi_j) &= 0 \\ \mathrm{M}(\Delta\xi_j \Delta\xi_{j'}) &= 0 \\ \mathrm{M}(\Delta\xi_j^* \Delta\xi_{j'}) &= \delta_{jj'} \Delta t \end{aligned} \tag{B.2}$$

and

$$\langle A \rangle = \int \mathcal{D}\pi_{\alpha\beta} \Psi^\dagger[\ldots, \pi_{\alpha\beta}, \ldots, t] A \Psi[\ldots, \pi_{\alpha\beta}, \ldots, t]. \tag{B.3}$$

The functional QHFT equation is

$$\Delta\Psi = -iH\Psi\Delta t + \sum_j \Big(\langle L_j^\dagger \rangle L_j - \frac{1}{2} L_j^\dagger L_j - \frac{1}{2} \langle L_j^\dagger \rangle \langle L_j \rangle \Big) \Psi \Delta t + \sum_j \Big(L_j - \langle L_j \rangle \Big) \Psi \Delta\xi_j, \tag{B.4}$$

and writing down $\Delta\Psi^\dagger$ for convenience:

$$\Delta\Psi^\dagger = +i\Psi^\dagger H^\dagger \Delta t + \Psi^\dagger \sum_j \Big(\langle L_j \rangle L_j^\dagger - \frac{1}{2} L_j L_j^\dagger - \frac{1}{2} \langle L_j \rangle \langle L_j^\dagger \rangle \Big) \Delta t + \Psi^\dagger \sum_j \Big(L_j^\dagger - \langle L_j^\dagger \rangle \Big) \Delta\xi_j^*. \tag{B.5}$$

[1] Adapted from notes by Kirsty Kitto

Now, because we are using Itô calculus, differentials up to the second power must be evaluated, so calculating the mean of the norm involves finding

$$
\begin{aligned}
& ||\Psi|| = M\int\mathcal{D}\pi\,\Big(\Psi^\dagger + \Delta\Psi^\dagger\Big)\Big(\Psi + \Delta\Psi\Big) \\
= \;& M\int\mathcal{D}\pi\,\Psi^\dagger\Psi + M\int\mathcal{D}\pi\,\Delta\Psi^\dagger\Psi + M\int\mathcal{D}\pi\,\Psi^*\Delta\Psi + M\int\mathcal{D}\pi\,\Delta\Psi^\dagger\Delta\Psi \\
& \text{(now substituting for } \Delta\Psi) \\
= \;& M\int\mathcal{D}\pi\,\Psi^\dagger\Psi \\
+ \;& iM\int\mathcal{D}\pi\,\Psi^\dagger H^\dagger\,\Psi\,\Delta t + M\int\mathcal{D}\pi\,\Psi^\dagger\sum_j\Big(\langle L_j\rangle L_j^\dagger - \frac{1}{2}L_jL_j^\dagger - \frac{1}{2}\langle L_j\rangle\langle L_j^\dagger\rangle\Big)\Psi\,\Delta t + \\
& M\int\mathcal{D}\pi\,\Psi^\dagger\sum_j\Big(L_j^\dagger - \langle L_j^\dagger\rangle\Big)\Psi\,\Delta\xi_j^* \\
- \;& iM\int\mathcal{D}\pi\,\Psi^\dagger H\,\Psi\,\Delta t + M\int\mathcal{D}\pi\,\Psi^\dagger\sum_j\Big(\langle L_j^\dagger\rangle L_j - \frac{1}{2}L_j^\dagger L_j - \frac{1}{2}\langle L_j^\dagger\rangle\langle L_j\rangle\Big)\Psi\,\Delta t + \\
& M\int\mathcal{D}\pi\,\Psi^\dagger\sum_j\Big(L_j - \langle L_j\rangle\Big)\Psi\,\Delta\xi_j \\
- \;& i^2M\int\mathcal{D}\pi\,\Psi^\dagger H^\dagger H\,\Psi\,dt^2 \\
+ \;& iM\int\mathcal{D}\pi\,\Psi^\dagger H^\dagger\,\sum_j\Big(\langle L_j^\dagger\rangle L_j - \frac{1}{2}L_j^\dagger L_j - \frac{1}{2}\langle L_j^\dagger\rangle\langle L_j\rangle\Big)\Psi\,\Delta t^2 + \\
& iM\int\mathcal{D}\pi\,\Psi^\dagger H^\dagger\,\sum_j\Big(L_j - \langle L_j\rangle\Big)\Psi\,\Delta t\Delta\xi_j \\
- \;& iM\int\mathcal{D}\pi\,\Psi^\dagger\sum_j\Big(\langle L_j\rangle L_j^\dagger - \frac{1}{2}L_jL_j^\dagger - \frac{1}{2}\langle L_j\rangle\langle L_j^\dagger\rangle\Big)H\,\Psi\;\,\Delta t^2 + \\
& M\int\mathcal{D}\pi\,\Psi^\dagger\sum_{j,k}\Big(\langle L_j\rangle L_j^\dagger - \frac{1}{2}L_jL_j^\dagger - \frac{1}{2}\langle L_j\rangle\langle L_j^\dagger\rangle\Big) \\
& .\Big(\langle L_k^\dagger\rangle L_k - \frac{1}{2}L_k^\dagger L_k - \frac{1}{2}\langle L_k^\dagger\rangle\langle L_k\rangle\Big)\Psi\,\Delta t^2 + \\
& M\int\mathcal{D}\pi\,\Psi^\dagger\sum_{j,k}\Big(\langle L_j\rangle L_j^\dagger - \frac{1}{2}L_jL_j^\dagger - \frac{1}{2}\langle L_j\rangle\langle L_j^\dagger\rangle\Big)\Big(L_k - \langle L_k\rangle\Big)\Psi\,\Delta t\Delta\xi_k \\
- \;& M\int\mathcal{D}\pi\,\Psi^\dagger\sum_j\Big(L_j^\dagger - \langle L_j^\dagger\rangle\Big)H\,\Psi\,\Delta\xi_j^*\Delta t + \\
& M\int\mathcal{D}\pi\,\Psi^\dagger\sum_{j,k}\Big(L_j^\dagger - \langle L_j^\dagger\rangle\Big)\Big(\langle L_k^\dagger\rangle L_k - \frac{1}{2}L_k^\dagger L_k - \frac{1}{2}\langle L_k^\dagger\rangle\langle L_k\rangle\Big)\Psi\,\Delta\xi_j^*\Delta t + \\
& M\int\mathcal{D}\pi\,\Psi^\dagger\sum_{j,k}\Big(L_j^\dagger - \langle L_j^\dagger\rangle\Big)\Big(L_k - \langle L_k\rangle\Big)\Psi\,\Delta\xi_j\Delta\xi_k^*
\end{aligned}
$$

(B.6)

H is hermitian, $\Delta t^2 = 0$, and $M(\Delta\xi_j) = M(\Delta\xi_j^*) = 0$, so the equation reduces to

$$\begin{aligned} ||\Psi|| &= M\int \mathcal{D}\pi\ \Psi^\dagger\Psi + M\int \mathcal{D}\pi\ \Psi^\dagger \sum_j \Big(\langle L_j\rangle L_j^\dagger - \frac{1}{2}L_jL_j^\dagger - \frac{1}{2}\langle L_j\rangle\langle L_j^\dagger\rangle \Big)\Psi\ \Delta t + \\ & M\int \mathcal{D}\pi\ \Psi^\dagger \sum_j \Big(\langle L_j^\dagger\rangle L_j - \frac{1}{2}L_j^\dagger L_j - \frac{1}{2}\langle L_j^\dagger\rangle\langle L_j\rangle \Big)\Psi\ \Delta t + \\ & M\int \mathcal{D}\pi\ \Psi^\dagger \sum_{j,k} \Big(L_j^\dagger - \langle L_j^\dagger\rangle \Big)\Big(L_j - \langle L_j\rangle \Big)\Psi\ \Delta t, \end{aligned} \tag{B.7}$$

because $M(\Delta\xi_j\Delta\xi_k^*) = \delta_{j,k}\Delta t$. Now if $L_j^\dagger L_j = L_jL_j^\dagger$, and so the three last terms cancel, and we are left with conservation of the norm, i.e.

$$||\Psi|| = M\int \mathcal{D}\pi\ \Psi^\dagger\Psi = 1 \tag{B.8}$$

if Ψ itself is normalised.

Appendix C

Flow Equations

Here we show in detail that the new 'fluid flow' theory of gravity is almost uniquely determined by some very simple physical arguments. As noted in Sect.7.1 the Newtonian equation for the gravitational acceleration field,

$$\nabla.\mathbf{g} = -4\pi G\rho, \tag{C.1}$$

may be exactly re-written, for zero vorticity, in terms of a velocity field according to

$$\frac{\partial}{\partial t}(\nabla.\mathbf{v}) + \nabla.((\mathbf{v}.\nabla)\mathbf{v}) = -4\pi G\rho, \tag{C.2}$$

where now

$$\mathbf{g} = \frac{\partial \mathbf{v}}{\partial t} + (\mathbf{v}.\nabla)\mathbf{v} = \frac{d\mathbf{v}}{dt}, \tag{C.3}$$

which involves the Euler total time derivative of $\mathbf{v}$ familiar from fluid mechanics. This gives the acceleration of an element of fluid, even when the velocity field is stationary, that is, not changing with time. Then the 'inverse square law' solution of (C.1) in vacuum,

$$\mathbf{g} = -\frac{GM}{r^2}\hat{\mathbf{r}}, \tag{C.4}$$

has the corresponding velocity field

$$\mathbf{v}(\mathbf{r}) = -\sqrt{\frac{2GM}{r}}\hat{\mathbf{r}}. \tag{C.5}$$

First note that it is the occurrence of the total derivative in (C.2) that leads to the 'inverse square law'; namely that this law is now seen to be mandated by the use of the velocity field formalism. But this 'flow equation' is not that of a conserved quantity, for which $\nabla.\mathbf{v} = 0$. Whence the matter density on the RHS of (C.2) plays the role of a 'sink', and that the Newtonian gravitational constant G determines the rate at which matter dissipates 'space'. However once the velocity field formalism is introduced, as above, we see immediately that it must be generalised. The first

generalisation is that a term may be added to (C.2) that is identically zero for the in-flow in (C.5),

$$\frac{\partial}{\partial t}(\nabla.\mathbf{v}) + \nabla.((\mathbf{v}.\nabla)\mathbf{v}) + C(\mathbf{v}) = -4\pi G\rho, \tag{C.6}$$

where

$$C(\mathbf{v}) = \frac{\alpha}{8}((trD)^2 - tr(D^2)). \tag{C.7}$$

It is this new 'spatial dynamics' term that explains the so-called 'dark matter' effect, and that the experimental data has indicated that the new dimensionless second gravitational constant α is non-other than the fine structure constant. So α determines the strength of the spatial self-interaction. Then it immediately follows that we can think of this new term in the context of (C.2) as an effective 'dark matter' density, by considering it placed on the RHS in the form $-4\pi G\rho_{DM}$, so in a form analogous to that for the matter density,

$$\rho_{DM}(\mathbf{r}) = \frac{\alpha}{32\pi G}((trD)^2 - tr(D^2)), \tag{C.8}$$

where

$$D_{ij} = \frac{1}{2}\left(\frac{\partial v_i}{\partial x_j} + \frac{\partial v_j}{\partial x_i}\right). \tag{C.9}$$

Both (C.6) and (C.7) imply that the spatial flow dynamics involves the tensor D_{ij}. Of course the occurrence of G in connection with the 'dark matter' density is somewhat misleading, for the 'dark matter' effect is independent of the value of G. To proceed with the further required generalisation we note that (C.6) is not acceptable as it stands on simple physical grounds; while the velocity flow field is defined relative to an inertial observer, and the total derivative transforms appropriately for that purpose, the absolute velocity of the matter with respect to space has not yet entered into the flow dynamics, as one would expect it to do so. The simplest generalisation to incorporate this is to use D_{ij} as a means to connecting $\mathbf{v}$ to $\mathbf{v}_R$, where

$$\mathbf{v}_R(\mathbf{r}_0(t), t) = \mathbf{v}_0(t) - \mathbf{v}(\mathbf{r}_0(t), t), \tag{C.10}$$

is the absolute velocity of the matter relative to space itself. This leads to the formalism

$$\frac{dD_{ij}}{dt} + A\delta_{ij}tr(D^2) + BD_{ij}trD + C\delta_{ij}(trD)^2 = -4\pi G\rho(\frac{\delta_{ij}}{3} + \frac{v_R^i v_R^j}{2c^2} + ..), \tag{C.11}$$

where all possible terms on dimensional grounds are included[1], with coefficients A, B and C, to be determined by comparison with (C.6), and by insisting that the velocity field (C.5) is an exact solution in vacuum for all terms $i, j = 1, 2, 3$. This

[1]We have excluded here the inclusion of the possible term $\delta_{ij}d(trD)/dt$ from the total time derivative part of (C.11).

procedure ensures that Kepler's laws remain exact, when we have small test objects in orbit about a large central spherically symmetric 'space' 'sink' such as the sun, neglecting for the moment the relativistic corrections to the acceleration **g** given in Sect.7.3. We then find on using, valid for zero vorticity,

$$(\mathbf{v}.\nabla)(trD) = \nabla.(\mathbf{v}.\nabla)\mathbf{v}, \tag{C.12}$$

in evaluating dD_{ij}/dt, that $A = 1/3 - \alpha/24$, $B = 1/2$, and $C = -1/6 + \alpha/24$, giving

$$\frac{dD_{ij}}{dt} + \frac{\delta_{ij}}{3}tr(D^2) + \frac{trD}{2}(D_{ij} - \frac{\delta_{ij}}{3}trD)$$
$$+\frac{\delta_{ij}}{3}\frac{\alpha}{8}((trD)^2 - tr(D^2)) = -4\pi G\rho(\frac{\delta_{ij}}{3} + \frac{v_R^i v_R^j}{2c^2} + ..). \tag{C.13}$$

The LHS of this 'flow equation' is most remarkable. Even though it was determined by Kepler's laws, it involves the product of $trD = \nabla.\mathbf{v}$ and $(D_{ij} - \frac{\delta_{ij}}{3}trD)$; the first factor is the well known measure of the rate of 'fluid' loss, while the second term is the traceless part of D_{ij} that is well known in fluid mechanics to characterise the distortion of a cell of fluid as it flows, without taking account of the rotation of that cell. This means that in general a spherical cell of 'fluid' evolves into an ellipsoid. However an interpretation of $tr(D^2)$ in the context of conventional fluid mechanics is not known. Finally to include rotational effects, we need to include the vorticity vector field $\omega = \nabla \times \mathbf{v}$ via the second-rank antisymmetric tensor

$$\Omega_{ij} = \frac{1}{2}\left(\frac{\partial v_i}{\partial x_j} - \frac{\partial v_j}{\partial x_i}\right) = -\frac{1}{2}\epsilon_{ijk}\omega_k = -\frac{1}{2}\epsilon_{ijk}(\nabla \times \mathbf{v})_k \tag{C.14}$$

Including the symmetric construct $(D\Omega - \Omega D)_{ij}$ then couples the vorticity into the flow dynamics, giving

$$\frac{dD_{ij}}{dt} + \frac{\delta_{ij}}{3}tr(D^2) + \frac{trD}{2}(D_{ij} - \frac{\delta_{ij}}{3}trD) + \frac{\delta_{ij}}{3}\frac{\alpha}{8}((trD)^2 - tr(D^2)) + (\Omega D - D\Omega)_{ij}$$
$$= -4\pi G\rho(\frac{\delta_{ij}}{3} + \frac{v_R^i v_R^j}{2c^2} + ..), \quad i,j = 1,2,3, \tag{C.15}$$

$$\nabla \times (\nabla \times \mathbf{v}) = \frac{8\pi G\rho}{c^2}\mathbf{v}_R, \tag{C.16}$$

where this last equation explicitly determines the vorticity tensor. In (C.15) the coupling between D and Ω has been chosen to agree with that for GR, as we see below. The required physical argument that would determine this coupling is not known at this stage. The tensor structure of the RHS of (C.15) involves the absolute velocity $\mathbf{v}_R$, as required; the factor of $1/2$ is conjecture only at this stage. Of course in the final analysis it is experiment and observation that determine the efficacy of this theory of gravity. As argued in this book there is considerable evidence for that

efficacy, particularly the explanation of the 'dark matter' effect in various guises, and not just its singular occurrence in spiral galaxy rotation anomalies.

The above flow equations would appear very strange to workers in General Relativity whose value system is focused on the primacy of the metric $g_{\mu\nu}$. However as noted in Sect.7.6 when the Panlevé-Gullstrand metric, appropriate to an in-flow interpretation of gravity, is substituted into the Hilbert-Einstein equation, we obtain in vacuum the tensor equations

$$(trD)^2 - tr(D^2) = 0, \tag{C.17}$$

$$(\nabla \times (\nabla \times \mathbf{v}))_i = 0, \tag{C.18}$$

$$\frac{d}{dt}(D_{ij} - \delta_{ij} trD) + (D_{ij} - \frac{1}{2}\delta_{ij} trD)trD - \frac{1}{2}\delta_{ij} tr(D^2) - (D\Omega - \Omega D)_{ij} = 0. \tag{C.19}$$

This system differs from (C.15)-(C.16) in that (C.17) forces the 'dark matter' effect to be absent. This requirement is a legacy of the Newtonian theory of gravity because, in part, GR was derived by forcing it to agree with the Newtonian theory of gravity in the appropriate limits. We see here also, and this is exact for the Panlevé-Gullstrand metric in GR, that the Euler fluid-flow total time derivative arises. Again we can explicitly check that the in-flow field in (C.5) satisfies all equations in (C.17)-(C.19), so that this system also agrees with Kepler's laws. So the extravagant formalism of GR, in the case of the Schwarzschild metric, is nothing more than the 'inverse square law' in disguise.

Finally we note the mathematical structure of (C.15)-(C.16), particularly from the point of view of computing numerical solutions. Imagine that we have computed the velocity field up to time t, and that the matter velocity $\mathbf{v}_R$ has also been computed up to that time. Then the flow equations determine both D_{ij} and Ω_{ij} at the next time step $t + \delta t$. Then

$$\frac{\partial v_i}{\partial x_j} = D_{ij} + \Omega_{ij} \tag{C.20}$$

determines v_i by integration.

Appendix D

Numerical Techniques

Various numerical solutions of the flow equations have been given above, and here we indicate the numerical techniques that have been used. In principle one needs to solve for the time-dependent velocity potential $u(\mathbf{r}, t)$ even in the simplest vorticity-free approximation, as discussed in Sect.8.1, which gives

$$\frac{\partial u(\mathbf{r}, t)}{\partial t} = -\frac{1}{2}(\nabla u(\mathbf{r}, t))^2 + \frac{1}{4\pi}\int d^3r' \frac{C(\nabla u(\mathbf{r}', t))}{|\mathbf{r} - \mathbf{r}'|} - \Phi(\mathbf{r}, t), \tag{D.1}$$

where Φ is the Newtonian gravitational potential

$$\Phi(\mathbf{r}, t) = -G\int d^3r' \frac{\rho(\mathbf{r}', t)}{|\mathbf{r} - \mathbf{r}'|}. \tag{D.2}$$

So here we ignore also the velocity field $\mathbf{v}_R$. However obtaining time-dependent solutions is computationally intensive, and only time-independent solutions are reported herein. In this case we can write (D.1) in the form

$$|\mathbf{v}(\mathbf{r})|^2 = \frac{2}{4\pi}\int d^3r' \frac{C(\mathbf{v}(\mathbf{r}'))}{|\mathbf{r} - \mathbf{r}'|} - 2\Phi(\mathbf{r}). \tag{D.3}$$

This non-linear equation clearly cannot be solved for $\mathbf{v}(\mathbf{r})$ as its direction is not specified. It is for this reason that we expect time-dependent fluctuations in the velocity field, since it is most likely that no unique static solution exists, although this is not yet proven. We have computed solutions to (D.3) by using the *ansatz* that the direction of $\mathbf{v}(\mathbf{r})$ is the same as the direction of $\nabla(\mathbf{v}(\mathbf{r}))^2$. Then (D.3) can be solved iteratively until numerical convergence is obtained. Note that when a non-minimal gravitational attractor is present $C(\mathbf{v}(\mathbf{r}))$ is non-zero at all distances. In this case the space has been divided into two regions by using a spherical surface, where inside this surface numerical methods are used, and the contribution to v^2 from outside of that surface is computed analytically. The integrations in (D.1) and (D.2) were represented by a cubic lattice, with point masses located at the centre of each cube. Then the mass at each centre had the form $\rho_{ijk} + \rho_{DMijk}$ with ρ_{DMijk} variable over iterations. This allows the integration to represented by analytic forms.

Appendix E

Fresnel Drag

Fresnel drag is the observed effect in which motion of a transparent medium partially drags the light, so that instead of the speed being $V = c/n$ it is increased to the extent given in (E.2). The explanation for this effect is yet to be determined, although over the years a variety of explanations have been produced. Fresnel in considering the possible nature of the aether[1] assumed that the density of the aether in a transparent material is proportional to the square of the refractive index n: $\rho_m/\rho_v = n^2$. When the matter moves through the aether that part of the aether in excess of the vacuum value is carried along: $\rho_m - \rho_v = (n^2 - 1)\rho_v$. Then the centre of mass of the aether moves with speed

$$v_{cm} = \frac{(n^2-1)v + 1.0}{(n^2-1)+1} = \left(1 - \frac{1}{n^2}\right) v, \tag{E.1}$$

where v is the velocity of the matter. This velocity is added to the velocity c/n of light in the body, so that

$$V = \frac{c}{n} + \left(1 - \frac{1}{n^2}\right) v, \tag{E.2}$$

and $f = (1 - 1/n^2)$ is known as the Fresnel drag coefficient. Fizeau confirmed this result using moving water in 1851. Michelson and Morley in 1886 confirmed the result using transparent liquids such as water, carbon disulfide and others with a high n.

Stokes in 1842 gave another derivation assuming that the aether was a compressible but conserved fluid. If the aether has an apparent speed v with respect to the transparent matter then let $v' = (1 - \kappa)v$ be the drag speed. If the aether density is $\rho = \rho_0$ in vacuum, then the density is $\rho' = n^2\rho_0$ in the matter. If the aether is conserved then $\rho_0 v = \rho' v' = n^2(1-\kappa)\rho_0 v$, and so $\kappa = 1 - 1/n^2$. Lorentz in 1892 gave another derivation based on the microstructure of the moving transparent medium.

The Fresnel drag may also be derived as a consequence of the relativistic velocity transformation, which follows from the Lorentz transformation. The mathematics

[1] Adapted from notes by G.F. Smoot

of this is straightforward. The Lorentz transformation gives the velocity addition rule:

$$V = \frac{v + v'}{1 + \dfrac{vv'}{c^2}}. \tag{E.3}$$

The meaning of this is that if an observer O' measures a light wave moving at speed v', and O' is moving with speed v relative to observer O, then (E.3) gives the speed V of that light wave according to O. Then for $v' = c/n$ we obtain (E.2). However the meaning of this mathematical derivation is not so clear as the argument does not coincide with the actual physical situation. The Fresnel drag effect is that if an observer measures the speed of the light wave to be c/n when the matter is at rest with respect to that observer, then the speed measured by the same observer when the matter is moving at speed v is given by (E.2).

Appendix F

Michelson Interferometer Analysis - no Fresnel Drag

Here is a simplified analysis of the Michelson interferometer when the Fresnel drag is neglected and when for simplicity the arms are parallel/orthogonal to the direction of motion, as shown in Fig.10.2. Let the arms have lengths L_1 and L_2 when at rest. The Fitzgerald-Lorentz effect is that the arm AB parallel to the direction of motion is shortened to

$$L_{\|} = L_1\sqrt{1-\frac{v^2}{c^2}} \tag{F.1}$$

by absolute motion. We consider the case when the apparatus is moving at speed v through space, and that the photon states travel at speed $V = c/n$ relative to the quantum-foam which is space, where n is the refractive index of the gas and c is the speed of light, in vacuum, relative to the space. Let the time taken for ψ_1 to travel from $A \to B$ be t_{AB} and that from $B \to A$ be t_{BA}. In moving from the beamsplitter at A to B, the photon state ψ_1 must travel an extra distance because the mirror B travels a distance vt_{AB} in this time, thus the total distance that must be traversed is

$$Vt_{AB} = L_{\|} + vt_{AB}. \tag{F.2}$$

Similarly on returning from B to A the photon state ψ_1 must travel the distance

$$Vt_{BA} = L_{\|} - vt_{BA}. \tag{F.3}$$

Hence the total time t_{ABA} taken for ψ_1 to travel from $A \to B \to A$ is given by

$$t_{ABA} = t_{AB} + t_{BA} = \frac{L_{\|}}{V-v} + \frac{L_{\|}}{V+v} \tag{F.4}$$

$$= \frac{L_{\|}(V+v) + L_{\|}(V-v)}{V^2-v^2} \tag{F.5}$$

$$= \frac{2L_1V\sqrt{1-\frac{v^2}{c^2}}}{V^2-v^2}. \tag{F.6}$$

Now let the time taken for the photon state ψ_2 to travel from $A \to C$ be t_{AC}, but in that time the apparatus travels a distance vt_{AC}. Pythagoras' theorem then gives

$$(Vt_{AC})^2 = L_2^2 + (vt_{AC})^2 \tag{F.7}$$

which gives

$$t_{AC} = \frac{L_2}{\sqrt{V^2-v^2}}, \tag{F.8}$$

and including the return trip $C \to A, t_{CA} = t_{AC}, t_{ACA} = t_{AC} + t_{CA}$ results in

$$t_{ACA} = \frac{2L_2}{\sqrt{V^2-v^2}}, \tag{F.9}$$

giving finally for the time difference for the two arms

$$\Delta t_0 = \frac{2L_1V\sqrt{1-\frac{v^2}{c^2}}}{V^2-v^2} - \frac{2L_2}{\sqrt{V^2-v^2}}. \tag{F.10}$$

Now let the two arms be rotated through 90^0, so that the roles of L_1 and L_2 become interchanged. Then the difference in travel time becomes

$$\Delta t_{90} = \frac{2L_1}{\sqrt{V^2-v^2}} - \frac{2L_2V\sqrt{1-\frac{v^2}{c^2}}}{V^2-v^2}. \tag{F.11}$$

Then on rotation the change in difference of the travel times, which gives the observed fringe shift, is given by

$$\Delta t = \Delta t_0 - \Delta t_{90} = \frac{2(L_1+L_2)V\sqrt{1-\frac{v^2}{c^2}}}{V^2-v^2} - \frac{2(L_1+L_2)}{\sqrt{V^2-v^2}}, \tag{F.12}$$

so that the effective arm length is $L = (L_1 + L_2)/2$, which is the average. For $V = c/n$ appropriate for no Fresnel drag, and for $v \ll c$ we obtain for $n \approx 1^+$

$$\Delta t = 2\frac{(n^2-1)L}{c}\frac{v^2}{c^2} + O(v^4). \tag{F.13}$$

Appendix G

Michelson Interferometer Analysis - with Fresnel Drag

Now consider the derivation in Appendix F when the Fresnel drag is included. Consider the Michelson interferometer operating in a gas which is moving with the interferometer at speed v. The motion of the gas relative to space results in a Fresnel drag effect. For simplicity consider only the cases when the arms are parallel/orthogonal to the direction of motion, as shown in Fig.10.2. Let the arms have equal lengths L when at rest. The Fitzgerald-Lorentz relativistic effect is that the arm AB parallel to the direction of motion is shortened to

$$L_{\parallel} = L\sqrt{1 - \frac{v^2}{c^2}} \tag{G.1}$$

by absolute motion, while the length L of the transverse arm is unaffected. We work in the absolute rest frame. Consider the photon states in the AB arm. They travel at speed $V = c/n \pm bv$ relative to the quantum-foam which is space, where n is the refractive index of the gas and c is the speed of light in vacuum and relative to the space. Here $b = 1 - 1/n^2$ is the Fresnel drag coefficient which is well established experimentally. The motion of the gas through the quantum foam slightly 'drags' the light. The effect on the speed is $\pm bv$ depending on the direction of the light relative to the direction of absolute motion. Then the total travel time t_{ABA} is

$$t_{ABA} = t_{AB} + t_{BA} = \frac{L_{\parallel}}{\frac{c}{n} + bv - v} + \frac{L_{\parallel}}{\frac{c}{n} - bv + v} \tag{G.2}$$

$$= \frac{2Ln}{c}\sqrt{1 - \frac{v^2}{c^2}}\frac{1}{1 - \frac{v^2}{n^2c^2}}. \tag{G.3}$$

For the orthogonal arm we have by Pythagoras' theorem

$$(Vt_{AC})^2 = L^2 + (vt_{AC})^2. \tag{G.4}$$

The speed V of light travelling from A to C (and also from C to A) is

$$V = \frac{c}{n} + bv\cos(\alpha), \tag{G.5}$$

where α is the angle of the transverse light path to the direction of motion of the interferometer, as shown in Fig.10.2, and is given by

$$\cos(\alpha) = \sqrt{1 - \frac{L^2}{(Vt)^2}}. \tag{G.6}$$

Solving (G.4), (G.5) and (G.6) for V we obtain

$$V = \frac{1}{2}\left(\frac{c^2}{n^2} + \sqrt{\frac{c^2}{n^2} + 4bv^2}\ \right). \tag{G.7}$$

Then (G.4) gives t_{AC}, and we obtain, with $t_{ACA} = t_{AC} + t_{CA} = 2t_{AC}$, and for $v \ll c$

$$\Delta t = 2(t_{ABA} - t_{ACA}) = -2\frac{(n^2-1)(2-n^2)L}{nc}\frac{v^2}{c^2} + O(v^4), \tag{G.8}$$

for the change in relative travel times when the apparatus is rotated through 90^0. The factor of 2 arises because then the role of each arm is interchanged. For gases $n \approx 1^+$ and we obtain

$$\Delta t \approx -2\frac{(n^2-1)L}{c}\frac{v^2}{c^2} + O(v^4). \tag{G.9}$$

The major significance of this result is that this time difference is not zero when a gas is present in the interferometer, as confirmed by all gas-mode interferometer experiments. Of course this result also shows that vacuum-mode experiments, with $n = 1$, will give null results, as also confirmed by experiment. In the case of a gas inclusion of the Fresnel drag effect results in only a change of sign for Δt, as shown by comparison of (F.13) and (G.9) .

Appendix H

Michelson Interferometer and the Einstein Postulates

The Einstein postulates (7.57) require that the Michelson interferometer gives a null effect even when operating with a dielectric, whether a gas or a solid, and so contrary to experiment in the case of gas-mode. So it is interesting to see an explicit demonstration of this[1].

Let L = proper length of each arm, $V = c/n$ = speed of photon in rest frame of dielectric, and take $c = 1$. Relative to 'stationary' observer S: v = speed of interferometer apparatus, V_{out} = speed of outbound photon in longitudinal arm, V_{ret} = speed of returning photon in longitudinal arm, V_{tran} = speed of photon in transverse arm (both ways), $L_{long} = L(1-v^2)^{1/2}$ = length of longitudinal arm, and length of transverse arm = L.

Consider the longitudinal arm: The velocity transformation/composition formula gives

$$V_{out} = \frac{V+v}{1+vV} \quad \text{photon \& frame velocities 'add',} \tag{H.1}$$

$$V_{ret} = \frac{V-v}{1-vV} \quad \text{photon \& frame velocities 'subtract'.} \tag{H.2}$$

For free-space propagation, $V = 1$, these reduce to $V_{out} = 1$ and $V_{ret} = 1$, as required by the second postulate. From these:

$$V_{out} - v = \frac{(1-v^2)V}{1+vV}, \tag{H.3}$$

$$V_{ret} + v = \frac{(1-v^2)V}{1-vV}. \tag{H.4}$$

[1] Adapted from notes by Ron Burman.

Note parenthetically that

$$V_{out} - V_{ret} = \frac{2v(1-V^2)}{1-(Vv)^2}, \tag{H.5}$$

reducing to 0 for the vacuum ($V = 1$) case.

Hence S calculates the out and back times in this arm, as in Appendix F:

$$\begin{aligned} t_{out} &= \frac{1}{V_{out} - v} L_{long}, \\ &= \frac{1+vV}{(1-v^2)V} L_{long}, \end{aligned} \tag{H.6}$$

$$\begin{aligned} t_{ret} &= \frac{1}{V(ret) + v} L_{long}, \\ &= \frac{1-vV}{(1-v^2)V} L_{long} \end{aligned} \tag{H.7}$$

Adding these and incorporating the Fitzgerald-Lorentz contraction, S considers the round trip time in this arm to be

$$t_{trip} = \frac{2L}{V}(1-v^2)^{-1/2}. \tag{H.8}$$

Eqn.(H.8) reducing simply to the vacuum result when $V = 1$.

Now consider the transverse arm: A photon in this arm has only a transverse velocity component, $\pm V$, in the rest frame of the apparatus. The velocity transformation formula yields these velocity components in S (relativistic aberration):

$$\text{longitudinal component} = v, \tag{H.9}$$

$$\text{transverse component} = \pm V(1-v^2)^{1/2}. \tag{H.10}$$

The relativistic factor arises from time dilation and means that the motion in the transverse arm is relativistically aberrated. Thus S calculates the photon's resultant speed to be V_{tran}:

$$V_{tran}^2 - v^2 = (1-v^2)V^2. \tag{H.11}$$

Using this result, S calculates the round trip travel time in this arm, as in Appendix F

$$\begin{aligned} t_{trip} &= \frac{2L}{(V_{tran}^2 - v^2)^{1/2}}, \\ &= \frac{2L}{V}(1-v^2)^{-1/2}. \end{aligned} \tag{H.12}$$

Thus the travel times in the two arms, (H.8) and (H.12), are identical, whether in a dielectric or not. This is because of a combination of Fresnel drag in the

longitudinal arm and relativistic aberration (via time dilation) in the transverse arm. So according to the Einstein postulates the effect is always null and void. While the above derivation may have some validity when the dielectric is a solid, it is clearly in disagreement with experiment when the dielectric is a gas. So the Einstein formalism lacks the contextuality that reality displays.

References

Bibliography

[1] D.R. Griffin, Ed., *Physics and the Ultimate Significance of Time: Bohm, Prigogine, and Process Philosophy*, (Albany: State University of NY Press, 1986).

[2] D. Browning and W.T. Myers, Eds., *Philosophers of Process*, 2nd ed. (Fordham Univ. Press, 1998).

[3] T.E. Eastman and H. Keeton, *Resource Guide to Physics and Whitehead*, *Process Studies Supplement, 2003*, http://www.ctr4process.org/publications/PSS/index.htm.

[4] T.E. Eastman and H. Keeton, Eds., *Physics and Whitehead: Process, Quantum and Experience*, (SUNY Press, 2003).

[5] D.R. Griffin, *Unsnarling the World-Knot: Consciousness, Freedom and the Mind-Body Problem*, (Univ. of California Press, 1998).

[6] R.T. Cahill, *Process Physics: Inertia, Gravity and the Quantum*, *Gen. Rel. and Grav.* **34**, 1637-1656(2002).

[7] R.T. Cahill, *Process Physics: From Quantum Foam to General Relativity*, gr-qc/0203015.

[8] R.T. Cahill and C.M. Klinger, *Bootstrap Universe from Self-Referential Noise*, gr-qc/9708013.

[9] R.T. Cahill and C.M. Klinger, *Self-Referential Noise and the Synthesis of Three-Dimensional Space*, *Gen. Rel. and Grav.* **32**(3), 529(2000); gr-qc/9812083.

[10] R.T. Cahill and C.M. Klinger, *Self-Referential Noise as a Fundamental Aspect of Reality*, Proc. 2nd Int. Conf. on Unsolved Problems of Noise and Fluctuations (UPoN'99), Eds. D. Abbott and L. Kish, Adelaide, Australia, 11-15th July 1999, **Vol. 511,** p. 43 (American Institute of Physics, New York, 2000); gr-qc/9905082.

[11] R.T. Cahill, C.M. Klinger, and K. Kitto, *Process Physics: Modelling Reality as Self-Organising Information*, *The Physicist* **37**(6), 191(2000); gr-qc/0009023.

[12] R.T. Cahill and K. Kitto, *Michelson-Morley Experiments Revisited and the Cosmic Background Radiation Preferred Frame*, *Apeiron* **10**, No.2. 104-117(2003); physics/0205070.

[13] R.T. Cahill, *Analysis of Data from a Quantum Gravity Experiment*, physics/0207010.

[14] R.T. Cahill, *Absolute Motion and Quantum Gravity*, physics/0209013.

[15] R.T. Cahill, *Gravity as Quantum Foam In-Flow*, *Apeiron*, **11**, No.1, pp. 1-52(2004).

[16] R.T. Cahill, *Absolute Motion and Gravitational Effects*, *Apeiron*, **11**, No.1, pp. 53-111(2004).

[17] R.T. Cahill, *Quantum Foam, Gravity and Gravitational Waves*, in *Relativity, Gravitation, Cosmology*, pp. 168-226, eds. V. V. Dvoeglazov and A. A. Espinoza Garrido (Nova Science Pub., NY, 2004).

[18] R.T. Cahill, *Gravitation, the 'Dark Matter' Effect and the Fine Structure Constant*, *Apeiron*, **12**, No. 2, pp. 144-177(2005).

[19] R.T. Cahill, *'Dark Matter' as a Quantum Foam In-Flow Effect*, in *Trends In Dark Matter Research*, ed. J. Val Blain (Nova Science Pub., NY, 2005).

[20] R.T. Cahill, *The Speed of Light and the Einstein Legacy: 1905-2005*, *Infinite Energy*, **10**, Issue 60, pp. 28-37(2005).

[21] K. Kitto, *Dynamical Hierarchies in Fundamental Physics*, p55, in *Workshop Proceedings of the 8th International Conference on the Simulation and Synthesis of Living Systems (ALife VIII)*, E. Bilotta *et al.*, Eds. (Univ. New South Wales, Australia, 2002).

[22] M. Chown, *Random Reality*, *New Scientist*, Feb 26, **165**, No 2227, 24-28(2000).

[23] B. Müller, J. Reinhardt and M.T. Strickland, *Neural Networks - An Introduction*, 2nd ed. (Springer).

[24] Y. Bar-Yam, *Dynamics of Complex Systems*, (Addison-Wesley, 1997)

[25] E. Nagel and J.R. Newman, *Gödel's Proof*, (New York Univ. Press, 1995).

[26] G.J. Chaitin, *Information, Randomness and Incompleteness*, 2nd ed. (World Scientific, 1990).

[27] G.J. Chaitin, *The Unknowable*, (Springer-Verlag, 1999).

[28] G.J. Chaitin, *Exploring Randomness*, (Springer-Verlag, 2001).

[29] G. Priest, *Beyond the Limits of Thought*, (Cambridge Univ. Press, 1995).

[30] F.Th. Stcherbatsky, *Buddhist Logic*, (Dover Pub. New York, 1962).

[31] J.A. Wheeler *Law without Law*, in *Quantum Theory of Measurement*, J.A. Wheeler and W.H. Zurek, Eds. (Princeton Univ. Press, 1983).

[32] P.A. Schilpp, Ed. *The Philosophy of Rudolf Carnap*, (Cambridge Univ. Press, 1963), p37.

[33] P. Bak, C. Tang and K. Wiesenfeld, *Phys. Rev. Lett.* **59**, 381(1987); *Phys. Rev. A* **38**, 364(1988).

[34] R.T. Cahill, *Hadronisation of QCD*, *Aust. J. Phys.* **42**, 171(1989); R.T. Cahill, *Hadronic Laws from QCD*, *Nucl. Phys. A* **543**, 63(1992); R.T. Cahill and S.M. Gunner, *The Global Colour Model of QCD for Hadronic Processes: A Review*, *Fizika B* **7**, 171 (1998).

[35] G. Parisi and Y. Wu, *Perturbation Theory without Gauge Fixing*, *Scientia Sinica* **24**, 483(1981).

[36] E. Schrödinger, *What is Life?*, (Cambridge Univ. Press, 1945).

[37] G. Nicholis and I. Prigogine, *Self-Organization in Non-Equilibrium Systems: From Dissipative Structures to Order Through Fluctuations*, (J. Wiley & Sons, New York, 1997).

[38] G. Nagels, *A Bucket of Dust*, *Gen. Rel. and Grav.* **17**, 545(1985).

[39] J.A. Wheeler, *Relativity, Groups and Topology*, B.S. Dewitt and C.M. Dewitt, Eds. (Gorden and Breach, New York, 1964).

[40] R.W. Ogden, *Non-Linear Elastic Deformations*, (Halstead Press, New York, 1984).

[41] N.S. Manton and P.J. Ruback, *Skyrmions in Flat Space and Curved Space*, *Phys. Lett. B* **181**, 137(1986).

[42] N.S. Manton, *Geometry of Skyrmions*, *Comm. Math. Phys.* **111**, 469(1987).

[43] T. Gisiger and M.B. Paranjape, *Recent Mathematical Developments in the Skyrme Model*, *Physics Reports* **36**, 109(1998).

[44] S. Coleman, J.B. Hartle, T. Piran and S. Weinberg, eds., *Quantum Cosmology and Baby Universes*, (World Scientific, Singapore, 1991).

[45] I.C. Percival, *Quantum State Diffusion*, (Cambridge Univ. Press, 1998).

[46] R. Penrose, *The Emperors New Mind: Concerning Computers, Minds and the Laws of Physics*, (Oxford Univ. Press, Oxford, 1989).

[47] R.E. Marshak, *Conceptual Foundations of Modern Particle Physics*, (World Scientific, 1993).

[48] J-J. Dugne, S. Fredriksson, J. Hansson and E.Predazzi, *Preon Trinity: A New Model of Leptons and Quarks*, 2nd International Conference Physics Beyond The Standard Model: Beyond The Desert 99: Accelerator, Nonaccelerator and Space Approaches, Proceedings, ed. H.V. Klapdor-Kleingrothaus, I.V. Krivosheina. Bristol, IOP, 1236(2000), hep-ph/9909569.

[49] B. Bollabás, *Random Graphs*, (Academic Press, London, 1985).

[50] A. Riess *et al.*, *Observational Evidence from Supernovae for an Accelerating Universe and a Cosmological Constant*, *Astron. J.* **116**, 1009(1998); S. Perlmutter, *et al.*, *Measurements of Omega and Lambda from 42 High Redshift Supernovae*, *Astrophys. J.* **517**, 565(1999).

[51] T. Toffoli, in *Complexity, Entropy and the Physics of Information*, p 301, W.H. Zurek, Ed. (Addison-Wesley, 1990).

[52] A. Unzicker, *What Can Physics Learn From Continuum Mechanics?*, gr-qc/0011064.

[53] H. Günther, *On Lorentz Symmetries in Solids*, *Physica Status Solidi*, **A 62**, 131(1988).

[54] W.G. Unruh, *Experimental Black Hole Evaporation*, *Phys. Rev. Lett.* **46**, 1351(1981).

[55] J.S. Bell, *Speakable and Unspeakable in Quantum Mechanics*, (Cambridge Univ. Press, 1987).

[56] P. Panlevé, *C. R. Acad. Sci.*, **173**, 677(1921).

[57] A. Gullstrand, *Ark. Mat. Astron. Fys.*, **16**, 1(1922).

[58] G. Pugh, in *Nonlinear Gravitodynamics: The Lense - Thirring Effect*, eds. R. Ruffini and C. Sigismondi, *World Scientific Pub. Co., 2003, pp 414-426*, (Based on a 1959 report).

[59] L.I. Schiff, *Phys. Rev. Lett.* **4**, 215(1960).

[60] R.A. Van Patten and C.W.F. Everitt, *Phys. Rev. Lett.* **36**, 629(1976).

[61] C.W.F. Everitt *et al.*, in: *Near Zero: Festschrift for William M. Fairbank*, ed. C.W.F. Everitt, (Freeman Ed,. S. Francisco, 1986).

[62] J.P. Turneaure, C.W.F. Everitt, B.W. Parkinson, *et al.*, *The Gravity Probe B Relativity Gyroscope Experiment*, in *Proc. of the Fourth Marcell Grossmann Meeting in General Relativity*, ed. R. Ruffini, (Elsevier, Amsterdam, 1986).

[63] S. Weinberg, *Gravitation and Cosmology: Principles and Applications of the General Theory of Relativity*, (John Wiley & Sons, 1972).

[64] G.M. Clemence, *Astron. Papers Am. Ephemeris*, **II**, part 1 (1943); *Rev. Mod. Phys.*, **19**, 361(1947).

[65] R.T. Cahill, *Novel Gravity Probe B Frame-Dragging Effect*, physics/0406121.

[66] R.T. Cahill, *Novel Gravity Probe B Gravitational Wave Detection*, physics/0408097.

[67] J.H. Oort, *Bull. Astr. Inst. Netherlands*, **6**, 249(1932).

[68] F.D. Kahn and L. Woltjer, *ApJ*, **130**, 705(1959).

[69] F. Zwicky, *Helv. Phys. Acta.*, **6**, 110(1933).

[70] J. Einasto, *Astrofizika*, **5**, 137(1969).

[71] V.S. Sizikov, *Astrofizika*, **5**, 317(1969).

[72] K.C. Freeman, *ApJ*, **160**, 811(1970).

[73] M. Allais, *AeroSpace Eng.*, Sept.-Oct. **18**, p.46(1959); http://allais.maurice.free.fr/English/Science.htm

[74] E.J. Saxl and M. Allen, *1970 Solar Eclipse as "Seen" by a Torsional Pendulum*, *Phys. Rev.*, **D3**, 823(1971).

[75] S.W. Zhou and B.J. Huang, *Abnormalities of the Time Comparisons of Atomic Clocks during the Solar Eclipses*, *Il Nuovo Cimento*, **15C**, N.2, 133(1992).

[76] S.E. Shnoll, *et al.*, *Realization of Discrete States During Fluctuations in Macroscopic Processes*, *Physics-Uspekhi* **41** (10) pp.1025-1035(1998); *Fine Structure of Distributions in Measurements of Different Processes as Affected by Geophysical and Cosmological Factors*, *Phys. Chem. Earth (A)*, **24**, No.8, pp.711-714(1999); *Regular Variation of the Fine Structure of Statistical Distributions as a Consequence of Cosmological Agents*, *Physics-Uspekhi* **43** (2) pp.205-209(2000).

[77] F.D. Stacey *et al.*, *Phys. Rev.* D**23**, 2683(1981).

[78] S.C. Holding, F.D. Stacey, and G.J. Tuck, *Phys. Rev.* D**33**, 3487(1986).

[79] S.C. Holding and G.J. Tuck,*Nature (London)* **307**, 714(1987).

[80] F.D. Stacey, G.J.Tuck, G.I. More, S.C. Holding, B.D. Goodwin and R. Zhou, *Geophysics and the Law of Gravity*, *Rev. Mod. Phys.* **59**, 157(1987).

[81] M.E. Ander *et al.*, *Test of Newton's Inverse-Square Law in the Greenland Ice Cap*, *Phys. Rev. Lett.* **62**, 985(1989).

[82] J. Thomas, *et al.*, *Testing the Inverse-Square Law of Gravity on a 465-m Tower*, *Phys. Rev. Lett.*, **63**, 1902(1989).

[83] C. Jekeli, D.H. Eckhardt, and A.J. Romaides, *Phys. Rev. Lett.* **64**, 1204 (1990).

[84] M. Zumberge *et al.*, *Submarine Measurements of the Newtonian Gravitational Constant*, *Phys. Rev. Lett.* **67**, 3051(1991).

[85] P.R. Heyl and P. Chrzanowski, *J. Res. Nat. Bur. Standards* **29**(1942)1.

[86] L. Facy and C. Pontikis, *Comptes Rendus des Scéances de l'Académie des Sciences de Paris* **272**, Série B, (1971)1397.

[87] J. Renner, in *Determination of Gravity Constant and Measurement of Certain Fine Gravity Effects*, Y. D. Boulanger and M. U. Sagitov (Eds.), (National Aeronautics and Space Administration, Washington, 1974), pp. 26-31

[88] M.U. Sagitov *et al.*, *Dok. Acad. Nauk SSSR* **245**(1979)567.

[89] G.G. Luther and W. Towler, *Phys. Rev. Letters* **48**(1982)121.

[90] J.-Cl. Dousse and Ch. Rhême, *Am. J. Phys.* **55**(1987)706.

[91] H. de Boer, H. Haars and W. Michaelis, *Metrologia* **24**(1987)171.

[92] M.A. Zumberge *et al.*, *J. Geophys. Res.* **95**(1990)15483.

[93] A. Cornaz, B. Hubler and W. Kündig, *Phys. Rev. Letters* **72**(1994)1152.

[94] B. Hubler, A. Cornaz and W. Kündig, *Phys. Rev.* **D51**(1995)4005.

[95] M.P. Fitzgerald and T.R. Armstrong, *IIIE Trans. Instrum. Meas.* **44**(1995)494.

[96] C.H. Bagley and G.G. Luther, *Phys. Rev. Letters* **78**(1997)3047.

[97] J. Luo *et al.*, *Phys. Rev.* **D59**(1998) 042001.

[98] J. P. Schwarz *et al.*, 1998, *Science* **282**(1998)2230.

[99] O.V. Karagioz, V.P. Izmaylov and G.T. Gillies, *Grav. Cosmol.* **4**(1998)239.

[100] J. Schurr, F. Nolting and W. Kündig, *Phys. Rev. Letters* **80**(1998)1142.

[101] M.P. Fitzgerald and T.R. Armstrong, *Meas. Sci. Technol.* **10**(1999)439

[102] F. Nolting, J. Schurr, S. Schlamminger and W. Kündig, *Meas. Sci. Technol.* **10**(1999)487.

[103] S.J. Richman, T.J. Quinn, C.C. Speake and R.S. Davis, *Meas. Sci. Technol.* **10**(1999)460.

[104] U. Kleinevoss, H. Meyer, A. Schumacher and S. Hartmann, *Meas. Sci. Technol.* **10**(1999)492.

[105] J. H.Gundlach and S.M. Merkowitz, *Phys. Rev. Letters* **85**(2000)2869 and SISSA preprint gr-qc/0006043.

[106] T.J. Quinn, C. C. Speake, S. J. Richman, R. S. Davis and A. Picard, *Phys. Rev. Letters* **87**(2001)111101.

[107] P. Baldi *et al.*, *Phys. Rev.* **D64**(2001)082001.

[108] G.T. Gillies, *The Newtonian Gravitational Constant: Recent Measurements and Related Studies*, *Rep. Prog. Phys.* **60**(1997)151-225.

[109] J. Gerssen, R. P. van der Marel, K. Gebhardt, P. Guhathakurta, R.C. Peterson and C. Pryor, *Hubble Telescope Evidence for an Intermediate-Mass Black Hole in the Globular Cluster M15 II. Kinematic Analysis and Dynamic Modelling*, *Astron.J.* **124**, pp. 3270-3288(2002); Addendum **125**, 376(2003).

[110] K. Gebhardt, R.M. Rich and L. C. Ho, *A 20 Thousand Solar Mass Black Hole in the Stellar Cluster G1*, *Astrophysical J.*, **L41**, 578(2002).

[111] B.W. Murphy, H.N. Cohn, P.N. Lugger and J.D. Dull, *Dynamical Models of the Globular Clusters M15*, *Bulletin of the Am. Astron. S.*, **26**, No.4, 1487(1994).

[112] M. Persic, P. Salucci, F. Stel, *The Universal Rotation Curve of Spiral Galaxies: I The Dark Matter Connection*, *Mon.Not.R.Astronom.Soc.* **281**, 27(1996).

[113] A.J. Romanowsky, *et al.*, *A Dearth of Dark Matter in Ordinary Elliptical Galaxies*, *Science* **301**, 1696(2003).

[114] J. Bahcall, *Phys. Rev. Lett.* 12, 300(1964).

[115] R. Davis, *Phys. Rev. Lett.* 12, 303(1964).

[116] L. Van Waerbeke *et al.*, *Detection of Correlated Galaxy Ellipticities from CFHT Data: First Evidence for Gravitational Lensing by Large-Scale Structures*, A&A, **393**, 30(2000).

[117] D.M. Wittman *et al.*, *Detection of Weak Gravitational Lensing Distortions of Distant Galaxies by Cosmic Dark Matter at Large Scales*, *Nature*, **405**, 143-149(2000).

[118] J.D. Anderson *et al.*, *Indication, from Pioneer 10/11, Galileo, and Ulysses Data, of an Apparent Anomalous, Weak, Long-Range Acceleration*, *Phys. Rev. Lett.* **81**, 2858-2861(1998).

[119] Descartes, *Principles of Philosophy*, V.R. Miller and R.P. Miller (trans), (Reidel Publishing, Dordrecht 1983).

[120] I. Newton, *Principles of Natural Philosophy*, 1729, trans. by A. Motte, (Dawsons).

[121] A.A. Michelson, *Amer. J. Sci.* **S. 3 22**, 120-129(1881).

[122] A.A. Michelson and E.W. Morley, *Philos. Mag.* S.5, **24**, No. 151, 449-463(1887), (available at http://www.scieng.flinders.edu.au/cpes/people/cahill_r/processphysics.html)

[123] D.C. Miller, *The Ether-Drift Experiment and the Determination of the Absolute Motion of the earth*, *Rev. Mod. Phys.* **5**, 203-242(1933).

[124] G.F. Fitzgerald, *Science*, **13**(1889)420.

[125] H.A. Lorentz, *Electric Phenomena in a System Moving With Any Velocity Less Than That of Light*, in *The Principle of Relativity*, (Dover, New York 1952).

[126] J. Larmor, *Phil. Trans. Roy. Soc. London*, 190-205(1897).

[127] R.S. Shankland, S.W. McCuskey, F.C. Leone and G. Kuerti, *New Analysis of the Interferometer Observations by Dayton C. Miller*, *Rev. Mod. Phys.* **27**(2), 167-178(1955).

[128] K.K. Illingworth, *Phys. Rev.* **30**, 692-696(1927).

[129] G. Joos, *Ann. d. Physik* [5], **7**, 385(1930).

[130] W.M. Hicks, *Phil. Mag*, [**6**], 3, 256, 555(1902); 9, 555(1902).

[131] L. Swenson, *The Ethereal Aether: A History of the Michelson-Morley-Miller Aether Drift Experiments*, (U. Texas Press, Austin, 1972).

[132] J. DeMeo, *Dayton Miller's Ether-Drift Experiments: A Fresh Look*, http://www.orgonelab.org/miller.htm

[133] R.W. Clark, *Einstein: The Life and Times*, (World Publishing C., NY 1971).

[134] H.A. Munéra, *Aperion* **5**, No.1-2, 37-54(1998).

[135] C. Lineweaver et al., *Astrophysics J.* **470**, 38(1996).

[136] T.S. Jaseja, A. Javan, J. Murray and C.H. Townes, *Test of Special Relativity or Isotropy of Space by Use of Infrared Masers*, *Phys. Rev.* **A 133**, 1221(1964).

[137] R. DeWitte, http://www.ping.be/˜pin30390/.

[138] D.G. Torr and P. Kolen, in *Precision Measurements and Fundamental Constants*, B.N. Taylor and W.D. Phillips, Eds. *Natl. Bur. Stand.(U.S.), Spec. Publ.* 617, 675(1984).

[139] H.P Kennedy and E.M. Thorndike, *Phys. Rev.* **42**, 400(1932).

[140] A. Brillet and J.L. Hall, *Phys. Rev. Lett.* **42**, No.9, 549-552(1979).

[141] C. Braxmaier, H. Müller, O. Pradl, J. Mlynek, A. Peters and S. Schiller, *Phys. Rev. Lett.* **88**, 010401(2002).

[142] J.A. Lipa, J.A. Nissen, S. Wang, D.A. Striker and D. Avaloff, *Phys. Rev. Lett.* **90**, 060403-1(2003).

[143] H.P. Robertson, *Rev. Mod. Phys.*, **21**, 378(1949).

[144] R.M. Mansouri and R.U. Sexl, *J. Gen. Rel. Grav.*, **8**, 497(1977), **8**, 515(1977), **8**, 809(1977).

[145] J. Shamir and R. Fox, *Il Nuovo Cimenta*, **LXII B** N.2, 258(1969).

[146] G.G. Stokes, *Phil. Mag.* **27**, 9(1845).

[147] W. Voigt. An English translation and commentary on Voigt's paper are found in A. Ernst and Jong-Ping Hsu, *First Proposal of the Universal Speed of Light by Voigt in 1887*, *Chinese Journal of Physics*, **39**, No. 3, 211-230(2001).

[148] R. Shankland, *Applied Optics*, **12**(10), 2280-2287(1973).